REPORT DOCUMENTATION PAGE

Form Approved
OMB No. 0704-0188

1. AGENCY USE ONLY *(Leave blank)*	2. REPORT DATE 4 August 1998	3. REPORT TYPE AND DATES COVERED

4. TITLE AND SUBTITLE
NANOPHASE SEPARATION AND PHOTOCHEMICAL REACTION OF RODCOIL MOLECULES, LIQUID CRYSTAL MOLECULES AND BINARY MIXTURES

5. FUNDING NUMBERS

6. AUTHOR(S)
Kyle Daniel Gresham

7. PERFORMING ORGANIZATION NAME(S) AND ADDRESS(ES)
University of Illinois at Urbana-Champaign

8. PERFORMING ORGANIZATION REPORT NUMBER

98-033

9. SPONSORING/MONITORING AGENCY NAME(S) AND ADDRESS(ES)
THE DEPARTMENT OF THE AIR FORCE
AFIT/CIA, BLDG 125
2950 P STREET
WPAFB OH 45433

10. SPONSORING/MONITORING AGENCY REPORT NUMBER

11. SUPPLEMENTARY NOTES

12a. DISTRIBUTION AVAILABILITY STATEMENT
Unlimited distribution
In Accordance With AFI 35-205/AFIT Sup 1

12b. DISTRIBUTION CODE

13. ABSTRACT *(Maximum 200 words)*

14. SUBJECT TERMS

15. NUMBER OF PAGES
210

16. PRICE CODE

17. SECURITY CLASSIFICATION OF REPORT	18. SECURITY CLASSIFICATION OF THIS PAGE	19. SECURITY CLASSIFICATION OF ABSTRACT	20. LIMITATION OF ABSTRACT

NANOPHASE SEPARATION AND PHOTOCHEMICAL REACTION OF RODCOIL MOLECULES, LIQUID CRYSTAL MOLECULES AND BINARY MIXTURES

Kyle Daniel Gresham, Ph.D.
Department of Materials Science and Engineering
University of Illinois at Urbana-Champaign, 1998
Samuel I. Stupp, Advisor

This work presents the synthesis and characterization of three related organic systems designed for self-assembly into ordered materials such as two dimensional objects and nanostructures. A family of reactive block molecules referred to as "rodcoils" was synthesized for the purpose of forming nanostructures. In these reactive rodcoil molecules rod-like segments are covalently attached to less rigid coil-like segments. These rodcoil molecules were found to assemble into extremely small aggregates of dimensions on the order of 2-3 nm. New reactive thermotropic liquid crystalline compounds with structure similar to the rod segments of the rodcoil molecules were synthesized and their mesophase behavior characterized. These compounds contained photochemically sensitized groups such as anthracene and diacetylene segments. Irradiation of these materials at various temperatures led to the formation of distinct dimesogens and other high molecular weight material which allowed one of the reactive liquid crystals to act as a negative photoresist for the lithographic formation of 3-5μm features on a silicon wafer. A new methodology for the formation of nanostructures that is presented for the first time in this work is the use of binary mixtures of rodcoil molecules and chemically similar rod molecules. This system was found to form two different types of nanomorphology seen by TEM. The first was a kinetically trapped, striped nanomorphology that was still reactive to topochemical reaction of the rods and which disappeared upon heating to 120°C. Secondly, nanocrystals, with dimensions of 3-

19980811 033

10 nm were found in the striped regions of as-cast films believed to contain mostly rodcoil molecules. These nanocrystals became more prevalent throughout the film upon heating to 100°C whereas the striped morphology disappeared. At 120°C, the nanocrystals also melt to form a new mixed phase exhibiting characteristic X-ray and electron diffraction patterns. Interestingly, the size and shape of the nanocrystals was constant upon heating which is in contrast to what would be expected of classic nucleation and growth behavior. This is thought to be due to interactions of the rodcoils and rods which limits the size of the aggregates and allows for the formation of a more thermodynamically stable phase containing nanocrystals surrounded by a less ordered matrix.

NANOPHASE SEPARATION AND PHOTOCHEMICAL REACTION OF RODCOIL MOLECULES, REACTIVE LIQUID CRYSTAL MOLECULES, AND BINARY MIXTURES

BY

KYLE DANIEL GRESHAM

B.S., United States Air Force Academy, 1991
M.S., University of Illinois, 1992

THESIS

Submitted in partial fulfillment of the requirements
for the degree of Doctor of Philosophy in Materials Science and Engineering
in the Graduate College of the
University of Illinois at Urbana-Champaign, 1998

Urbana, Illinois

UNIVERSITY OF ILLINOIS AT URBANA-CHAMPAIGN

THE GRADUATE COLLEGE

November 1997

WE HEREBY RECOMMEND THAT THE THESIS BY

KYLE DANIEL GRESHAM

ENTITLED NANOPHASE SEPARATION AND PHOTOCHEMICAL REACTION OF

RODCOIL MOLECULES, LIQUID CRYSTAL MOLECULES AND BINARY MIXTURES

BE ACCEPTED IN PARTIAL FULFILLMENT OF THE REQUIREMENTS FOR

THE DEGREE OF DOCTOR OF PHILOSOPHY

_____
Director of Thesis Research

_____
Head of Department

Committee on Final Examination†

_____ Chairperson

_____

_____

_____

† Required for doctor's degree but not for master's.

O-517

NANOPHASE SEPARATION AND PHOTOCHEMICAL REACTION OF RODCOIL MOLECULES, LIQUID CRYSTAL MOLECULES AND BINARY MIXTURES

Kyle Daniel Gresham, Ph.D.
Department of Materials Science and Engineering
University of Illinois at Urbana-Champaign, 1998
Samuel I. Stupp, Advisor

This work presents the synthesis and characterization of three related organic systems designed for self-assembly into ordered materials such as two dimensional objects and nanostructures. A family of reactive block molecules referred to as "rodcoils" was synthesized for the purpose of forming nanostructures. In these reactive rodcoil molecules rod-like segments are covalently attached to less rigid coil-like segments. The rod segments contained photochemically active groups such as diacetylene segments designed to "stitch" covalently the aggregates following nanophase separation of rodcoil molecules. These rodcoil molecules were found to assemble into extremely small aggregates of dimensions on the order of 2-3 nm. New reactive thermotropic liquid crystalline compounds with structure similar to the rod segments of the rodcoil molecules were synthesized and their mesophase behavior extensively characterized by variable temperature powder X-ray diffraction. These compounds contained photochemically sensitized groups such as anthracene and diacetylene segments. Irradiation of these materials at various temperatures led to the formation of distinct dimesogens and other high molecular weight material which allowed one of the reactive liquid crystals to act as a negative photoresist for the lithographic formation of 3-5μm features on a silicon wafer. Various one-dimensional objects such as comb, ladder, comb-ladder and/or two-dimensional polymers might have formed upon irradiation of these reactive liquid crystal molecules. A new methodology for the formation of nanostructures that is presented for the first time in this work is the use of binary mixtures of rodcoil molecules

and chemically similar rod molecules. This system was found to form two different types of nanomorphology seen by transmission electron microscopy (TEM). The first was a kinetically trapped, striped nanomorphology that was still reactive to topochemical reaction of the rods and which disappeared upon heating to 120°C. Secondly, nanocrystals, with dimensions of 3-10 nm were found in the striped regions of as-cast films believed to contain mostly rodcoil molecules. These nanocrystals became more prevalent throughout the film upon heating to 100°C whereas the striped morphology disappeared. At 120°C, the nanocrystals also melt to form a new mixed phase exhibiting characteristic X-ray and electron diffraction patterns. Interestingly, the size and shape of the nanocrystals was constant upon heating which is in contrast to what would be expected of classic nucleation and growth behavior. This is thought to be due to interactions of the rodcoils and rods which limits the size of the aggregates and allows for the formation of a more thermodynamically stable phase containing nanocrystals surrounded by a less ordered matrix.

Acknowledgments

I would like to thank my advisor, Professor Samuel I. Stupp, for providing me the opportunity to do research in his group. I greatly admire his capacity for critical thinking about science and hope that I may achieve some level of this in my future work. I would also like to acknowledge the various members of his group who have provided motivation, insight, and knowledge through countless discussions that have truly rounded out my Ph.D. experience. Finally, I would like to thank Mom, Dad, Ross, and Nicole, who listened patiently to me as I described such things as "the quals" and "nanostructures" and who provided an infinite amount of encouragement during my time here.

I would like to thank the Air Force Institute of Technology/Civilian Institutions office, which sponsored me for this Ph.D. Finally I would like to acknowledge the National Science Foundation and the Army Research Office for partial support of my research.

Table of Contents

Chapter 1 Introduction

1.1 Objectives and Significance

The objective of the author's work has been the synthesis and characterization of organic molecules that self assemble into nanostructures and two-dimensional objects. Much of the work has been done using novel, diblock rodcoil molecules that undergo nanophase separation in solvent cast films. Another motif investigated was the use of thermotropic liquid crystalline compounds as a means for achieving ordered layers that could lead to the formation of two-dimensional objects. These liquid crystal molecules are similar in structure to the rod segments of the rodcoil molecules and were specifically designed to be crosslinked within an ordered liquid crystalline layer in an attempt to form shape persistent, or shape invariant two dimensional analogs of classical one dimensional polymers. One of these materials proved effective as a photoresist material using conventional semiconductor processing techniques. Lastly, the new idea of binary mixtures of rodcoil molecules with chemically similar rod molecules was investigated as a potential system for the formation of nanomorphologies. The binary mixtures were observed to nanophase separate into two distinct morphologies, stripes and nanocrystals that were not found in either component in their pure state.

Due to the difficulties of chemically synthesizing organic nanostructures bond-by-bond, self-assembly and supramolecular chemistry will be one of the important means to achieve controlled synthesis of objects on the nanoscale. The goal would be the formation of many supramolecular units, with similar shape and size, that could be interesting building blocks for materials because of the way they pack to fill space most efficiently.[1] Nanostructures with specially designed surfaces could subsequently lead to materials which also evidence surfaces

with different properties due to their nanostructure.

1.2 Nanostructures

Nanostructures are objects with dimensions between one and one hundred nanometers. This is the realm of proteins, viruses, and liposomes and hence is commonly studied by biologists and biochemists. But in the last two decades, interest in nanostructures by other areas of science has dramatically increased. Physicists interested in quantized materials, particularly semiconducting materials, have found many paths to create inorganic nanostructures with optical and electrical properties that are significantly different than those of the same material in the bulk.[2-7] Another area where work is approaching the nanoscale is the area of semiconductor devices. In an effort to increase the device density on integrated circuit microprocessors, smaller feature sizes are required. Current photolithographic techniques are not capable of making nanostructures although advances are made on a yearly basis. The smallest feature size attainable in photolithography is proportional to the wavelength of the exposure tool. Currently, exposure tools that output 365 nm wavelengths are being upgraded to KrF excimer lasers which output 248 nm light.[8] The next resolution advancement in photolithography is expected to come with the ArF excimer laser that produces a wavelength of 193 nm and will require new photoresist chemistries that can operate in the deep UV region.[9] Researchers in materials science and in the field of supramolecular chemistry are interested in building nanoscale devices from the molecular scale up, rather than trying to engineer current photolithographic techniques down. The benefit of building structures from the molecule up lies in the flexibility inherent to organic chemistry. But while potentially very promising, the nanoscale size regime is not easily attained with the chemical compounds

common in organic chemistry. Organic chemistry has evolved greatly to the point that the total synthesis of complex natural products such as palytoxin is possible.[10] But molecules such as palytoxin (2680 daltons) are small in size (~1 nm) and can not be considered a true nanostructure. Also, the synthesis of compounds like palytoxin is arduous and not a likely candidate for scale up. So another methodology other than bond-by-bond construction must be found to produce new materials that have controllable features on the nanoscale.

One new route to nanostructures using covalent synthesis is Moore's work with rigid phenyl acetylene dendrimers.[11] This work has led to discrete molecules with dimensions on the order of 10 nm in only a few generations of growth and is one example of covalent synthesis that could potentially lead to large-scale synthesis of nanostructures. Another route that nature uses quite successfully is the use of combinations of two or more organic molecules which self assemble into nanostructures. A well-studied example of this type of natural self-assembled nanostructure is the tobacco mosaic virus (TMV) which is cylindrical in shape and is 300 nm long by 18 nm wide.[12, 13] The TMV consists of a single strand of RNA that is surrounded by 2130 identical protein units that self assemble to form a helical coat. What is fascinating about the TMV is that it can be dissociated into its RNA and 2130 protein coat subunits which under appropriate conditions, spontaneously self assemble back into an identical and fully infective virus. Thus, self-assembly is a powerful means of constructing ordered nanostructures and will be the preferred methodology in this investigation

1.3 Self Assembly

Thermodynamically, self-assembly of a nanostructure is controlled by both enthalpy

and entropy. Aggregation requires that many weak, noncovalent bonds overcome the translational, rotational, and conformational entropic costs of bringing many molecules together.[14-17] Because the process is an equilibrium process, the final product is at a thermodynamic minimum. As the structure is assembling, errors tend to be discarded and replaced by orientations that are enthalpically favorable. In this way, biologically self-assembled structures are built error free. Hydrogen bonds are favored for self-assembly due to their relatively high strength, 1-5 kcal/mol, compared to polar, hydrophobic, π-π stacking, and Van der Waals interactions. In order to begin to quantify values for translational entropy, the major entropic term for relatively short and stiff molecules, Whitesides has employed an interpretation of the Sackur-Tetrode equation used by Williams.[15, 18] The form of the Sackur-Tetrode equation used by Williams for a perfect, monatomic gas is,

$$S_{trans}(g) = 5R/2 + (5R/2) \ln T - R \ln P + R \ln [(2\pi m/h^2)^{3/2} k^{5/2} \qquad (1)$$

where   R = gas constant
        P = pressure
        T = temperature
        m = molar mass
        h = Planck's constant
        k = Boltzmann constant

By substituting values of 298 K and 1 atm into eq. 1, one obtains eq 2,

$$S_{trans}(g) = 108.8 + 12.47 \ln(RMM) \text{ J/K mol} \qquad (2)$$

where RMM = relative molar mass, g/mol

Because Williams was interested in the translational entropy loss caused by dimerization in aqueous solution, gas phase information was not adequate. Therefore, to convert these values of entropy in a gas to entropy in dilute solution, Williams imagined the gas being condensed

into a pure liquid of itself, and then being diluted to 1 M solution. Trouton's rule states that the entropy of condensation for a wide range of liquids is ~85 J/K mol while ΔS of dilution can be approximated by

$$\Delta S = R \ln (M_1/M_2) \tag{3}$$

where M_1 is the initial concentration and M_2 is the final concentration. Williams assumes the pure liquid has the density of water (1g/L) and because $M_2 = 1$ M, eq. 3 becomes

$$\Delta S = R \ln (1000/RMM) \tag{4}$$

Therefore, to calculate the loss in translational entropy caused by the assembling of a number of individual molecules in solution, $T\Delta S_{trans}(1$ M$)$, one must calculate $S_{trans}(1M)$ for both the free and assembled case in the gas phase (eq1), convert to the pure liquid state (-85 J/K mol for each molecule), calculate the entropy of dilution (eq 4) and then take the difference between the two states. This process for the dimerization of two molecules of relative molar mass 100 under standard conditions is illustrated in Fig 1.1. If this treatment is applied to the aggregation of 2, 10, and 100 of these same molecules then $T\Delta S_{trans}(1M)$ is calculated to be -5.9 kcal/mol, -64 kcal/mol, and -433 kcal/mol, respectively. While these calculations are rough, they vividly display one problem inherent in the self assembly of many molecules into one. Thus self assembly requires more than just a handful of hydrogen bonds to come about. It requires a careful consideration of entropy and enthalpy, and how they interact at different points in the assembly process of supramolecular structures.

2 Macromolecules(g), mw = 100 g/mol

$S_{trans} = 2 \times 166 = 332$ J/K mol

> (S = 2 x 85 = -170 J/K mol
>
> Trouton's Rule

2 Macromolecules(l), mw = 100 g/mol

$S_{trans} = 332 + (-170) = 162$ J/K mol

> $\Delta S = 2 \times R \ln(1000/100)$
>
> = 38 J/K mol

2 Macromolecules(1 M sol), mw = 100 g/mol

$S_{trans} = 162 + 38 = 200$ J/K mol

Macromolecule Dimer(g), mw = 200 g/mol

$S_{trans} = 1 \times 175 = 175$ J/K mol

> (S = 1 x 85 = -85 J/K mol
>
> Trouton's Rule

Macromolecule Dimer(l), mw = 200 g/mol

$S_{trans} = 175 + (-85) = 90$ J/K mol

> $\Delta S = R \ln(1000/200)$
>
> = 27 J/K mol

Macromolecule Dimer(1 M sol), mw = 200 g/mol

$S_{trans} = 90 + 27 = 117$ J/K mol

$T\Delta S_{trans}$ for dimerization at (T=298K) = -24.7 kJ/mol

= -5.9 kcal/mol

Figure 1.1 Calculation of the translational entropy loss for dimerization of two molecules (100 daltons) in a 1 M solution using method of Doig and Wiliams.[18]

1.4 Supramolecular chemistry

The field of supramolecular chemistry received the highest recognition in science in 1987 when the Nobel Prize in Chemistry was given to Lehn, Pedersen, and Cram for work done in this field.[19-21] In his Nobel Lecture, Lehn stated "Supramolecular chemistry may be defined as 'chemistry beyond the molecule,' bearing on the organized entities of higher complexity that result from the association of two or more chemical species held together by intermolecular forces."[19] Lehn and others have reviewed the topic of supramolecular chemistry in the last few years.[22-25] A major theme of much of the recent research is the use of hydrogen bonds as the intermolecular force that joins molecular aggregates together.[26-29] Directionality and strength of the hydrogen bond lends itself to the design of intricate molecular assemblies that have complementary cavities and surfaces.[30-33] These cavities and surfaces are potential sites for substrates and molecular recognition events, all of which are important properties of biological assemblies. Lehn has proposed and worked on many different receptor/substrate systems with a variety of potential applications in molecular devices. Whitesides has published extensive work on a model molecular system that forms discrete structures through a network of hydrogen bonds that are fairly stable in some organic solvents and have molecular weights on the order of 5000 daltons.[34-36] Stoddart has taken another approach to building nanostructures through the use of rotaxanes.[25] Generally, these are a class of molecules where a cyclic macrocycle encircles a dumbbell shaped molecule that can not withdraw itself due to the two capped ends. The synthesis uses secondary interactions between the macrocycle and the "bar" of the "dumbbell" to hold the "bar" inside the macrocycle. The "bar" is then capped with bulky head groups and the "dumbbell" is complete

and can not easily withdraw itself from the macrocycle. Thus, the structure is held together mechanically rather than by covalent or secondary bonds. This technique has been used to synthesize an enormous number of systems with increasing complexity, including a molecular switch that involved the shuttling of a macrocycle between two positions by chemical or electrochemical stimulus.[37, 38]

1.5 Reaction in Ordered Media

A specific area of research in the field of self assembly of biological structures is the study of bilayer membranes. Bilayer membranes are present in all forms of life and are composed of lipids (double-chain amphiphiles with a polar head group) which form bilayers due to the hydrophobic effect. Various groups have synthesized new lipids that assemble into Langmuir-Blodgett films, vesicles, or free standing bilayers.[39, 40] Related to this work is the incorporation of diacetylene groups in the long chains of artificial lipids.[41-44] Wegner decades ago described the ability of diacetylene groups to undergo topochemical polymerization to form polydiacetylene chains.[45-47] Thus, lipids with the diacetylene group can be polymerized with UV light while the biomembrane is intact. This leads to trapping of structures such as vesicles that are much more robust than natural bilayer membrane structures. Work has also been done in the formation of thin films of diacetylenic materials, by Langmuir-Blodgett techniques and others, which leads to enzymatically functionalized surfaces and potential lithographic uses.[48-50]

Polymerization of thermotropic liquid crystal mesophases has also been investigated as a way to form orientated polymer networks with valuable anisotropic thermal, mechanical, electrical, and optical properties.[51-53] The benefit of such an approach is to try and

control the kinetics of the polymerization reaction and control the structure of the resulting polymer. Polymerization in the nematic phase does not lead to substantial benefits in properties probably because the nematic phase and isotropic phase are similar. But, the more ordered smectic phases do offer increased order within the material over an isotropic system and this leads to anisotropic gels which could serve such roles as ferroelectric switching devices in the future.[54-56] Diacetylene groups are just one of the reactive groups placed in liquid crystal mesogens. Polymerization of the diacetylenes has been reported in liquid crystalline phases at temperatures as high as 210°C.[57, 58]

1.6 Rodcoil Molecules

Currently, work is done in the Stupp group on the self assembly of diblock and triblock molecules called rodcoil molecules.[1, 59-62] An example is shown below,

1

$\overline{n}$ and $\overline{(x+y+z)}$ ~ 9
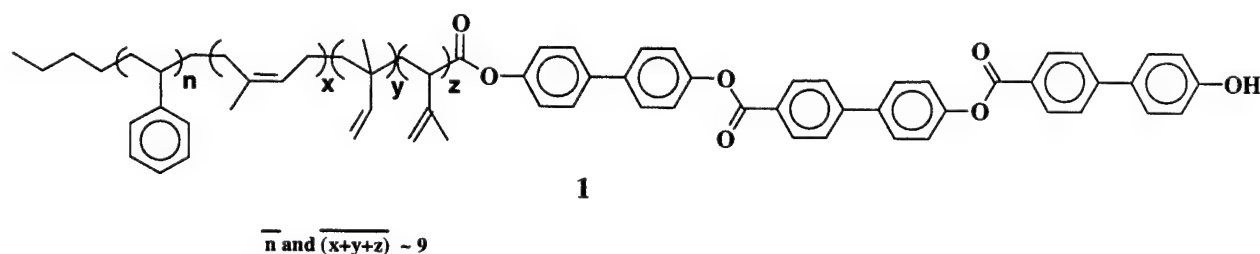
Ober, Thomas, and others have also reported findings on rodcoil systems, including extensive TEM studies of the different morphologies formed by microphase separation due to the mutual repulsions of the dissimilar blocks.[63-67] But there are two differences between these systems and the Stupp rodcoil molecules. First of all, these other rodcoil systems are of much larger molecular weight, approaching that of a true polymer. Second of all, the rod block

of these larger rodcoil molecules is not perfectly discrete monodisperse, but of oligomeric or polymeric lengths with a distribution of molecular weight.

The term rodcoil molecule refers to a block structure consisting of a rigid, rod-like segment covalently attached to a flexible coil-like molecular segment. Those studied in the Stupp group have been found to self assemble into aggregates with dimensions on the nanoscale depending on certain properties such as coil length and rod volume. [61] A variety of chemically different rodcoil systems including one with a poly(ethylene oxide) coil segment and another with a photoluminescent poly(p-phenylene vinylene) rod segment are currently being investigated in the Stupp group.[68] Thus the rodcoil strategy for the self assembly of nanostructures is a general one and can accommodate a wide chemical variety.

The goal of the rodcoil work is to explore the formation of supramolecular nanostructures of similar size and shape. Such nanostructures, or shape persistent macromolecules, could prove to have interesting properties as materials because their defined shape will dictate how the materials will pack in the bulk.[1] By chemical design of the rodcoil molecule precursor, the surfaces of the nanostructures can be altered to provide different properties and functional three dimensional structures. There is also potential to create novel properties in molecular materials creating topographies in nanostructures.

One of the most recently investigated rodcoil molecules is **1**.[1] When this rodcoil molecule is solvent cast as a film, it is likely that the rod segments of the molecules will prefer to crystallize. The coil segments, however, can not in the case of **1** because of styrene atacticity, various modes of isoprene addition, and distribution of coil molecular lengths. Hence, as the rods densify to increase favorable secondary interactions, the coil segments can not pack with the same density and a packing density mismatch begins to occur between

the crystalline rods and the amorphous coil which is covalently attached.[1] Because of their greater cross sectional area, the coil segments will experience repulsive forces at certain degrees of aggregation. These repulsive forces may cause the coil segments to splay out in an effort to relieve the hard core interactions experienced by the coil. It may take a certain number of molecules for repulsive forces to build up, but at some degree of aggregation, the repulsive forces in the coil segments are likely to overcome any favorable interactions of the rod segments and the aggregate of rodcoil molecules will stop growing. Based on transmission electron microscopy (TEM) and second harmonic generation experiments it is believed that these rodcoil molecules aggregate into "mushroom" shaped nanostructures whose size is limited thermodynamically and which polar stack throughout the bulk of a macroscopic film.[1] Rodcoil molecules with much longer (40-100 repeat units) and more flexible poly(isoprene) coil segments have also been studied in the author's laboratory.[60, 61] The repulsive arguments may not play as important a role here as it did for the shorter, bulkier copolymer block. The poly(isoprene) has a smaller cross section than oligo(styrene) and will be more capable of matching the density of the rod segments. But doing this will require the stretching of flexible poly(isoprene) segments. Calculations done by Williams and Fredrickson on the free energy of coil stretching indicate the size of the assembly may be limited by the loss of entropy associated with the stretching of longer poly(isoprene) coil segments.[69]

1.7 Plan of Study

The purpose of this work has been to utilize supramolecular chemistry and self assembly of organic molecules to form ordered nanostructures. For this purpose, the author

synthesized various reactive rodcoil molecules, and reactive liquid crystal molecules. The solid state behavior of these two types of molecular systems was studied individually and in a binary mixture of the two.

Chapter 2 describes the work done with diblock rodcoils, materials with narrow molecular weight distributions, which were substituted with diacetylene reactive groups and other chromophores capable of photochemical reaction upon irradiation with UV light. These materials differed fundamentally from previous rodcoils investigated in the author's group due to their homoblock as opposed to diblock copolymer architecture in the coil and the placement of reactive groups on the rod portion of the molecule. The complete synthesis and characterization are given. Chapter 3 begins with a review of the basics of thermotropic liquid crystals and then describes the mesophase behavior of several liquid crystal molecules with structures similar to the rodcoil molecules discussed in Chapter 2. A combination of Differential Scanning Calorimetry (DSC), Polarized Optical Microscopy (POM), and Variable Temperature X-ray Diffraction was used to assign the different mesophases to these liquid crystals. Irradiation of films of these liquid crystals led to the formation of photoproducts that were investigated by Gel Permeation Chromatography (GPC), UV/Vis, and fluorescence spectroscopy. Proton, carbon, and various 2D nuclear magnetic resonance techniques were also used to further elucidate the structures of the photoproducts. Chapter 4 describes the use of one reactive liquid crystalline material as a photoresist using common semiconductor processing techniques to transfer 3-5 μm features onto a silicon wafer. Finally, Chapter 5 describes investigation of binary mixtures of rodcoils (Chapter 2) with discrete liquid crystalline molecules (Chapter 3) which form nanomorphologies when cast from solution. TEM and X-ray diffraction were used to characterize these morphologies. Investigation of

the order within the material was also probed by visually monitoring topochemical

polymerization within the mixtures.

Chapter 2 Self-Assembling Reactive Rodcoil Molecules

2.1 Introduction

Due to the success with various rodcoil systems in achieving self-assembly of ordered nanostructures, as discussed in Chapter 1, work was continued using this approach but with some fundamental shifts in strategy. Two general changes in the molecular architecture of the rodcoil were proposed. First, the coil portion would be changed to consist only of a bulky, non-reactive, homoblock oligomer, and secondly, the rod would be modified to act both as a mesogen and a reactive site for covalent linkage with adjoining rods. The rod segment continues to play an important role in the formation of ordered nanostructures from rodcoil molecules. Layering is important because it is one way to confine the crosslinking or "stitching" reactions to well-defined planes. The author's group has done this by synthesis of molecules which form layers due to liquid crystalline interactions[1, 70] although it can also be accomplished using Langmuir troughs, vesicles and surfaces.[42, 71, 72] If the reactive groups are allowed to react randomly in three dimensions, a network results and it is not possible to control the stitching of ordered nanostructures. Removing the reactive oligo(isoprene) from the coil segment should affect greatly the ability of the rods to aggregate and may limit the size of the aggregates formed. This assumption is based on the possibility of greater steric repulsion and therefore, possible differences in packing density. As mentioned in Chapter 1, the rod portions of the rodcoil molecules favor crystallization and therefore dense packing to maximize π-π stacking. The atactic oligo(styrene) may favor a random coil conformation and has a much wider cross sectional area due to the aromatic side groups. Therefore, coils on adjacent rodcoil molecules will experience hard core interactions and repulse each other at the same time as the rod portions are attempting to densify. In the previous system, **1**, the

oligo(isoprene) served as a flexible linker with a cross sectional area intermediate between the rods and the oligo(styrene). It is likely that its presence helped to lessen the packing density mismatch between rod and coil segments. In the new architecture, the oligo(isoprene) spacer is no longer present and the packing density mismatch should have a greater effect on aggregation of the molecules. Another effect of removing the oligo(isoprene) will be the absence of the large number of crosslinking sites available in a length of oligo(isoprene). Each repeat unit of oligo(isoprene) has a double bond that can potentially act as a crosslinking site. Before reaction of the isoprene double bonds, **1** forms a smectic melt upon heating above 130°C and becomes an isotropic liquid at 260°C. Thermally initiated free radical reaction of the isoprene double bonds leads to a material which now forms a birefringent melt above 250°C but does not undergo isotropization before it decomposes. It is not known whether the isoprene reaction takes place strictly within the nanostructured "mushroom" or whether the reaction can take place throughout the bulk of the film. In any event, a single "mushroom" nanostructure has not been isolated to date and the new rodcoil architecture was specifically designed with the idea of "capturing" the nanostructure by selective reaction in only the rod portion of the molecule rather than the uncontrolled crosslinking of the oligo(isoprene). The molecules made for this purpose are shown in Fig 2.1 (**2-7**).

The first target of this new rodcoil architecture was **2**. These molecules contain an oligomeric length of styrene covalently attached to a liquid crystalline mesogen possessing a reactive diacetylene group as a potential linker between adjacent rods. As discussed in Chapter 1, adjacent diacetylene groups within a proper distance (≈4-5 Å) and orientation can undergo a thermally or photochemically initiated reaction to form
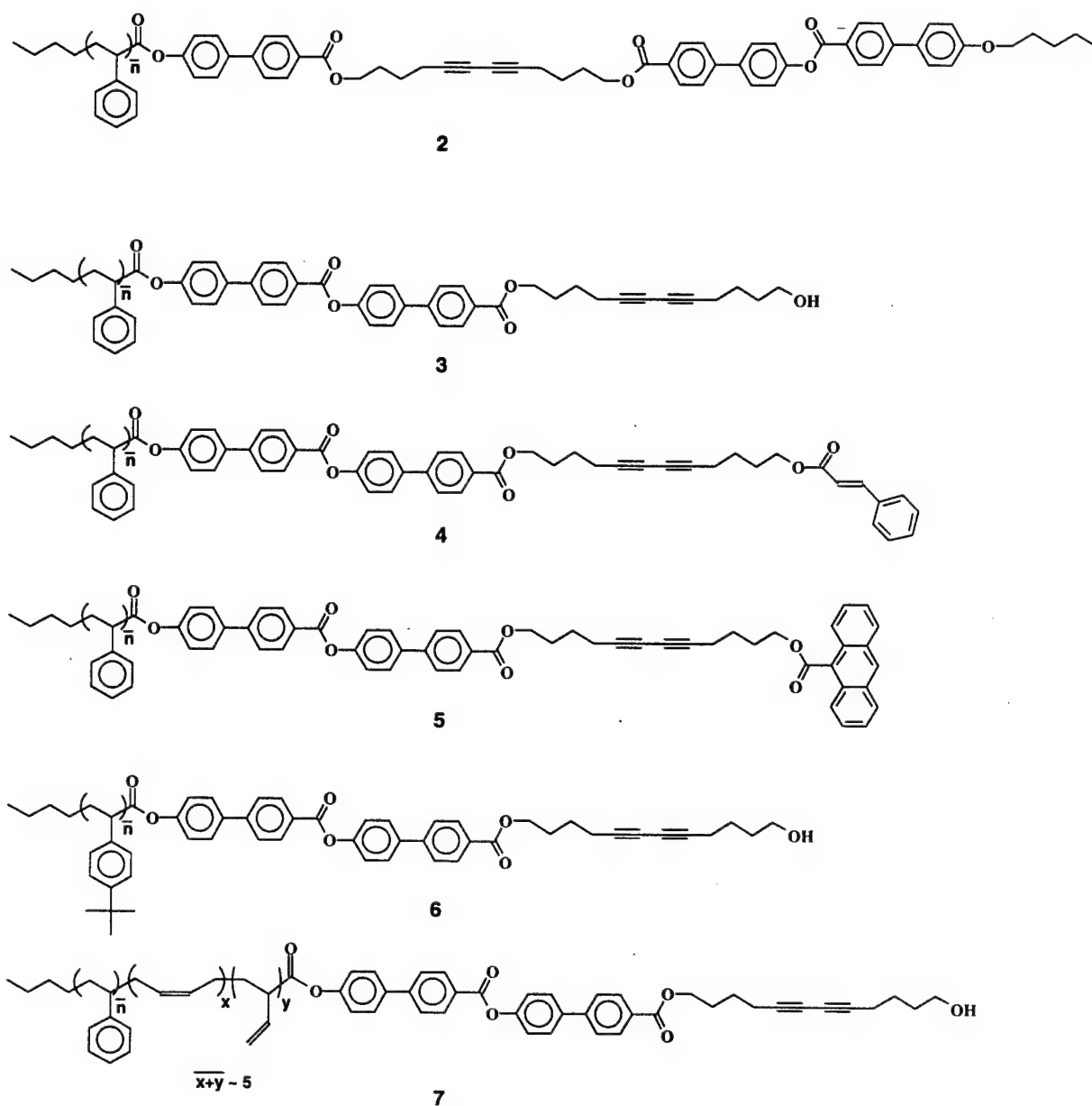
Figure 2.1 Reactive rodcoil molecules synthesized, **2-7**, $\overline{n}$ = 10, average number of repeat units

poly(diacetylene) as illustrated in Fig 2.2.[45-47] Poly(diacetylene) is highly colored

depending on degree of polymerization, and can be made conductive by doping.[73-77] The

polymerization occurs instantly in room light in some highly crystalline samples.[45-47, 78, 79]

2.2 Results and Discussion

2.2.1 Rodcoil Molecules 2 and 3

When **2** was examined by polarized optical microscopy (POM), it exhibited a small

and diffuse amount of birefringence with no assignable texture. This diffuse birefringence

will be elaborated on in the discussion of the other reactive rodcoil molecules. Transmission

electron microscopy (TEM) was performed on films of the

material which were cast from chloroform onto water and picked up with a copper grid. The

electron micrograph revealed that there was no superlattice in the film although the film was

broken up into domains of approximately 1-3 nm (Fig 2.3). Electron diffraction revealed

polycrystalline rings and an amorphous halo. It is suggested that the observed crystallinity is

due to the ordering of small domains of rod segments while the amorphous halo results from

scattering by regions contain atactic oligo(styrene) segments or rodcoil molecules that have

not formed crystalline aggregates. Heating and irradiation failed to cause a color change in

the material indicating either very small or no reaction among the diacetylene groups in the

material to form poly(diacetylene). Gel Permeation Chromatography (GPC) indicated that

formation of higher molecular weight material did not occur. While electron diffraction

indicated that the material was crystalline, it may have been in a crystal lattice that was not

conducive to topochemical polymerization.

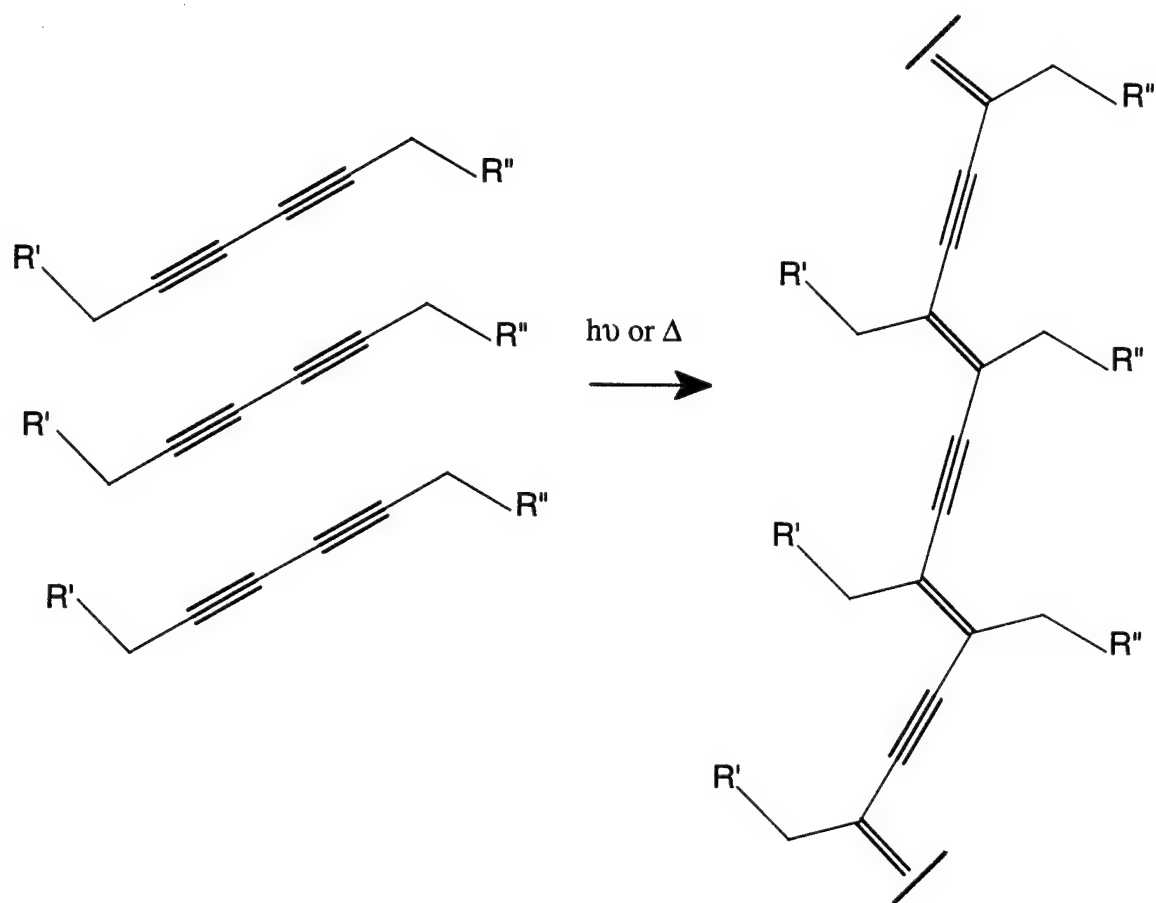**Figure 2.2** Schematic of the 1,4 diacetylene topochemical polymerization reaction
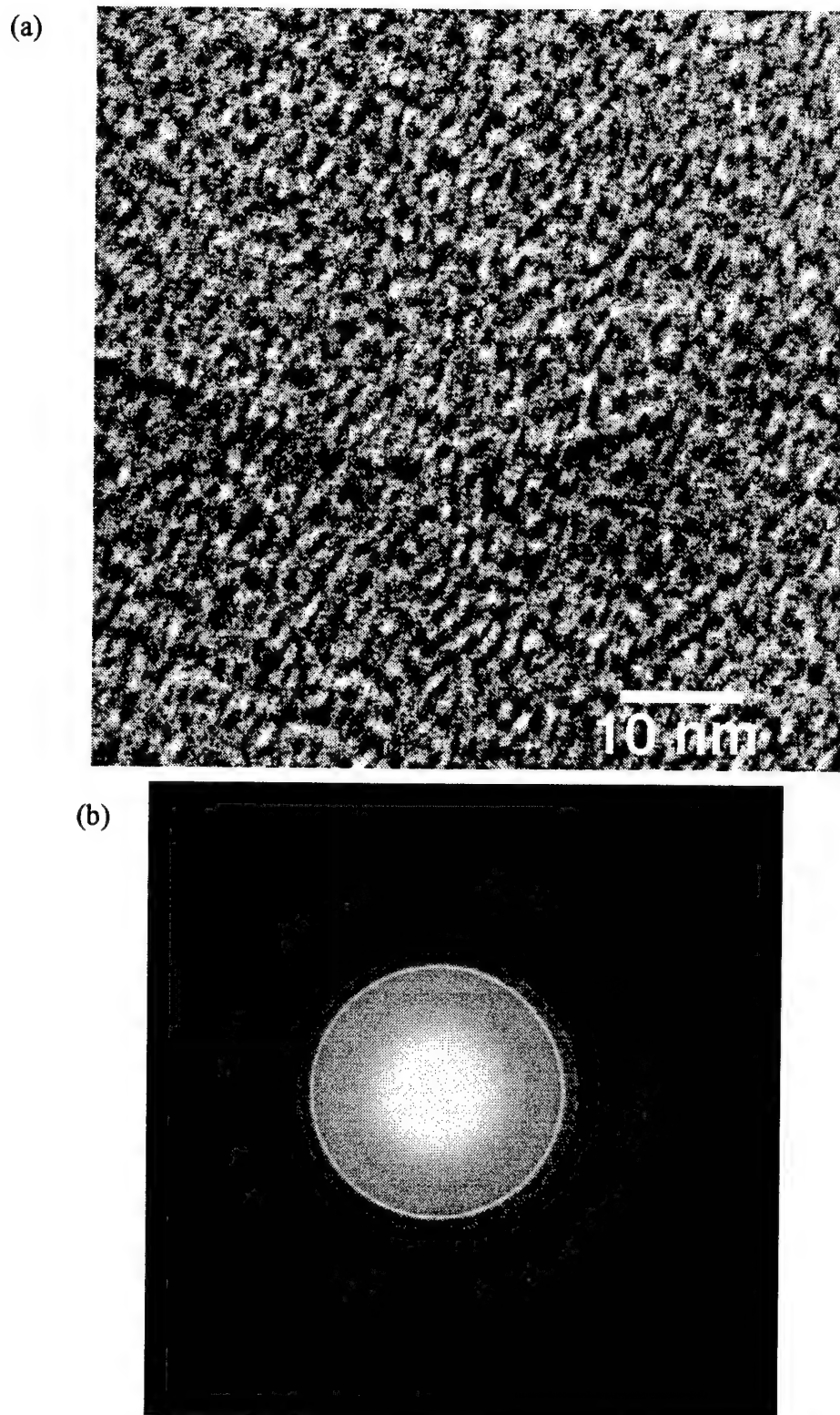
(a)

(b)

Figure 2.3 (a) Transmission Electron Micrograph of film of **2** (b) Wide angle electron diffraction pattern of same film indicating polycrystalline material

Wegner found that only diacetylenes containing hydrogen bonding or high dipole moment substituents undergo solid state reaction.[47] Thus how the substituent affects the structure of the lattice is important. It may be that the oligo(styrene) was too disruptive for topochemical reaction of the diacetylene bonds to occur.

The next rodcoil molecule synthesized, **3**, did have a hydrogen bonding group and studies of the small molecule analog, **8** (discussed more in Chapter 3 and Chapter 5), had found the terminal –OH group to undergo polymeric hydrogen bonding. Molecule **8** was observed to undergo topochemical polymerization spontaneously in room light.[78, 79] Also, the terminal hydroxy group allowed easy derivatization and led subsequently to molecules **4-6**. Synthesis of **3** is outlined in Scheme 1 and Scheme 2 (Scheme 3 shows the relatively simple synthesis of **2** from **3c** and **8**). Scheme 1 outlines the different coil segments synthesized while Scheme 2 details the covalent attachment of the completely monodisperse rod segment to complete the rodcoil molecule synthesis. The synthesis starts with the anionic polymerization of styrene quenched with CO_2 to form end functionalized oligo(styrene) molecules with carboxylic acid groups. The oligo(styrene) coil was characterized by proton nuclear magnetic resonance (NMR) and molecular weight distributions were measured by both GPC and field desorption mass spectroscopy (FD). Examples of both GPC and FD performed on the same batch of carboxylated oligo(styrene) are shown in Fig 2.4 and 2.5. Three values of interest in characterizing the oligocoil are number average molecular weight, M_n, weight average molecular weight, M_w, and polydispersity index. The formulas for all three are below.[80]

$$\overline{M_n} = \frac{\Sigma N_i M_i}{\Sigma N_i}$$

$$\overline{M_w} = \frac{\Sigma \, N_i M_i^2}{\Sigma \, N_i M_i}$$

$$\text{polydispersity index} = \frac{\overline{M_w}}{\overline{M_n}}$$

M_i = molecular weight of species i

N_i = number of moles of species i

Polydispersity values for the carboxylated coil ranged between 1.04 to 1.18 depending on the batch and the technique used to determine the molecular weight distributions. The molecular weight distributions were calculated from the FD data using a spreadsheet program and the formulas listed above.[81, 82] The polydispersity of a Poisson distribution for an average coil length of 10 can be calculated using the following expression,[83]
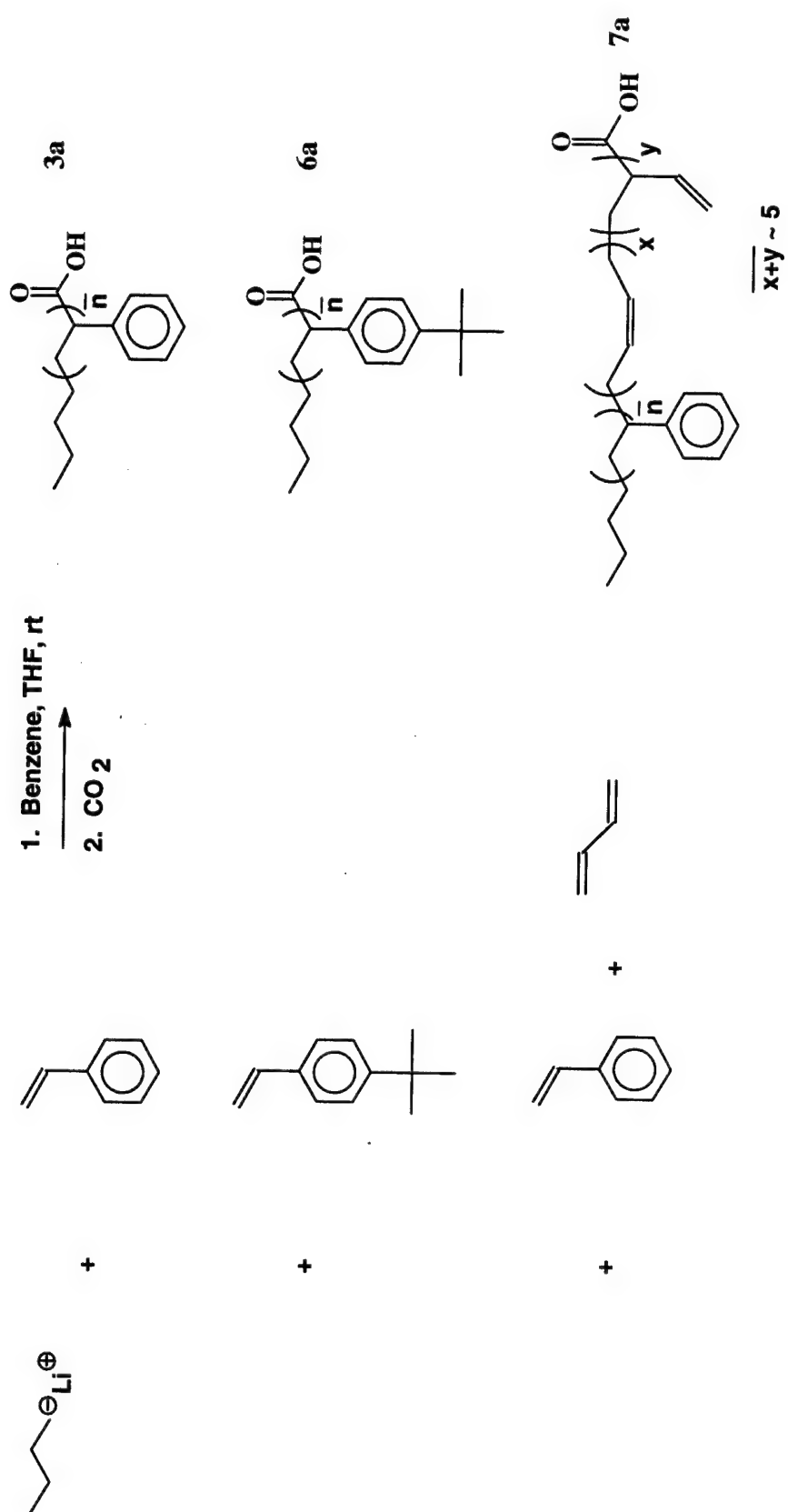
$$\text{polydispersity} = 1 + v/(v+1)^2$$
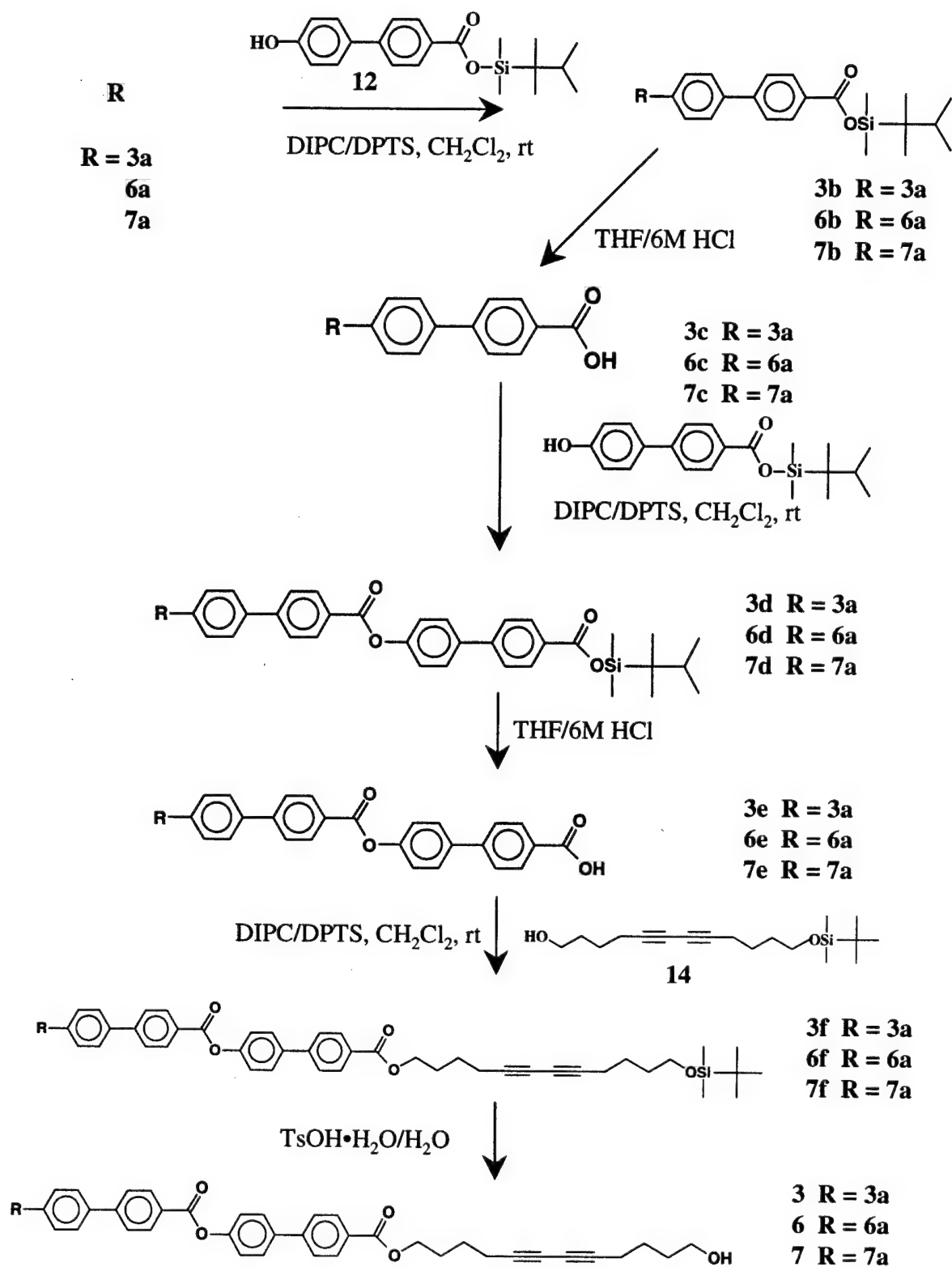
where v = kinetic chain length

Therefore, for $v=10$, the polydispersity of a Poisson distribution would be 1.08. The carboxylation step to functionalize only the living ends with carboxylic acid groups and the subsequent purification may in fact lead to distributions with lower polydispersity than the theoretical Poisson distribution.

The coil is covalently linked to 4-hydroxy-4'-biphenyl carboxylic acid protected as a dimethylthexyl silyl ester (12) [Scheme 2]. The 'thexyl' group is bulkier than the more common t-butyl dimethyl silyl (TBDMS) group and increases the solubility of the biphenyl molecule 'rod' piece in the esterification reaction which is done at room temperature in

Scheme 1

$$\xrightarrow[\text{2. CO}_2]{\text{1. Benzene, THF, rt}}$$

3a

6a

O OH 7a

$\overline{x+y \sim 5}$

Scheme 2

R

R = 3a
6a
7a

12

→ DIPC/DPTS, CH₂Cl₂, rt

3b R = 3a
6b R = 6a
7b R = 7a

THF/6M HCl

3c R = 3a
6c R = 6a
7c R = 7a

DIPC/DPTS, CH₂Cl₂, rt

3d R = 3a
6d R = 6a
7d R = 7a

THF/6M HCl

3e R = 3a
6e R = 6a
7e R = 7a

DIPC/DPTS, CH₂Cl₂, rt   14

3f R = 3a
6f R = 6a
7f R = 7a

TsOH•H₂O/H₂O

3 R = 3a
6 R = 6a
7 R = 7a

Scheme 3

3c

+

8

DIPC/DPTS, CH$_2$Cl$_2$, rt

2

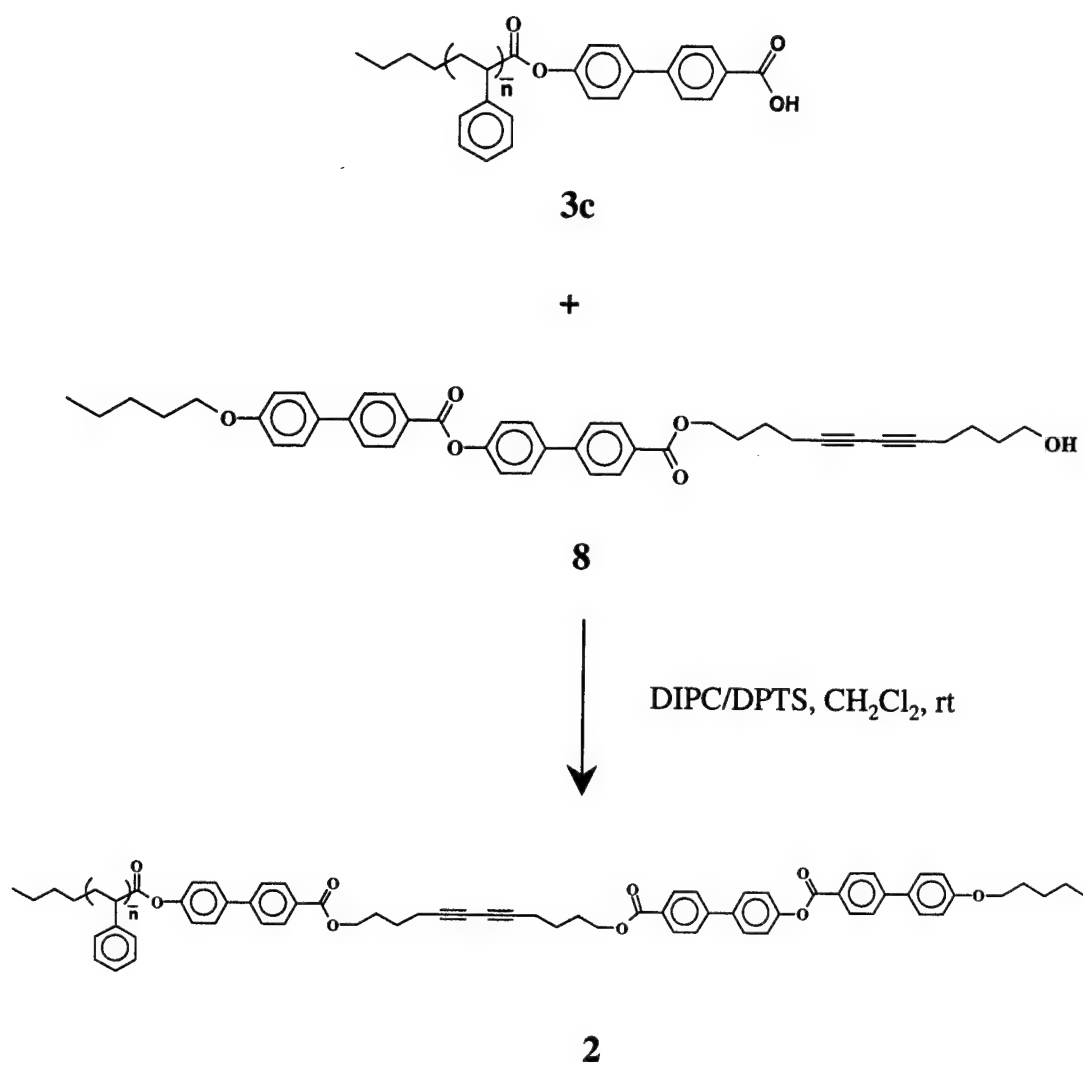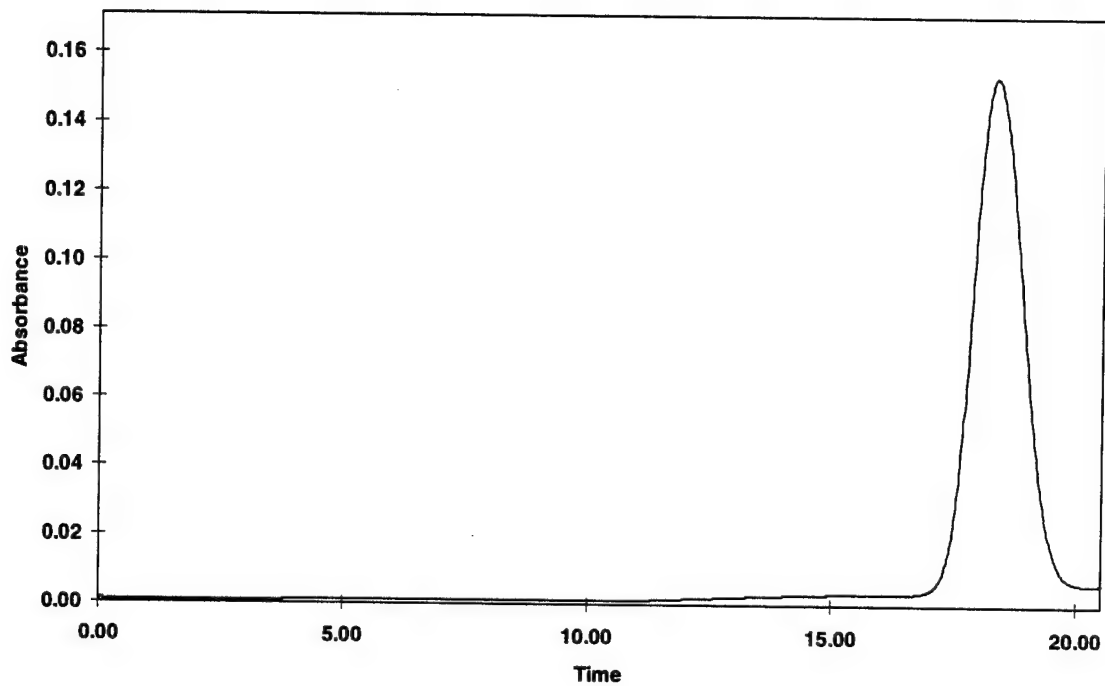**Figure 2.4** Gel Permeation Chromatography trace of **3a** in THF. Average M_n = 1304, Average M_w = 1541, polydispersity index = 1.18
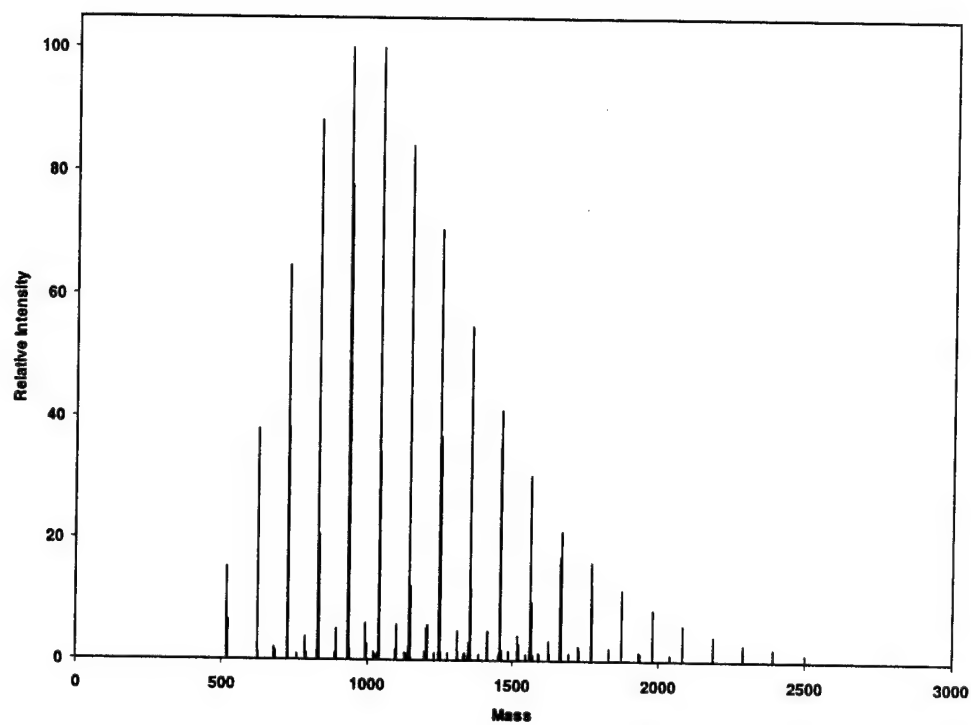
Figure 2.5 Field Desorption Mass Spectroscopy spectrum of same batch of **3a** analyzed in Fig 2.4. Average M_n = 1137, Average M_w = 1219, polydispersity index = 1.07

CH_2Cl_2 as described by Moore and Stupp.[84] After coupling the coil to the first biphenyl

"rod" piece, deprotection of the 'thexyl' group using a solution of 6M HCl in THF affords a

compound (**3c**) with a carboxylic acid end group in almost quantitative yield.[85, 86] The

biphenyl esterification reaction and the thexyl deprotection reaction are then repeated to build

the complete rigid rod segment (**3e**). To the end of the rod segment is added a monoprotected,

diacetylene diol (**14**). Deprotection to remove the TBDMS group and form the terminal

alcohol completes the synthesis of **3**.

GPC of **3** (pure by NMR and TLC) showed it to be a fairly monodisperse material

(polydispersity index = 1.07). This result was substantiated by matrix-assisted laser

desorption/ionization (MALDI)[87-89] from which a value for the polydispersity index was

calculated to be 1.08. Others have found that broad molecular weight distributions are not

accurately analyzed by MALDI while narrow distributions can be accurately resolved. The

problem with the broad distributions is the differences in the ionization ability of the largest

and smallest members of the distribution [89, 90]. Larger members require more laser power to

undergo ionization which leads to smaller peak areas for the higher molecular weight material

which will skew the calculated distribution. Because the materials discussed here are of

narrow distribution, this is not thought to be a problem. The results from both methods for

the same sample are illustrated in Fig 2.6 and Fig 2.7 along with the molecular weight

distributions. Average molecular weights measured by GPC are higher than those measured

with MALDI. This would be expected because while **3** has a portion of linear oligo(styrene),

the rest of the molecule is much more rigid and would be expected to remain straighter and

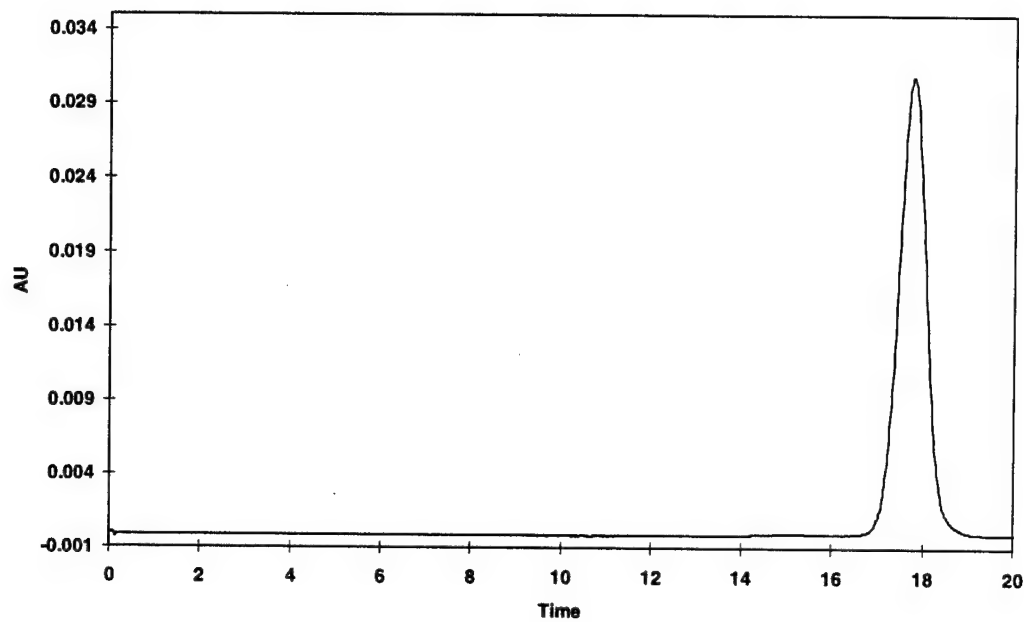sweep out a larger hydrodynamic volume per unit weight than a similar length of more

Figure 2.6 Gel Permeation Chromatography trace of **3** in THF. Average M_n = 2435, Average M_w = 2614, polydispersity index = 1.07
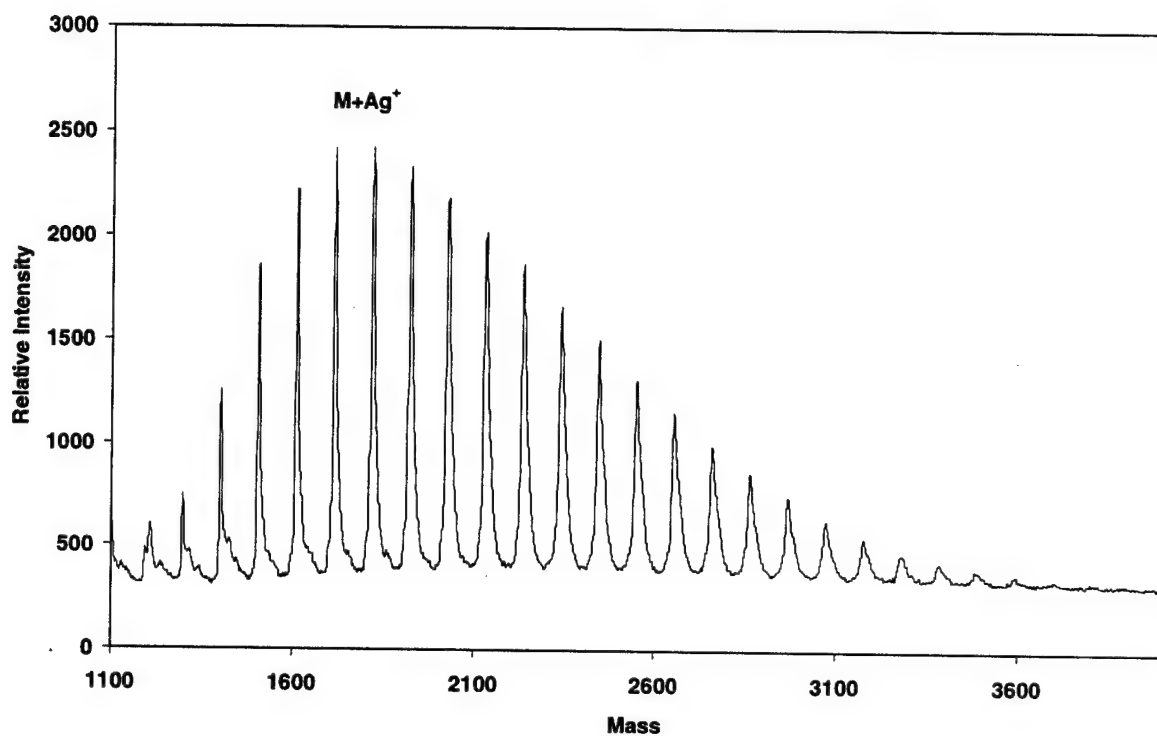
Figure 2.7 Matrix Assisted Laser Desorption/Ionization spectrum of same batch of **3** analyzed in Fig 2.6. Average M_n = 2057, Average M_w = 2222, polydispersity index = 1.08

flexible oligo(styrene). Thus **3** will appear to be a larger molecule when compared to linear poly(styrene) which is what the GPC is calibrated against.

NMR was used after every step to confirm that addition of the rod pieces had occurred (proton NMR of the final product, **3**, is shown in Fig 2.8). Notice that it is possible to identify the majority of the biphenyl protons as sharp multiplets between 7.6 and 8.4 ppm even in the oligo(styrene) derivatives. Protons from the oligo(styrene) show up as broad peaks centered at 7.1 and 6.6 ppm. Analysis by POM could not conclusively assign any mesophases based upon the observed textures. There was only a diffuse birefringence that did not change greatly with changes in temperature nor present a distinguishable pattern that could be assigned as is done with conventional, small molecule liquid crystals. A second order transition is observed at approximately 50°C by DSC as the only feature in the trace of **3** [see Fig 2.9]. This supports the POM data that indicated that no distinct, first order transitions occur in this material. A relationship for the calculation of Tg for poly(styrene) has been developed based on the free volumne of chain ends and is shown below.[91]

$$1/Tg = 1/Tg^{\infty} + A/M$$

A = 0.515 for poly(styrene)

M = number average molecular weight

When the molecular weight of a 10 repeat oligo(styrene) chain is substituted for M, the calculated value for Tg = 42°C which is in close agreement with the DSC experiment.

Molecule **3** is not without molecular order as is dramatically evidenced in the TEM micrograph and wide angle electron diffraction patterns shown in Fig 2.10. At the top of this figure a TEM image shows that the material is made up of small aggregates approximately 1-5 nm in size and it is not a homogeneous amorphous film. The diffraction patterns are the

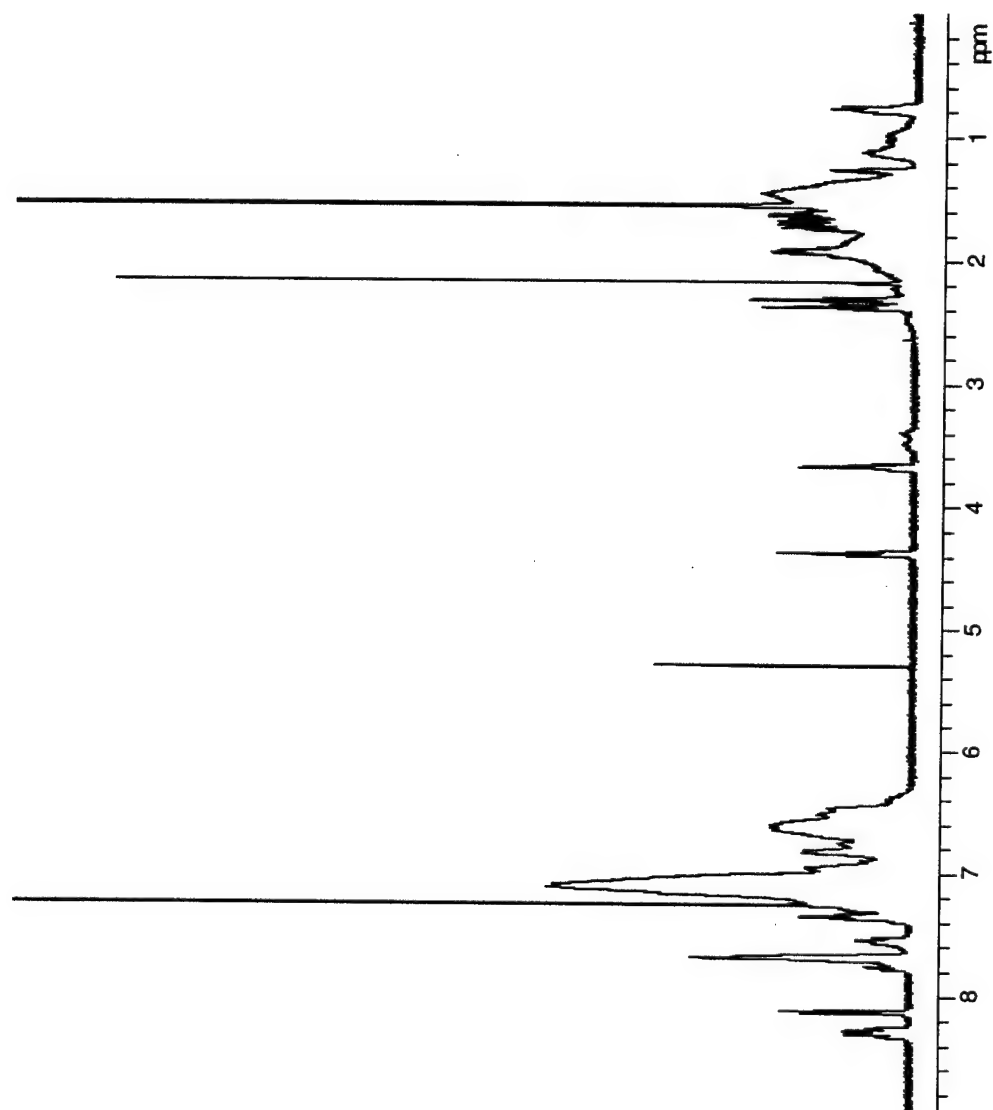**Figure 2.8** Proton NMR of **3** in CDCl₃ (400 MHz)

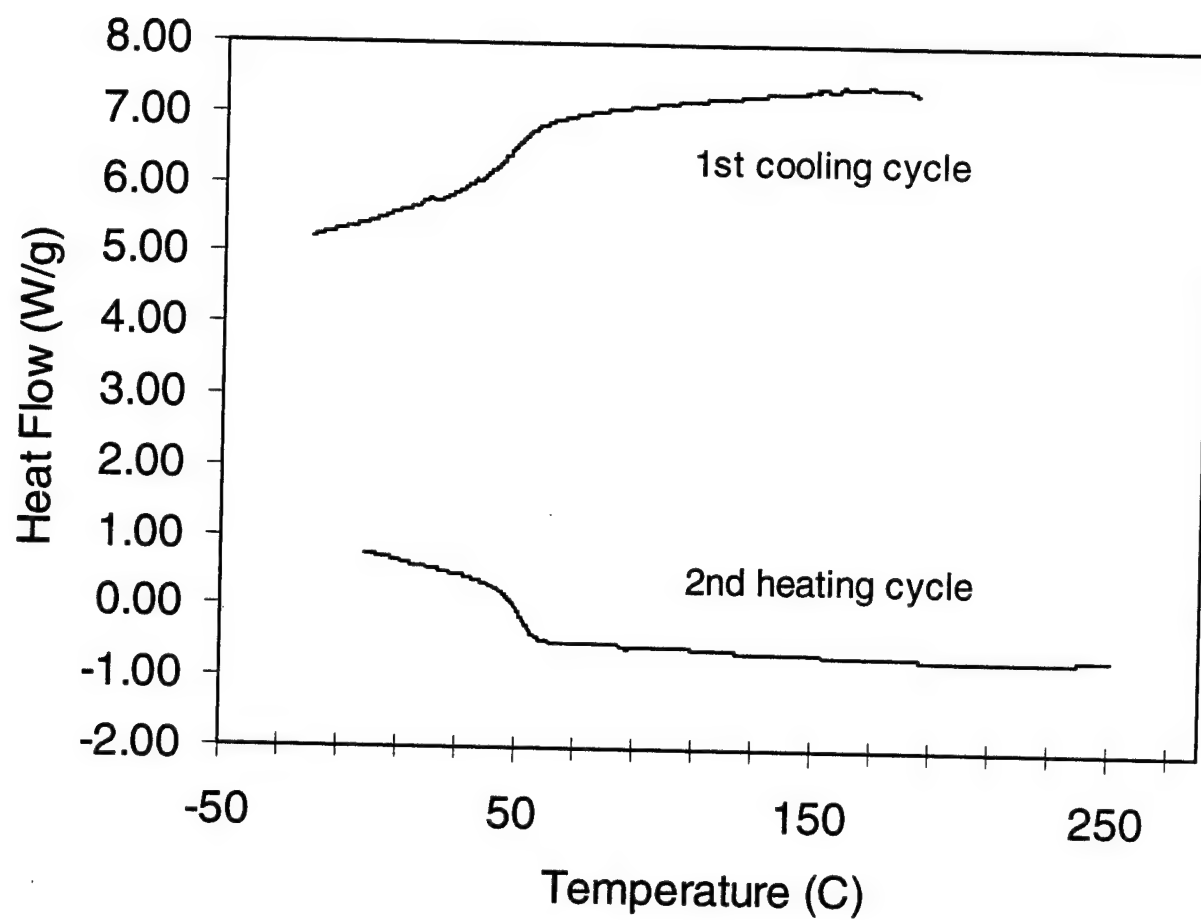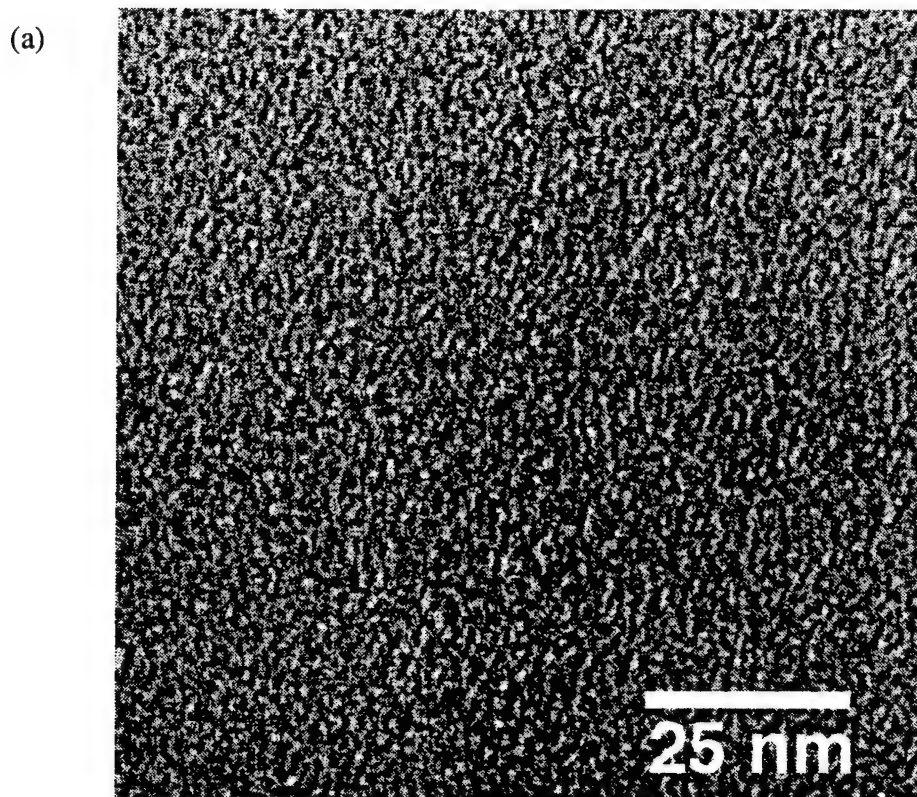**Figure 2.9** Differential Scanning Calorimetry of **3** obtained at 10°C/min during both the 1st cooling and 2nd heating cycle
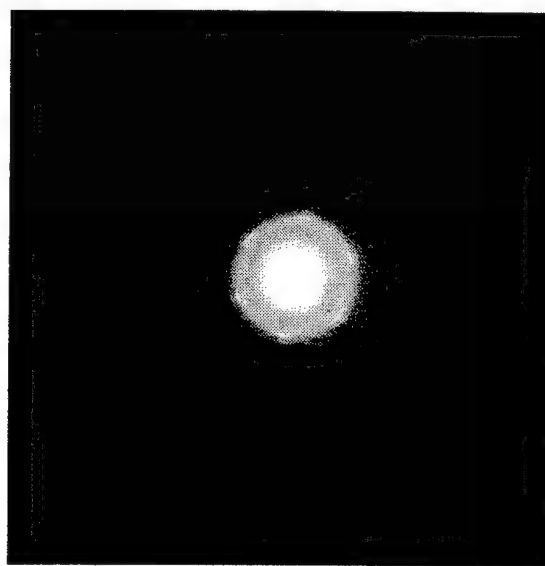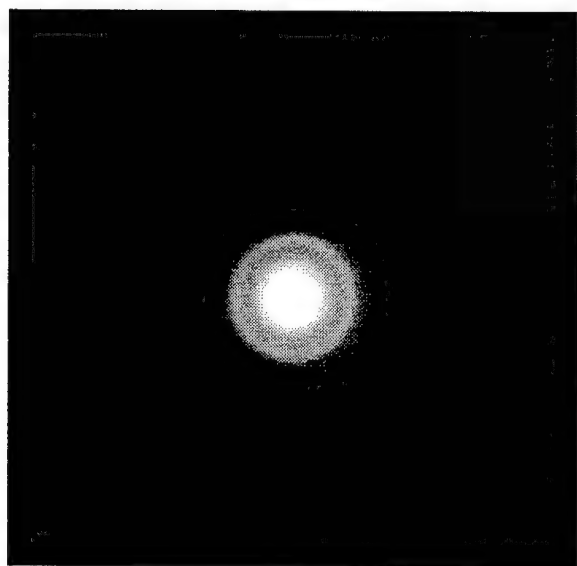
Figure 2.10 (a) Transmission Electron Micrograph of 3; (b) and (c) Wide angle electron diffraction patterns showing amorphous and crystal E order in different regions of the film using selective area diffraction of ~ 1 micron areas

result of selective area electron diffraction obtained from two different regions of the film (~ 1 µm diameter area) although the morphology is the same as Fig 2.10 (a) throughout the film. The first diffraction pattern [Fig 2.10 (b)] shows amorphous scattering characteristic of isotropic material. The second diffraction pattern [Fig 2.10 (c)] is characteristic of a region containing a highly ordered crystal E phase (often called S_E phase) superimposed on an amorphous halo. The crystal E phase is an orthogonal system with the long axis of the molecules perpendicular to the ab plane. The crystal E diffraction patternis not characteristic of the entire film but only a small localized region. It may be an artifact of the solvent casting process where rodcoils with shorter coils precipitated out first and were able to aggregate without the disruptive presence of the longer oligo(styrene) coils. It may also be due to electron beam damage to the sample that cleaved the coil segment from the rod segment and allowed the rod segments to order.

The atactic oligo(styrene) coil can not crystallize and thus explores conformational space. But this amorphous portion of the rodcoil material can not be the only part contributing to amorphous scattering because the area of the film analyzed by selective area electron diffraction is much larger than the 1-5 nm domains of the material. Thus many of the light and dark domains are being probed simultaneously. In the case of the crystal E diffraction pattern [Fig 2.10 (c)], this must have been a region that due to the process of film casting, formed many 1-5 nm crystalline domains which also happened to have a large amount of crystallographic registry among them (note the short arcs in the electron diffraction pattern). The underlying amorphous halo is of course still present because of the amorphous oligo(styrene) which is covalently linked to the rods. Any crystalline aggregates are going to be nanoscale size and surrounded by amorphous material. The fact that there is only small

range order within the material may explain why POM detects so little birefringence and DSC does not detect first order transitions in the material even though electron diffraction indicates there are highly ordered regions. Small Angle X-ray Scattering (SAXS) done on powder samples of **3** revealed no diffraction corresponding to the formation of a layered material.

Attempts were made to react the diacetylene groups in films of **3** that were solvent cast onto glass. Cast films were treated by in three different ways: 1) heat treated to 200°C, 2) irradiated at 254 nm irradiation, and (3) heated and irradiated simultaneously. The films were then dissolved in tetrahydrofuran and analyzed by GPC to see if any increase in molecular weight was detectable. While there was some broadening of the peak in GPC, there was no substantial amount of high molecular weight material that would indicate poly(diacetylene) formation after any of the above three treatments. Additional evidence for lack of diacetylene reaction is that while the films often turned a light brown color (likely due to decomposition) upon annealing, they never turned the characteristic colors of poly(diacetylene) (blue, red, or orange). These colors are due to long conjugation lengths in the polymer backbone, narrowing the band gap of the material into the visible range. That large, ordered domains of poly(diacetylene) were not formed is not surprising in light of the TEM results which showed that the material did not form large domains at all, but instead formed nanoscale domains approximately 1-5 nm in size. Thus, bulk topochemical reaction of the diacetylenes can not occur and no visible color change is noted by the naked eye. Any poly(diacetylene) formed would be confined to the nanoscale domains formed by the rod segments which were possibly in close proximity and in the right configuration to react. The steric forces of the oligo(styrene) coil appeared to have the desired affect in that the crystalline aggregates were nanoscale and in some cases had a high degree of order (crystal E). The reason that no

poly(diacetylene) was detected may be due to crystal E ordering in only a small percentage of the film. Alternatively, the rod segments may not have been in the correct configuration for diacetylene reaction.

2.2.2 Rodcoil Molecules 4 and 5—Additional Crosslinking Groups

One of the goals with this new class of rodcoil molecules was to design them so they would self assemble and then "capture" the self assembled structure by crosslinking the rods to form some type of shape persistent macromolecule which might have new and interesting properties. While **3** did show evidence for the formation of ordered domains on the nanoscale, these domains were not successfully "stitched" together to form a new type of shape persistent macromolecule. The "stitching" reaction in this case would only have formed a rigid linear polymer because there was only one reactive diacetylene group per rodcoil molecule. In an attempt to augment the rodcoil molecule's ability to cross link within the crystalline aggregates, a second crosslinking group was added on the end of **3.** Ideally, this second reactive group would be decoupled from the diacetylene reaction so as to "stitch" in two dimensions. If both groups reacted in concert in the same direction then a type of one-dimensional ladder polymer instead of a shape persistent aggregate would be formed. Putting the second reactive group at the end of the molecule was favored for the following reasons. First, synthetically it was relatively simple to functionalize the terminal alcohol of **3** with various acid groups. Secondly, by placing the group at the terminus, disturbance of rod packing would be minimized in comparison to placing the second reactive group as a side chain on the rod. Two crosslinking groups were investigated, 9-anthracene carboxylic acid and cinnamic acid, both of which undergo photochemical dimerization reactions.[92-96] The

synthesis used to derivatize **3** with these two acid groups is shown in Scheme 4.

2.2.2.1 Cinnamic Acid Derivative (4)

Trans cinnamic acid can undergo a photochemical (2π-2π) cycloaddition with an

adjacent cinnamic acid group to form two single bonds and give a cyclobutane derivative [Fig

2.11(a)]. The reaction has been very well studied in the solid state where it occurs as a

topochemical reaction when the distance between the reactive ethene groups is $\approx$3.6Å. [97]

Films of **4** showed no distinct birefringence and SAXS did not show evidence for layer

packing of the rodcoil molecules. Cast films were irradiated at room temperature for 1 hour

and 24 hours at 300nm. Only the sample irradiated for 24 hours showed any crosslinking

which was evidenced by the small shoulder observed in the GPC trace [Fig 2.12].

Presumably this shoulder corresponds to dimeric molecules and other higher oligomers. POM

of the films after irradiation did show more birefringent regions than before irradiation but it

was not homogeneous throughout the sample. Samples were also irradiated at higher

temperature, 190°C for 24 hours which resulted in almost no reaction at all as evidenced by

GPC. Therefore, the molecule may not have been in the correct orientation for cinnamic acid

dimerization at these higher temperatures where there was likely much more molecular

motion which prevented topochemical reaction.

2.2.2.2 Anthracene Derivative (5)

Photodimerization of anthracene has been widely investigated since the first published

study done in 1876.[92, 93, 98-103] Anthracene dimerizes via a singlet arene excimer when

irradiated at 366 nm and this reaction is reversible both thermally and by irradiation with

higher energy radiation (254 nm) [see Fig 2.11(b)]. Anthracene substituted at the 9-

Scheme 4

3

refluxing CH₂Cl₂
pyridine/DMAP

4a

4

3

refluxing CH₂Cl₂
pyridine/DMAP

5a

5
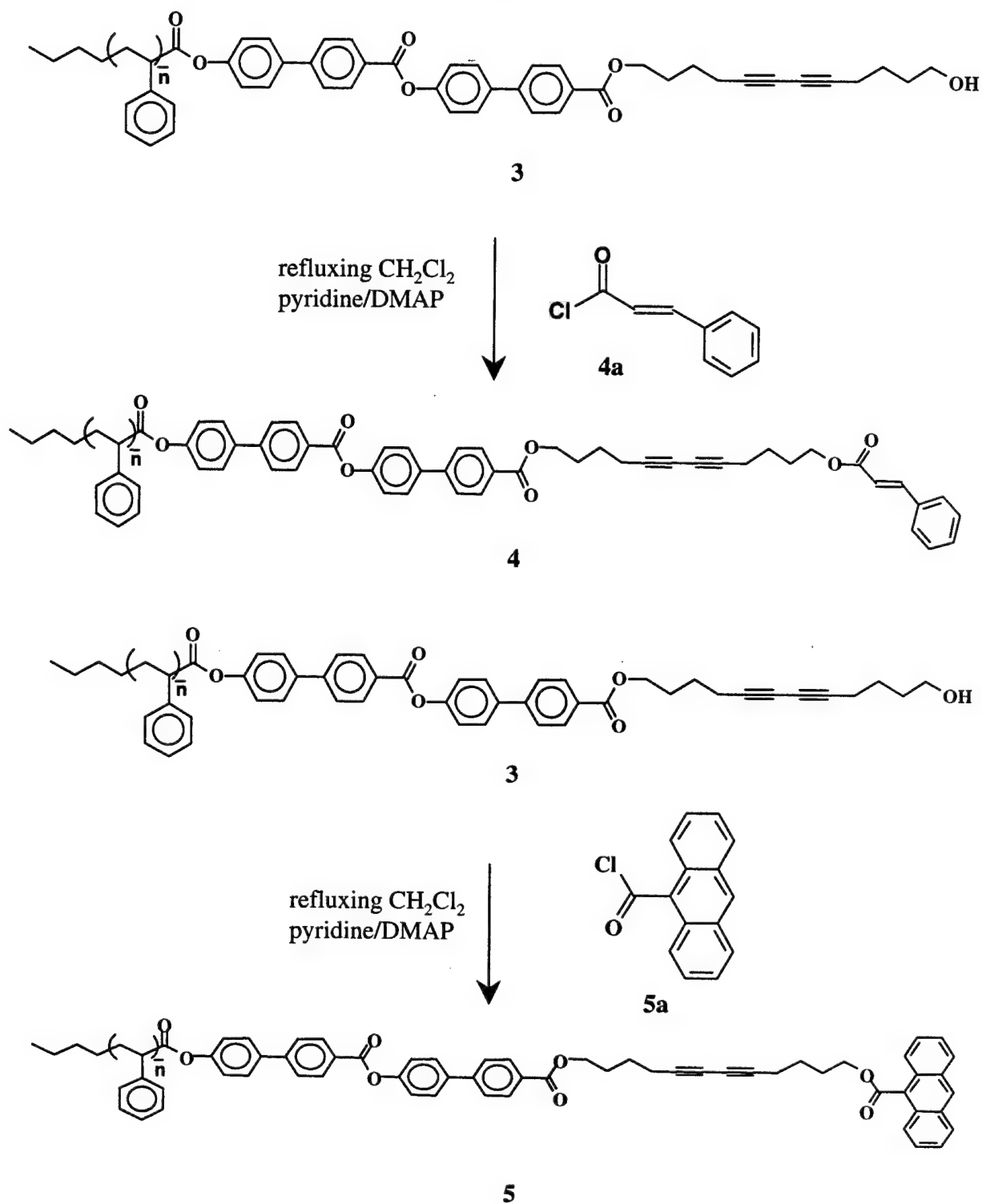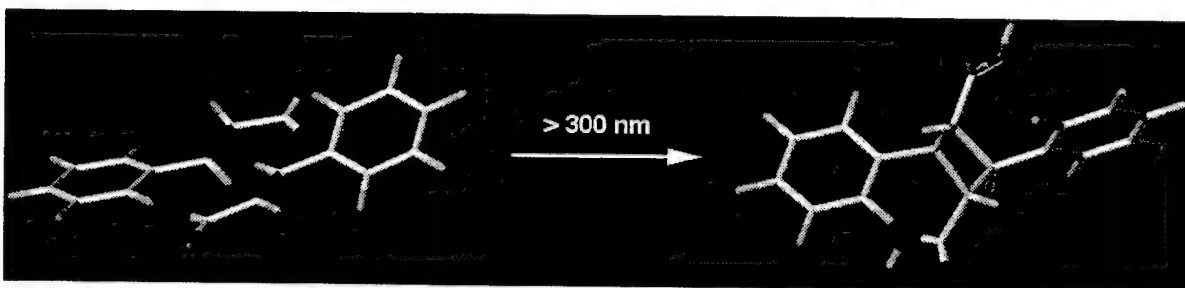
(a) Cinnamic acid photodimerization
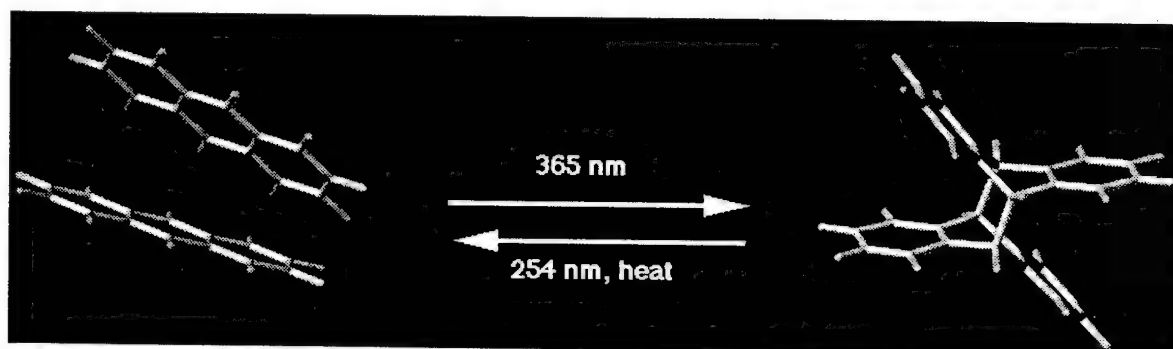
(b) Anthracene photodimerization

Figure 2.11 Photochemical crosslinking reactions of cinnamic acid and anthracene

Figure 2.12 Gel Permeation Chromatography trace of **4** after irradiation for 24 hours at >300 nm

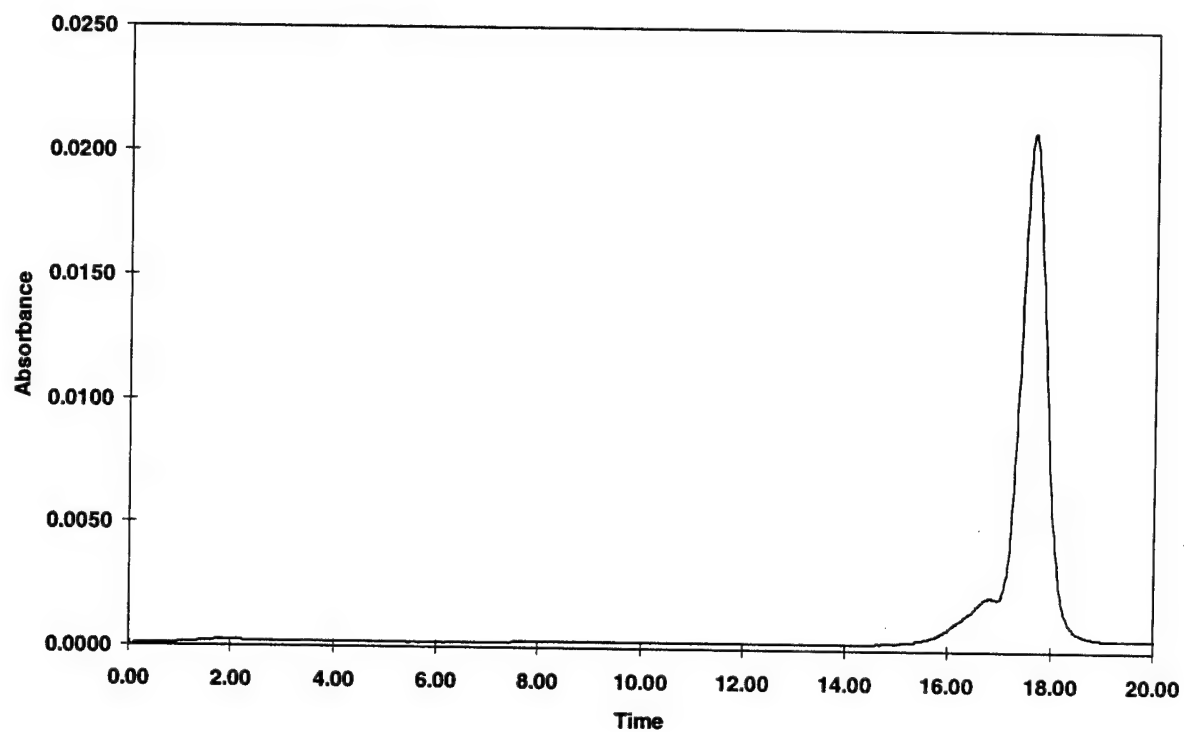position also undergoes photodimerization but now two constitutional isomers can be formed; a head-to-head dimer and a head-to-tail dimer, as shown in Figure 2.13. In almost all cases, the head-to-tail dimer is the only species detected upon photodimerization of 9-substituted anthracene. This is believed to be mainly due to electronic effects. Bouas-Laurent has observed head-to-head photodimers in solution and has isolated head-to-head dimers that were formed from a solution containing both 9-methoxy- and 9-cyanoanthracenes. These molecules formed the

mixed head-to-head dimer in high yields with the other products being the two respective homodimers. [94, 104] Films of **5** showed faint amounts of birefringence under crossed-polars but no distinct textures were seen as is the case with **3** and all of its derivatives. SAXS showed no evidence for the formation of layers.

Attempts to photocrosslink **5** with 366 nm radiation were successful in creating dimers from this material. Higher temperatures (200°C) and 254 nm radiation were tried to determine if diacetylene polymerization could be induced (note that anthracene dimerization is reversed under these conditions) but no high molecular weight material was detected. A GPC trace of the material resulting from the irradiation at 366 nm is shown in Fig 2.14. Thus it would appear that irradiation at 366 nm successfully led to dimerization of the anthracene group but no diacetylene reaction occurred. The success of the anthracene group in dimerizing at the terminus of a rodcoil molecule was encouraging and became the motivation to study the reactive liquid crystalline molecules discussed in Chapter 3.

2.2.3 Changing the Cross Sectional Area of the Coil

To further investigate the effect of the hard core repulsions of the coil, a bulkier coil of

44

(a) Head to Head Isomer

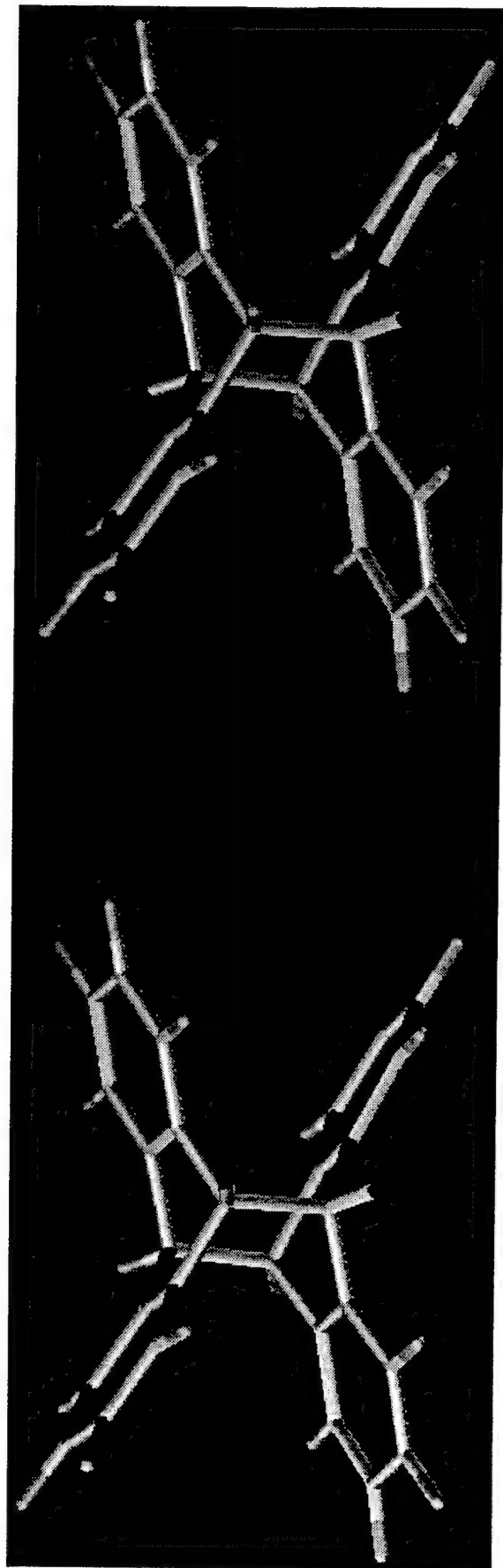(b) Head to Tail Isomer

Figure 2.13 The two constitutional isomers of the 9-substituted anthracene photodimer (a) head-to-head (b) head-to-tail
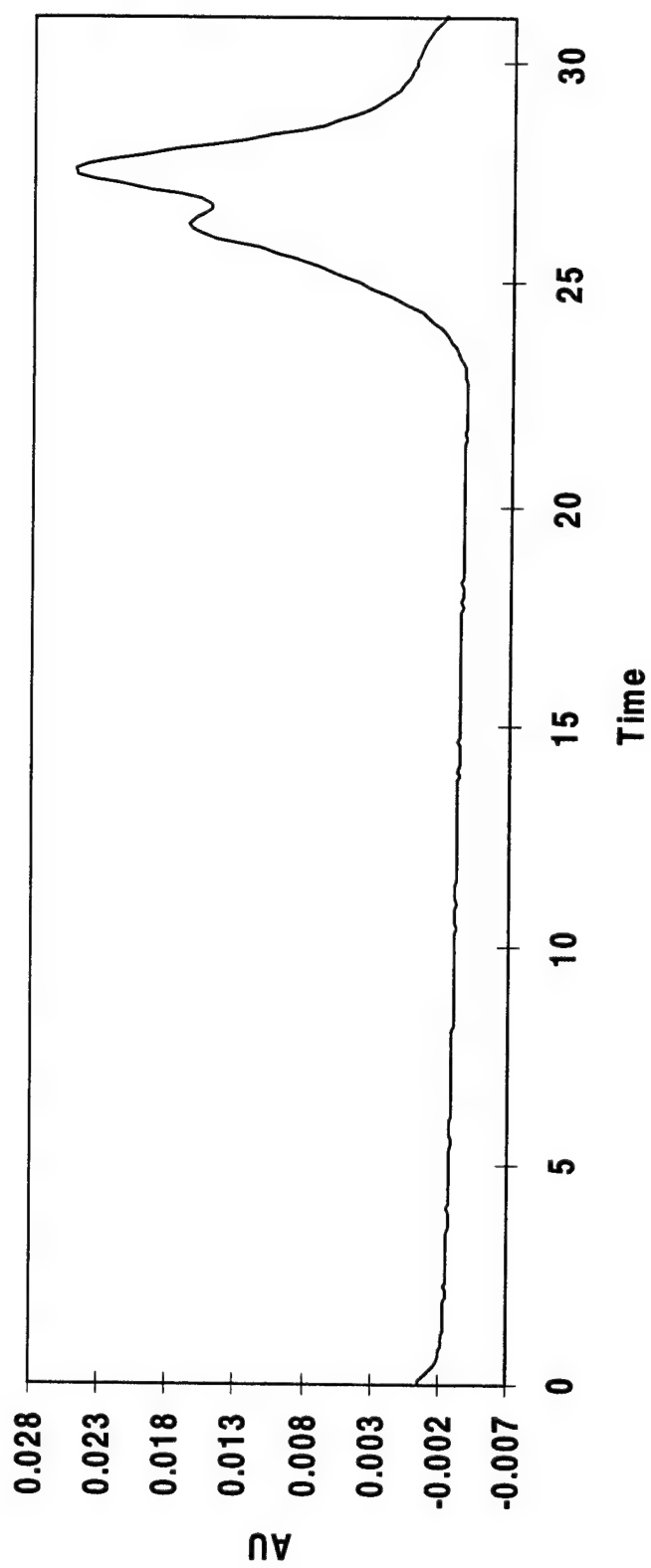
Figure 2.14 Gel Permeation Chromatography trace of **5** after irradiation at room temperature

t-butyl styrene was attached to the same two biphenyl rod segment used in **3**. This new material, **6**, had a coil whose $M_n = 2047$ by FD. After subtracting for the end groups, this is equivalent to an average degree of polymerization of 12. Using optical microscopy and SAXS no evidence could be obtained for smectic-like layering of molecules. TEM of the material revealed that it formed an amorphous film that gave no crystal E diffraction as observed in **3**. One explanation may be that the rods could not aggregate at all because of the highly disruptive nature of the greater cross sectional area of the oligo(t-butyl styrene). To help illustrate this, a molecular simulation was run on 13 molecule aggregates of both **3** and **6**. The rod segments of both rodcoil molecules are identical so the first step was to construct a 13 member rod aggregate placing rods on an orthorhombic lattice with parameters determined from both electron and X-ray diffraction. This aggregate of rods was then minimized. Thirteen coil aggregates of **3a** and **6a** (with ten monomer units per coil) were then minimized separately and covalently attached to the rods in the orthorhombic lattice and the whole assembly minimized to convergence. Figure 2.15 shows the minimized aggregates and the calculated volumes of the two different coil segments (shown in yellow on the figure). The volume of the oligo(t-butyl styrene) was 1.7 times greater than the oligo(styrene) and thus it seems possible that the bulkier oligo(t-butyl styrene) coil would hinder formation of layers. Another explanation for the lack of nanophase separation in the case of **6** may be a kinetic one. The T_g of poly(styrene) is 100°C while the T_g of poly(t-butylstyrene) is 130°C.[105] Thus, solvent-cast films of **6** may not relax as rapidly as **3** and this may explain the lack of nanomorphology seen in TEM samples.

Attempts to lessen the effect of the coil on the crystallization of the rods were made with **7**, the last material synthesized in this homologous series of styrene derivatives. A
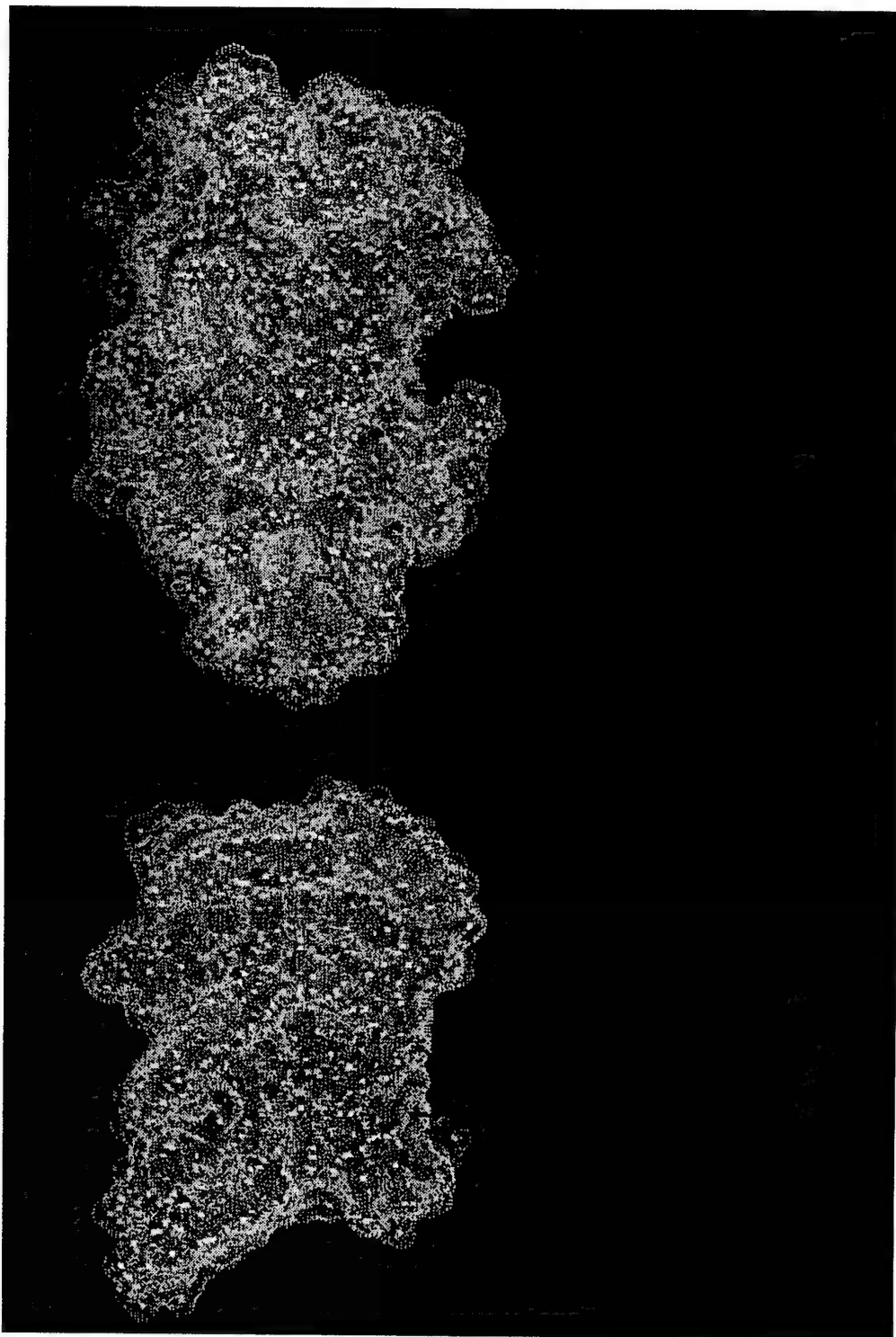
Figure 2.15 Representation of aggregates containing 13 rodcoil molecules with rod segments on identical, fixed orthorhombic lattices (Cerius^2). Coil length is ten repeat units for all coils (a) **3,** total coil volume = 19,000 Å^3 (b) **6,** total coil volume = 32,000 Å^3

segment of oligo(butadiene) was added to oligo(styryl) to form a diblock coil using typical anionic polymerization techniques.[106] Characterization of the coil by proton NMR indicated a high percentage of 1,2 addition vs. 1,4 addition of the butadiene due to the presence of tetrahydrofuran (a polar solvent) in the reaction solvent system. A solvent system of benzene:THF in the volume ratio 3:1 was used to help break up the anion-cation pair leading to more efficient carboxylation of the coils.[107, 108] The average number of repeat units of styrene was approximately 10 and the number of oligo(butadiene) units was approximately five by NMR analysis. While POM did not reveal a substantial increase in the birefringence of the material, SAXS did show a broad peak at large d-spacing $\approx 70\text{Å}$, after the film was annealed to 160°C in N_2 and then slowly cooled [Fig 2.16]. It is presumed that the oligo(butadiene) segments did not react because of the mild temperatures and lack of O_2 while annealing. SAXS of the unannealed sample showed no diffraction. The extended length of a representative rodcoil with 10 repeat units of styrene, and 5 repeat units of butadiene in its fully stretched conformation is 74Å as determined in the molecular graphics program SYBYL. Thus the x-ray peak corresponding to a d-spacing of 70Å is very likely due to layers of the extended rod coil. Electron diffraction did not indicate any ordering within the layer nor did TEM show a superlattice of uniform supramolecular aggregates. Therefore the oligo(butadiene) spacer did allow **7** to form layers after thermal annealing, whereas **3** could not. TEM confirmed that the material formed a homogeneous film which may indicate the formation of S_A or S_C infinite layers rather than the nanostructures that were formed in films of **1** and the nanoaggregates formed in films of **2** and **3**.
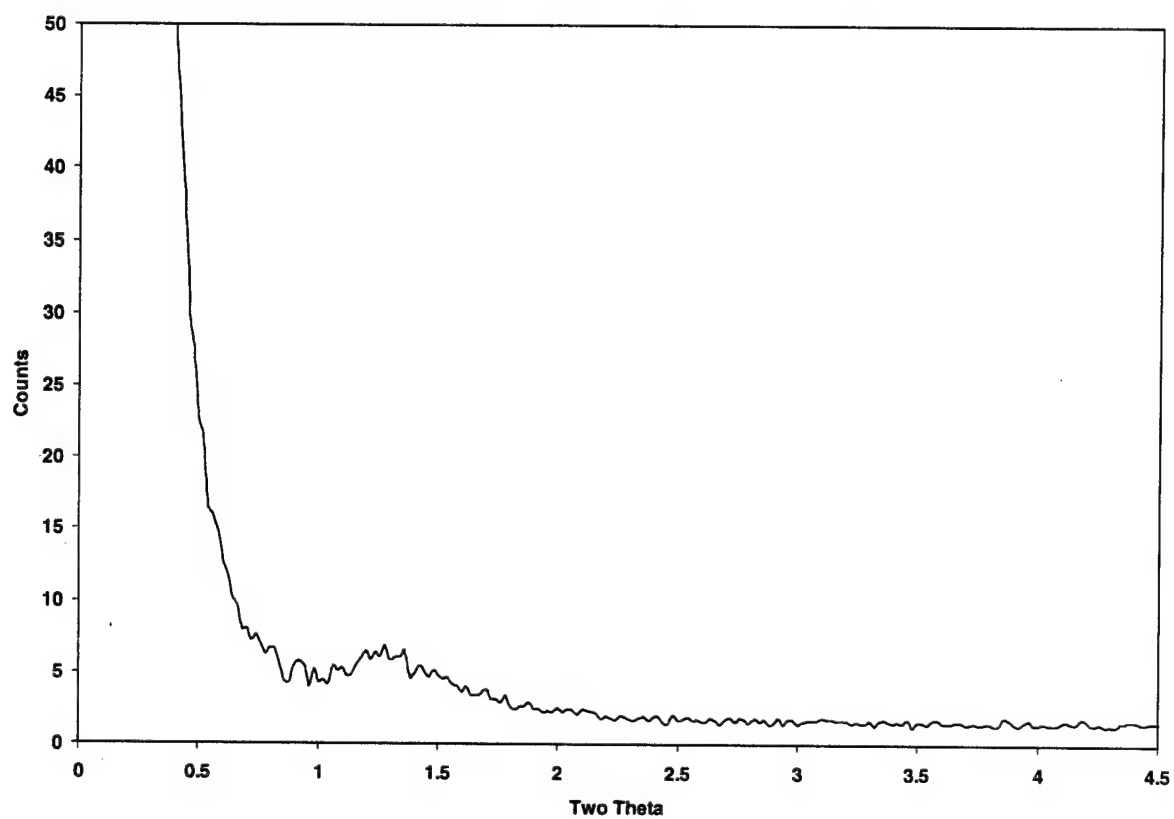
2.3 Conclusions

Figure 2.16 SAXS of **7** after annealing at 160°C and slow cooling to room temperature

In conclusion, rodcoil molecules containing an oligo(styrene) coil and a reactive mesogenic rod segment showed an interesting array of abilities to form nanodomains in the solid state. Characterization of these materials is greatly helped by the use of FD and MALDI mass spectrometry that allows one to observe the entire distribution of rodcoil molecules. Nanophase separation in these materials could be completely hindered by changing the oligo(styrene) coil to the much bulkier oligo(t-butyl styrene) coil. Adding an oligo(butadiene) spacer segment to the oligo (styrene) coil helped the formation of layers as detected by SAXS. Addition of a photocrosslinkable end group to the end of the rod allowed the formation of dimers among rodcoil molecules and was the motivation to continue work with anthracene as a crosslinking agent. None of the molecules investigated revealed long range order. However, evidence was found for the existence of ordered nanosized aggregates that in turn exhibited short range order. Thus, investigation of lower molar mass chemical compounds similar to the reactive rodcoils was undertaken to understand further self-assembly in the organic solid state.

Chapter 3 Reactive liquid crystals

3.1 Introduction

As discussed in Chapter 1, liquid crystalline molecules are very useful in the design of self assembling systems because of their ability to form various anisotropic phases over a variety of temperature ranges (thermotropic liquid crystals) or mixed with a solvent in various concentrations (lyotropic liquid crystals). The ability to form layered structures, some with degrees of order similar to crystals, makes liquid crystals a useful tool for the synthesis of self assembling organic molecules. These layered structures are free standing in that they do not require a specially treated support, interface, or surface to form a two-dimensional layered structure. By changing the temperature, in the case of thermotropic liquid crystals, these materials can also experience polymorphism forming less ordered phases upon heating and more ordered phases upon cooling. Thus, a liquid crystalline material is usually not locked into only one type of architecture, but potentially has many. How liquid crystals transform to different mesophase, and the make-up of these mesophases is important for understanding their use in self assembling systems. The primary interest of this chapter will be the study and characterization of thermotropic liquid crystals containing reactive groups that can undergo a crosslinking reaction for the purpose of forming ordered two-dimensional structures. It is important to know the relative position, orientation, and location of adjacent molecules before attempting to crosslink any type of ordered system. Thus it is necessary to understand the mesomorphic behavior of the reactive liquid crystals in detail. Before discussing the specific molecules of this study, it is appropriate to review some of what is known about liquid crystals.

In general, liquid crystals are materials that have order to a degree intermediate

between a three-dimensional crystal and an isotropic liquid. Commonly, these materials will flow and have anisotropic properties. An interesting historical footnote is that one of the first written accounts of an anisotropic fluid is from 1837, not from a scientific journal, but rather from the pen of Edgar Allen Poe! [109, 110] The first work on liquid crystals was done during the latter half of the 19th century on lyotropic liquid crystals. Virchow described the birefringent properties of myelin in water in 1854, which would make the phospholipids of the myelin sheath the first reported liquid crystals.[111] In 1888, Reinitzer gave a detailed description of the iridescent colors produced by a material which "…has two melting points, if it can be expressed in such a manner."[112] This material was a cholesteryl ester, a thermotropic liquid crystal, from which the cholesteric phase gets its name. Another important scientist in the early history of liquid crystals was Otto Lehmann, an expert in the field of crystallization microscopy during this period. His expertise made him an important collaborator of Reinitzer and others in the early investigations of the optical properties of liquid crystals. Lehmann authored the first monograph on liquid crystals in 1904 and he is credited with being the creator of the term "liquid crystal".[113, 114]

3.2 Molecular Architecture of Liquid Crystals

The generic structure of a thermotropic liquid crystal (remaining discussion will now focus on thermotropic liquid crystals so the designation thermotropic will be dropped) is that of a long, rigid rod terminated by various alkyl groups depicted as X and Y in the drawing below.[115, 116]
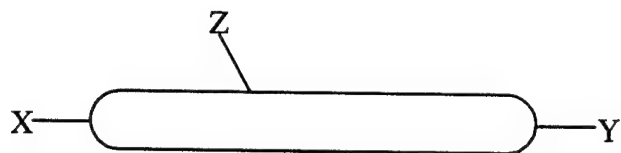
The rigid, central core of the molecule is commonly made up of linked aromatic rings, due to their rigidity, but any fairly linear molecule with sufficient stiffness will serve the same purpose. Experimentally it has been found that a length to width ratio $\geq$ 4-6 is required for the formation of a nematic phase. Theoretically, Onsager described liquid crystals as a fluid of hard rods with the only forces between them being that they could not interpenetrate.[117, 118] At low densities, these hard rods can take on any orientation and the fluid remains isotropic. But as the density of rods in the fluid is increased, excluded volume interactions become important and the rods tend to align in a uniaxial fashion. While this is just one explanation for the formation of the nematic phase, it is the theory most often cited. Lateral substitutions on the core, Z, tend to depress the temperature ranges of the liquid crystalline mesophases, while terminal groups X, and Y, that increase the length of the molecule without increasing the width tend to stabilize the mesophases of the molecule. Another type of molecular architecture that exhibits liquid crystalline behavior is disc-shaped molecules with relatively flat cores and four to six radial substituents that extend from the center in a star shape. These molecules tend to align with the plane of the flat cores parallel to one another. These 'discotic' liquid crystals were discovered in 1977 and a typical structure is shown below.[119]

$$R = \quad \text{—} \quad O(CH_2)_nCH_3$$
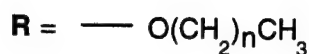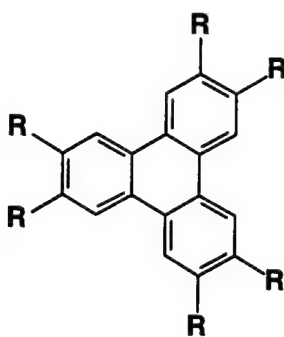
3.3 Classification

Traditionally, thermotropic liquid crystals have been divided into three major classes, nematic, cholesteric, and smectic.[120] While this classification system is still valid, refinements in the classifications can be made based on structural information provided by x-ray and neutron scattering experiments. This refined classification system, as described by Leadbetter, is illustrated in Table 1.[121] Many of the previously called "smectic" phases, such as S_E, S_H, are now referred to as disordered crystal phases (others have suggested the term smectic crystal phases[122]). This is based on the results of scattering experiments that show these phases have long range positional order of the molecules in three dimensions, and thus are better described as crystals, but they have molecular orientation disorder, and so are called disordered crystals. Phases with order less than a disordered crystal but greater than an isotropic liquid are called liquid crystals, and include the familiar nematic, cholesteric, smectic A (S_A), and smectic C (S_C) mesophases.

| Ordered Crystal	Disordered Crystal	Liquid Crystal		Nematic	Isotropic Liquid
	Layer Structure	Smectic		Nematic	
	Cubic **D**	Weakly ordered layers, two dimensional	One dimensional density wave		
k	Orthogonal **E** **B**	$S_B{}^h$	S_A	**n** **n*** (cholesteric)	**i**
	Tilted **H** **G** **K** **J**	S_F S_I	S_C		

Decreasing Order →

Table 3.1 Structural classification of lath-like, thermotropic liquid crystals. From *Thermotropic Liquid Crystals*, G.W. Gray, ed. Copyright Joh Wiley & Sons Limited. Reproduced with permission.

3.3.1 Nematics and Cholesteric Phases

The nematic mesophase is the most commonly found liquid crystalline phase. It is an anisotropic fluid with no positional order, but with orientational order of the long axes of the molecule along a director, **n** [123, 124][Fig 3.1(a)]. The cholesteric mesophase, also called the chiral nematic or twisted nematic mesophase, has a helical twist of the liquid crystal director as one move perpendicular to the director [Fig 3.1(b)]. A given plane in Fig 3.1(b) is ordered as a nematic phase, but above and below, the directors of the nematic phases are slightly rotated. The depiction of "layers" in Figure 3.1(b) is only intended to show a rotation of the director and does not imply that the cholesteric phase is layered. The pitch of this helix is often on the order of the wavelength of visible light leading to Bragg scattering of incident white light producing the iridescent color effects for which this phase is known. Because of the similarities between the two phases, the cholesteric phase is included in Table 1 under the nematic phase. Another chiral phase related to the nematic and cholesteric is the blue phase that gets its name from its distinct color when viewed in reflective mode optical microscopy.[122] This phase exists in a very narrow temperature range (< 0.5 °C) between the cholesteric phase and the isotropic liquid that has made it difficult to study. There are believed to be three such phases although their structure has not been definitively solved [121, 122].

3.3.2 Smectics Based on a One-Dimensional Density Wave

The S_A and S_C phases (depicted in Fig 3.2) have long range orientational order of their long axis along a director like the nematic phase. They are also characterized by
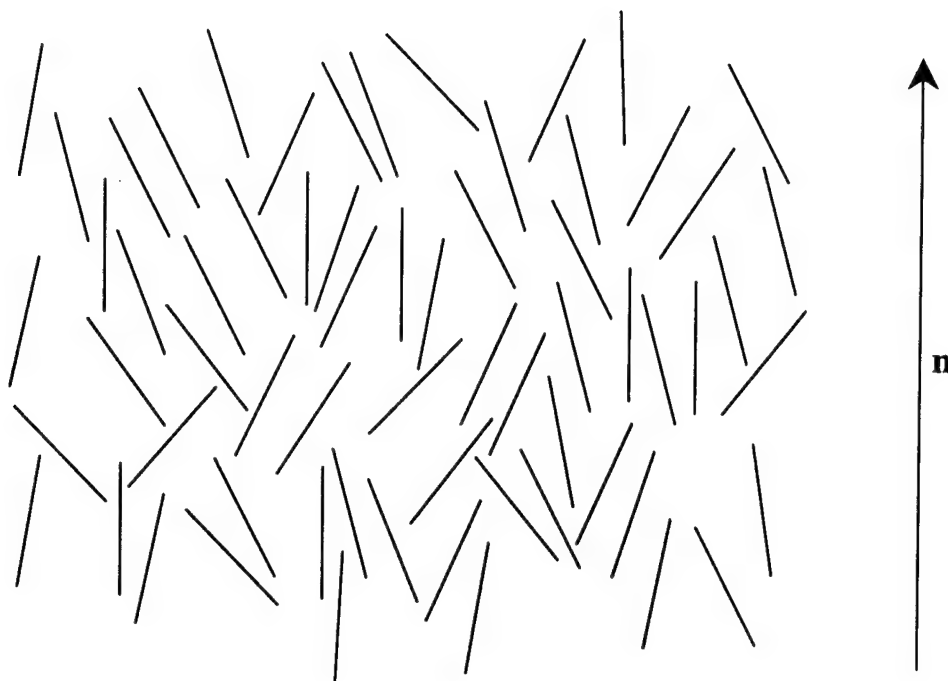
a) nematic mesophase with director n

Pitch
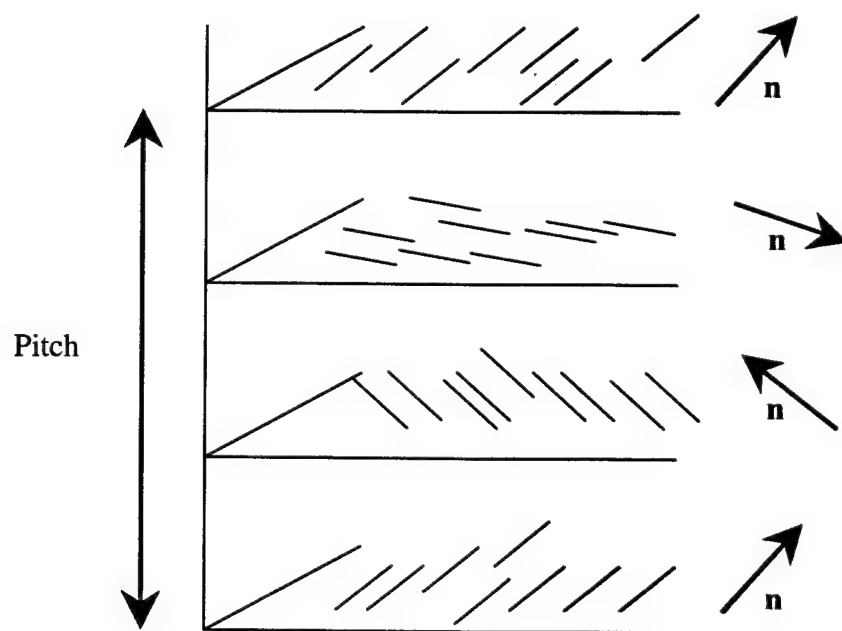
b) cholesteric mesophase

Figure 3.1 Schematics of the (a) nematic and (b) cholesteric mesophase
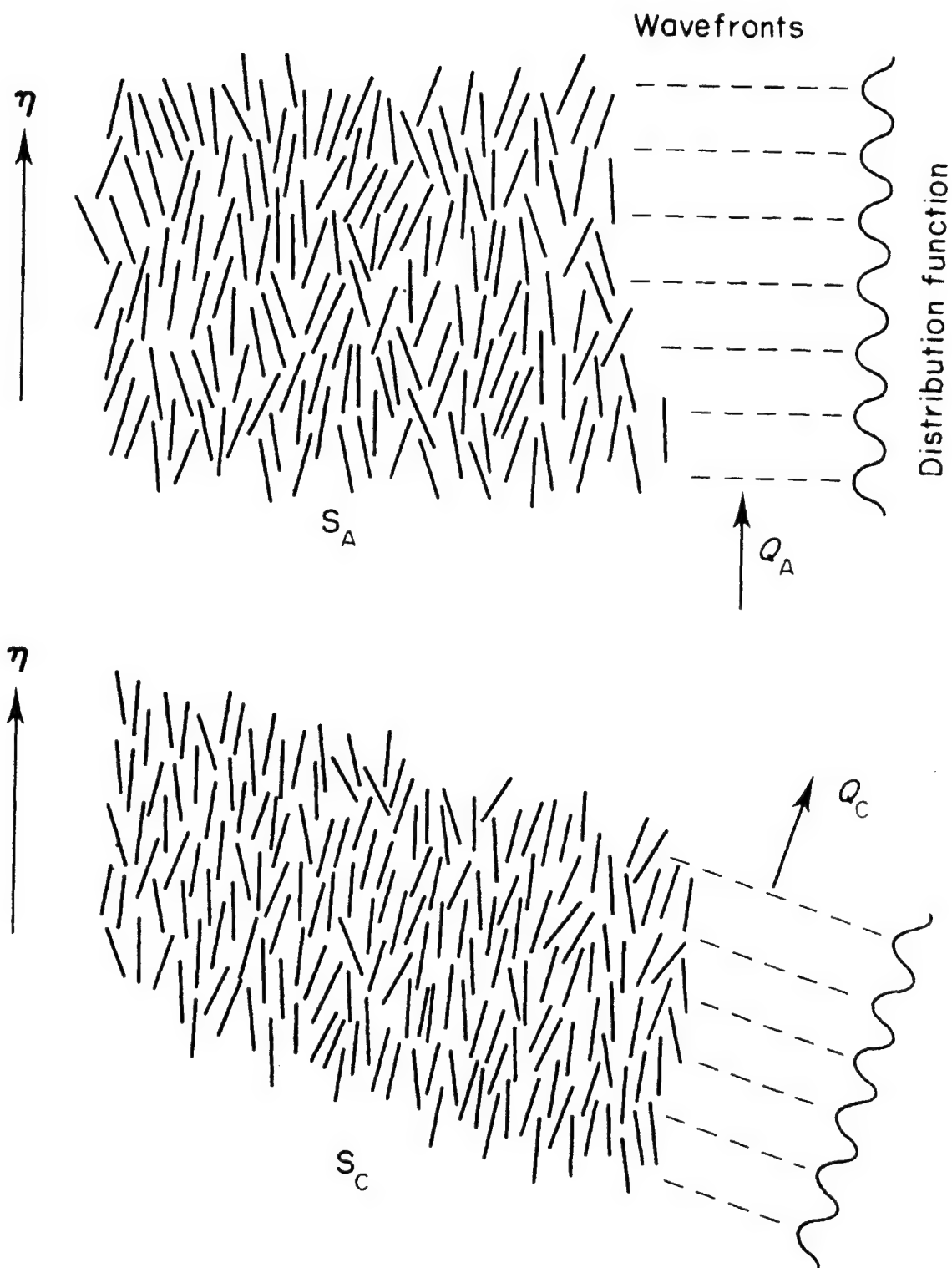
Figure 3.2 Representations of the S_A and S_C mesophases. From *Thermotropic Liquid Crystals*, G.W. Gray, ed. Copyright John Wiley & Sons Limited. Reproduced with permission

one-dimensional density waves parallel to the director (for S_A) and at a small angle to the director (for S_C), although there is no positional correlation between molecules within the layer. Commonly, these phases are depicted as stacks of finite, two-dimensional layers, when in fact, the density wave is sinusoidal and thus the layers should be thought of as being very diffuse.[121, 122] The single layer S_{A1} and S_{C1} were the first phases found but subsequently, other variations have been found and their nomenclature is listed below.[125-129]

S_{A1} and S_{C1}	normal one dimensional density wave with random head to tail orientation
S_{A2} and S_{C2}	bilayer packing with antiferroelectric ordering
S_{Ad} and S_{Cd}	interdigitated bilayer packing
S_A and S_C	"antiphase", modulated antiferroelectric ordering within the layer

3.3.3 Weakly Ordered Two Dimensional Smectics

These three mesophases, S_B^h, S_F, and S_I, are characterized by positional long range order within the layer one order of magnitude greater than the S_A and S_C phases. Order within the S_B^h layer is hexagonal, while the phases S_F, and S_I are quasi-hexagonal due to the tilt of the mesogens [Fig 3.3]. What is interesting about these phases is that they contain long range, bond orientation in three dimensions.[121, 122] Bond orientation has nothing to do with orientation of chemical bonds, rather, the 'bond' refers to a vector that joins two nearest-neighbors in the lattice. Figure 3.4 illustrates three situations with various degrees of positional order and bond orientational order. Figure 3.4(b) illustrates the current understanding of these two dimensional, hexatic phases that have long range bond
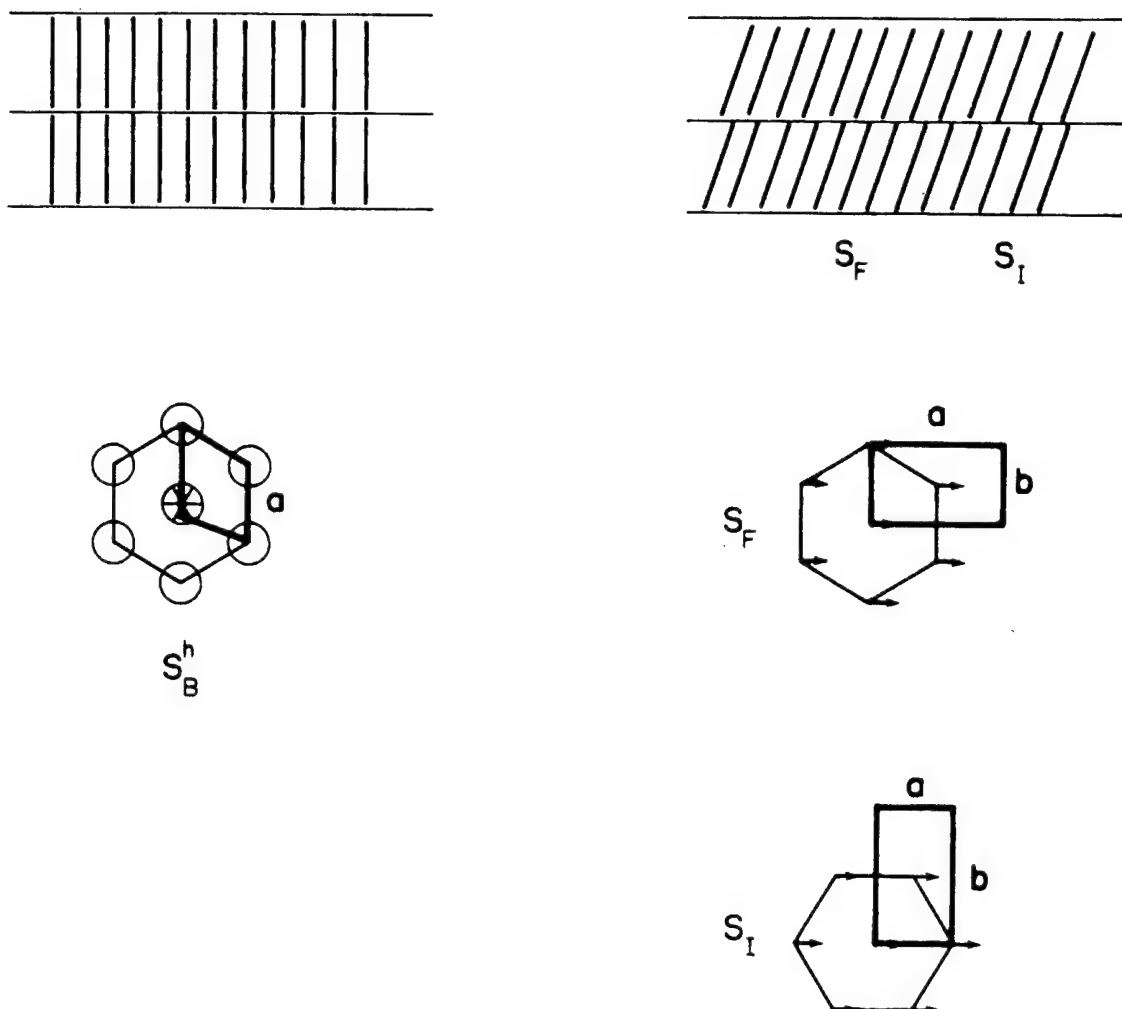
Figure 3.3 Short range order within the layers of $S_B{}^h$, S_F, and S_I mesophases. From *Thermotropic Liquid Crystals*, G.W. Gray, ed. Copyright John Wiley & Sons Limited. Reproduced with permission

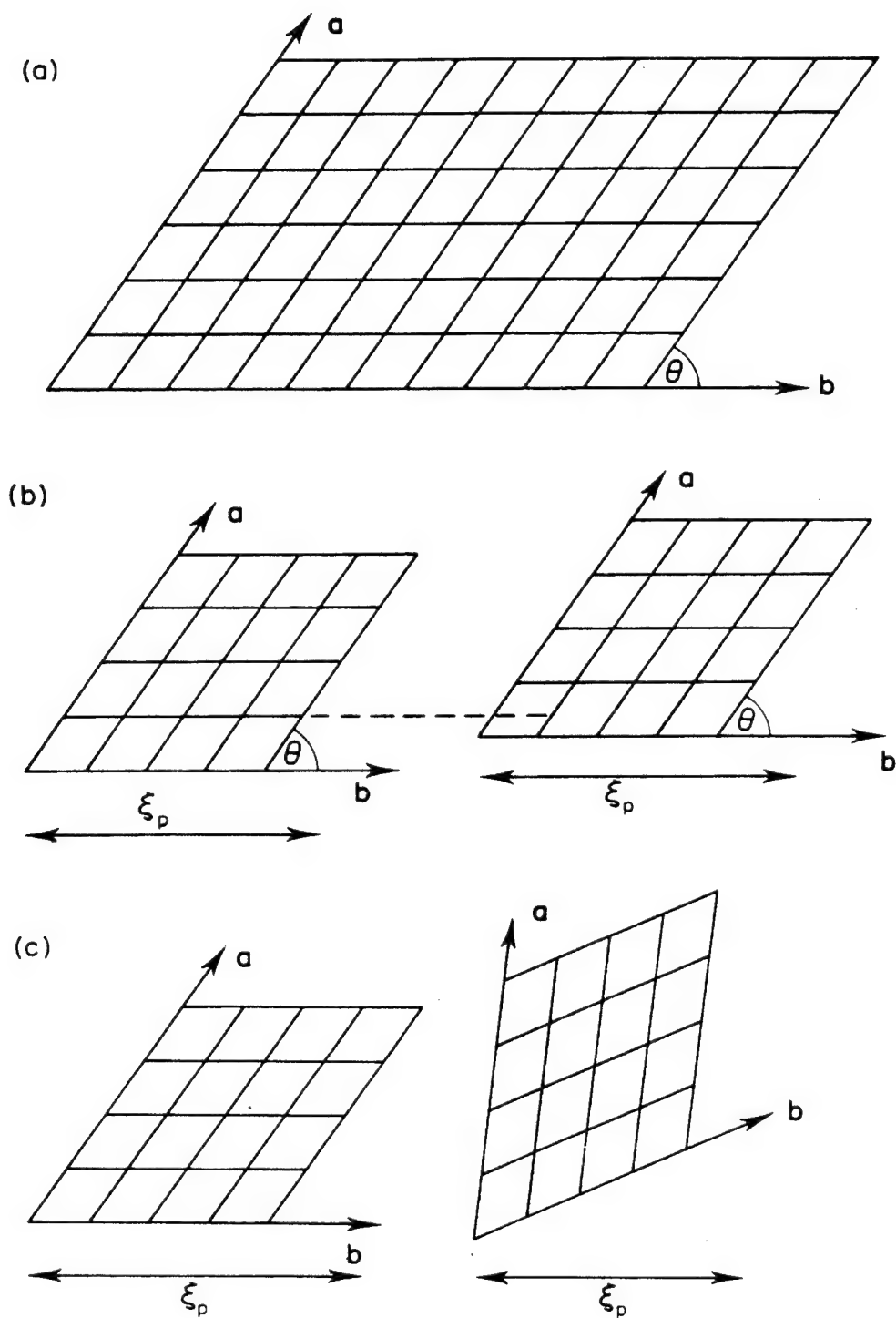**Figure 3.4** Different degrees of positional and bond orientational order. (a) long range bond orientational order and positional order; (b) long range bond orientational order; short range positional order; (c) short range bond orientational order; short range positional order. From *Thermotropic Liquid Crystals*, G.W. Gray, ed. Copyright John Wiley & Sons Limited. Reproduced with permission

orientational order in three dimensions, but only short range positional order within the layer.

3.3.4 Disordered Crystals

There are six general classes of disordered crystal phases known that are listed in Table 1 and whose structure is detailed in Fig 3.5. All of these structures have long range positional order in three dimensions, making them true crystals, although there is considerable orientational disorder of the molecules. Phases B, G, and J are based on the hexatic S_B^h, S_F, and S_I phases, respectively, gaining long range positional order in three dimensions. The E, H, and K phases are formed from the loss of free translational rotation in the B, G, and J phases, respectively which leads to the herringbone packing shown in Figure 3.5. This loss of translational freedom in the E, H, and K phases is not complete as neutron scattering studies have shown that there are still cooperative rotations of $< 180°C$ about the long axis of the molecule.[130]

3.3.5 Chiral Smectic Phases

Similar to the case of the cholesteric phase, incorporation of chiral molecules into a tilted smectic layer will lead to a phase that undergoes a macroscopic helical twist of the molecule's director on moving perpendicular to the planes.[123]
The S_C, S_F, and S_I phases, form this helix and show ferroelectric and optically active properties.[131] Helix formation in the disordered crystal phases, G, H, J, K, does not occur because of the long range positional order in the material.[132-134]
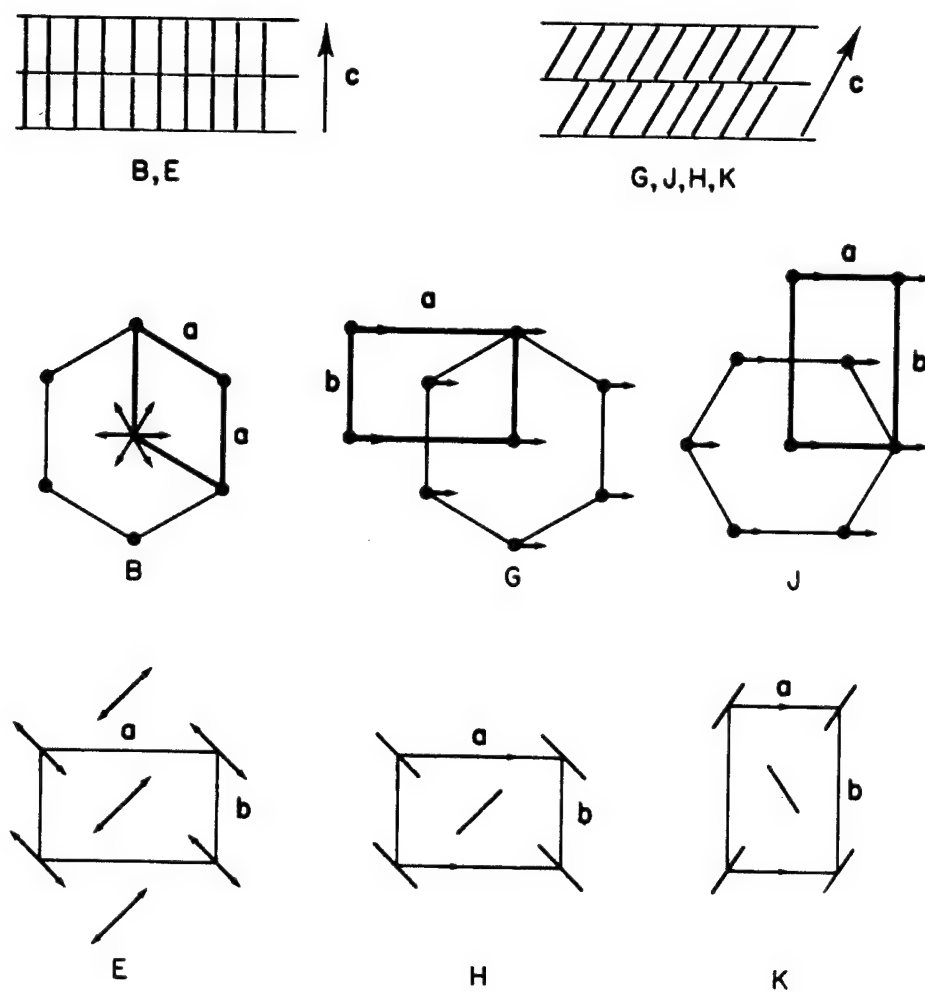
Figure 3.5 Order within the layers of the disordered crystal phases B, G, J, E, H, K. From *Thermotropic Liquid Crystals*, G.W. Gray, ed. Copyright John Wiley & Sons Limited. Reproduced with permission

3.3.6 Cubic phase

This phase has been found in only a few molecules but single domain x-ray studies has shown it to have long range positional order.[121, 122] The phase is optically isotropic and seems to be related to the S_C phase although the exact structure has yet to be elucidated.

The above discussion has detailed the structures of many of the known thermotropic liquid crystal phases. These descriptions will be useful in the following sections where the reactive liquid crystals in this study are found to have many phases beyond the more commonly known nematic and S_A mesophases.

3.4 Design of Reactive Liquid Crystals

The molecular structure of the liquid crystals (**8-11**) studied in this work are shown below:
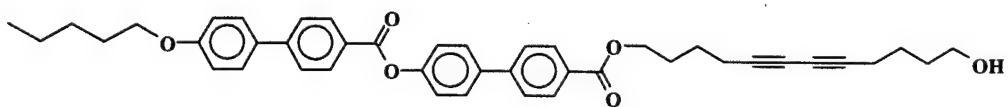
8
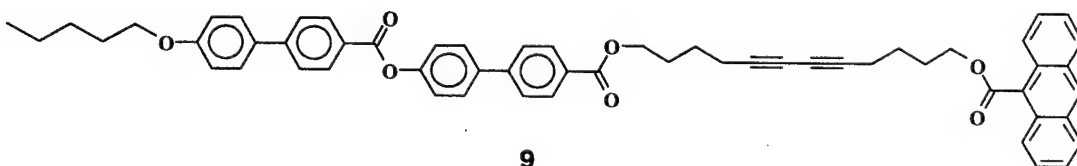
9

10

11

Molecule **8** has been studied in detail by others in the Stupp group and is shown here for comparative purposes while **9-11** are new ones synthesized by the author.[78, 79, 135] When in the crystalline state, **8** will react spontaneously under room light forming an insoluble blue solid (further work with this material will be described in Chapter 5). Molecule **9** was synthesized to investigate the ability of the anthracene group to act as a crossl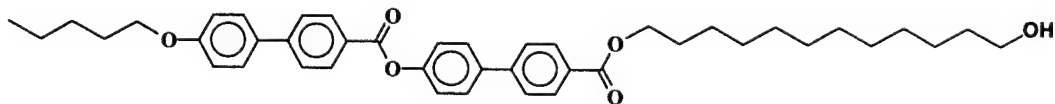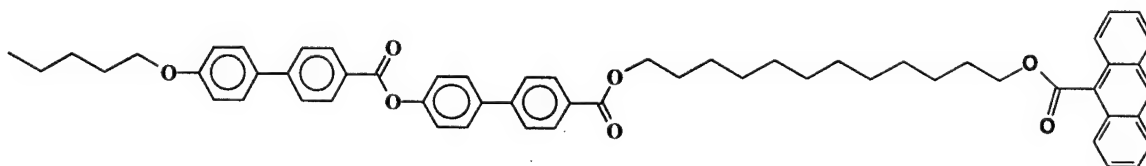inker in liquid crystalline materials. Because **9** proved to be a photoresist material (discussed in Chapter 4), the non-diacetylenic derivative, **11,** and its precursor **10** were synthesized to investigate the diacetylene's role in photoresist properties (Scheme 5). Molecules **10** and **11** also proved to have interesting liquid crystalline properties and are included in this chapter's discussion.

Inspection of molecules **9-11** reveals them to have many classic smectogen features. The rigid biphenyl groups linked by ester bonds and the terminal alkyl groups are all commonly seen in liquid crystals. One unique structural feature is the incorporation of a diacetylene group in **9** which makes for a more rigid alkyl segment that can also potentially react with adjacent diacetylene groups. Another unique structural feature is the placement of the anthracene group on the end of the molecule with its long axis perpendicular to the long axis of the existing mesogen. It was unknown how a group this large and rigid would affect the liquid crystalline properties when placed in this configuration. It should be noted that **8** is a thermotropic liquid crystal that forms a highly crystalline solid. It was hoped that placing the potentially disruptive terminal anthracene group on **8** (thus forming **9**) would lead to a mesogen that could undergo two "stitching" reactions--a diacetylene polymerization and a photodimerization of the anthracene at the end of the molecule. Earlier work by Stupp and Son illustrated the

Scheme 5
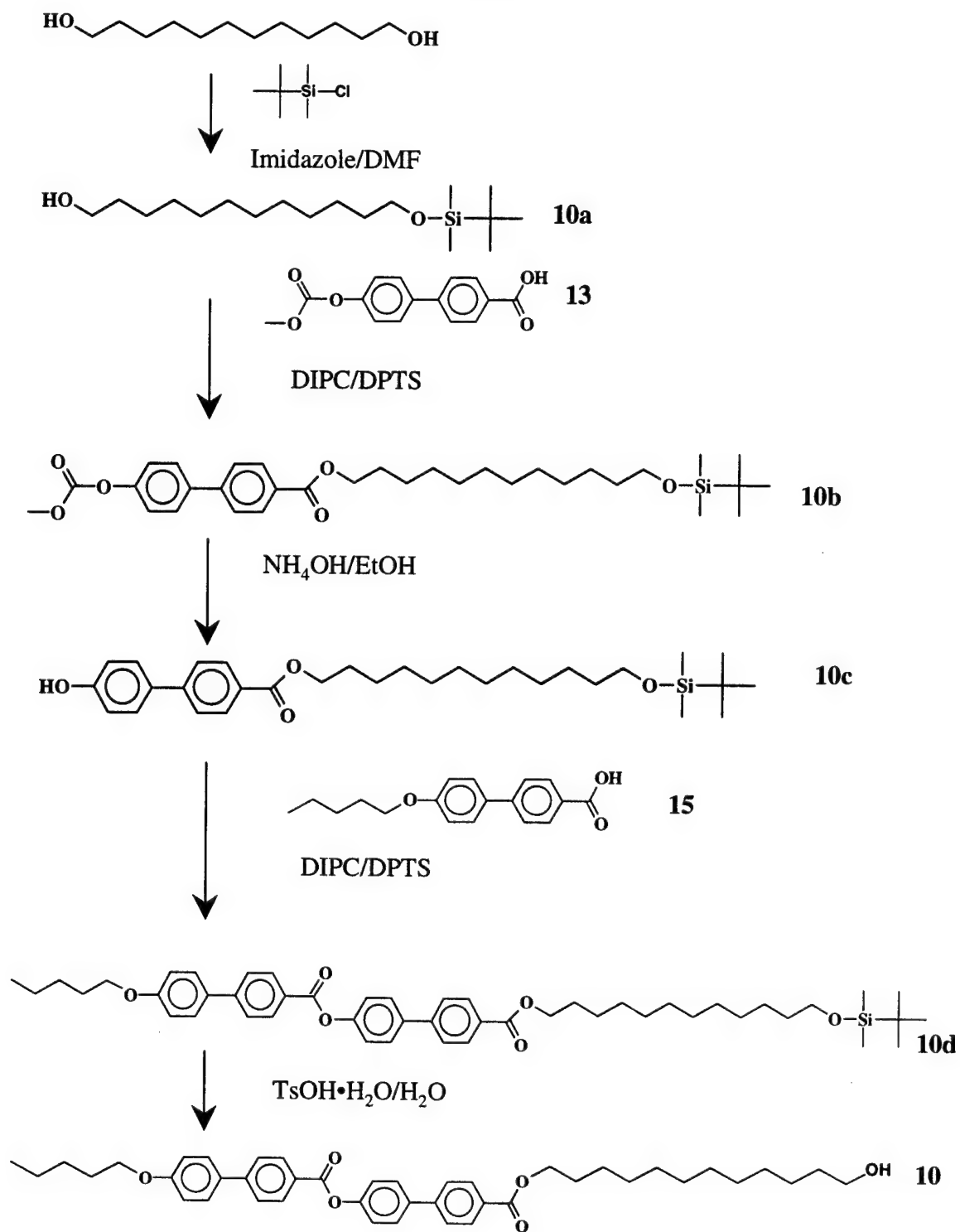
ability of a reactive liquid crystal molecule with two uncoupled reactive sites to form a two dimensional polymer.[70, 136] For this to occur with **9**, there are some important conditions that have to exist. First, the molecule would have to form an ordered layered structure with the reactive groups in the proper orientation and spacing to react with the adjacent mesogen. The formation of a layer with dimensions in the x and y direction much greater than the z direction is necessary for the formation of a two dimensional object. Secondly, the two reactive groups can not react in concert, but must react independently of one another. The various possible products formed by photochemical reaction of layers of **9** will be detailed in section Therefore, the formation of a two dimensional network using **9** will rely on a high degree of polymerization from the diacetylene groups.

3.4.1 Characterization of 9

Molecule **9** is a pale yellow solid that degrades over time if left exposed to room light. Based upon the evidence of POM, DSC, and X-ray diffraction, the following mesophase sequence is proposed for **9**:

$$g \ 15 \ E \ 111 \ S_B{}^h \ 128 \ S_{Ad} \ 205 \ n \ 213 \ i$$
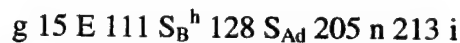
DSC results ([1st] cooling and [2nd] heating cycles at 5°/min) are shown in Fig 3.6 and reveal this material's mesophase behavior. There are four first order transitions and one second order transition which are listed in Table 3.2. Notice that the material does not form a true crystal at low temperature but instead undergoes a second order transition, or glass transition.

3.4.1.1 Variable Temperature X-ray diffraction

Perhaps the most powerful technique for the study of liquid crystal structure is variable temperature X-ray diffraction (which will be abbreviated VT SAXS for small
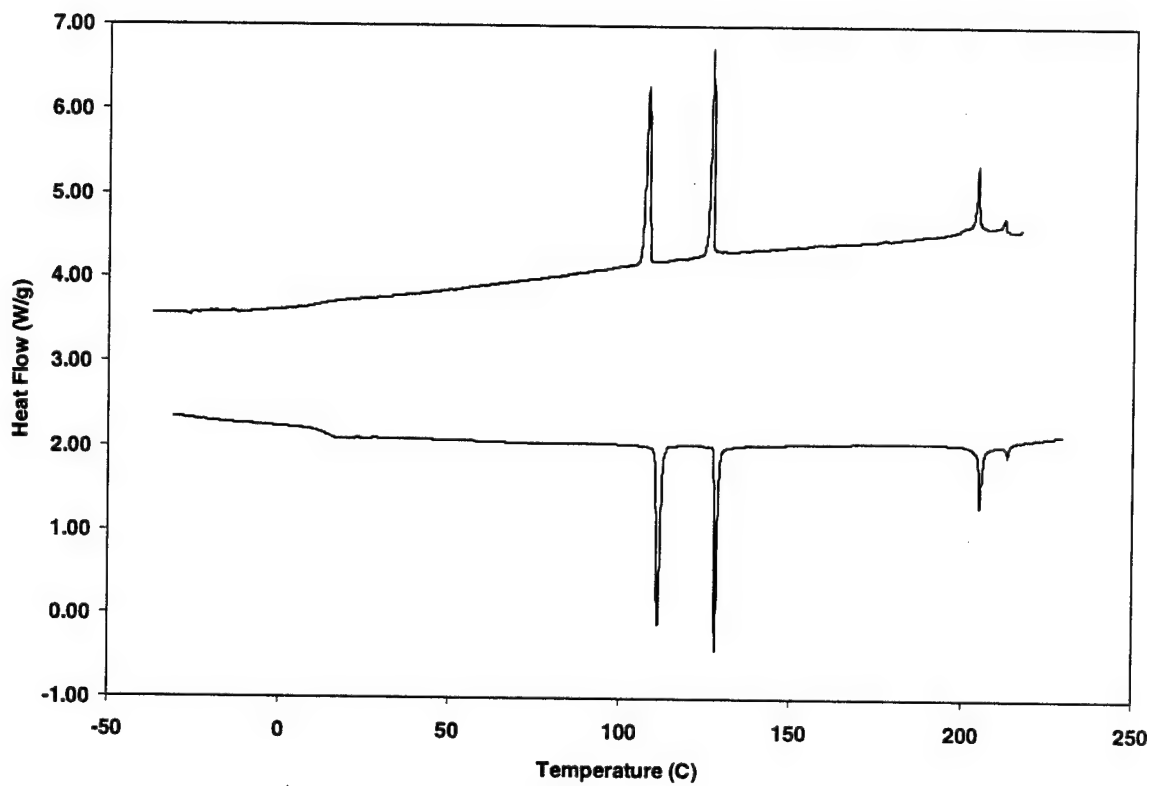
Figure 3.6 Differential Scanning Calorimetry scan of **9**. Top curve is 1st cool, bottom curve is 2nd heat; both done at 5°C/min

Table 3.2 Transition enthalpies of **9** determined by 2nd heating cycle (DSC)

Transition Temperature, °C	Phase Change	ΔH, kJ/mol
15	glass transition	---
111	$E \rightarrow S_B$	5.3
128	$S_B \rightarrow S_A$	4.0
205	$S_{Ad} \rightarrow n$	1.5
213	$n \rightarrow i$	0.2

angle measurements and VT WAXS for wide angle measurements). VT SAXS probes the

smectic layer thickness which can be used to differentiate between orthogonal and tilted

phases. The layer thickness of the tilted phases is usually less than the respective spacing of

the orthogonal phase and one can calculate the average tilt within the layer using the modeled

length of the liquid crystalline molecule. VT WAXS is valuable for determination of order

within the layers and allows easy differentiation, for example, between homeotropic $S_B{}^h$ and

S_A phases that can look identical under the optical microscope.

Because no variable temperature cell was available in current X-ray facilities for doing

bulk powder samples, the author designed a cell which is photographed in Fig 3.7-3.9. Figure

3.7 is a picture of the copper cell mounted on the rail which goes inside the SAXS machine.

The white Macor insulator blocks help to isolate the cell from the rest of the X-ray machine at

high temperatures. The two leads coming off the cell are for the substrate heater that controls

the temperature and a K-type thermocouple lead. The sample is placed inside the cell in 1.5

mm, glass capillary tubes. Figure 3.8 shows the cell mounted inside the SAXS machine
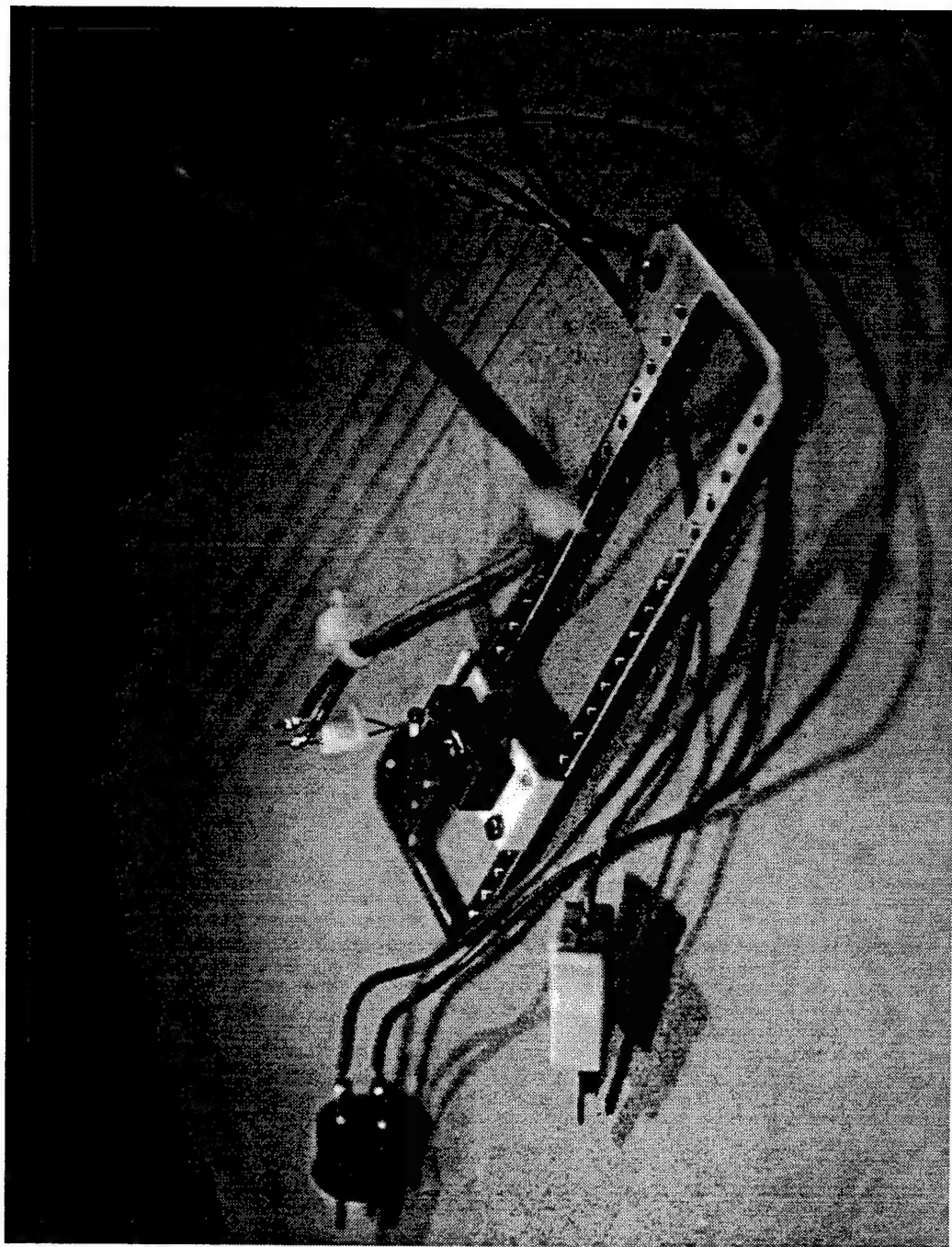
Figure 3.7 Variable Temperature X-ray cell mounted for Small Angle X-ray Scattering
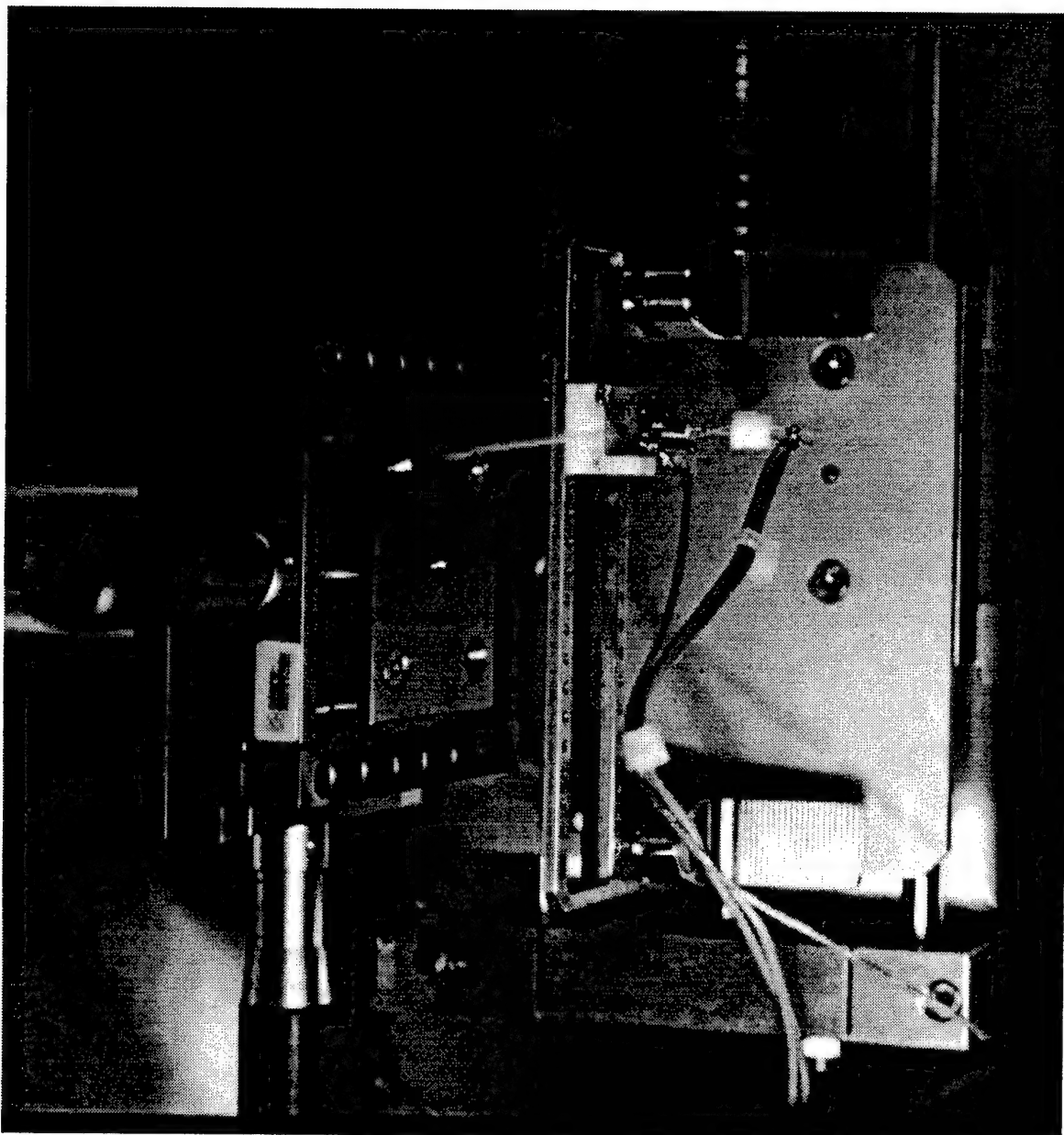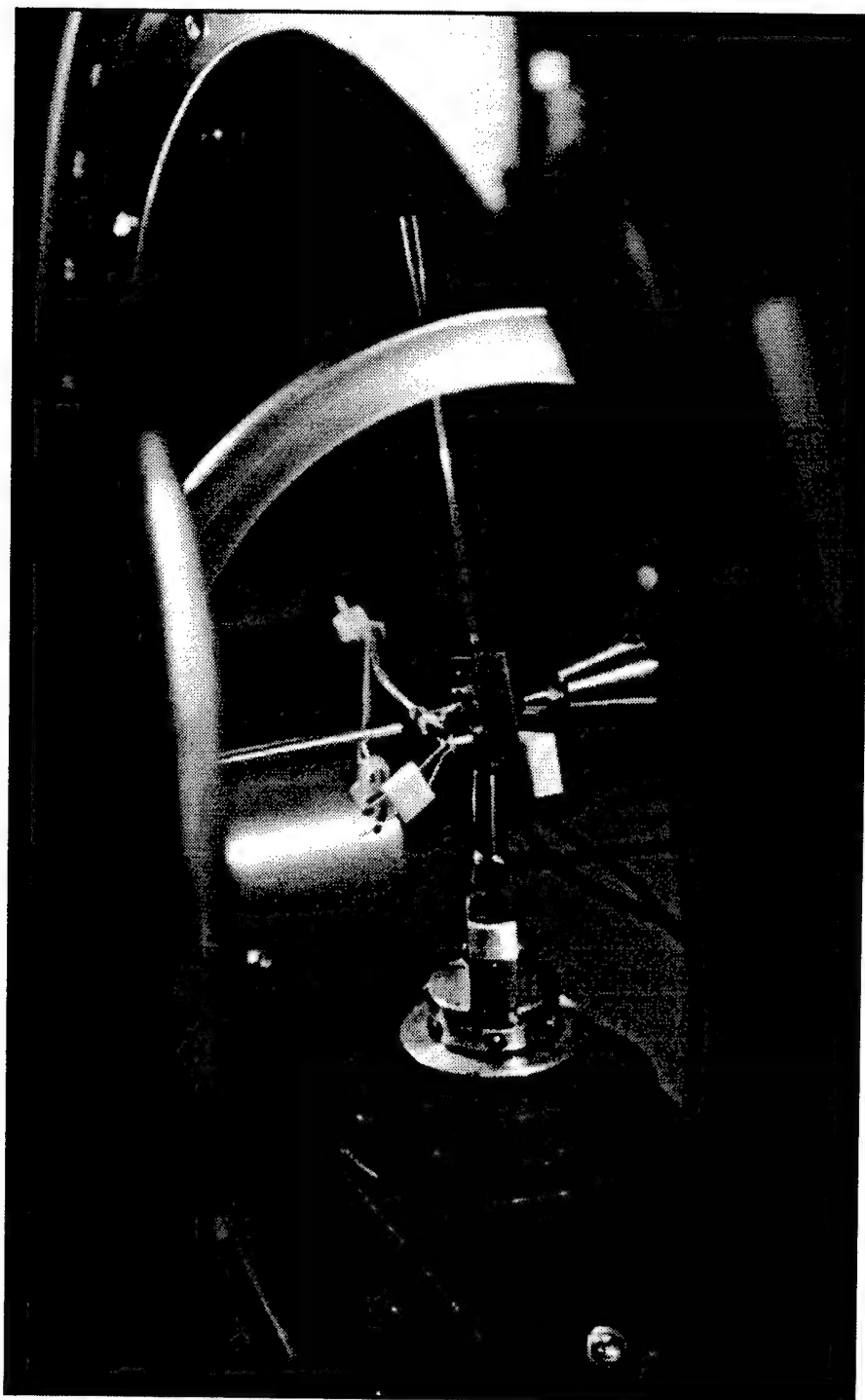
Figure 3.8 VT SAXS experimental set-up

Figure 3.9 VT WAXS experimental set-up

with the power and thermocouple leads attached to a feed through which allows operation under vacuum. Figure 3.9 shows the same cell, with minor modifications, mounted for used in the WAXS experiment. Thus, the same samples and the same cell can be used for both X-ray diffraction experiments. The cell was calibrated for temperature by analyzing stearic acid which melts at 67-69°C. The small angle spacing of stearic acid, 40Å, was observed to disappear at 70°C according to the thermocouple on the cell.

3.4.1.2 VT X-ray Analysis of 9

The d-spacing versus temperature as measured by VT SAXS is shown in Fig 3.10 for molecule **9**. The layer spacing, d, is fairly constant at 54Å from room temperature until about 140°C and then slowly decreases with increasing temperature from 54Å to 52Å. Renderings of molecules **9-11** in an extended confirmation were done in SYBYL and their lengths measured [Fig 3.11]. The extended length of the molecule, l, for **9** is 50.3Å. It is common to find that d for a S_{A1} layer is actually slightly smaller than l.[121, 122] Therefore, it is reasoned that the highest temperature smectic phase is a highly interdigitated S_{Ad} phase which accounts for $d>l$. An interdigitated packing scheme would also be favorable for incorporation of the bulky anthracene group into a layered structure. Others have also reported a slight decrease in d-spacing with increased temperature in the S_{Ad} mesophase.[127, 137] Final assignments of the mesophases below S_{Ad} in temperature were made with the help of VT WAXS that is able to probe order within the layer and detect three distinct liquid crystal phases [Fig 3.12]. Shown in Fig 3.12(a) is the diffuse scattering peak characteristic of liquid-like order within the layer and thus indicative of a one-dimensional smectic phase.[138] As the temperature drops to 120°C, the diffraction peak becomes much sharper and is characteristic of a hexatic phase,
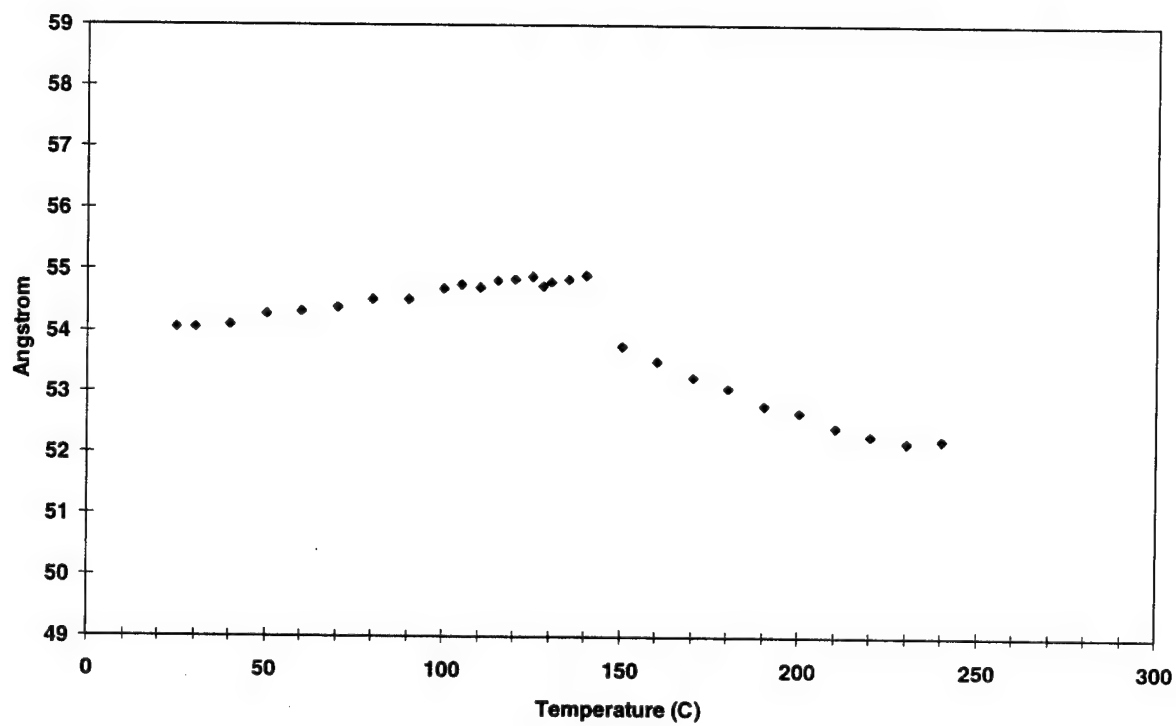
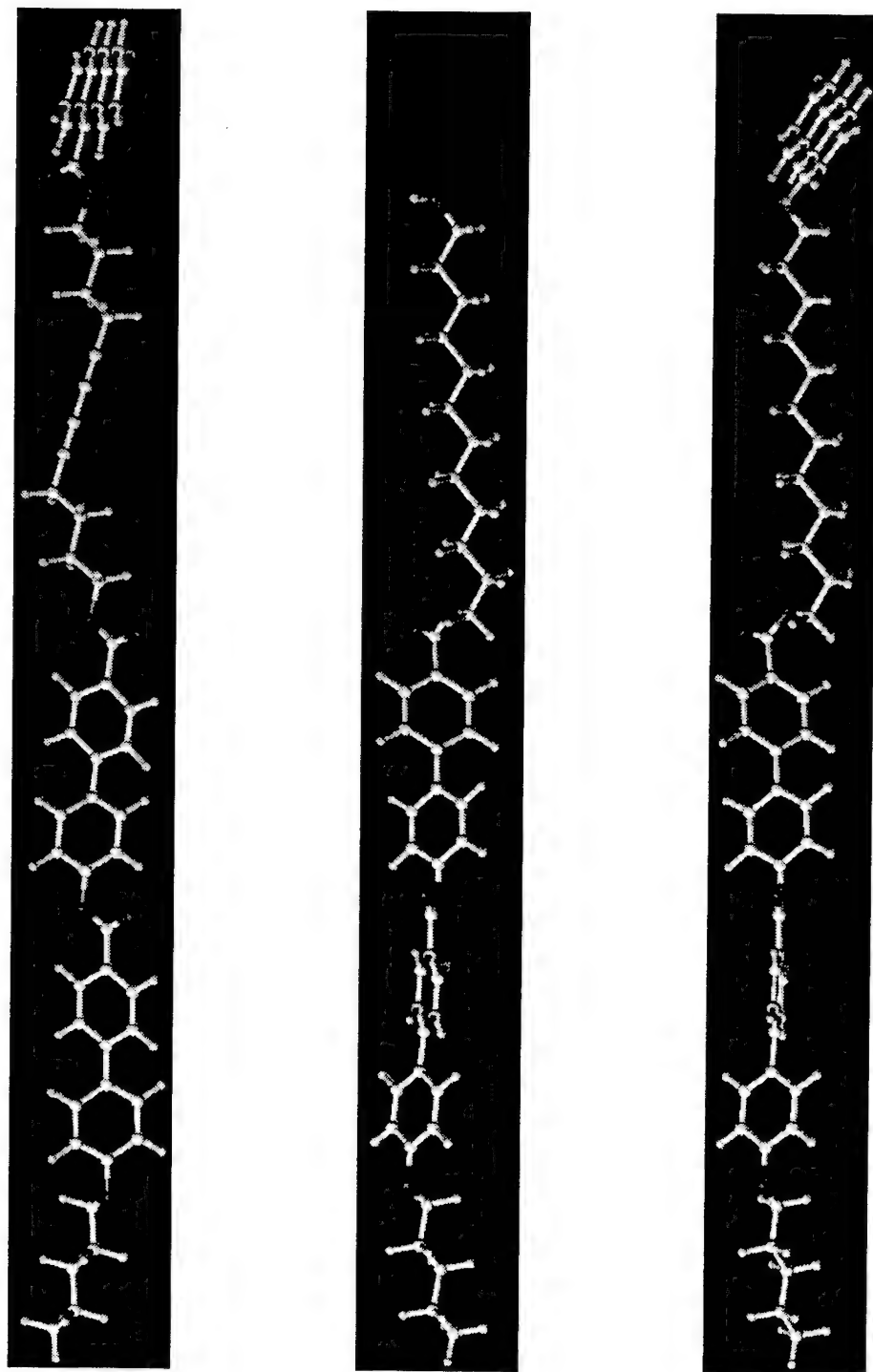**Figure 3.10** d-spacing of the 001 peak vs temperature for **9**

Figure 3.11 Molecular Graphics (SYBYL) renderings of molecules **9-11** in extended confirmation (a) **9**, extended length = 50.3Å (b) **10**, extended length = 42.7Å (c) **11**, extended length = 47.1Å
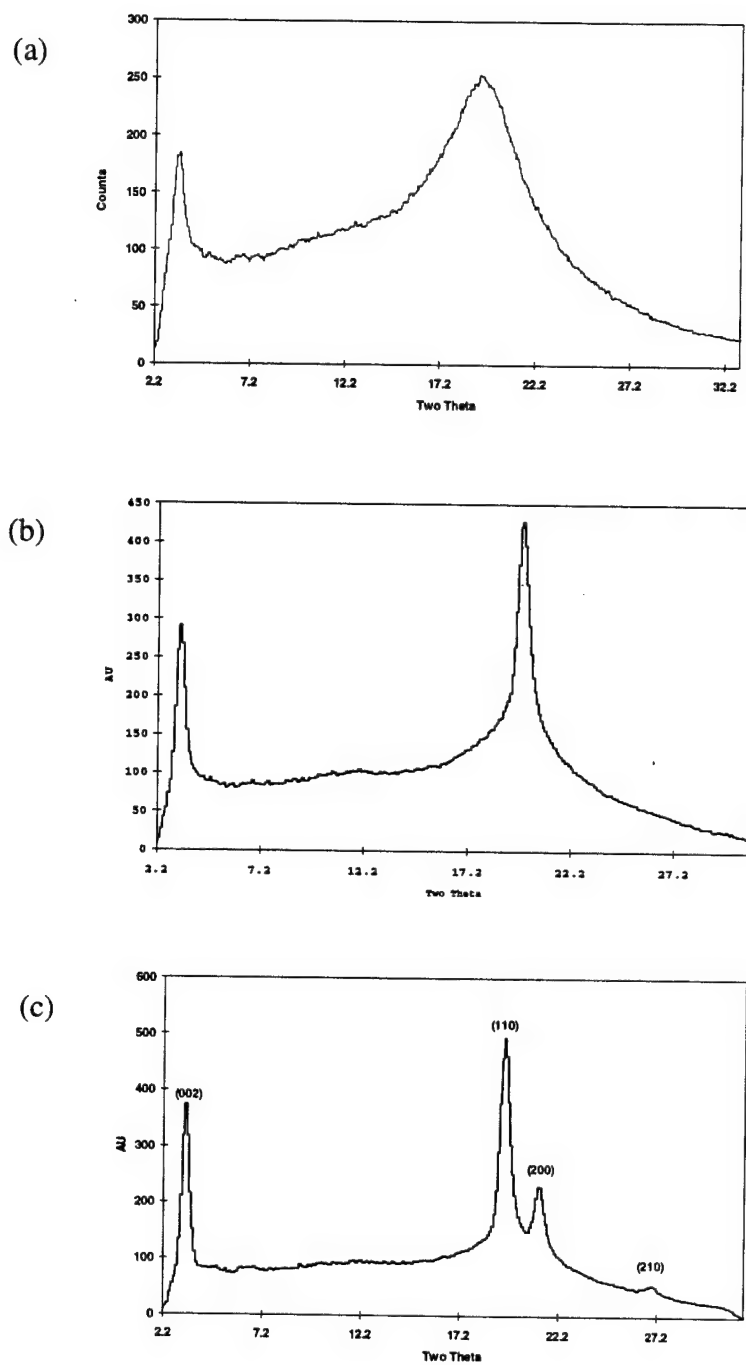
Figure 3.12 Debye-Scherrer patterns of **9** a) 150°C, S_A; b) 120°C, $S_B{}^h$; c) 108°C, crystal E

S_B^h, where the (200) and (110) peaks are superimposed.[139] Finally, another transition is detected as the temperature is dropped to 108°C. The diffraction pattern in Fig 3.12(c) has ratios indicative of orthorhombic packing with a = 8.36Å and b = 5.43Å. The probable (110), (200), (210) and (002) peaks are labeled on the figure. Using the measured lattice parameters of a = 8.36Å, b = 5.43Å, c = 53.7Å, a model was made of the crystal E structure using an orthorhombic interdigitated packing scheme in Cerius^2 which confirmed that the packing scheme was viable.

Textures of molecule **9** from polarized optical microscopy (POM) at various temperatures are shown in Fig 3.13 (a)-(e). POM revealed that the material cooled from the isotropic liquid to a very narrow nematic phase at ~ 210°C, Fig 3.13 (a), before becoming a homeotropic phase Fig 3.13 (b) that remained until 100°C. The homeotropic phase was investigated by conoscopic observation which revealed the phase to be uniaxial Fig 3.13 (c) which is characteristic of the S_A and S_B^h mesophase. Below 100°C the homeotropic phase became "mossy" or "sandy" in texture Fig 3.13 (d) and conoscopic observation showed the material to be biaxial [Fig 3.13 (e)-(f)]. Conoscopy is a quick indicator of whether a homeotropic phase is either uniaxial or biaxial. The black cross pattern seen for a uniaxial material Fig 3.13 (c) does not move upon rotation of the sample on the microscope stage. Biaxial materials form a dark hyperbola pattern, Fig 3.13 (e)-(f), under conoscopic observation that changes upon rotation of the sample. Upon rotation, the hyperbola, or isogyres, coalesce into a cross and then separate again into the hyperbola rotated 90° (illustrated in Fig 3.13 (e)-(f)). Conoscopic microscopy was important for molecules **10** and **11** as well, because they also formed homeotropic or pseudohomeotropic phases when observed between two glass coverslips. Fig 3.14 is a

(b)

(c)

(a)
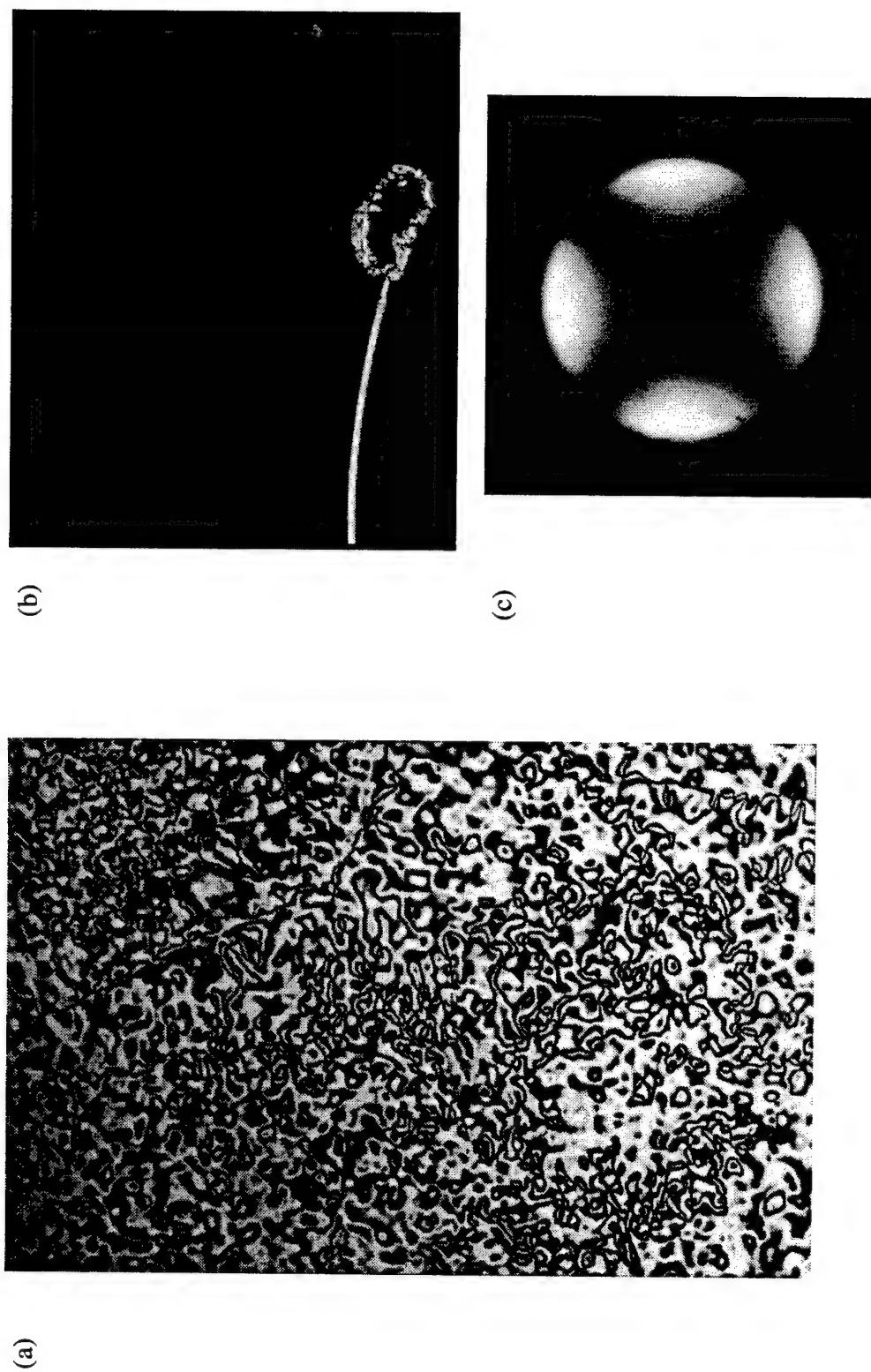
Figure 3.13 Polarized Optical Microscopy textures of **9** at (a) 208°C; nematic (b) 151°C; homeotropic S_{Ad} (c) 151°C; conoscopic image indicating uniaxial alignment

(e)

(f)

(d)
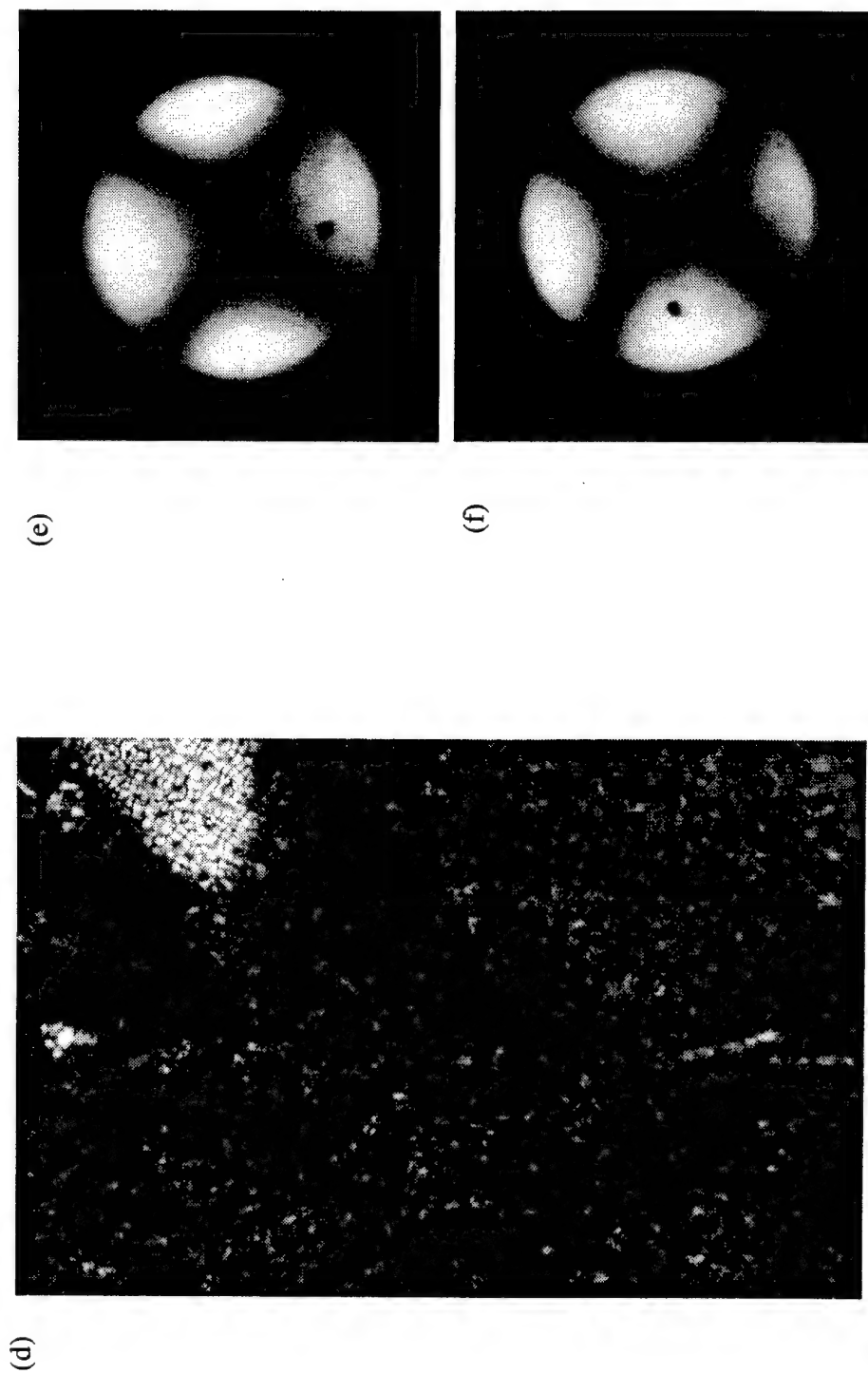
Figure 3.13 (cont.) (d) 95°C; crystal E (e) and (f) 21°C; conoscopic images of sample indicating biaxial alignment; (f) same area of sample as (e) but rotated ~ 180°C
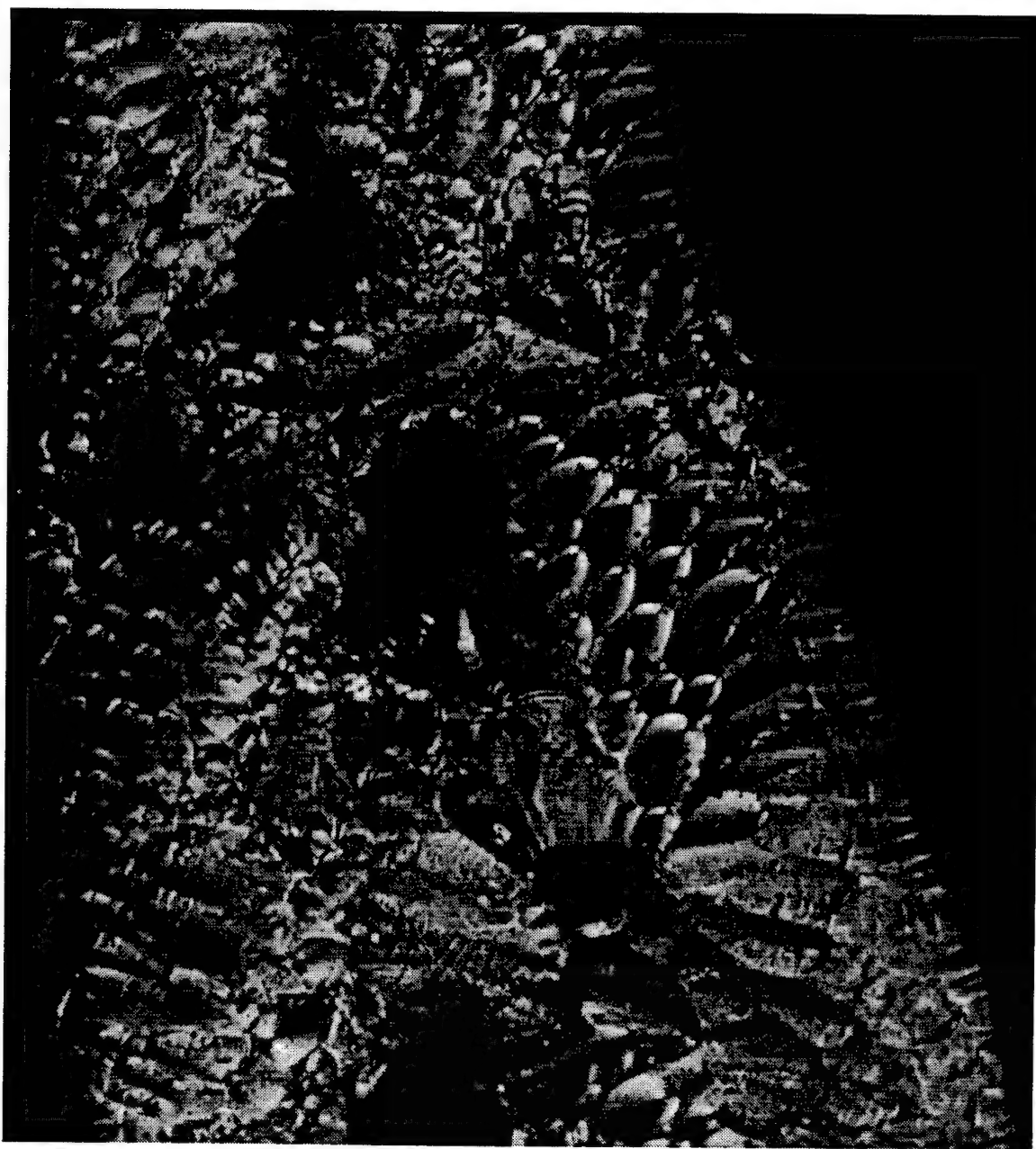
Figure 3.14 Polarized Optical Microscopy image of free standing droplet of **9** at 195°C. Image shows focal conic fans and black homeotropic regions characteristic of S_A mesophase

POM image of a free standing droplet of **9** at 195°C which has the characteristic focal conic fans and dark homeotropic regions of the S_A mesophase. Therefore, POM confirmed the presence, upon cooling, of a nematic phase followed by a homeotropic S_A phase. The transition to the $S_B{}^h$ phase was not detected because it was a uniaxial homoetropic phase as well and would not necessarily show any texture change. The "mossy" or "sanded" texture below 100°C was biaxial, but SAXS did not indicate a decrease in the layer spacing, d, therefore, the biaxial nature was not due to a tilt of the mesogens within the layer but rather from the "herringbone" packing of the crystal E phase.

3.4.2   *Characterization of 10*

Molecule **10** is the non-diacetylene version of **8** and was the precursor for **11**. This material is a white solid that has dramatically decreased solubility in chloroform (0.5 mg/mL) when compared to **8,9**, and **11**. This comparative insolubility is thought to be due to the twelve carbon, alkyl chain which does not have the diacetylene "kink" to break up the ability of the chain to crystallize. After attachment of the anthracene group to the end of **10** to make **11**, the solubility was improved. Based upon POM, DSC, and X-ray diffraction, the following mesophase behavior is proposed for molecule **10**.

k 110 G 139 S_F 150 S_C 257 i

DSC scans of the material are shown in Fig 3.15. Notice the presence of a supercooled transition in the 1st cooling cycle that is indicative of crystallization. Calculated enthalpies are listed in Table 3.3.
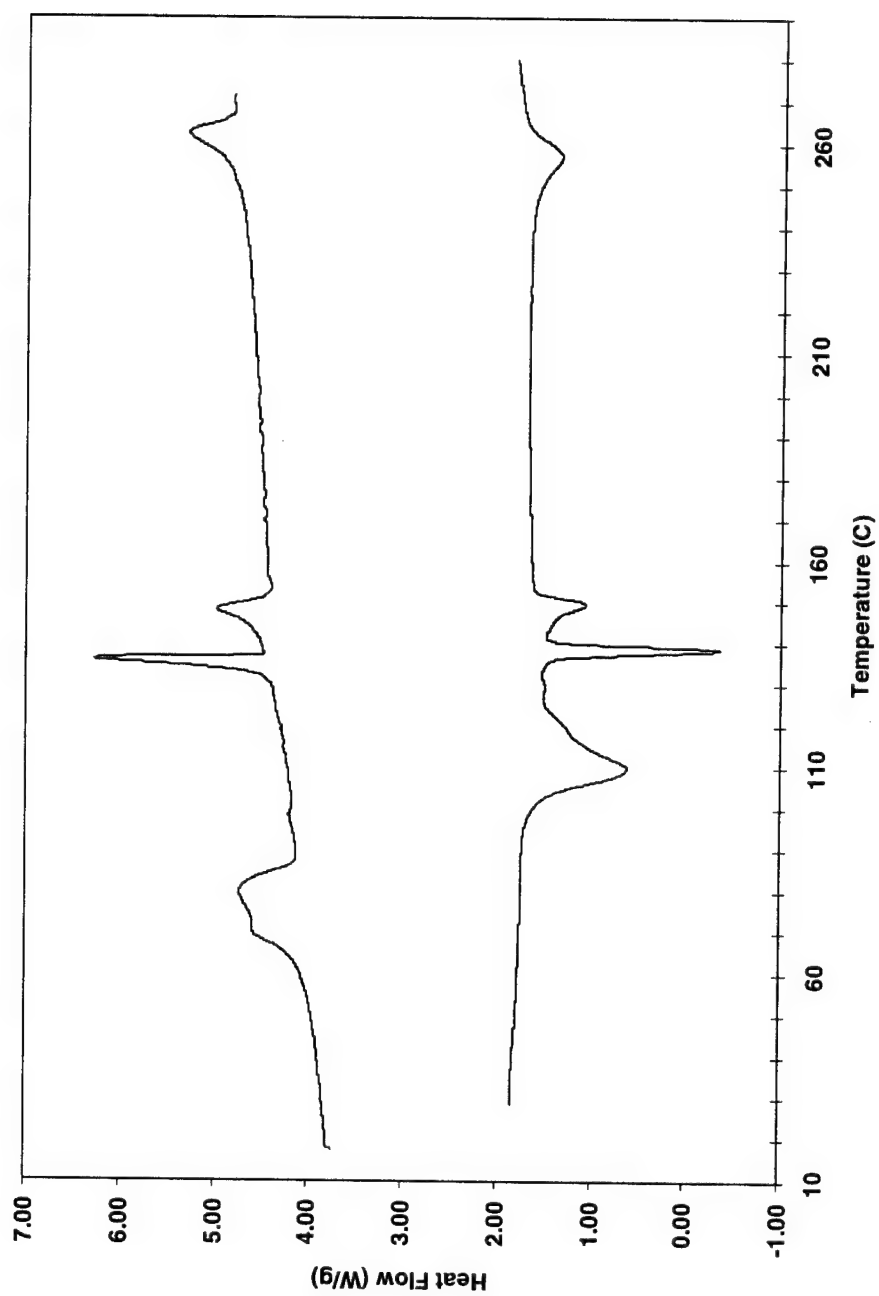
Figure 3.15 Differential Scanning Calorimetry scan of **10**. Top curve is 1st cooling cycle and bottom curve is 2nd heating cycle; both at 5°C/min

Table 3.3 Transition enthalpies of **10** determined by 2nd heating cycle (DSC)

Transition Temperature, °C	Phase Change	ΔH, kJ/mol
110	$k \rightarrow G$	12.4
139	$G \rightarrow S_F$	4.6
150	$S_F \rightarrow S_C$	2.4
257	$S_C \rightarrow i$	3.9

The results of the VT SAXS and VT WAXS experiments are shown in Fig 3.16 and Fig 3.17. An interesting result with this molecule is the formation of a tilted, bilayer phase detected in the VT SAXS data. Many of the first bilayer and interdigitated S_A mesophases were found for mesogens with polar end groups such as -CN and $-NO_2$.[129, 140] The highest temperature mesophase (between 150-250°C) was measured by SAXS to have a d-spacing of ~32Å which is much shorter than the molecule's calculated, extended length, 42.7Å [Fig 3.11(b)]. Therefore, the molecules must be tilted within the layer and are in the S_C mesophase. The biaxial nature of the homeotropic phase was confirmed by conoscopic observation, [Fig 3.18(a)]. As the material is cooled, there is a transition to the bilayer spacing of ~64Å between 140-130°C. This bilayer spacing remains constant upon further cooling of the material. Identification of this new smectic phase, [Fig 3.18(b)], depended on a combination of the VT WAXS and POM results. VT WAXS revealed a very slight narrowing of the diffuse, scattering as the material was cooled from 180°C to 124°C [Fig 3.17(a)-(b)]. This indicates the new phase has more order than a liquid but less than the $S_B{}^h$ phase [Fig 3.12(b)]. Therefore, this new phase could be either the S_F or S_I phase. It has been reported

Figure 3.16 Graph of d-spacing of (001) peak vs temperature for molecule **10**
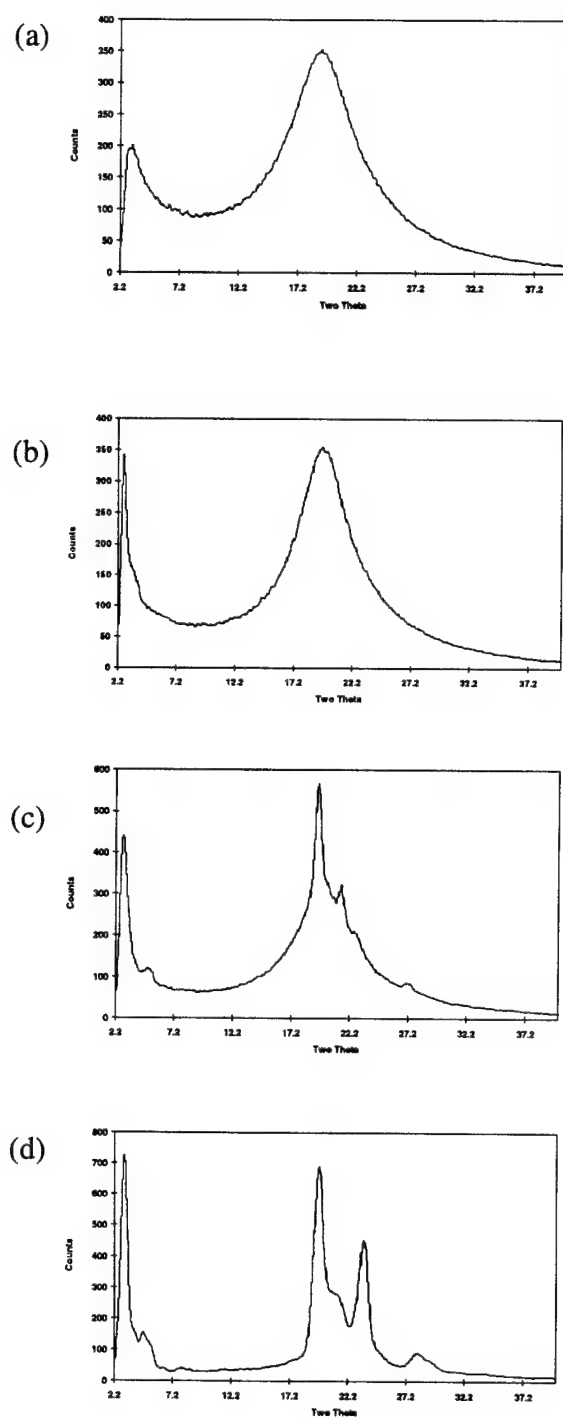
Figure 3.17 Debye-Scherrer patterns of **10** (a)180°C; S_C (b) 124°C; S_F
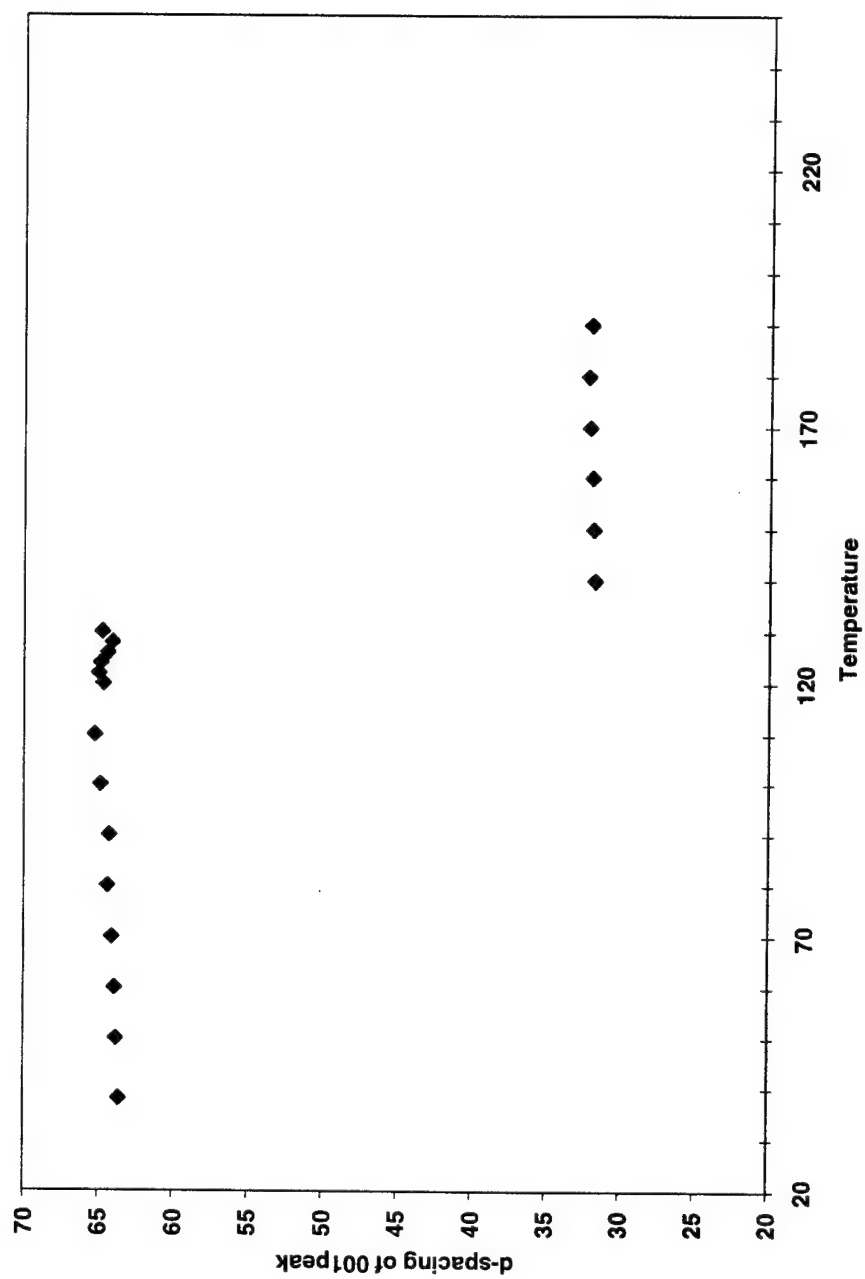(c) 120°C; G (d) 29°C, k
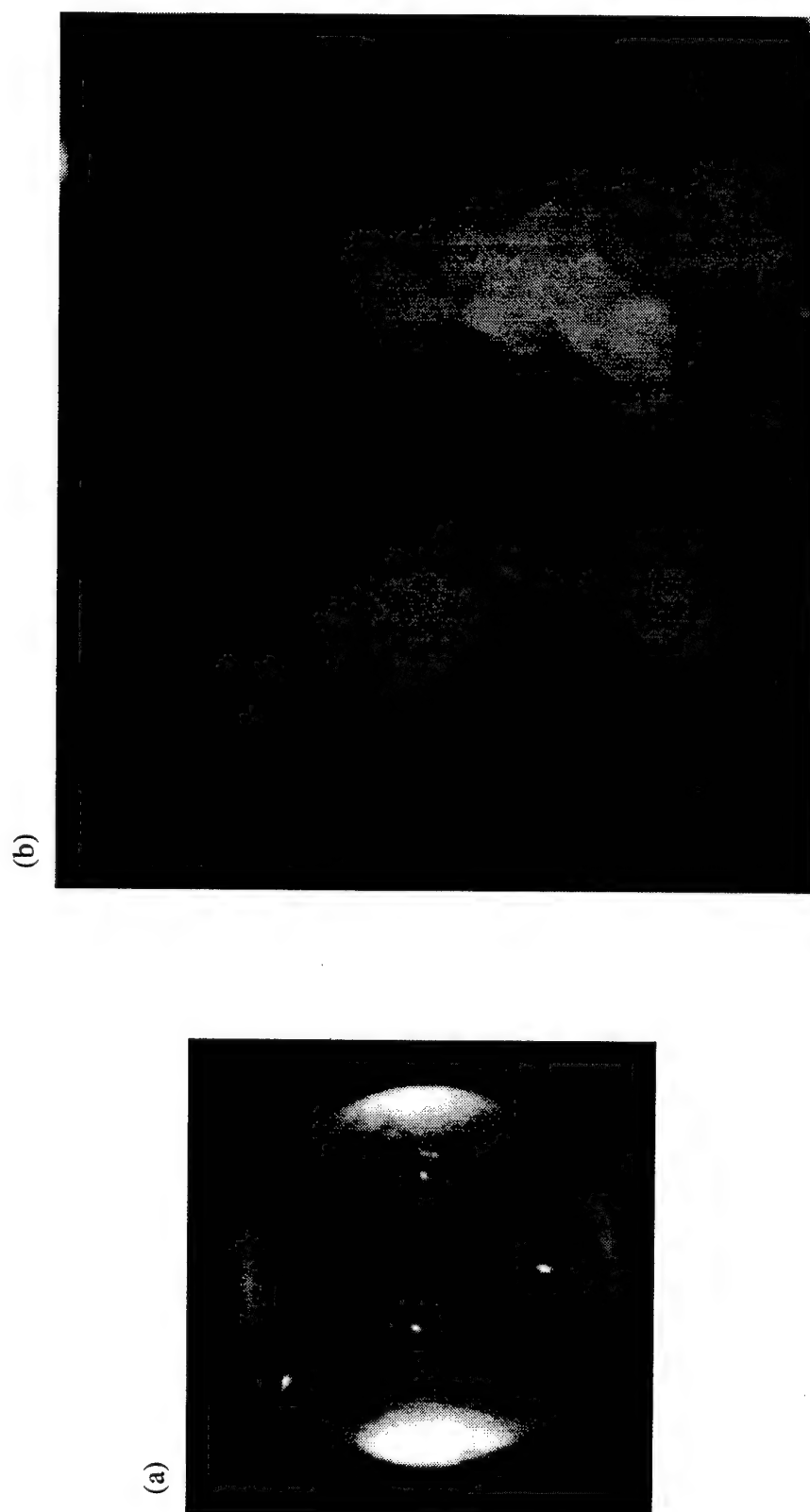
Figure 3.18 Polarized Optical Microscopy textures of **10** at (a) 196°C; conoscopic image indicating biaxial alignment (b) 122°C; S_F

(d)

(c)
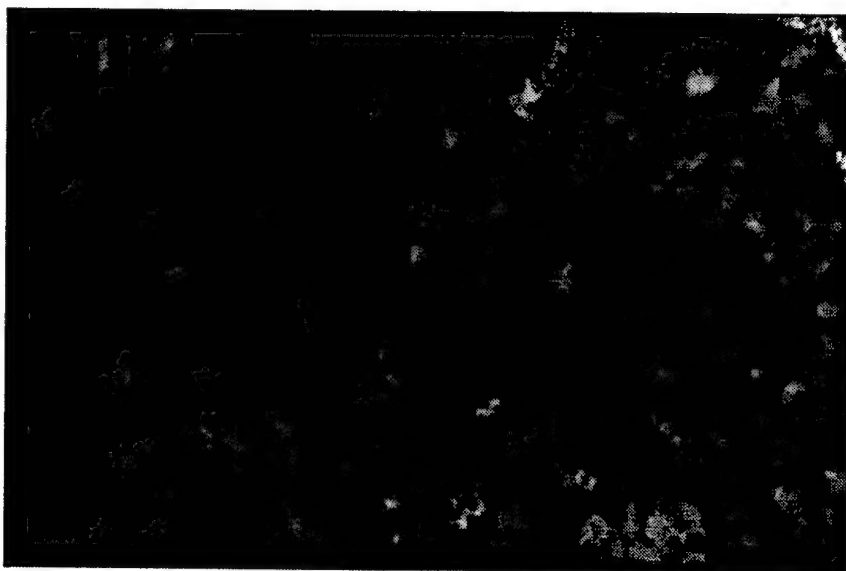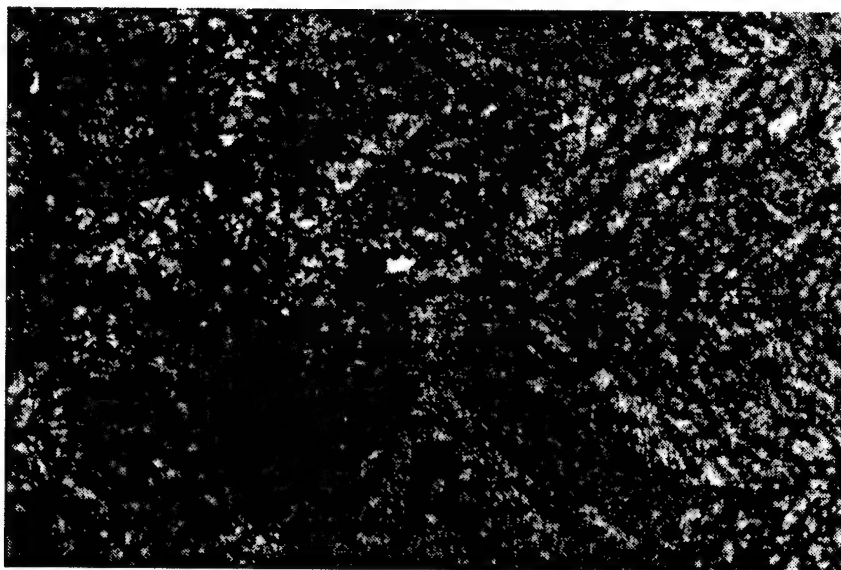
Figure 3.18 (cont.) (c) 118°C; G (d) 54°C; crystal

that the S_F phase has a more diffuse wide angle peak than the S_I phase[122, 133] and comparisons to POM textures in the literature led to the conclusion that the phase was the S_F phase. As the sample is cooled further, it undergoes another phase transition as evidenced by the appearance of a sharp peak in the wide angle diffraction along with weaker reflections, Fig 3.17(d) and a change in the POM texture to a darker, higher contrast texture [Fig 3.18(c)]. The X-ray diffraction data indicates more order within the layer, similar to the $S_B{}^h$, but this phase is of higher order as evidenced by the other weak diffraction peaks about the main peak. The G and S_F phase are related in that both mesophases have quasi-hexagonal packing with the mesogens tilted toward the sides of the hexagon (see sections 3.3.3 and 3.3.4). The difference between the phases is the G phase has long range positional order in three dimensions. Therefore, the mesophase between 139-110°C was assigned the G phase based on the wide angle diffraction and comparisons to POM textures from the literature. Below the G phase is a crystal phase with the wide angle diffraction pattern shown in Fig 3.17(d) and a POM texture shown in Fig 3.18(d).

3.4.3 Characterization of 11

Molecule **11** is a pale yellow solid. The proposed mesophase behavior for this molecule is,

k 89 E 139 $S_B{}^h$ 141 S_{Ad} 205 n 212 i
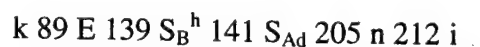
The DSC of this material is shown in Fig 3.19 while the enthalpies of the transitions are listed below in Table 3.4. This material was very similar to **9** in its phase behavior, with identical mesophase assignments. However, molecule **11** is without a diacetylene group and was able
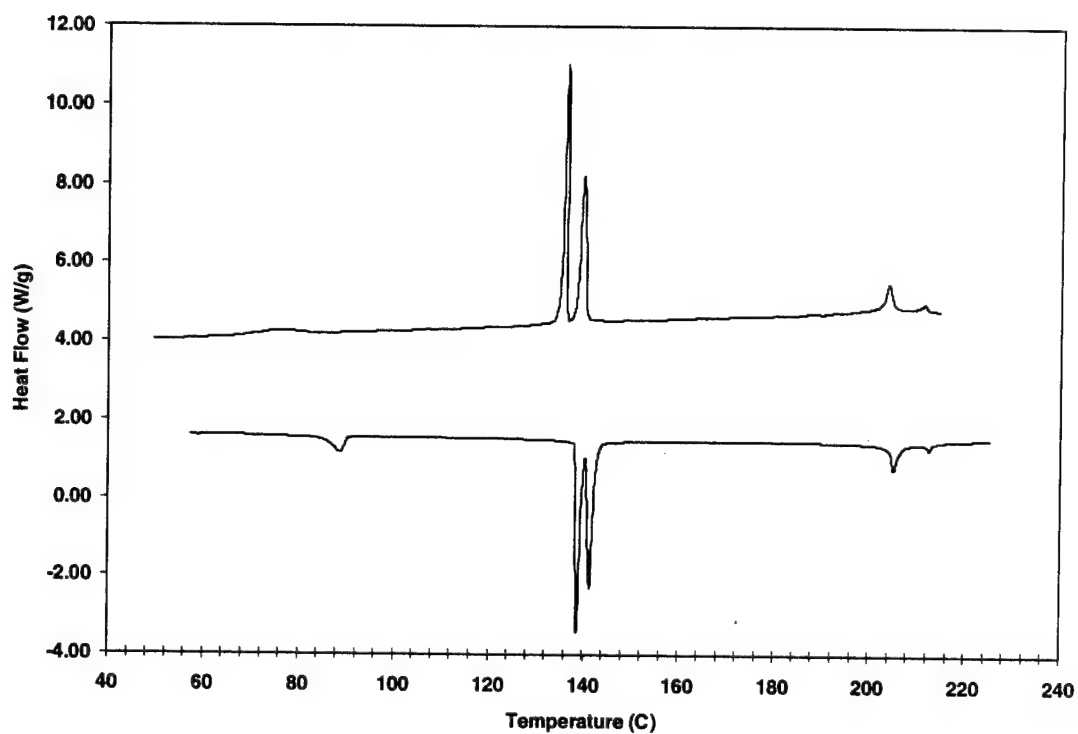
Figure 3.19 Differential Scanning Calorimetry scan of **11**. Top curve is
1st cooling cycle and bottom curve is 2nd heating cycle, both at 5°C/min

to crystallize and tended to have higher transition temperatures in the higher ordered smectic phases.

Analysis by X-ray diffraction, Fig 3.20 and Fig 3.21, was similar to that done for **9**. POM again revealed a high temperature uniaxial homeotropic phase, Fig 3.22(a)-(b), with layer spacing greater than the extended length of the molecule. Thus

Table 3.4 Transition enthalpies of **11** determined by 2nd heating cycle (DSC)

Transition Temperature, °C	Phase Change	ΔH, kJ/mol
89	$k \rightarrow E$	1.5
139	$E \rightarrow S_B^h$	6.1
141	$S_B^h \rightarrow S_{Ad}$	6.1
205	$S_{Ad} \rightarrow n$	1.3
212	$n \rightarrow i$	0.2

the material was also forming a S_{Ad} phase as **9** had. This phase showed the same small decrease in d-spacing as the temperature was increased from 140°C to 200°C, [Fig 3.20]. The S_B^h phase was not homeotropic in this case but showed a "cloudy" mosaic texture that was only obtainable by cooling at 0.2°/min because the mesophase had such a narrow range [Fig 3.22(c)]. The wide angle X-ray pattern of the phase was a characteristic single sharp peak at wide angles along with the (002) peak that is visible in all these WAXS patterns [Fig 3.21(b)]. Further cooling led to a change in the POM texture, [Fig 3.22(d)], and a change in the wide angle diffraction pattern, [Fig 3.21(c)]. The peaks in this pattern can be indexed in
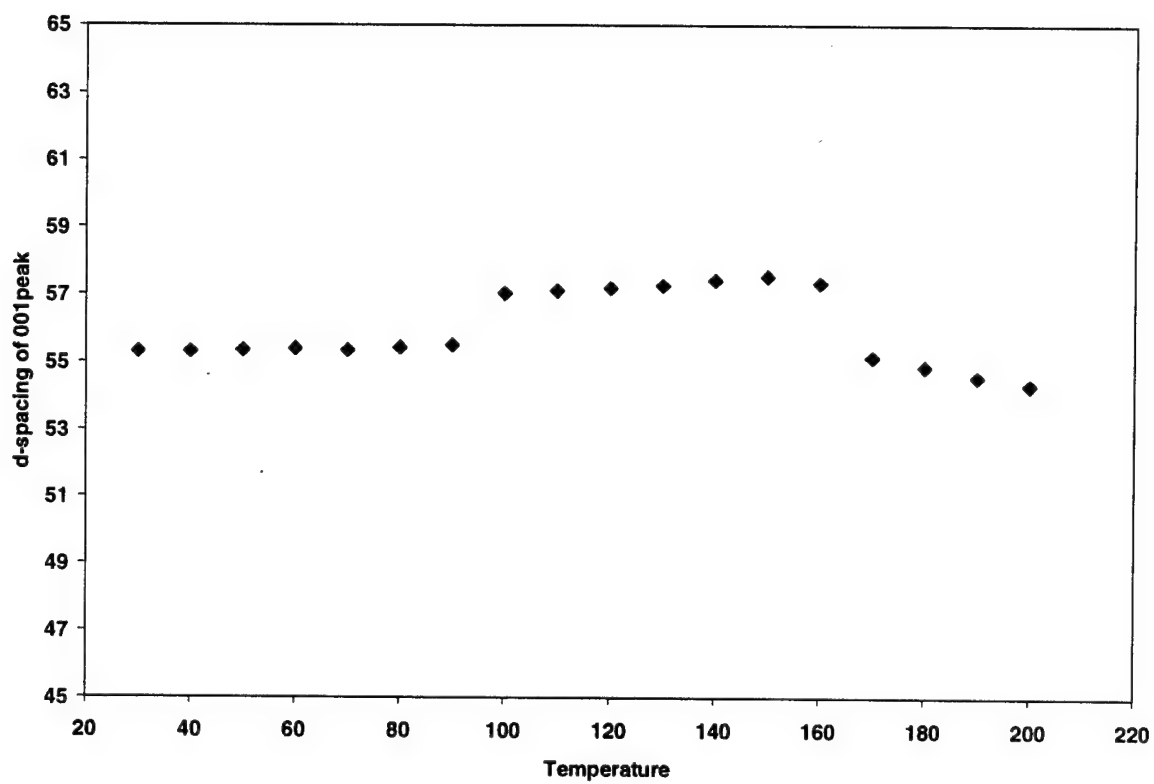
Figure 3.20 d-spacing of (001) peak vs. temperature for **11**
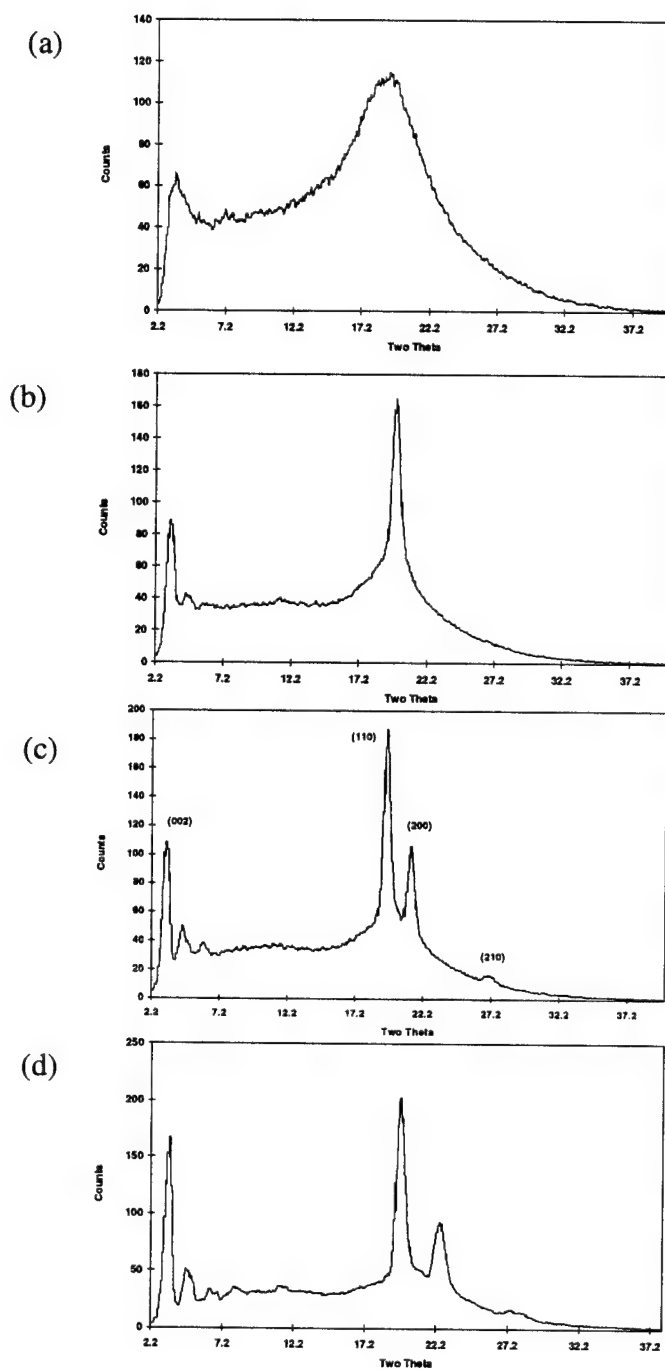
Figure 3.21 Debye-Scherrer patterns of **11** (a) 200°C; S_{Ad} (b) 140°C; S_B^h (c) 136°C; E (d) 25°C, crystal

94

(b)

(a)
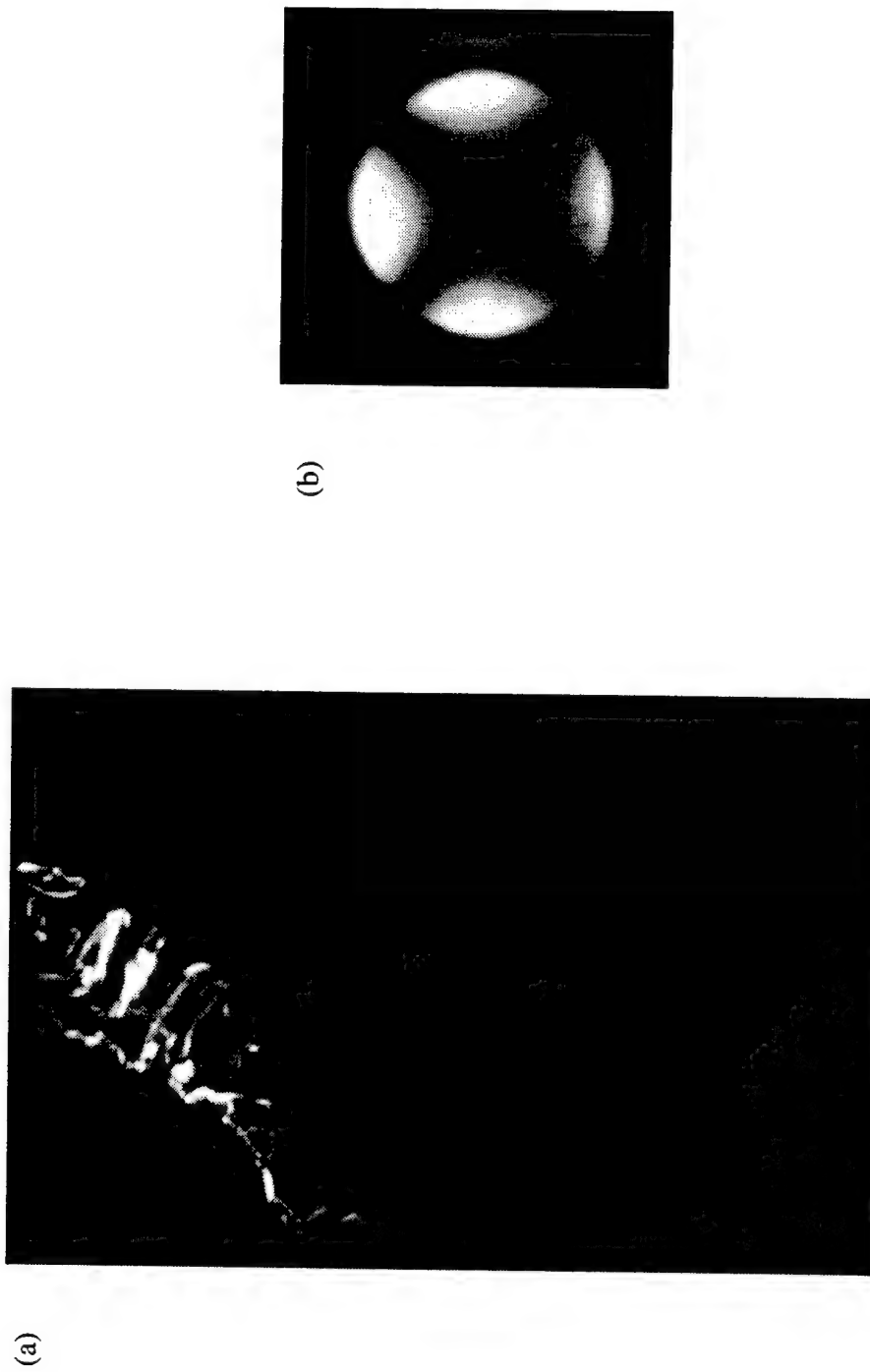
Figure 3.22 Polarized Optical Microscopy textures of **11** at (a) 143°C; homeotropic S$_{Ad}$ (b) 143°C; conoscopic image indicating uniaxial alignment
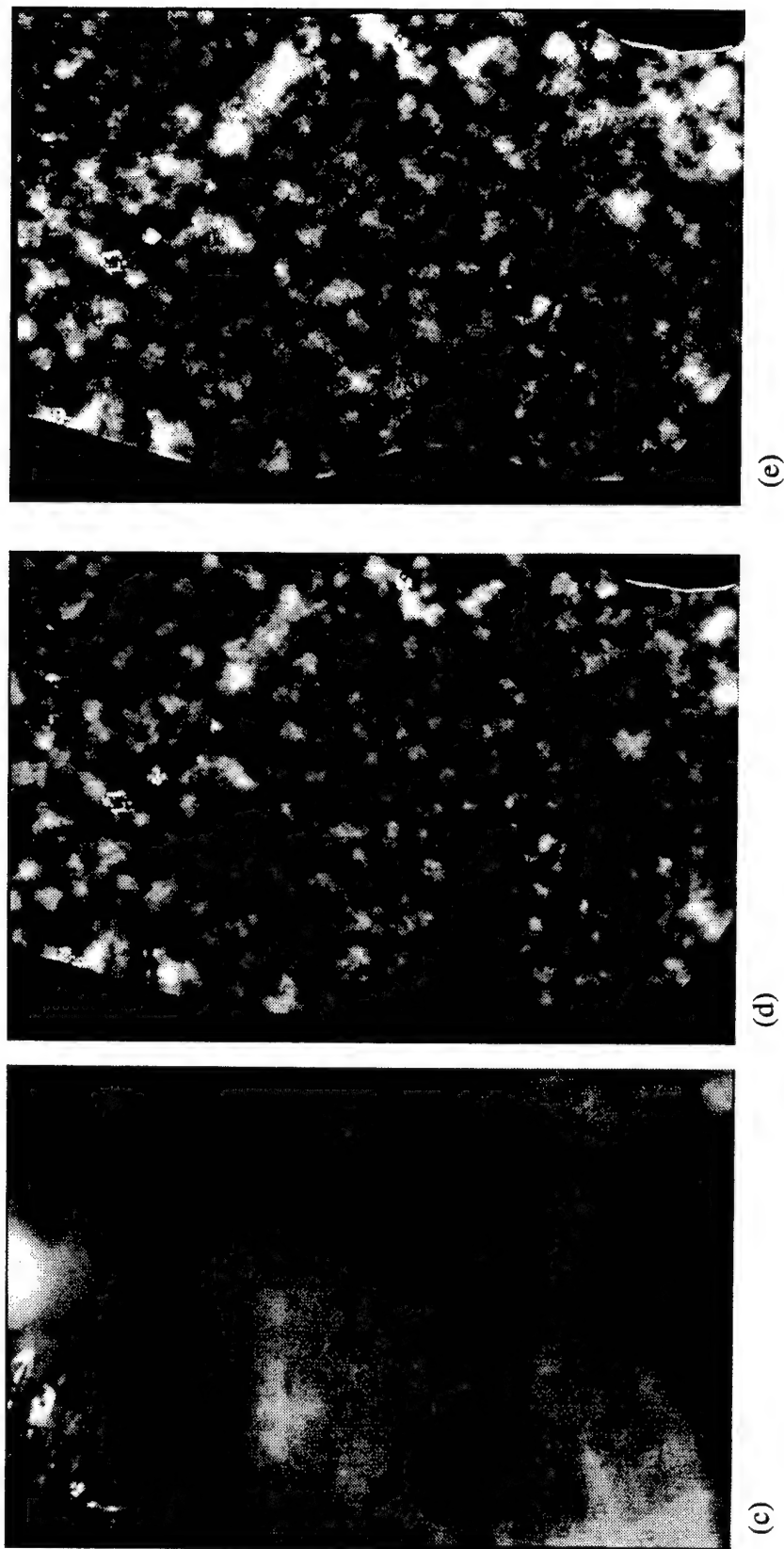
Figure 3.22 (cont.) (c) 139°C; S_B^h (d) 90°C; crystal E (e) 43°C, crystal

the same manner as they were for the crystal E phase of **9** [Fig 3.21(c). This material did undergo a decrease in layer spacing upon crystallization at 89°C that can be seen in Fig 3.20. The last phase change to the crystal can be seen in Figure 3.22(e) as many lines begin forming in the small domains from the previous E phase.

3.4.4   *Conclusions about Structure and Potential Reactivity*

Molecules **9-11** show a variety of layered phases. Because the layered structures formed by molecule **9** are interdigitated, the chances for photodimerization of the anthracene end groups *within* the layer are small (see Figure 3.23). Most likely, the anthracene photodimerization reaction will occur *between* layers. Therefore, one prediction is that the predominant photodimer will be the head-to-tail product and not the head-to-head product (Figure 3.24). As mentioned before, the head-to-tail product is the favored product in the photodimerization of 9-substituted anthracene. If the head-to-head product [Fig 3.24(a)] were to form, the chances of diacetylene reaction would be high due to their close proximity in this structure. An analogous diacetylene molecule having this 'hairpin'-like structure has previously been shown to be highly reactive to diacetylene polymerization.[78] A schematic of the various structures that could be formed if the head-to-tail demesogens where to undergo diacetylene polymerization is shown in Figure 3.25. All three covalent structures, comb, ladder, and comb-ladder polymer are one dimensional and will form depending on the extent of reaction in the two different planes of diacetylene groups. In order to form two dimensional polymers, poly(diacetylene) backbones need to form above and below the anthracene photodimer junction and most importantly, the direction of these backbones cannot be parallel. Perpendicular polymerization of the diacetylene groups in the two reactive

d > length of **9**
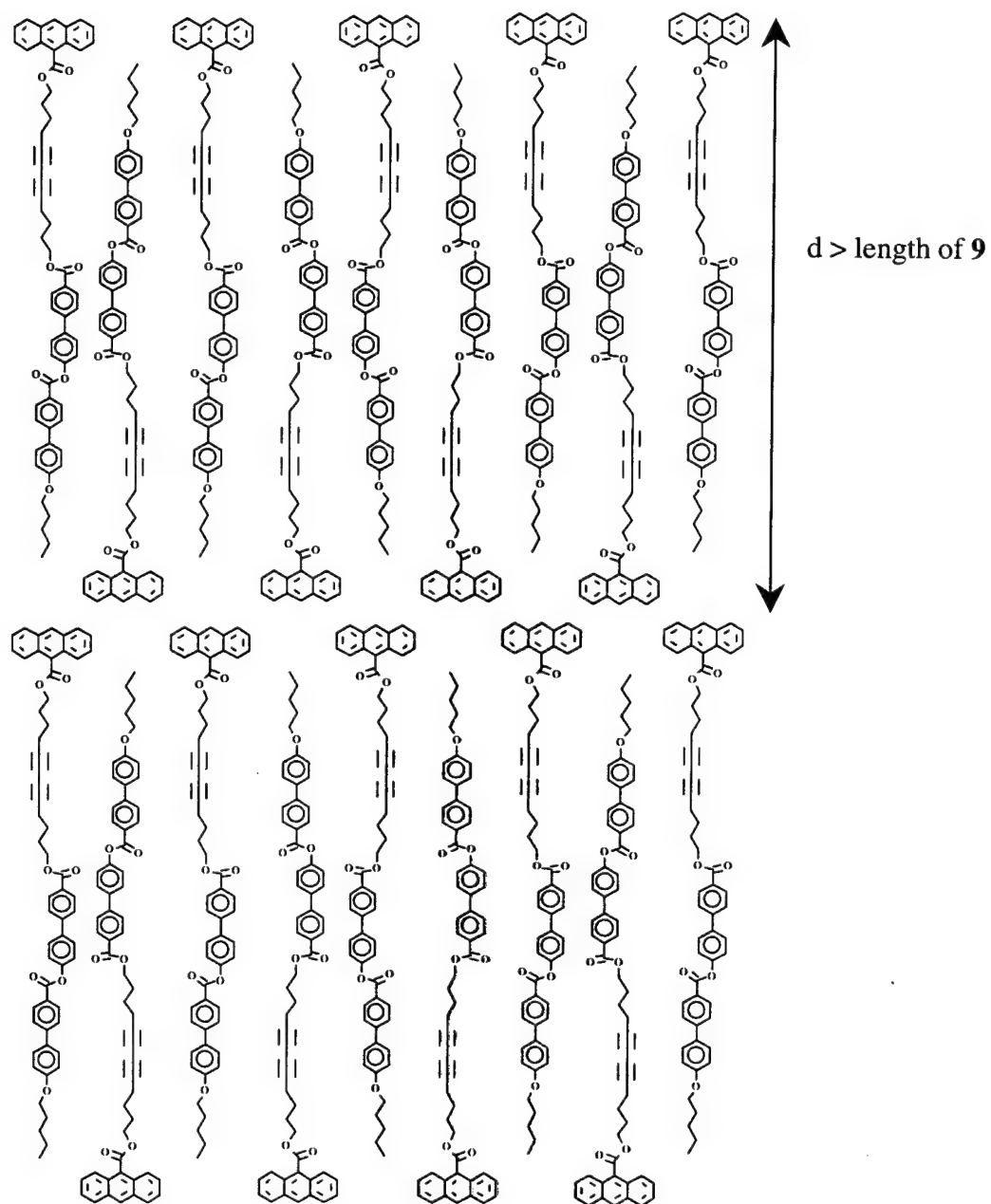
Figure 3.23 Schematic of interdigitated packing in S$_{ad}$ phase of **9**
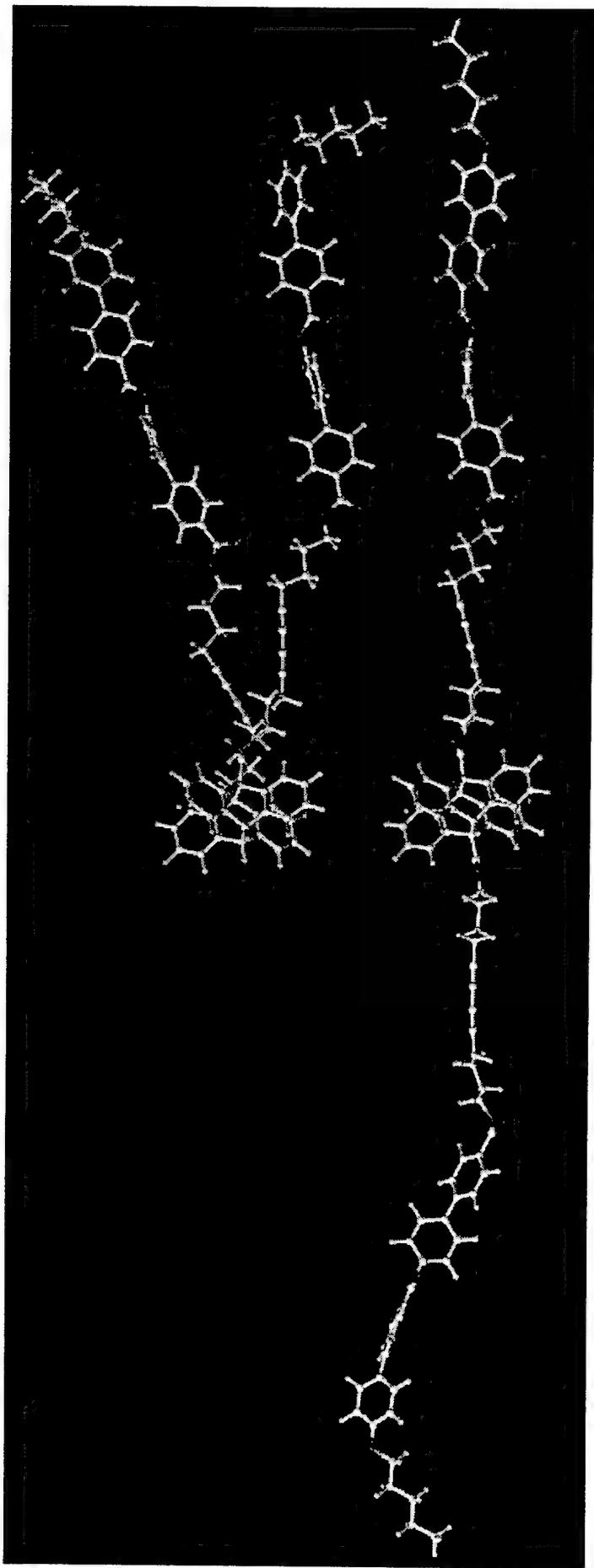
Figure 3.24 Rendering of the two constitutional isomers of the photodimer of **9** (a) head-to-head (b) head-to-tail

9

Comb

Ladder

Comb-Ladder
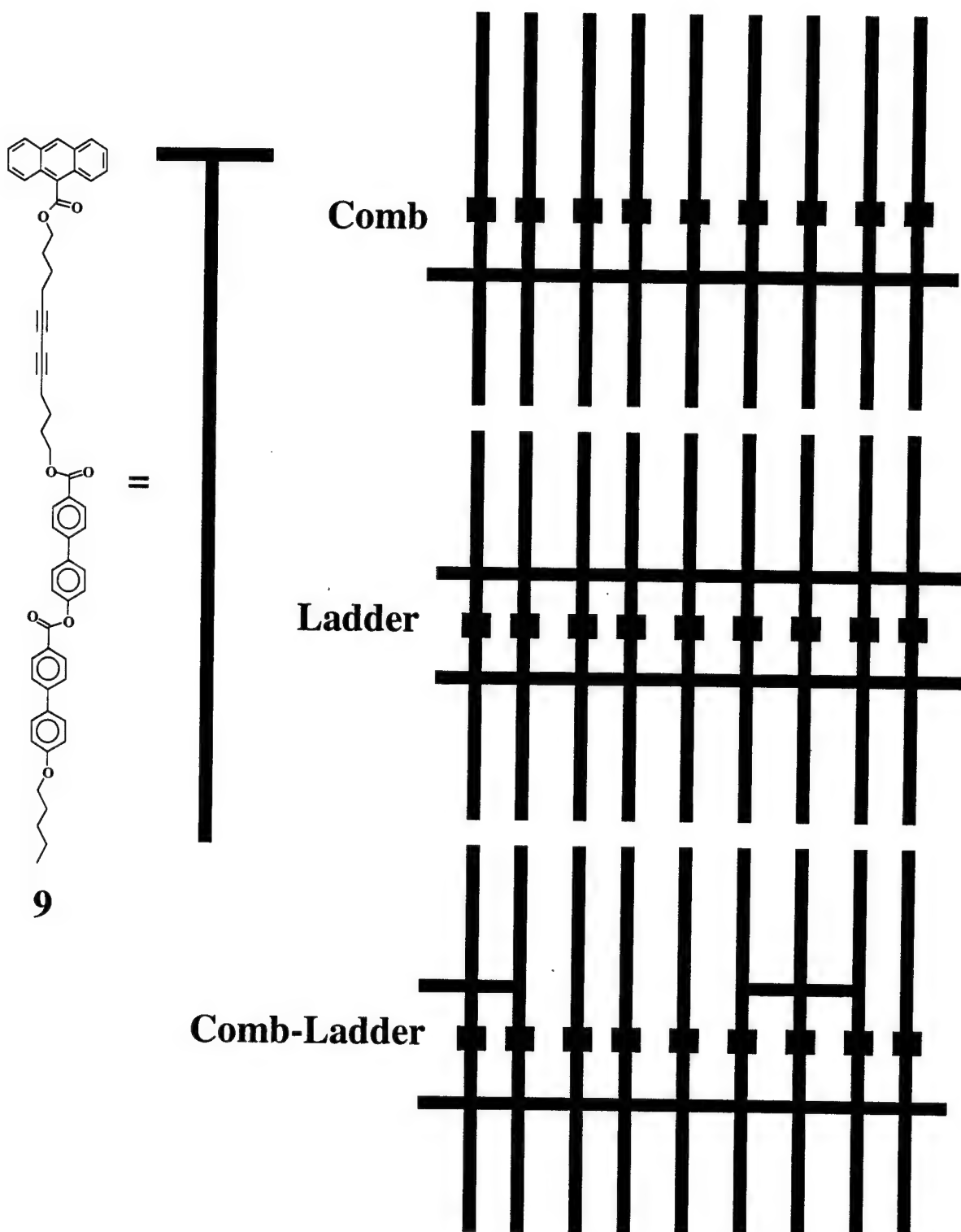
Figure 3.25 Potential one-dimensional polymers that could be formed by reaction of **9**

planes (shown in blue in Fig 3.25) would lead to the formation of two dimensional objects. One way to promote non-parallel polymerization of the diacetylene bonds may be to heat the material that would allow the dimesogens more freedom within the layer, and allow rotation of the molecules. This "spinning" of the reactive groups while still in a smectic layer, may promote uncorrelated diacetylene polymerization which in turn would lead to the formation of two dimensional objects.

3.5 Properties of 9

3.5.1 Absorption and Fluorescent Properties

The absorption spectra of **9** in solution and in the solid state are shown in Fig 3.26 and Fig 3.27, respectively. Figure 3.26 shows three absorption bands between 325-400 nm which are characteristic of the anthracene chromophore.[141, 142] The spectrum in Fig 3.27(a) was obtained (from a thin film of **9** spin coated onto a silicon wafer) using an integrating sphere showing the same three bands between 325-400 nm. Spin coated films were investigated because of the lithographic studies done on this material (described in Chapter 4). Irradiation at wavelengths above 300 nm causes a photodimerization reaction between two adjacent anthracene groups (see section 2.2.2.2). The absorption spectrum of the same film used in Fig 3.27(a) is shown in Fig 3.27(b) after a 30 minute irradiation with a 150W Xenon lamp. The relative absence of any remaining anthracene groups after this irradiation is apparent.

Linked to the change in the adsorption spectrum is a change in the fluorescent properties. Molecule **9** has a characteristic blue emission centered about 450 nm, both in solution and in the solid state, when irradiated with ultraviolet light between 254 and 365 nm. Figure 3.28 shows the fluorescent emission spectrum for a spin coated film of **9** on a
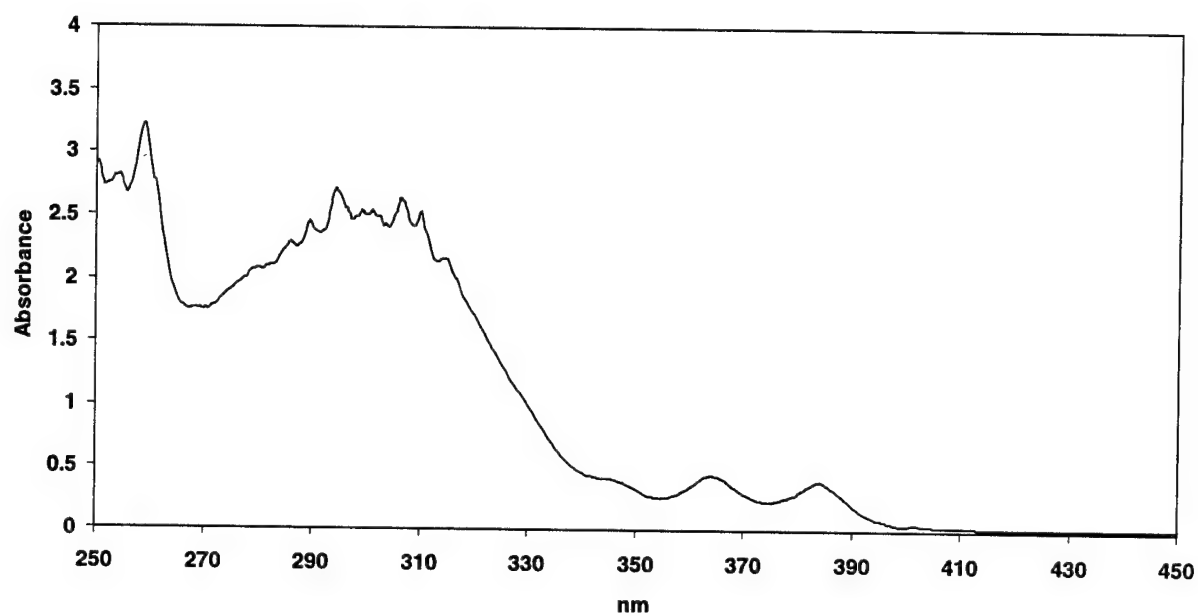
Figure 3.26 UV/Vis of **9** in solution of dichloromethane (1mg/mL)
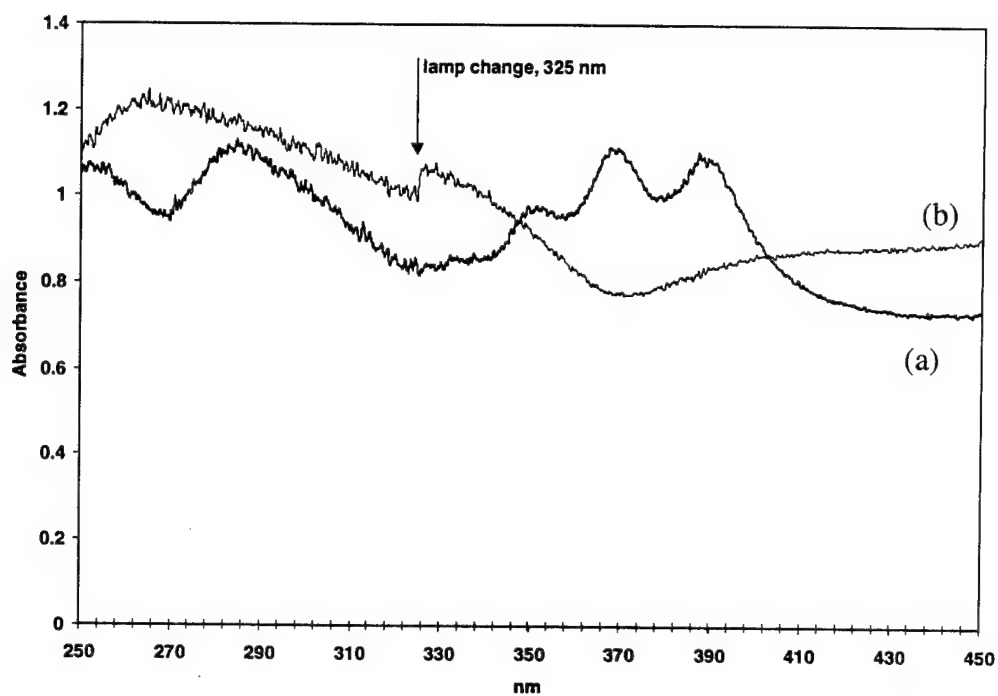
Figure 3.27 UV/Vis of spin coated film of **9** on Si wafer (a) before (b) after 30 minute irradiation with 150 W Xenon lamp
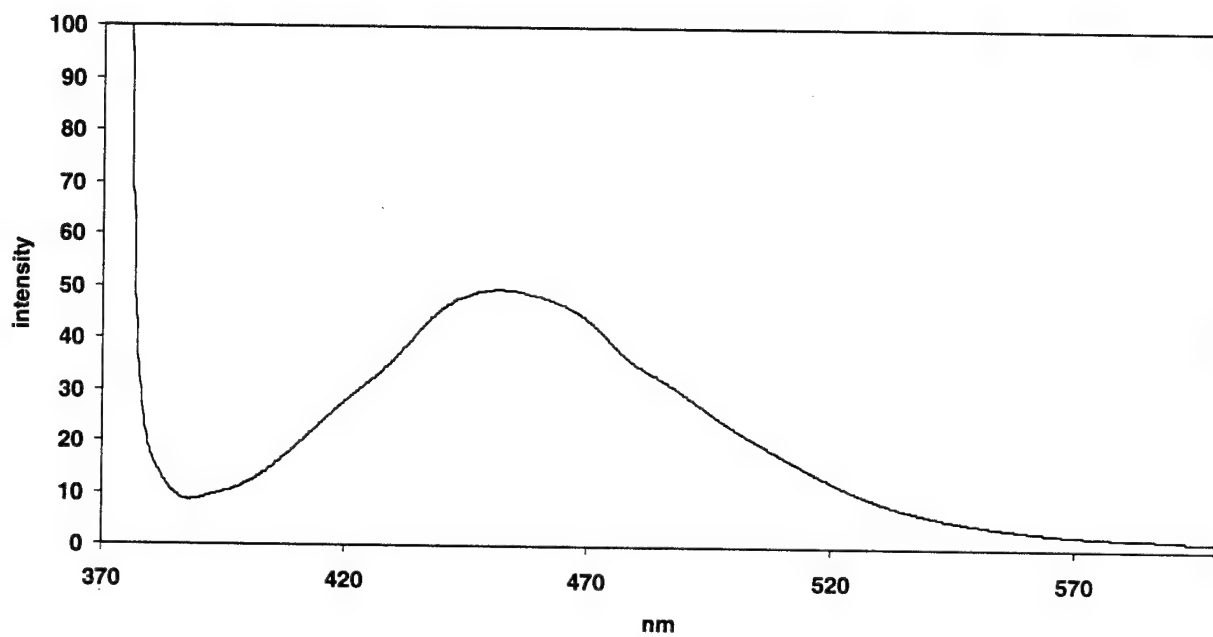
Figure 3.28 Fluorescence spectrum (excitation at 365 nm) of spin coated film of **9** on silicon wafer

silicon wafer. When this same film is then irradiated at >300 nm for 30 minutes, the fluorescent emission is dramatically reduced which indicates a high degree of reaction of the anthracene groups. Figure 3.29(a)-(b) shows the change in fluorescent emission at 450 nm over the excitation range of 220-430 nm for the (a) unirradiated and (b) irradiated film of **9** spin coated on silicon.

3.5.2   *Gel Permeation Chromatography*

Another tool used to characterize the photoproducts of the irradiation of **9** was GPC. Films of **9** were irradiated under various conditions and then removed from the substrate, dissolved in THF, filtered, and injected on the GPC column. Figure 3.30 shows the GPC spectrum of a film of **9** after irradiation with a 150W Xenon lamp for 30 minutes. The major products are the photodimer and the precursor monomer. But there is a small amount of higher molecular weight material above the dimer peak which must be caused by some process other than the photocycloaddition of anthracene. Irradiating films of **9** at 80°C where bulk samples of **9** are in the crystal E phase produced larger amounts of the photodimer. This is thought to be due to reorientation of the liquid crystalline mesogens at elevated temperature from the as-cast state allowing better alignment for photochemical cycloaddition. Figure 3.31 shows the GPC resulting from the irradiation of a film of **9** solvent cast on to glass and irradiated for 20 min with a 150 W Xenon lamp at 80°C. This sample was then used for NMR analysis of the photodimer as described in the next section.

3.5.3   *NMR Analysis of the photodimer*

NMR experiments were done on the photoproducts to prove that the photodimer was actually forming, and to determine whether it was adding in the head-to-head or head-to-
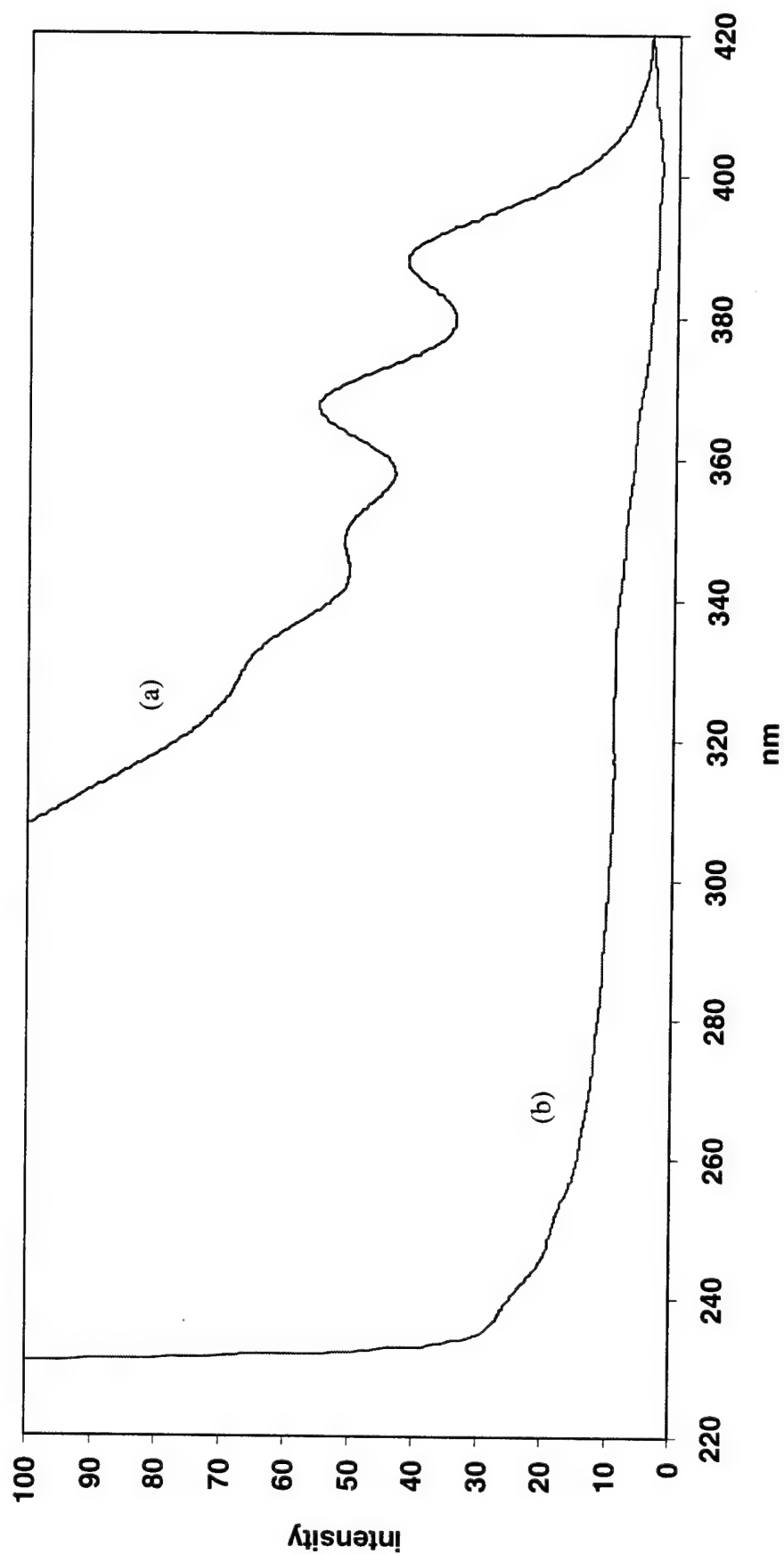
Figure 3.29 Fluorescence spectra (emission at 450 nm) of spin coated film of **9** on silicon wafer (a) before (b) after 30 minute irradiation with 150 W Xenon lamp
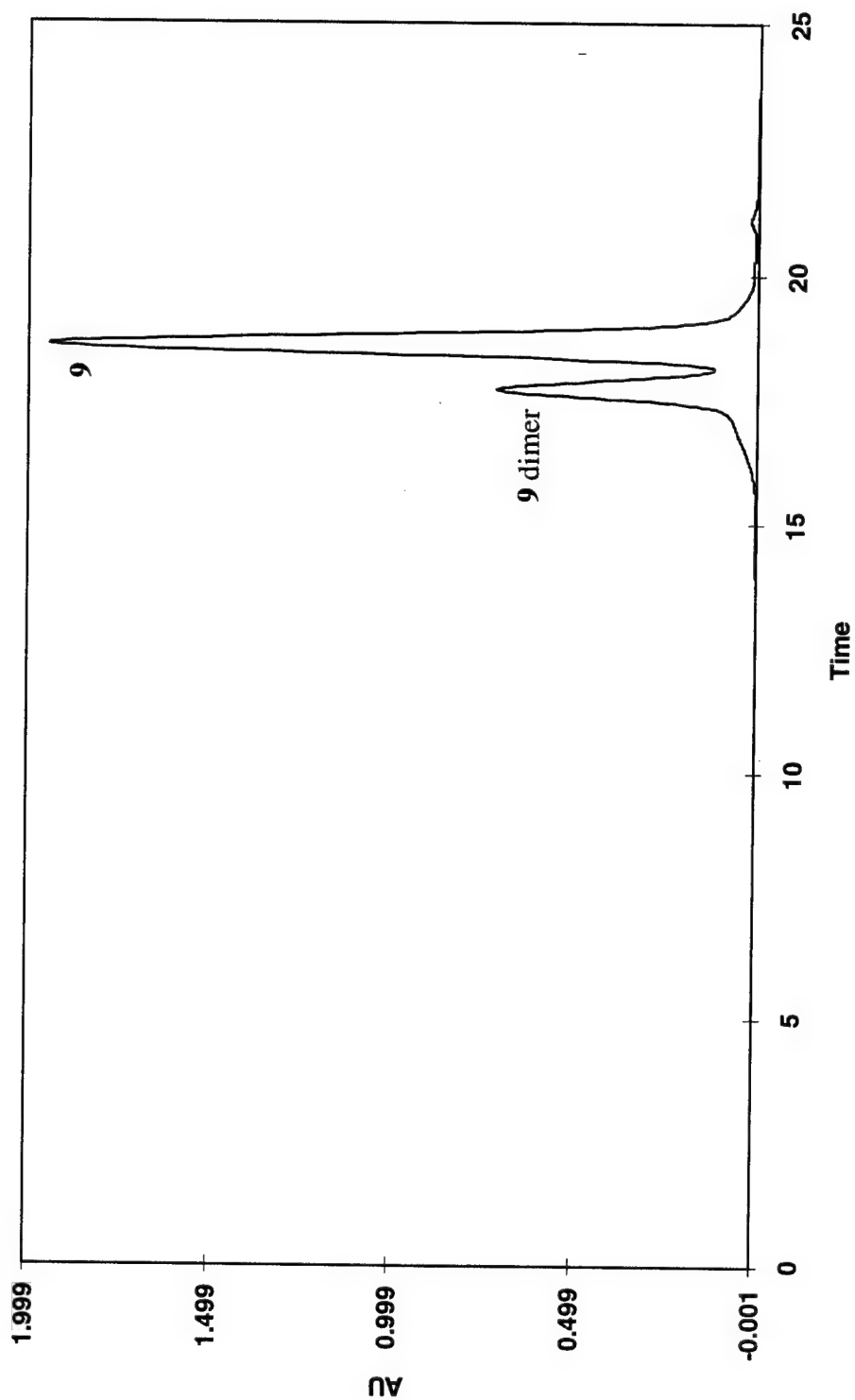
Figure 3.30 Gel Permeation Chromatography of **9** after irradiation in the solid state for 30 minutes with 150 W Xenon lamp
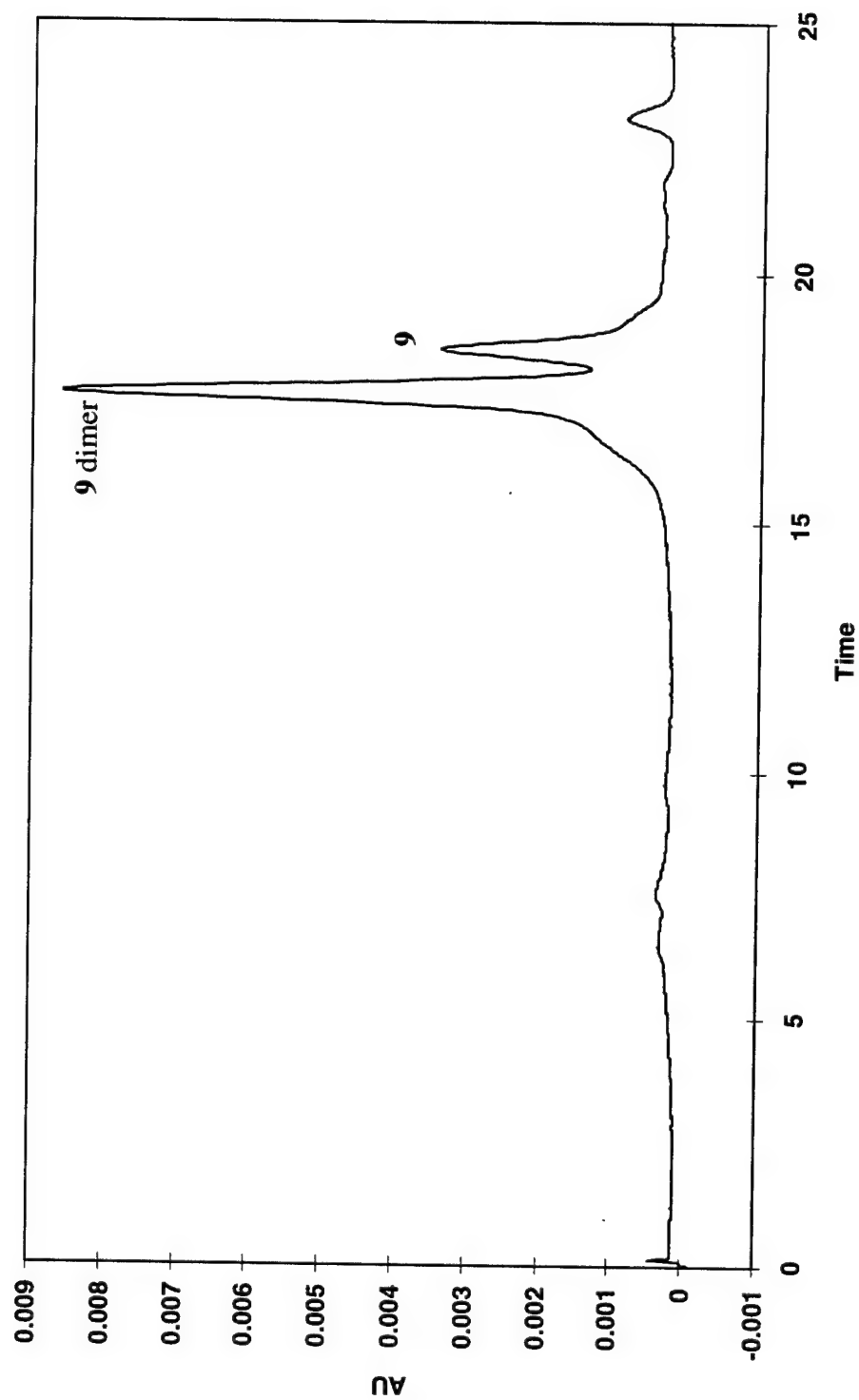
Figure 3.31 Gel Permeation Chromatography of **9** after irradiation for 20 minutes at 80°C yielding greater amount of photodimer compared to Fig 3.28

tail configuration (section 2.2.2.2). Another reason for doing NMR was to determine whether there was any reaction of the diacetylenes during the various irradiation processes.

3.5.3.1 Photodimer of 9-Anthracene Carboxylic Acid

To assist in the characterization of the photodimer of **9**, a simpler photodimer was synthesized from 9-anthracene carboxylic acid. This yellow precursor was dissolved in ethanol, placed in a quartz cuvette with a stir bar, and irradiated for 24 hours at >300 nm. The result of this reaction was a white powder that was not soluble in ethanol and whose proton NMR is shown in Fig 3.32(b) along with the NMR spectrum of the 9-anthracene carboxylic acid precursor, Fig 3.32(a). As shown by the integrations of the peaks, the number of protons has exactly doubled in (b), and the bridgehead proton(s) are now observed at 5.7 ppm instead of 8.6 ppm. Determination of the constitutional isomers (see Fig 2.13) was done by use of ^{13}C satellites as previously done by Chapman.[143, 144] In the head-to-tail configuration [Fig 2.13], the coupling constant between the two bridgehead protons will be close to zero. In the head-to-head configuration, their coupling constant could be expected to be ~6-10 Hz.[143] However, the two bridgehead protons of the anthracene dimer make up an A_2 spin system and thus, J_{AA} can not be determined directly from the proton spectrum. By taking advantage of the 1.1% natural abundance of ^{13}C at one of the bridgehead positions, it is possible to think of the system as a AA'X spin system where X is the ^{13}C attached to one of the bridgehead protons.[145] The results of this experiment are shown in Figure 3.33. Note that the two small peaks closest to the main peak at 5.72 ppm are spinning side bands. The two visible ^{13}C satellites reveal the $^1J(^{13}C\text{-}H)$ coupling constant to be 138 Hz and the J(AA') coupling constant to be zero. Therefore, the product of the photodimerization of 9-anthracene
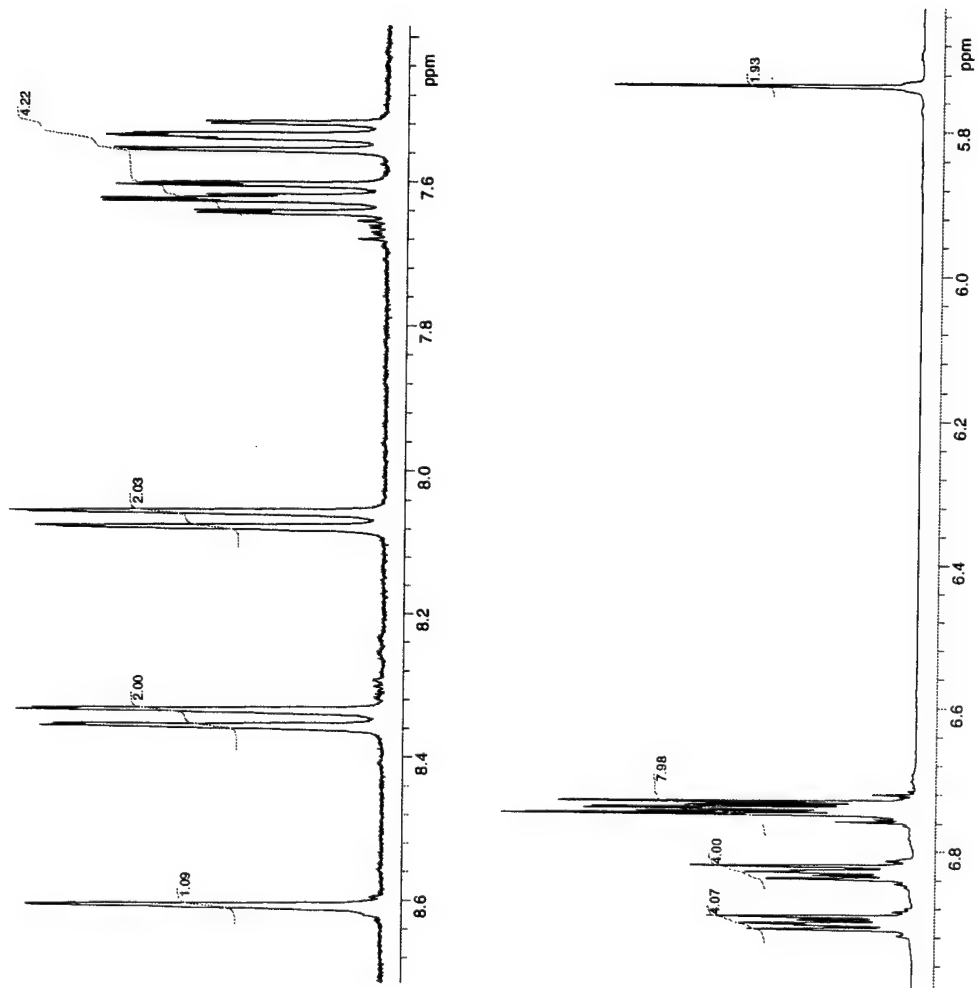
Figure 3.32 Proton NMR of (a) 9-anthracene COOH in CD_3Cl (b) 9-anthracene COOH photodimer in THF-d_6
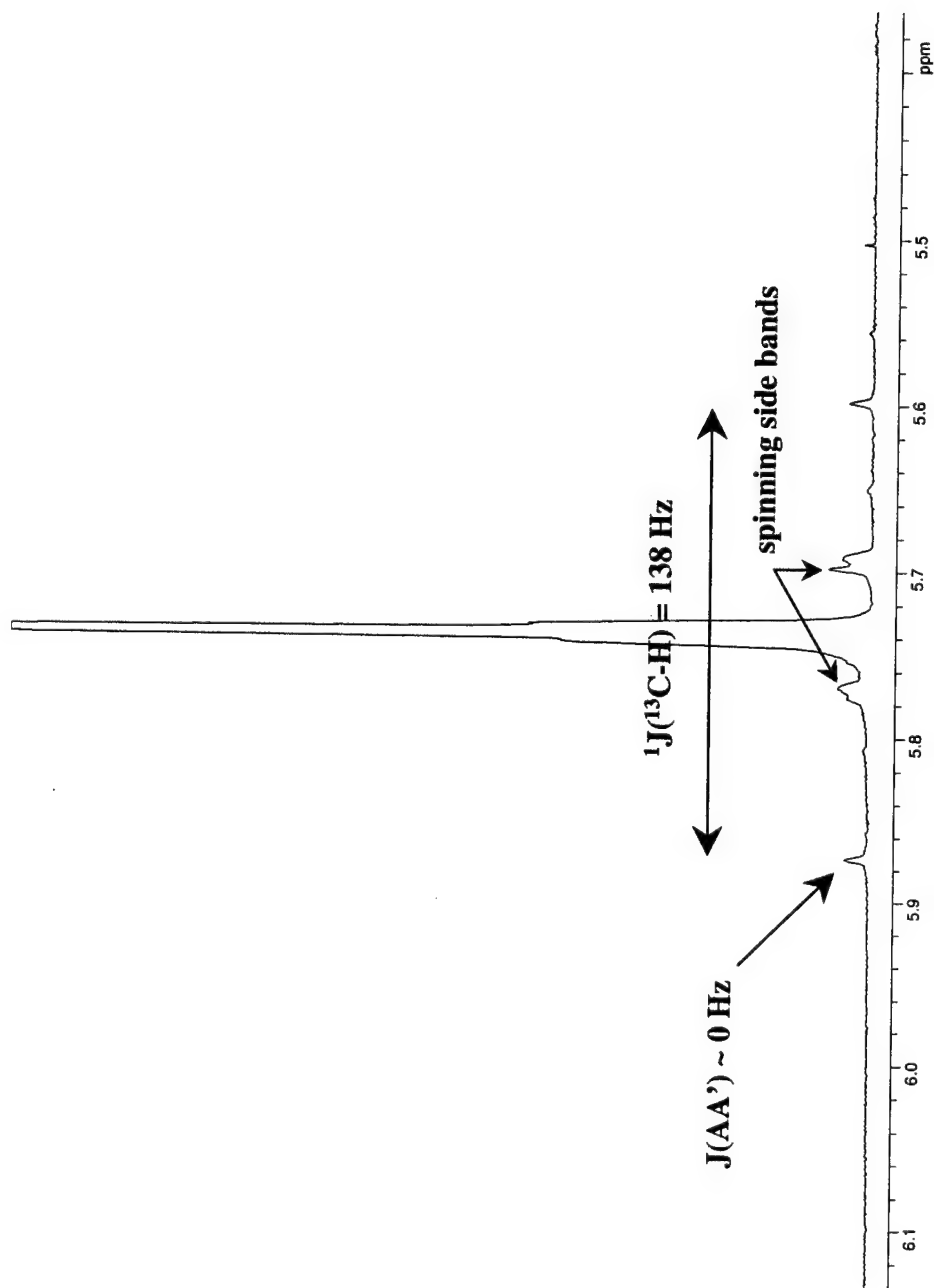
Figure 3.33 Proton NMR of photodimer of 9-anthracene carboxylic acid showing ^{13}C satellites (THF-d_6). No coupling between bridgehead protons is seen, indicating only head-to-tail photocycloaddition

carboxylic acid is head-to-tail in orientation.

3.5.3.2 Photodimer of 9

Characterization of the photodimer of **9** was not done using the ^{13}C satellite method because of a change to deuterated dichloromethane as the NMR solvent and due to the difficulty in making enough material for a concentrated sample. Instead, heteronuclear shift correlation experiments were done to determine the configuration of the photodimer. Specifically, inverse correlation techniques were used due to the increase in sensitivity (eight fold over a conventional HETCOR) gained by detecting the C-H correlation through the proton rather than the carbon.[146, 147] The results of proton NMR of the precursor **9** and its photoproducts are shown in Figure 3.34(a)-(b). Integrating the bridgehead protons at 5.7 ppm indicates that ~76% of the material has formed the photodimer. Integration of the precursor peak at 8.5 ppm indicates ~14% unreacted monomer. The last 10% of material may be explained by the high molecular weight shoulder seen in the GPC trace, [Fig 3.31]. Both Heteronuclear Multiple Quantum Coherence (HMQC) and Heteronuclear Multiple Bond Coherence (HMBC) experiments were done on the photoproducts of **9** to determine the constitutional isomers. The HMQC experiment is designed to correlate carbon and proton nuclei through ^{1}J(C,H).[147] The HMBC experiment correlates carbon and proton nuclei through ^{2}J(C,H) and ^{3}J(C,H) couplings. The goal of these experiments was to determine which carbon atoms the distinct bridgehead protons were coupling to through spin-spin coupling. Because of the wealth of information provided by these experiments, it is possible to assign the photodimer isomers by matching a handful of different correlations. Perhaps the most direct route is to determine whether the bridgehead protons are coupled to the carbonyl
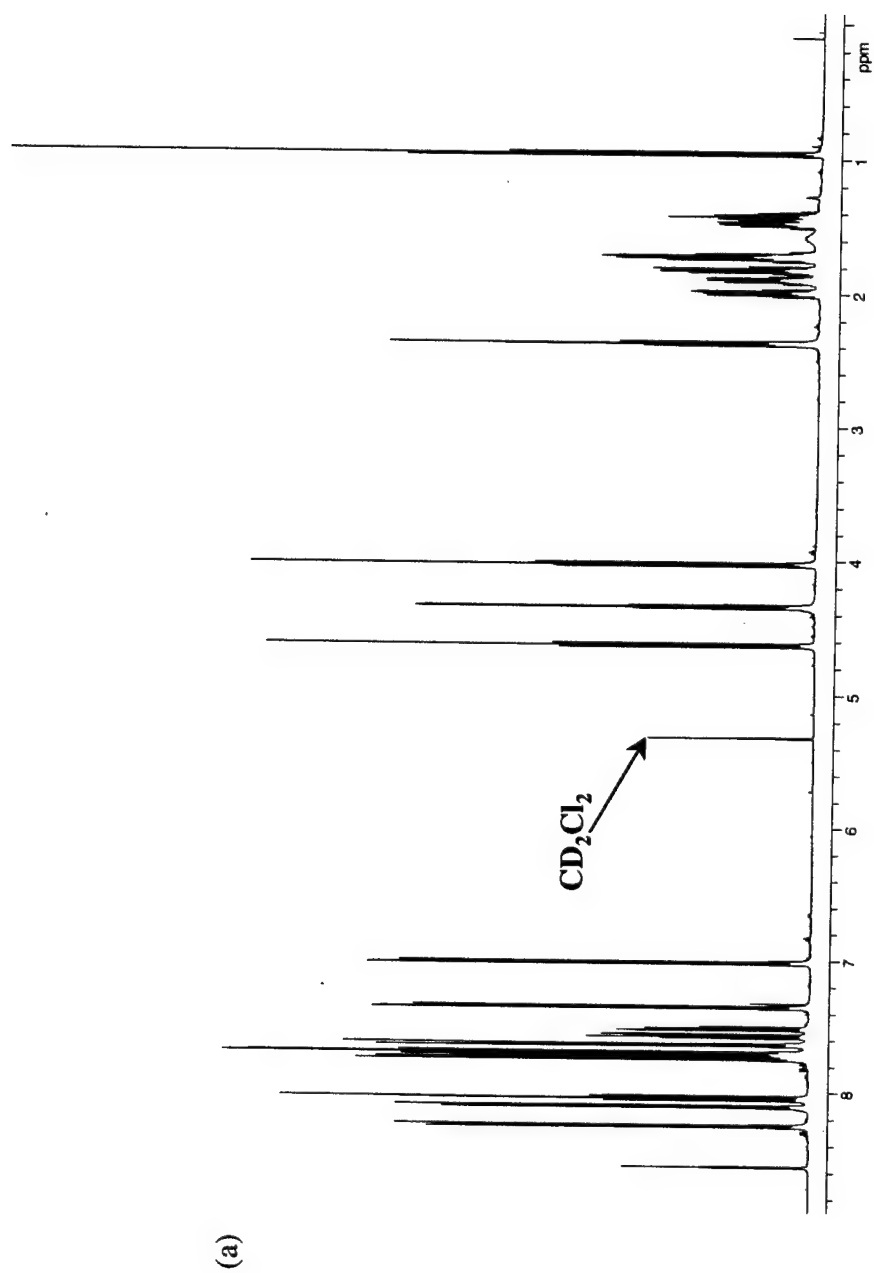
Figure 3.34 Proton NMR of (a) precursor **9** in CD_2Cl_2
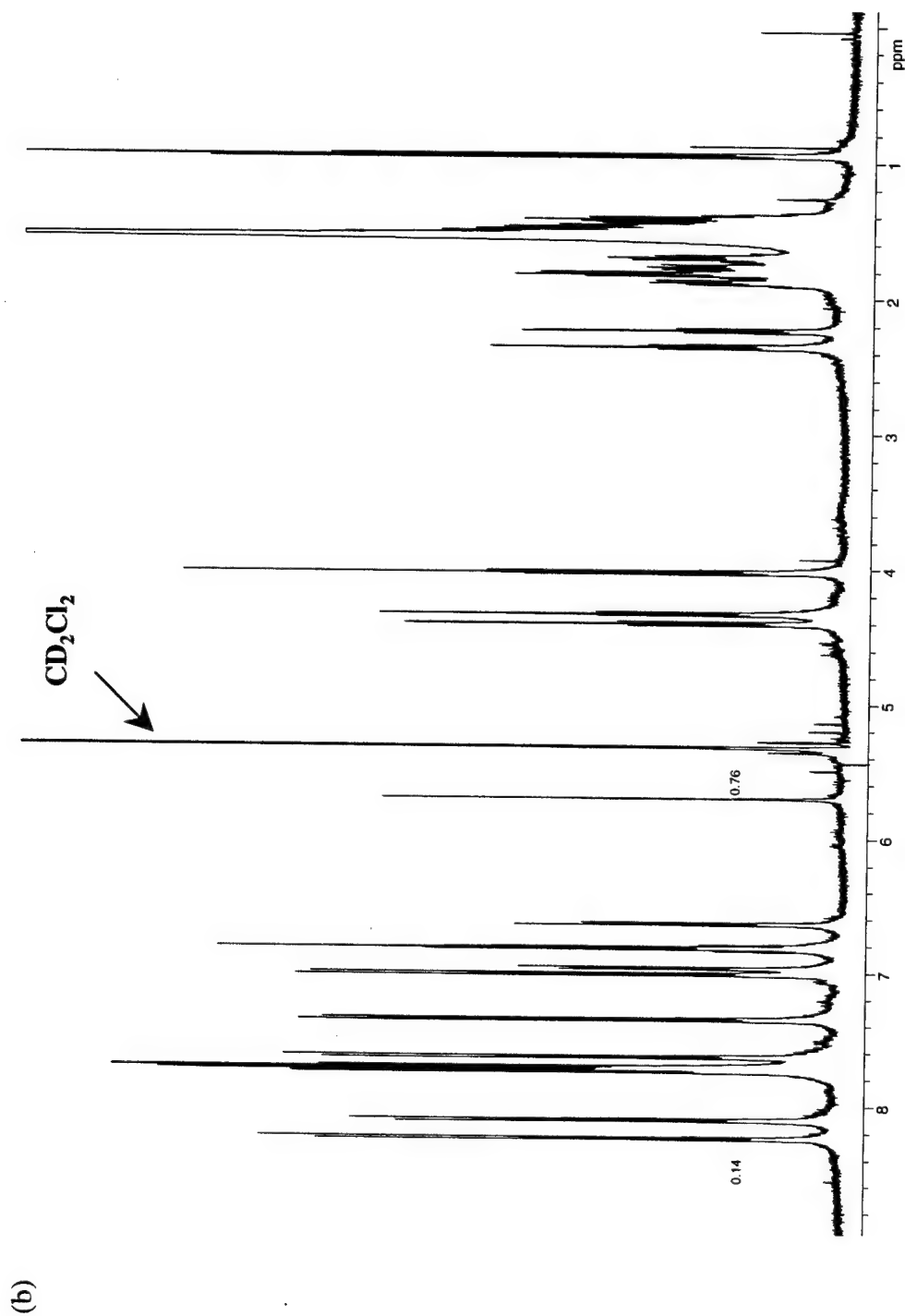
Figure 3.34 (cont.) (b) photoproducts after irradiation of **9** for 20 minutes at 80°C in CD$_2$Cl$_2$. Integration at 8.5 ppm is for unreacted **9**; integration at 5.7 ppm is for **9** photodimer

(b)

carbons of the adjacent anthracene group in the dimer (both photodimers are explicitly shown in Figure 3.24). If the photodimers are formed head-to-head, then coupling between the bridgehead proton and a carbonyl carbon would be $^5J(C,H)$ or $^6J(C,H)$ which would not be detected by the HMBC experiment which is tuned to look for $^2J(C,H)$ and $^3J(C,H)$ couplings. Conversely, if the photodimers are formed head-to-tail, then the bridgehead protons and the carbonyl carbons would have $^3J(C,H)$ coupling which should be detected by HMBC. Figure 3.35 shows a portion of the HMBC spectrum taken of the photoproducts of **9**. The signal for the carbonyl carbon attached to anthracene is 175 ppm. As can be seen in the HMBC spectrum, there is coupling between the bridgehead proton at 5.7 ppm on the proton axis, and the carbonyl carbons at 175 ppm on the carbon axis. Therefore, the photodimer of **9** was also found to be the head-to-tail dimer. This same analysis was also done on the 9-anthracene carboxylic acid photodimer discussed in section 3.5.3.1 and confirmed the results of the ^{13}C satellite experiment.

Substantial solubility differences were generated between the irradiated and unirradiated material (which was used to do lithography as described in Chapter 4). This was initially thought to be due to a combined anthracene photodimerization and diacetylene polymerization. At this time, the only direct evidence for higher molecular weight material comes from GPC traces of irradiated material. When these same films are placed in deuterated dichloromethane, there is a substantial amount of material that is not soluble and no poly(diacetylene) is detected. The ^{13}C signals for the diacetylene and soluble polydiacetylene carbons are well reported in the literature and shown below with the values in ppm placed over the corresponding carbon atom:[148-150]

—CH₂—C≡C—C≡C—CH₂— ⁶⁵ ⁷⁵ ¹⁹

C—C≡C—C ¹⁰⁰ ¹²⁹ ³⁵ CH₂

diacetylene group   poly(diacetylene) chain
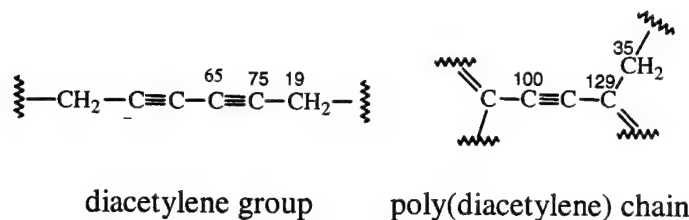
To confirm whether diacetylene reaction was occurring, carbon NMR was done on the same photoproducts of **9** that were investigated above by proton NMR. A portion of the carbon spectrum is shown in Figure 3.36 with the characteristic signals for the alkyne carbons marked. There are no peaks that would correspond to carbon atoms on a polydiacetylene chain at 100 or 35 ppm (the region around 129 ppm is masked with other aromatic carbon atoms). Therefore, it was concluded that no soluble poly(diacetylene) products were formed in films irradiated with light >300 nm. There is the possibility that any poly(diacetylene) formed is not soluble and thus would not be detectable by either NMR or GPC. More indirect evidence for the reaction of the diacetylene groups is given in Chapter 4 in comparisons of **9** and **11** as photoresists. Films were also irradiated with 254 nm irradiation in an attempt to react the diacetylene groups but again no polydiacetylene could be detected.

3.6 Reaction at higher temperature

As was mentioned in section 3.4, molecule **9** has the potential to form a two-dimensional structure, if certain requirements are met. These requirements are the formation of a layered structure, a significant amount of diacetylene polymerization, and the photodimerization of the anthracene end groups. From the above discussion, it is apparent that **9** readily forms layers, some of which are highly ordered, i.e. S_B^h and crystal E phase. The head-to-tail photodimer [Figure 3.24(b)] was the primarily product when films of **9** where irradiated
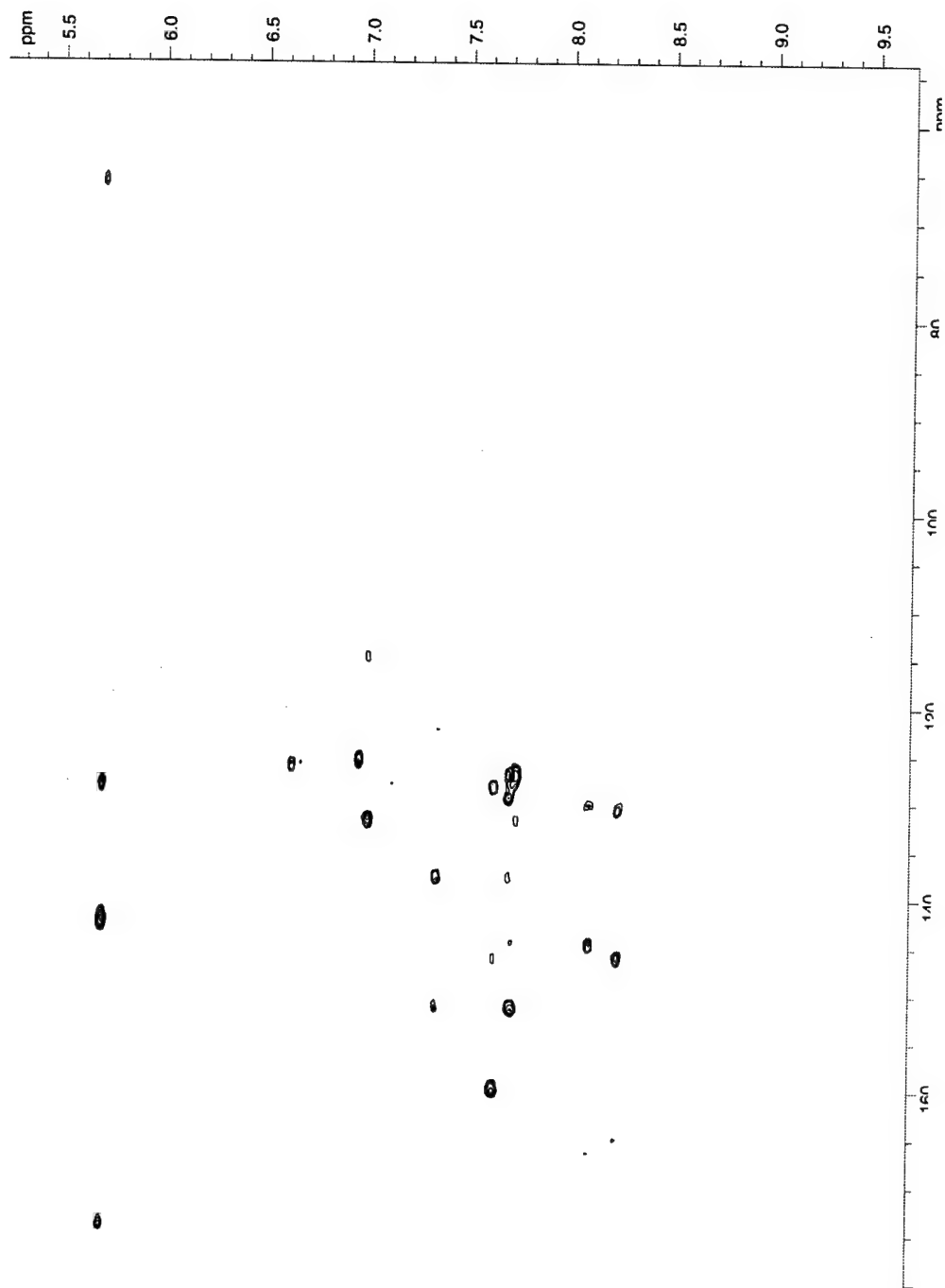
Figure 3.35 Heteronuclear Multiple Bond Correlation spectrum of photoproducts of **9** in CD$_2$Cl$_2$
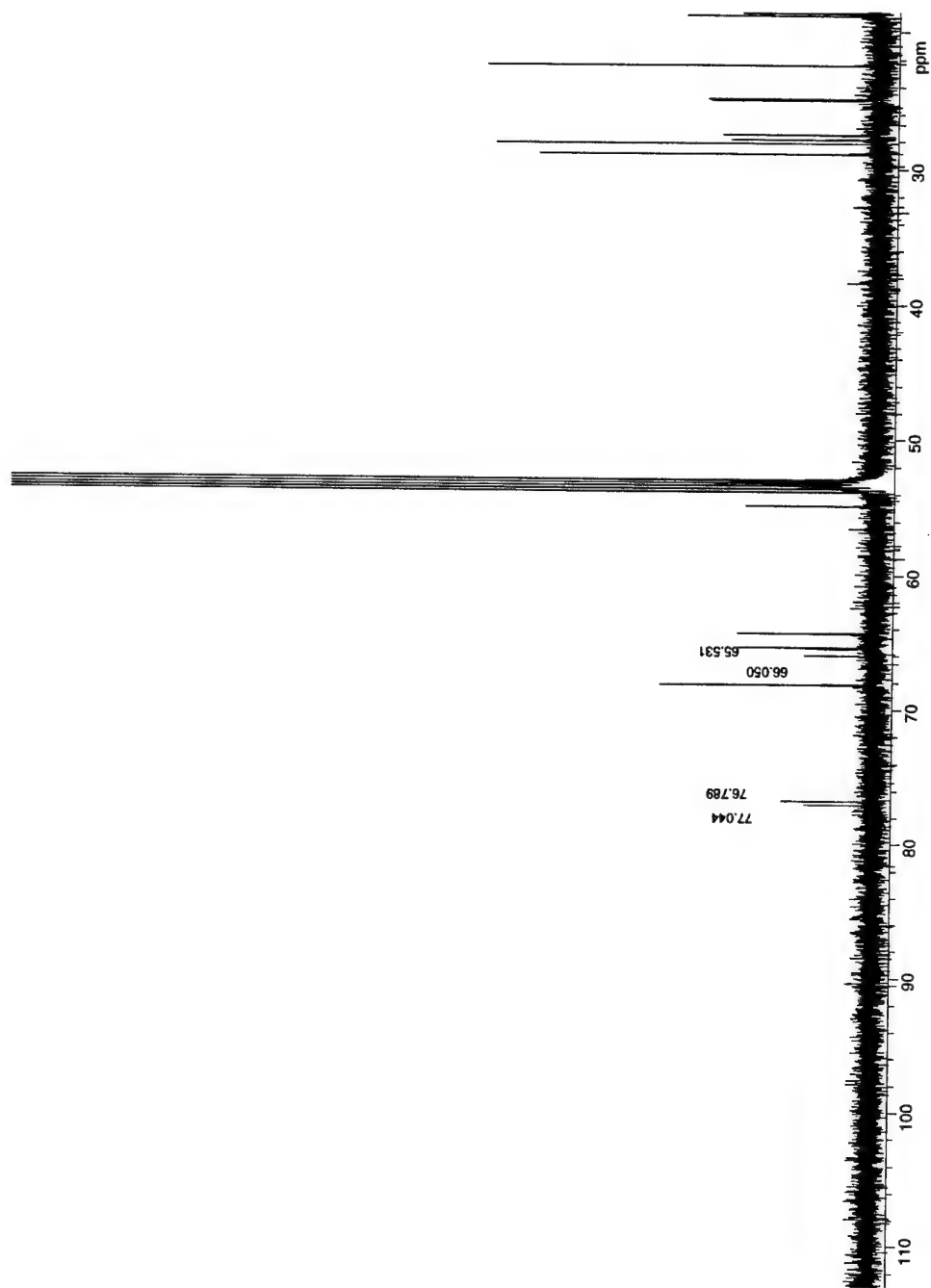
Figure 3.36 Carbon NMR of photoproducts of **9** in CD$_2$Cl$_2$

in the crystal E phase. Diacetylene polymerization to form poly(diacetylene) chains was not observed which may be expected due to the structure of the head-to-tail dimer, or dimesogen, which separates the two diacetylene groups rather than bringing them closer as would be the case in the head-to-head dimesogen [Figure 3.24(a)]. Because the diacetylene reaction is necessary for the formation of two-dimensional structures in this system, attempts were made at higher temperature to determine whether diacetylene polymerization could be induced in the other layered mesophases of the material. Films of **9** were irradiated in the S_B^h and S_A mesophases at 120°C and 145°C, respectively. Irradiation was done for 1 hour in both cases and the resulting GPC traces are shown in Figure 3.37. The peaks representing the mesogen and dimesogen are labeled on the traces. There is a dramatic decrease in the amount of the dimesogen formed at 145°C vs. 120°C. This may be due to the decreased order in the S_B^h and S_a mesophases leading to a smaller number of favorable interactions for photodimerization between adjacent anthracene molecules. A more likely reason is the known reversibility of the photodimer at elevated temperatures. This is observed in the proton NMR spectrum of the 145°C irradiated sample by an increase in the integrated regions of the monomer compared to the 80°C irradiated sample.

The shoulder in the GPC trace to higher molecular weight of the dimesogen peak has an onset of ~100,000 daltons in both spectra. This is believed to be due to some reaction in the diacetylene groups leading to some of the one dimensional materials drawn in Figure 3.** or possibly to two dimensional materials. A portion of the film irradiated at 145°C was not soluble in NMR solvent which may explain why no poly(diacetylene) chains were detected. Both the monomer, **9**, and the dimesogen were soluble and characterized by GPC and NMR. Poly(diacetylenes) are known to be insoluble which may mean that diacetylene reaction
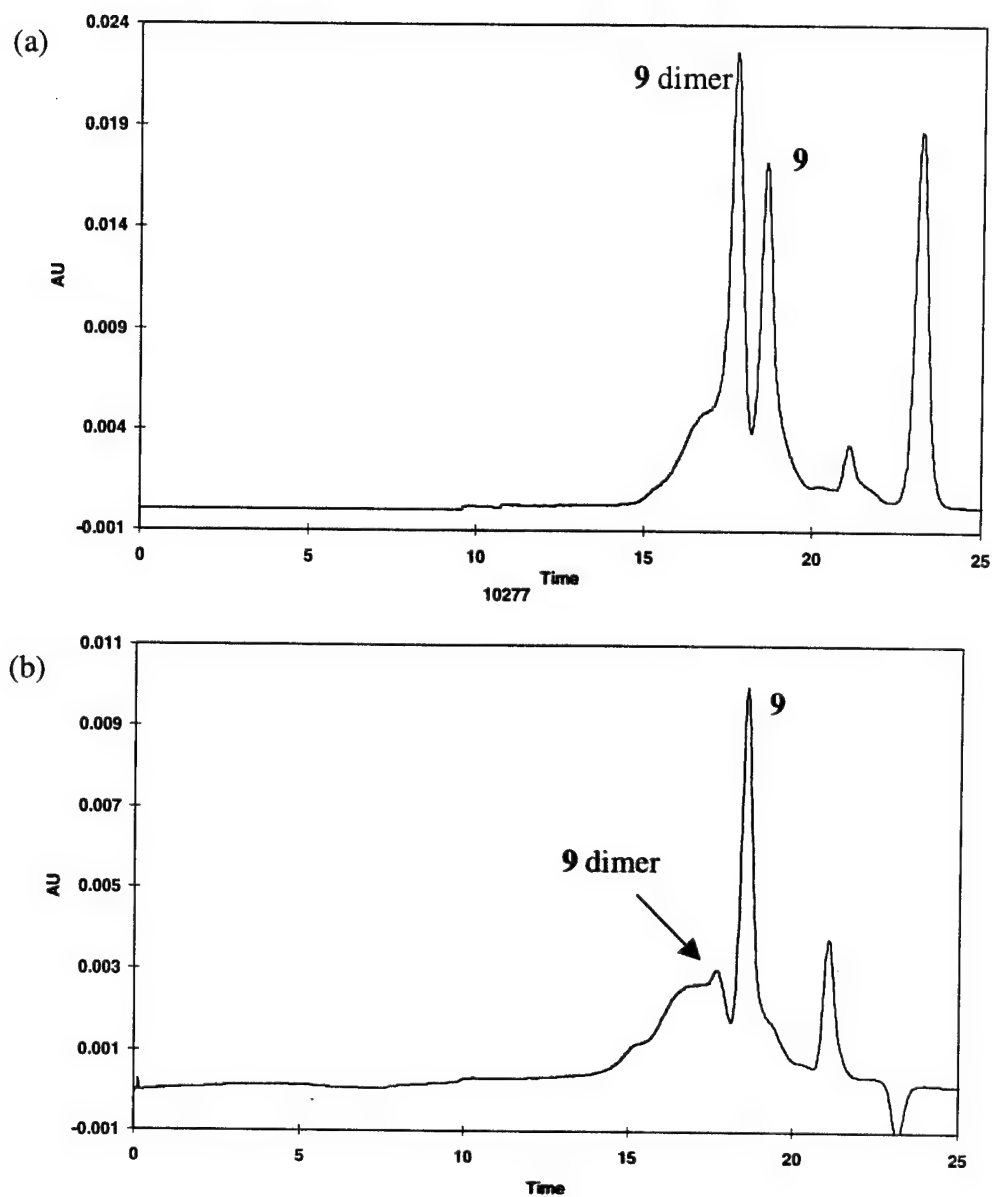
Figure 3.37 Gel Permeation Chromatography traces of (a) **9** irradiated for 1 hour at 120°C (b) **9** irradiated for 1 hour at 145°C

did occur and the formation of two dimensional objects can not be ruled out. Besides topochemical reaction of the diacetylenes, another explanation for the higher molecular weight material may be the known formation of endoperoxides when anthracene is irradiated with UV light in the presence of O_2.[92]
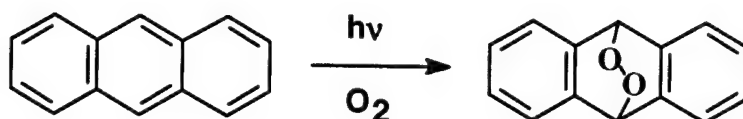
This endoperoxide may possibly initiate reaction with adjacent mesogens, and dimesogens to produce the higher molecular weight materials seen in the GPC traces in Figure 3.37.

3.7 Conclusions

Three structurally related liquid crystals were analyzed by DSC, POM, and X-ray diffraction to determine their mesophase behavior. The addition of anthracene with its long axis perpendicular to the main mesogen did not destroy molecule 8's ability to form anisotropic phases, and in fact enriched the mesomorphism. Removing the diacetylene moiety from the 12 carbon chain linking the main body of the mesogen with the anthracene, did not change the mesomorphism although it did allow 11 to crystallize. It was also determined that the extent of reaction of the anthracene groups in films of 9 irradiated in the crystal E phase was high, ~76% was converted to photodimer. Various NMR experiments were used to determine that the photodimer of 9 was formed in a head-to-tail fashion which is the usual case. No reaction of the diacetylene groups to form polydiacetylene was detected by NMR although there were insoluble products formed in films irradiated at 145°C which may represent very high molecular weight material linked by poly(diacetylene) chains and

anthracene photodimers.. The ability of **9** to form a two-dimensional structure at lower temperatures was hampered by the lack of topochemical reaction in the diacetylene groups. But the anthracene group was successfully photodimerized under various conditions and this reaction led to a significant change in the solubility of the products which was utilized in the next chapter dealing with lithography using reactive liquid crystals.

Chapter 4 Lithography with Reactive Liquid Crystals

4.1 Introduction

During the study of the photochemical reactions of **9**, a test was done to determine applicability as a photoresist using a TEM grid as a mask. Early experiments were successful in transferring the TEM grid pattern onto both glass and silicon wafers. Therefore, further investigation of lithography with **9** was begun. Lithography is the process of transferring a pattern from a mask to the surface of a substrate.[151, 152] In photolithography, light is passed through the mask to irradiate a photoresist layer in specific regions (Fig. 4.1). The pattern of the mask is imparted onto the photoresist layer through some type of photochemical reaction that causes a change in the solubility of the irradiated photoresist. The resist is then developed with a solvent system to produce a replica of the mask on top of the substrate. The photoresist then protects the substrate from various etching processes that transfer the mask pattern to the substrate. Thus the photoresist acts to 'resist' the etchant. Finally, a stripping process removes the photoresist and the substrate is ready for the next fabrication step.

As illustrated in Fig. 4.1, there are two general type of photoresists: positive and negative. The first resists used in integrated circuit fabrication produced a negative image and thus were called negative resists.[153] Irradiation of a negative photoresist layer through a mask creates patterned regions of relative insolubility (usually by crosslinking to form a network) compared to the unreacted photoresist. Rinsing with organic solvent washes away any portions that are not crosslinked and a pattern is left behind on the substrate. A positive resist works in the opposite fashion. The positive resist layer is insoluble in the development solution (commonly aqueous base) and only the regions that are irradiated become soluble and can be washed away. The manner in

LIGHT
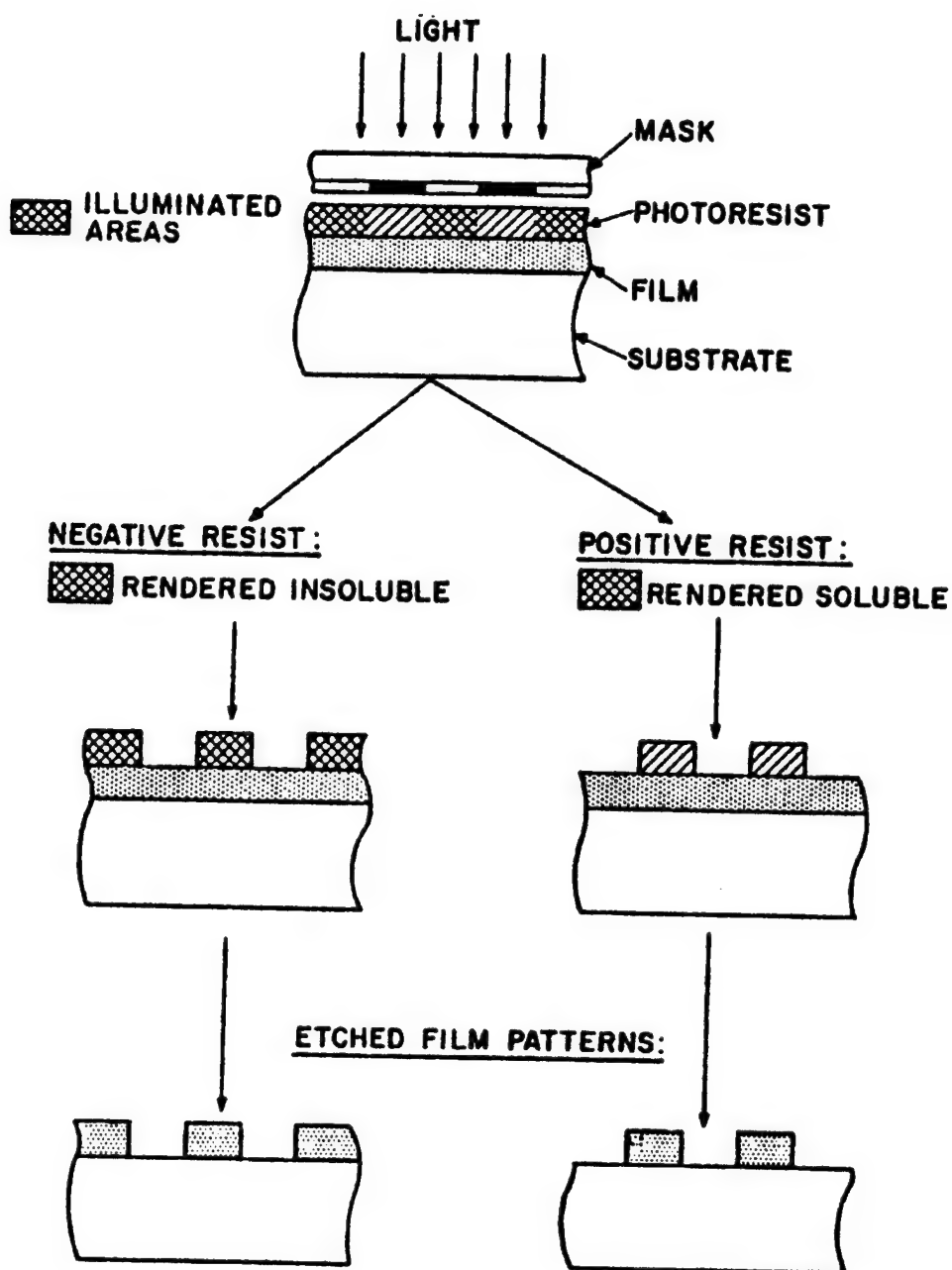
Figure 4.1 Exposure and development of positive and negative photoresists with subsequent etching of the substrate. Reprinted with permission from *Introduction to Microlithography* Thompson, L.F., Willson, C.G., Bowden, M.J., ed. (1983). Copyright 1983 American Chemical Society

which the negative and positive photoresist create a solubility difference is important in obtaining features of sub-micron size because of the nature of their respective development processes.[153, 154] In the negative photoresist process, the photoresist layer is completely soluble in the development solvent before the exposure. After exposure, while the crosslinked regions in the negative resist do not dissolve, they do swell in the developing solution which is a problem when trying to create sub-micron features. Thus, traditional negative resists see limited use in current semiconductor fabrication processes.[155] The effects of swelling can be lessened in some cases by rinsing the developed pattern with a sequence of solvents that have less and less affinity for the polymer resist.[151] Negative resists that generate insolubility by changing the polarity also avoid the problem of swelling.[156]

Frechet and co-workers introduced the important concept of chemical amplification to the field of photoresist chemistry in 1982.[157, 158] The photoresist developed by this group was a mixture of the polymer poly[4-[(*tert*-butyloxycarbonyl)oxy]styrene], **16**, and triphenylsulfonium hexafluoroantimonate, **17**.[159] The polymer, **16**, has labile *tert*-butyl carbonate groups which can be removed in the presence of a strong acid and mild heat. The onium salt, **17**, is a photoactive compound that generates a strong Lewis acid upon irradiation at 254 nm.[160] This photoactive group is often referred to as a photoacid generator (PAG).

Cleavage of the *tert*-butyl carbonate groups leads to the formation of polar phenol groups
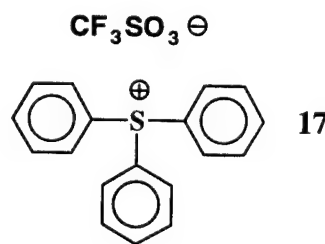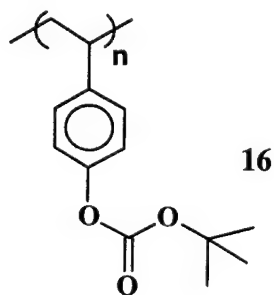
making that region of the polymer film soluble in aqueous base. Because the acid cleavage of t-butyl carbonates is catalytic, smaller exposure doses are required than with conventional, dissolution inhibitor positive resists.[161] Another feature of this photoresist system is the ability to act as either a positive or negative resist, depending on the development solvent. If nonpolar solvents are used, then the unirradiated regions of the polymer, still protected by the t-butyl carbonate groups, will dissolve leading to a negative image of the mask. Additionally, development with aqueous base will wash away the irradiated regions, containing polar phenol groups, leaving behind a positive image of the mask. Because polarity changes cause the differences in solubility, swelling is not a problem for this system acting in the negative mode. Acting as a negative photoresist for electron beam lithography, this system achieved 19 nm features.[162]

Current state of the art photoresists all tend to work in a positive manner using chemical amplification processes to generate solubility differences. Because exposure wavelengths are moving below 248 nm to Deep UV (DUV) wavelengths such as 193 nm, the polymer matrix is continually changing to those polymers with optical transparency in the DUV.[8, 9, 163] The polymer must also have adequate film-forming, adhesion, and etch resistance ability, as well as optical transparency at that exposure wavelength.[9, 151, 155]

4.2 Liquid Crystal Lithography

In light of the above discussion, it is clear that using molecule **9** as a photoresist is a new approach to photoresist formulation. This photoresist system consists of only two components, liquid crystal **9** and a solvent since the photoactive group is part of the molecule itself. Covalently attaching the photoreactive group to the polymer matrix of conventional

photoresists is common[152], but it is uncommon to replace the polymer matrix with a single molecule, liquid crystalline medium. As mentioned above, the polymer is important for film forming capability, adhesion, and etch resistance of the photoresist. Using a liquid crystalline substance to achieve or improve these same properties is a new approach and will be discussed below.

Anthracene has been incorporated into many polymeric and oligomeric systems to take advantage of its crosslinking and fluorescent abilities.[164-170] Some researchers have investigated a series of low molecular weight, alkyl systems which are bis- and tris-substituted with anthracene (**18-19**).[141, 171] These materials have been investigated for potential

18

19
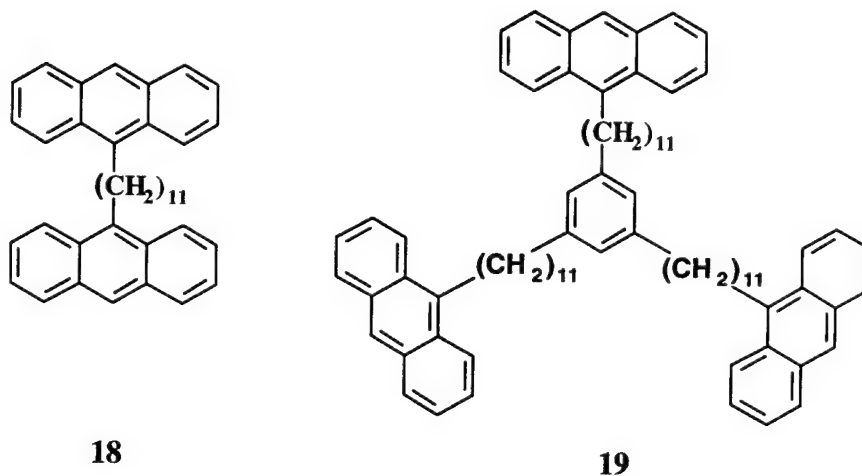
read/write and optical waveguide applications. These oligoanthrylenes are spin coated into films that are then irradiated with UV light to change various properties such as refractive index, and fluorescence due to anthracene cycloaddition. Only the trichromophoric material, **19**, is reported to give a solubility change adequate for negative photoresist application.[141]

These materials are not reported to be liquid crystalline and thus will form amorphous films much different than those of **9**.

4.3 Results

4.3.1 TEM Grid Mask

The first attempt at lithography was done on films cast from chloroform onto glass. A TEM grid with ~40 μm features was held in contact with a film of **9** using another glass slide. The film was irradiated with a 150 W Xenon lamp for 22 hours under nitrogen, then developed by rinsing with dichloromethane (10 mL). A negative image of the TEM grid was left on the glass as shown in the optical microscope image [Fig 4.2]. Optical microscopy done on the irradiated and developed films revealed that the remaining pattern was birefringent and did not go isotropic up to 250°C. Placing a cover slip on top of the film and shearing had little effect on the lithographic pattern which retained its features. Scanning electron microscopy (SEM) was used for closer inspection of the same pattern, this time formed on silicon [Fig. 4.3]. Note that [Fig 4.3 (a)] is an image of the photoresist pattern and the dark square regions are photoresist. Shown in [Fig 4.3 (b)] is the TEM grid used as a mask where now the square regions are holes and the light regions are the copper grid. A higher magnification SEM image of the photoresist pattern and the TEM grid mask are shown in Fig 4.4 (a) and (b) revealing clearly the replication of the mask by irradiated **9**. The silicon substrate, photoresist, copper grid, and holes are indicated in Fig 4.4.

As discussed in Chapter 3, photodimerization of the anthracene group leads to a change in its fluorescent properties. Specifically, fluorescence at 450 nm is destroyed in dimerized structures. Therefore, it is possible to write patterns into a film of **9** that can be
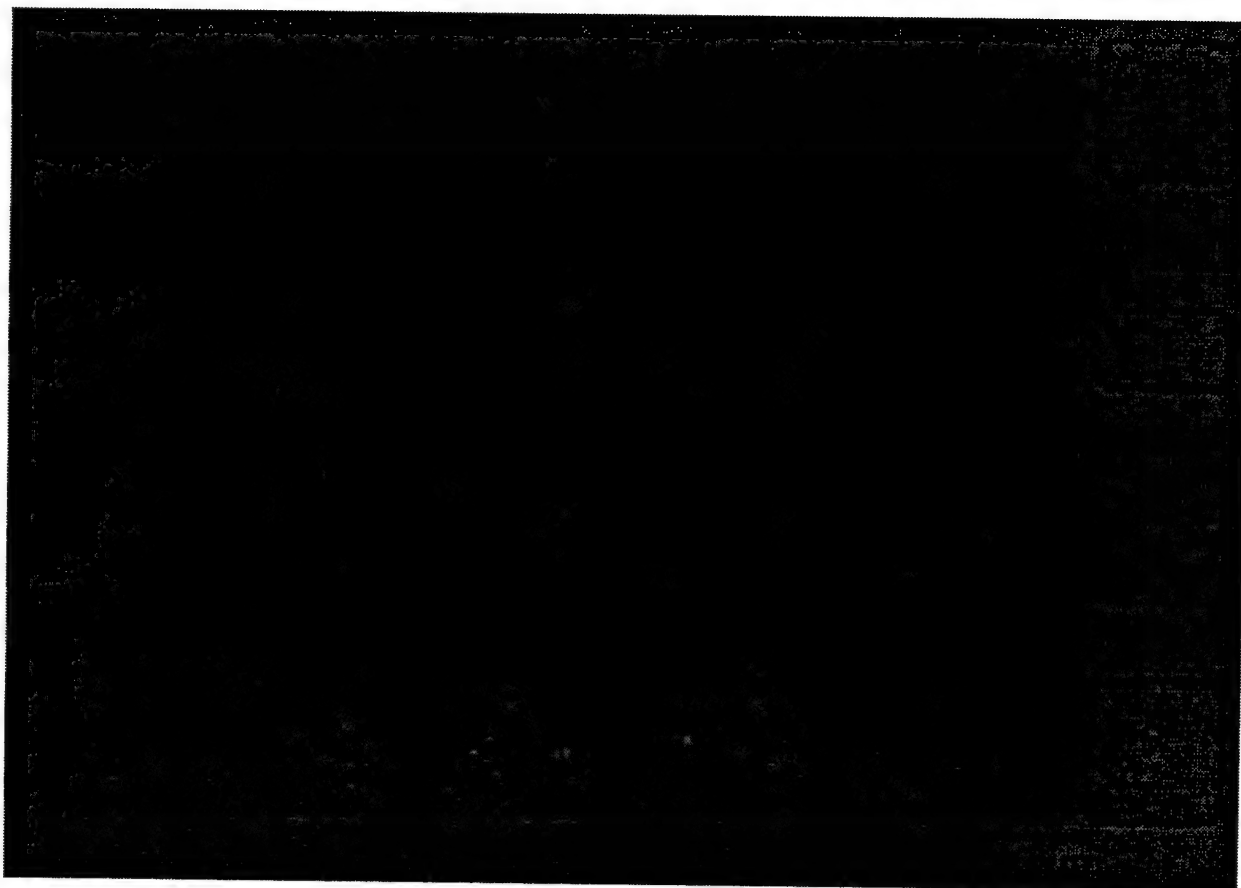
Figure 4.2 Optical micrograph of photoresist **9** patterned onto glass with a TEM grid

(a)
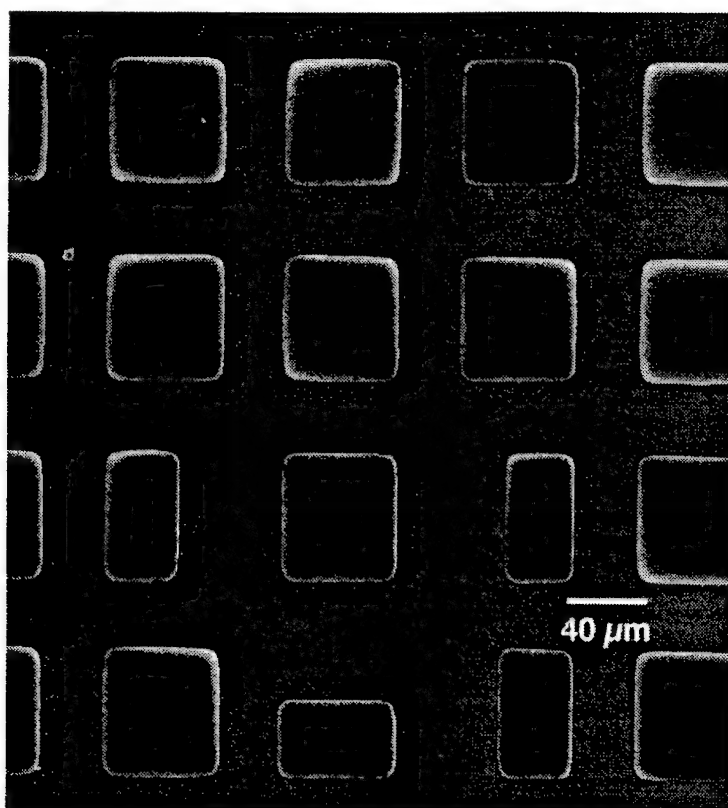
(b)
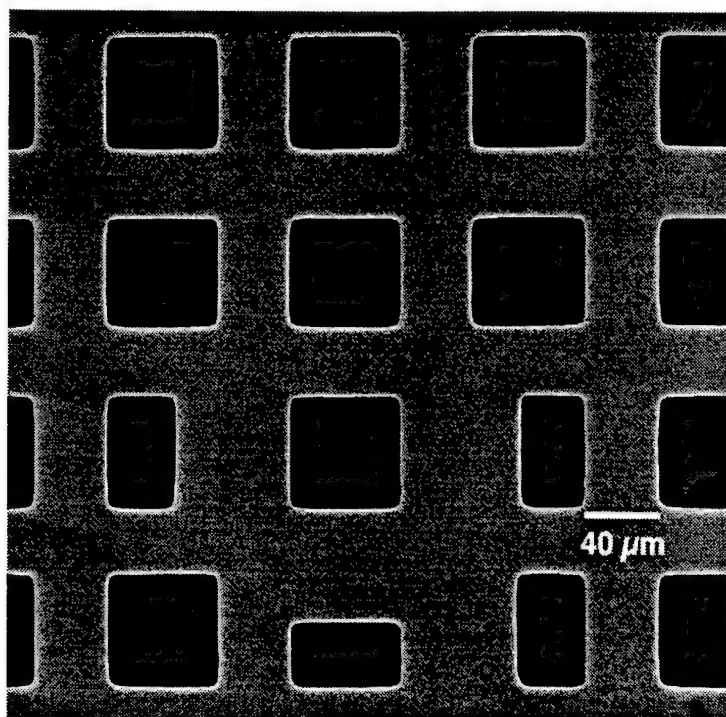
Figure 4.3 Scanning Electron Microscopy images

(a) patterned film of **9** on a Si wafer

(b) TEM grid used as a mask for patterning **9**
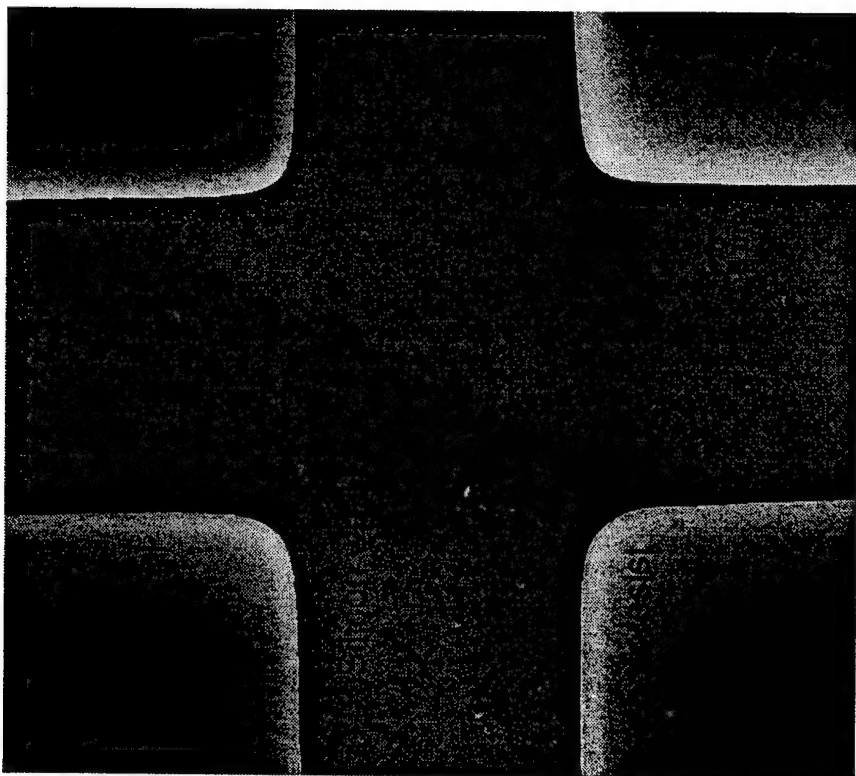
(a) Lithographic pattern of **9** on silicon wafer
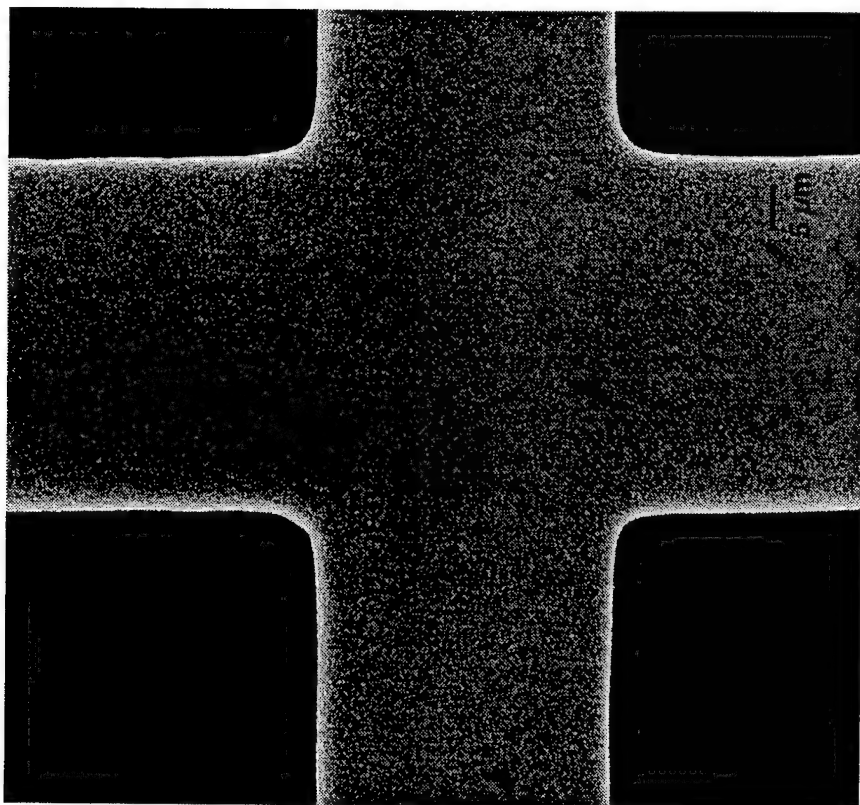
(b) TEM grid used as a mask to obtain (a)

Figure 4.4 Scanning Electron Microscopy images of photopatterned **9** and TEM grid mask

read based on the change in fluorescent properties after exposure and requires no solvent development at all. Figure 4.5 is an image taken with the optical microscope of a film of **9** that has been exposed through a TEM grid mask but not developed with solvent. The film is being excited from above with 365 nm radiation using a thin layer chromatography lamp, producing the fluorescing blue grid. Because the film is on a silicon wafer, the picture was taken with the microscope in reflectance mode with all light being collected for the picture coming from the fluorescence of the unreacted anthracene groups.

4.3.2 Higher Resolution Lithography

Previously, films were simply used as cast from solvent. For better control over film thickness and uniformity, it was necessary to apply the films with a spin coater. Another improvement in the lithography investigation was replacement of the TEM grid mask with a chrome on quartz mask with ~3-5 μm features. Films of **9** were spin coated from chloroform solutions (40 mg/mL) onto silicon wafers, with and without native oxide layers. Film thicknesses were 200-300 nm as measured by ellipsometry. These films were then exposed for 30 minutes with a 150 W Xenon lamp using a glass slide to cut off light < 300 nm. The films were then developed by flushing the wafer surface with 10 ml of development solvent (3:1, dichloromethane:acetone) followed by water rinse. An optical micrograph of the patterned photoresist is shown in Fig 4.6. A higher magnification SEM image of one of the features in the pattern is shown in Fig 4.7. Fig 4.8 is a close-up of the edge of a photoresist line where the photoresist is on the left of the picture and the bare substrate is on the right.

Exposure times were greatly decreased by use of a weaker development solvent for **9** (from 22 hours to 30 minutes). Acetone was not a good solvent for **9** so the original
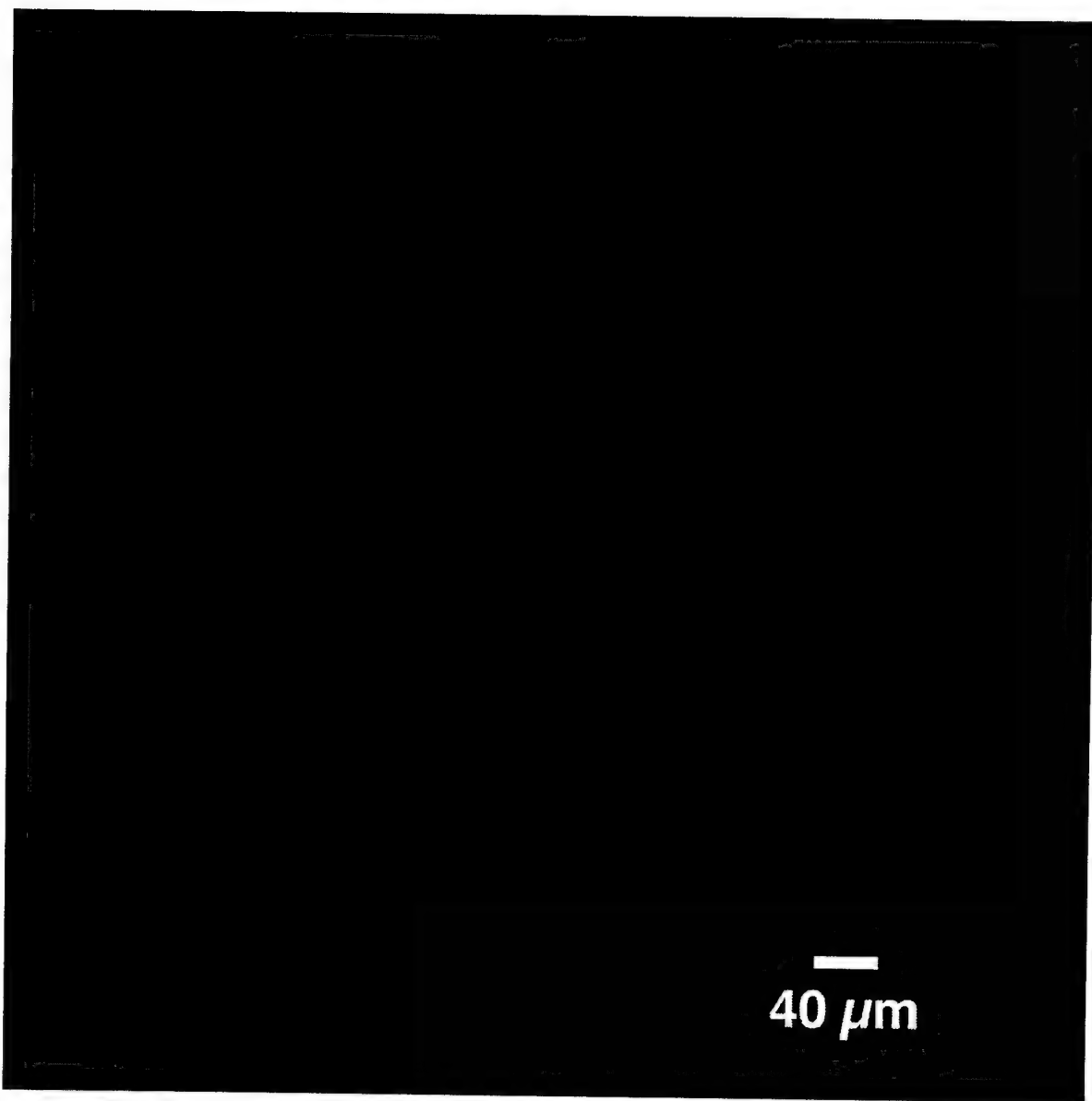
Figure 4.5 Fluorescent pattern in film of **9** resulting from the exposure and subsequent photodimerization of anthracene moieties. Image is taken in reflectance mode of a film on Si being illuminated at 365 nm.
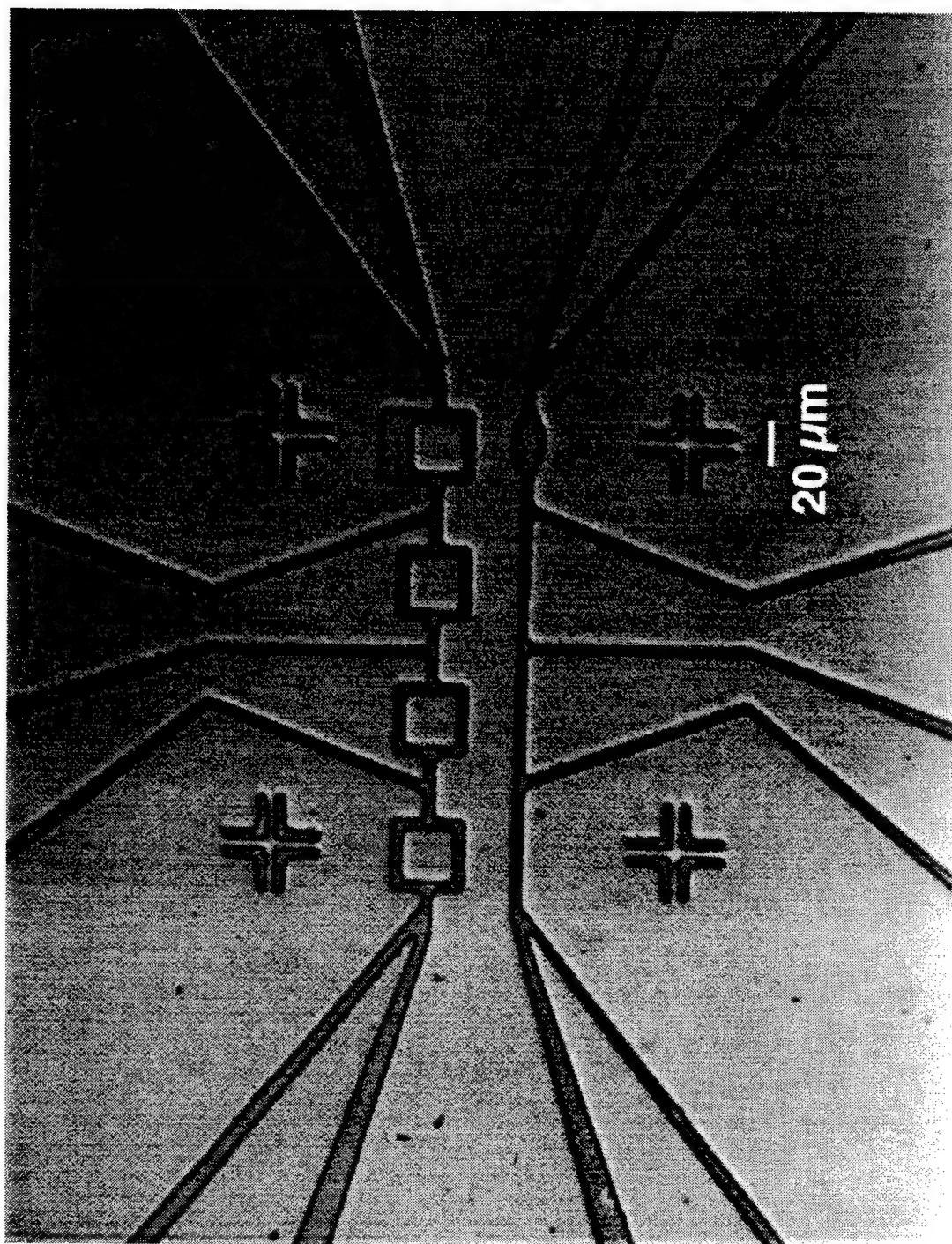
Figure 4.6 Optical Microscopy image of **9** patterned on silicon wafer
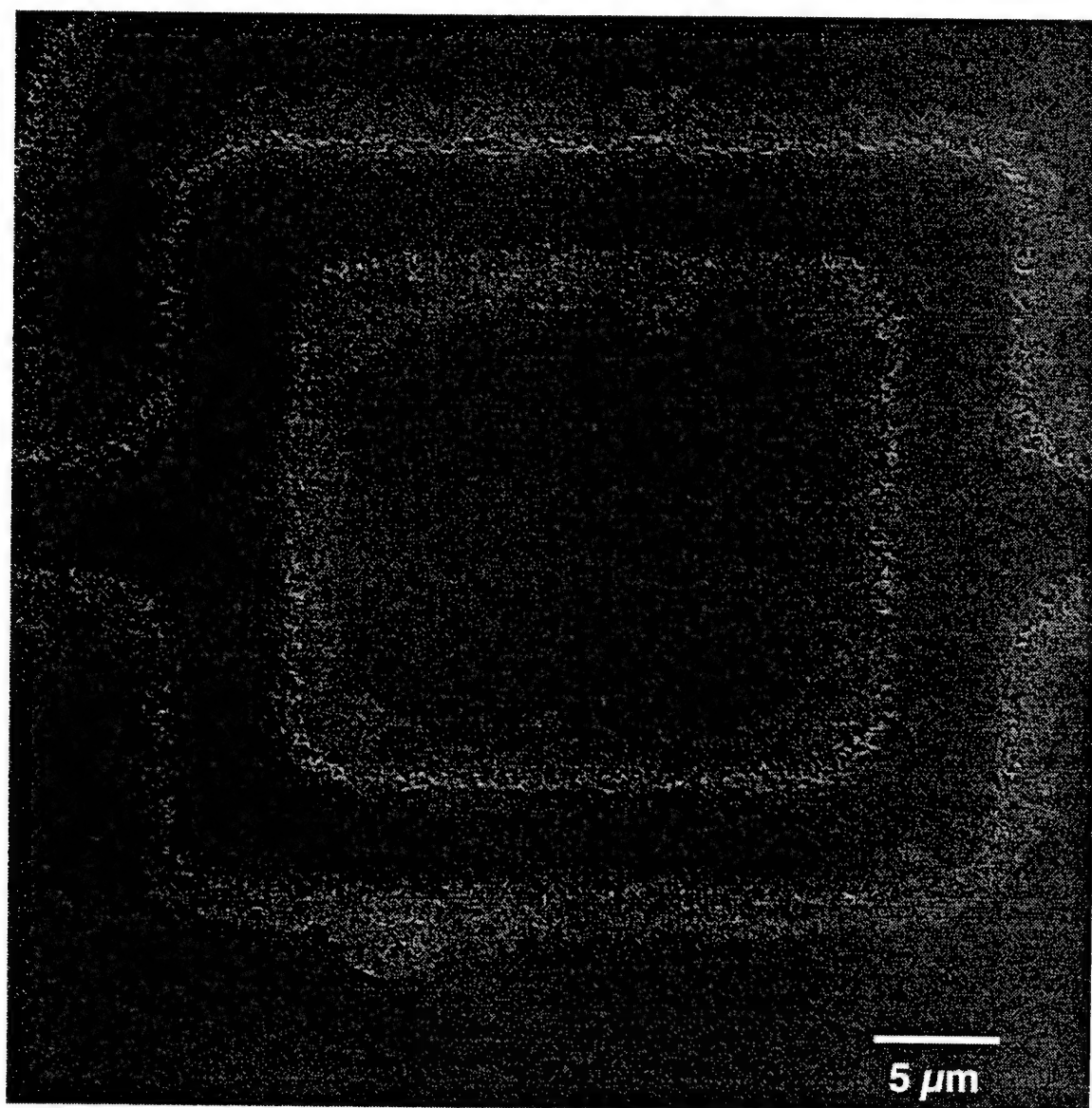
Figure 4.7 Scanning Electron Microscopy image of **9** patterned onto a silicon wafer
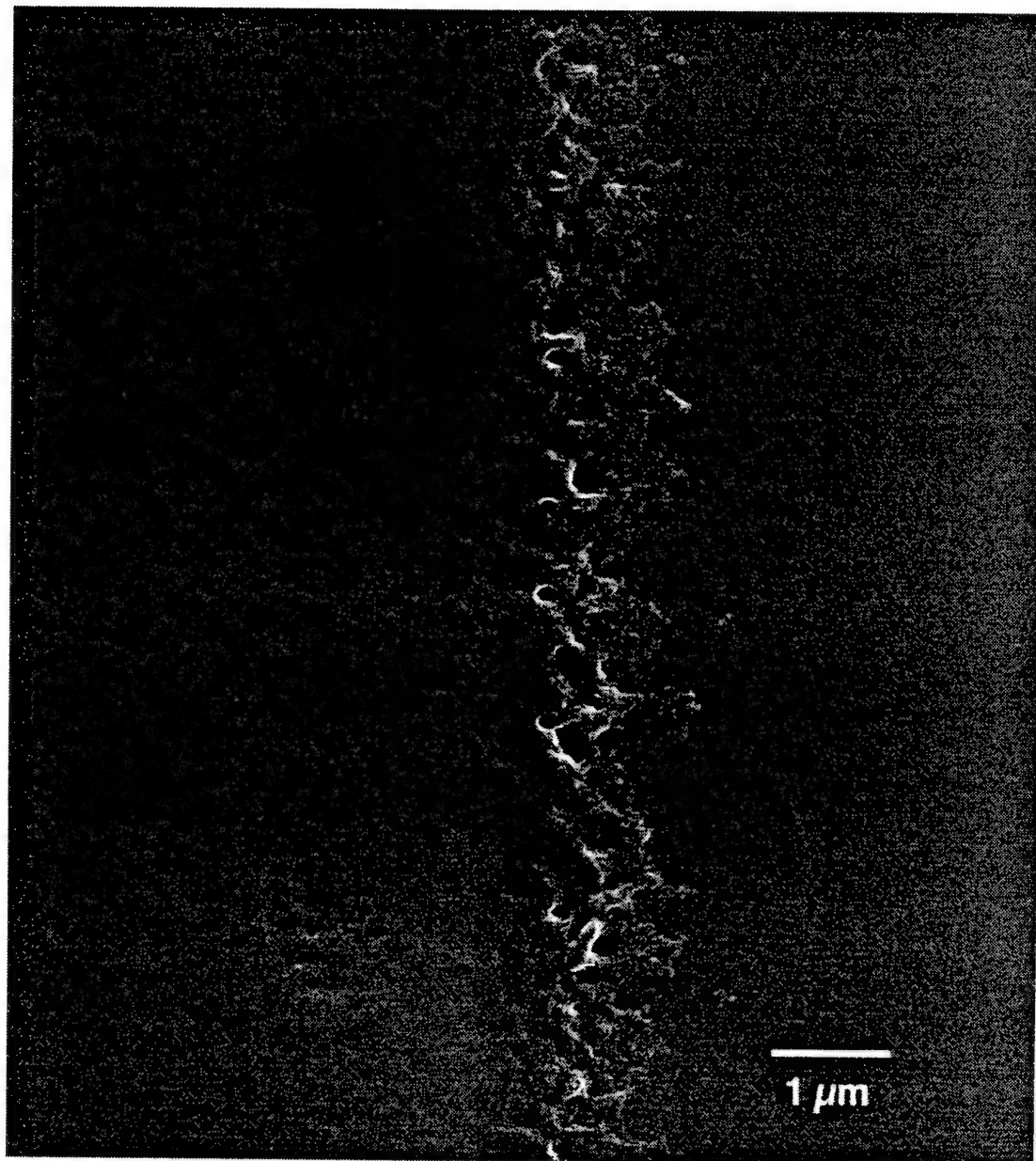
Figure 4.8 Scanning Electron Microscopy image showing edge resolution of photoresist **9** developed on Si

dichloromethane development solution was "poisoned" with 25% acetone to make it possible

_to achieve accurate patterning with as little as ten minutes of irradiation. Films that were

exposed for > 45 minutes were very robust and could not be removed even when placed in a

good solvent, such as dichloromethane or THF, and exposed to sonication. Therefore it is

possible that these films might have application were organic solvent resistance is important.

4.3.3 Reversibility

The photodimerization of anthracene is known to be reversible by application of heat

or higher energy UV radiation (< 300 nm).[102] But when the anthracene chromophore is

attached to a polymer or oligomeric system and then crosslinked, the photochemical

reversibility tends to be poor.[141, 165] Mullen reported photochemical reversibility rates of

20-40% and thermal reversibility rates between 40-60%.[141] One reason the yield of the

reverse reaction is so low in the solid state may be low mobility of the two anthracene groups

in the solid state once they dissociate from the photodimer structure. A biradical intermediate

has been suggested as an intermediate in both the cycloaddition and the dissociation

reaction.[172] Thus, in the solid state where the individual anthracene molecules are relatively

immobile, reformation of the photodimer can occur.[141] Another reason the

photodimerization may not be reversible is that oxygen can react with the anthracene

derivatives forming endoperoxides that will not degrade back into the anthracene precursor

upon heating or higher energy irradiation.[92] Attempts were made to reverse the patterns

using both higher energy UV and heat, but changes in fluorescent behavior and solubility

were not detected. Therefore it is reasoned that in addition to the cycloaddition reaction,

some other reactions are responsible for photoresist behavior.

Molecule **11** was synthesized to test the importance of the diacetylene group to the photoresist abilities of **9**. Originally, the solubility difference in irradiated **9** was thought to be a combination of the anthracene cycloaddition and some diacetylene polymerization to form poly(diacetylene) chains and thus a two dimensional network. Subsequent investigation of the photoproducts of **9** by NMR (section 3.5.3.2) failed to observe any poly(diacetylene) chains in the material. Therefore, the role of the diacetylene in the photoresist ability of **9** was not clear. To test this further, films of **11** were spin coated onto silicon and irradiated for 30 minutes with a 150 W Xenon lamp through a glass filter. Development with the usual solvent system, 10 mL, 3:1 dichloromethane:acetone, completely washed the pattern away. Development in a weaker solvent, acetone, left the outline of all the features but they were rough and not all of the unirradiated material was removed (Fig. 4.9). A side-by-side comparison (Fig 4.9) of the two patterns resulting from irradiation of films of **9** and **11** is also shown. The pattern resulting from **9** is sharp and all the unreacted material is removed by the solvent development. Because acetone has to be used to develop the pattern in **11**, there is still photoresist in the regions that are not irradiated that will lead to inaccurate patterning in subsequent etching steps. Also, the features are blurry and in the case of the "plus" sign in the bottom right portion of the pattern formed by **11**, not defined at all. Thus, **11**, was a much poorer photoresist than **9** with all structural features being equal except for the diacetylene group. Therefore, it is believed that the diacetylene polymerization is taking place and either leading to the one-dimensional structures described in Figure 3.25 or possibly two-dimensional polymer as indicated by GPC. Another explanation may be the phase the material is in during irradiation. Exposure of the films was done at room temperature where **9** is in the crystal E phase and **11** is a crystal. It could be that the crystal
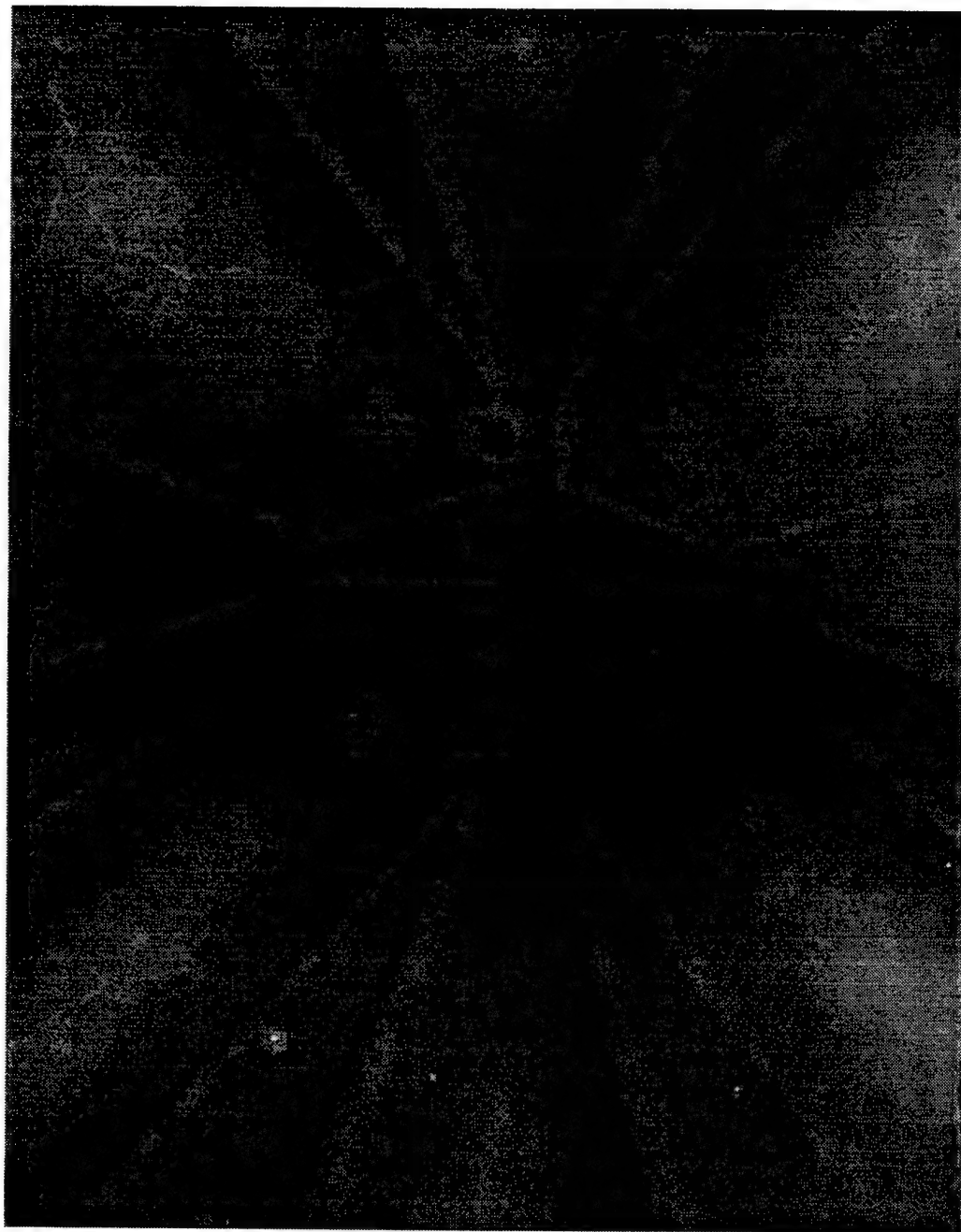
Figure 4.9 Optical Microscopy image of **11** patterned on silicon wafer. Notice how poorly the material replicates the pattern and the unreacted material left behind on the wafer due to the weak development solvent(see text)
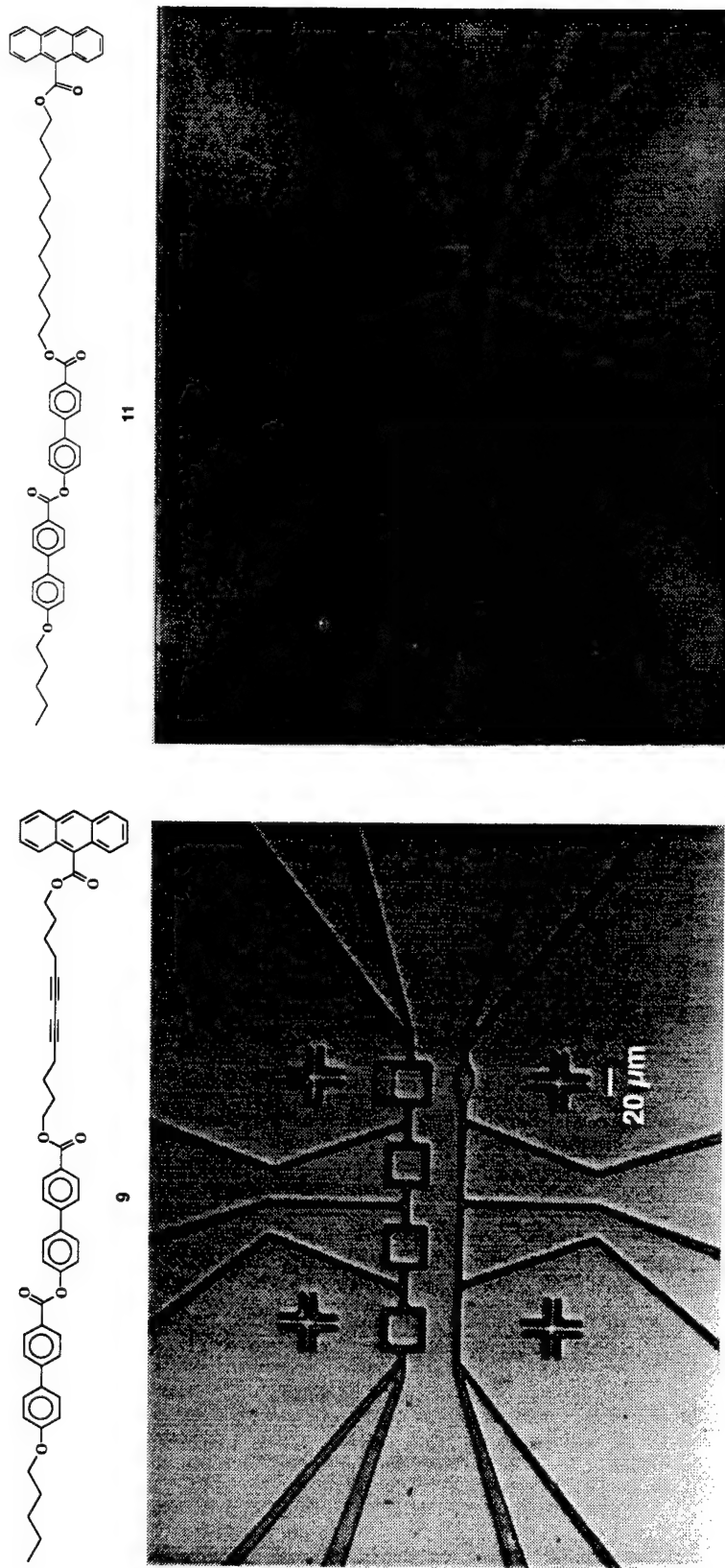
Figure 4.9 (cont) Comparison of **9** and **11** as photoresists. On the left molecule **9** after 30 minute irradiation and development with 10 mL(3:1 DCM:acetone) On the right molecule **11** after 30 minute irradiation and development with 1 mL acetone. Development of **11** with same solvent as **9** completely washes away the pattern

phase of **11** does not place the anthracene groups in the right orientation for cycloaddition while the crystal E phase of **9** does. It must be remembered that even in the highly ordered crystal E phase, the molecules are rotating about their long axis through an angle of $< 180°$ at 10^{11} second.[122] It could be that this mobility is necessary for the anthracene groups to orient properly for reaction and this mobility is not available in the crystal phase of **11**.

4.3.4 Anisotropic Etching

The goal of placing a photoresist pattern on a substrate is to use an etching process to pattern the underlying substrate, usually silicon, silicon dioxide or a metal. As minimum feature sizes have decreased well below one micron, the use of isotropic etching solutions has ceased. The amount of undercutting of the substrate beneath the photoresist is simply too great in comparison to the feature sizes. Therefore, anisotropic etching has become the method of choice for transferring features from the photoresist layer to the underlying substrate. Reactive Ion Etch (RIE) is the most common anisotropic technique used to etch silicon, silicon dioxide, and aluminum.[173] This technique combines the directional control of physical sputtering leading to highly anisotropic etching, with the chemical selectivity of reactive plasma. The plasma in RIE, usually a mixture of CF_4, O_2, and H_2, can etch different materials at different rates depending on its specific composition.[173]

Features were etched into silicon wafers patterned with films of **9** using RIE. After etching the silicon, an oxygen plasma was used to 'ash' the remaining photoresist layer and the wafers were examined by SEM. Fig 4.10 is an image of the same pattern shown in Fig 4.6, but in this case, the contrast is due to the height of the silicon step and not due to a photoresist layer. The step height of the thin lines in Fig 4.10 are 100 nm as measured by
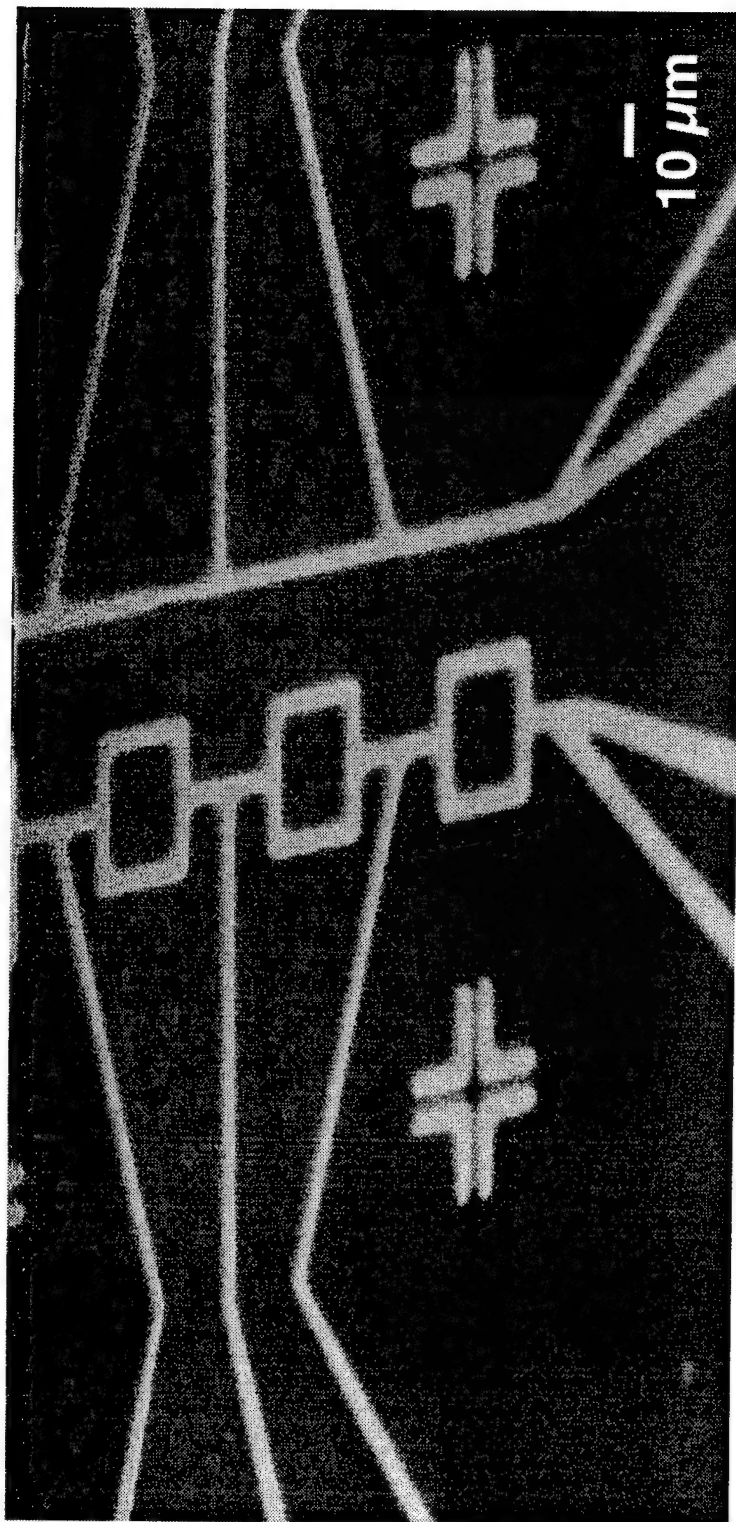
Figure 4.10 Low resolution Scanning Electron Microscopy image of pattern etched into Si by RIE using **9** as a photoresist

profilometry [Fig 4.11]. Fig 4.12 is magnified view of the center of the pattern.

One factor to consider when evaluating photoresists is the so-called proximity effect.[155, 174] The proximity effect refers to different geometrical shapes which are harder or easier for the two different types of photoresists to form. While an isolated line is easier for a negative resist to form, an isolated hole is easier for a positive resist to form. Thus, the "plus" sign shown in Fig 4.13 is the hardest part of the pattern for **9** to replicate as a photoresist. The last SEM image is a close-up of the edge of one of the larger lines to show the edge resolution achievable with this system [Fig 4.14]. The line in the middle of the image is actually raised above the substrate and not sunken in as it may appear.

4.4 Conclusions

A low molecular weight material was successfully used to photopattern 3-5 μm features on silicon using standard, integrated circuit fabrication techniques. While not designed specifically for this purpose, molecule **9** did raise the possibility of using reactive liquid crystalline substances of low molar mass as photoresists. This material acted as a negative resist but not through the formation of an insoluble network, as is common. Instead, the change in solubility came primarily from the formation of a head-to-tail photodimer of **9** which had decreased solubility in certain solvent systems. The structure of the material of higher molecular weight than the dimer detected by GPC (Chapter 3) is unknown at this time although it is likely that this played an important role is decreasing the solubility of the irradiated material. This higher molecular weight material may be caused by reaction of endoperoxides formed on the anthracene group with adjacent molecules leading to larger molecular weight material than the dimer.
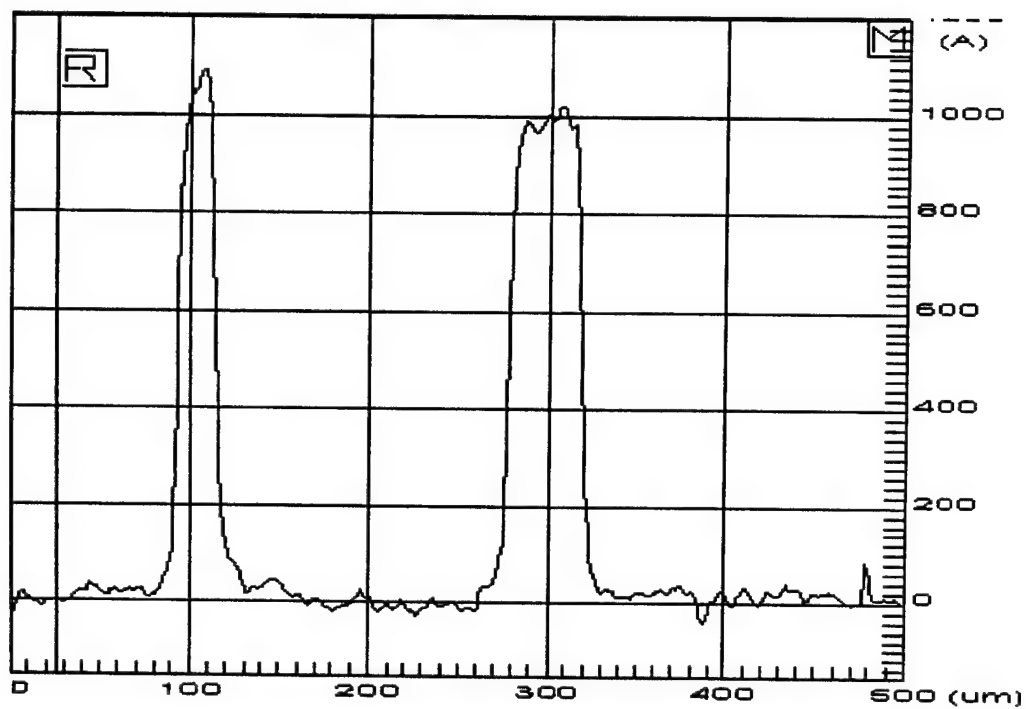
Figure 4.11 Profile trace of the narrow line features (Fig 4.9) etched on Si by RIE indicating a ~100 nm step height
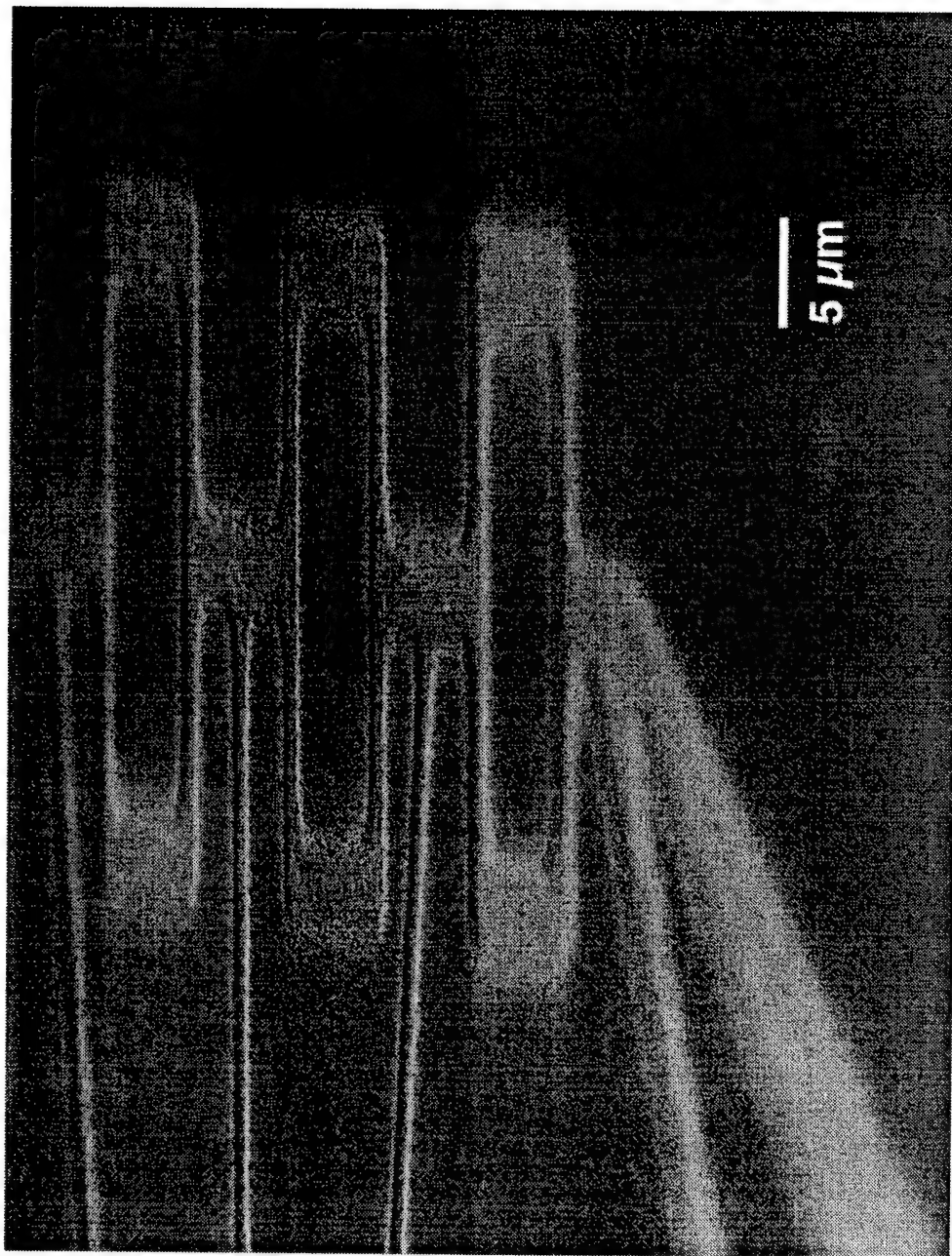
Figure 4.12 Scanning Electron Microscopy image of features etched into Si by RIE using **9** as a photoresist
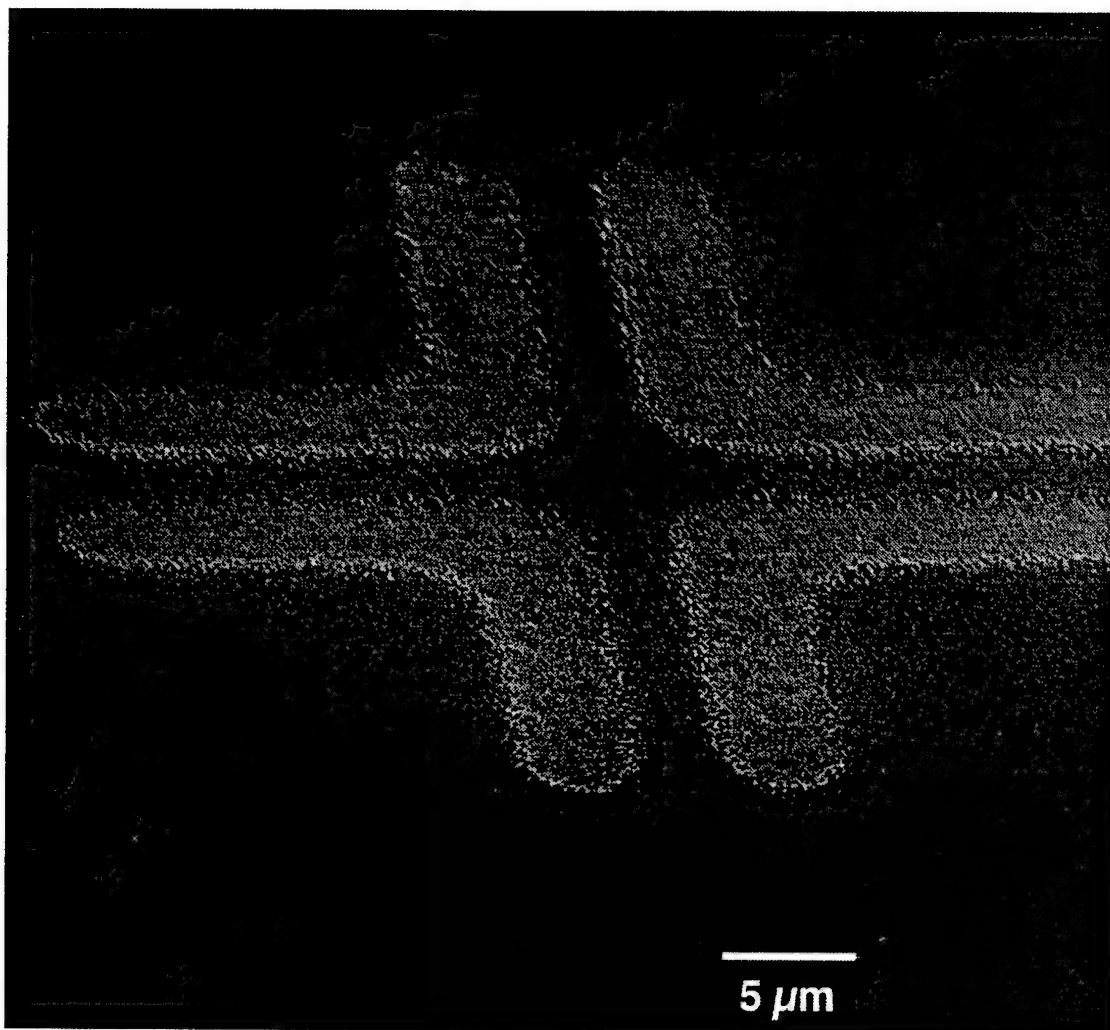
Figure 4.13 Scanning Electron Microscopy image of the 'plus' sign etdhed into Si by RIE using **9** as a photoresist
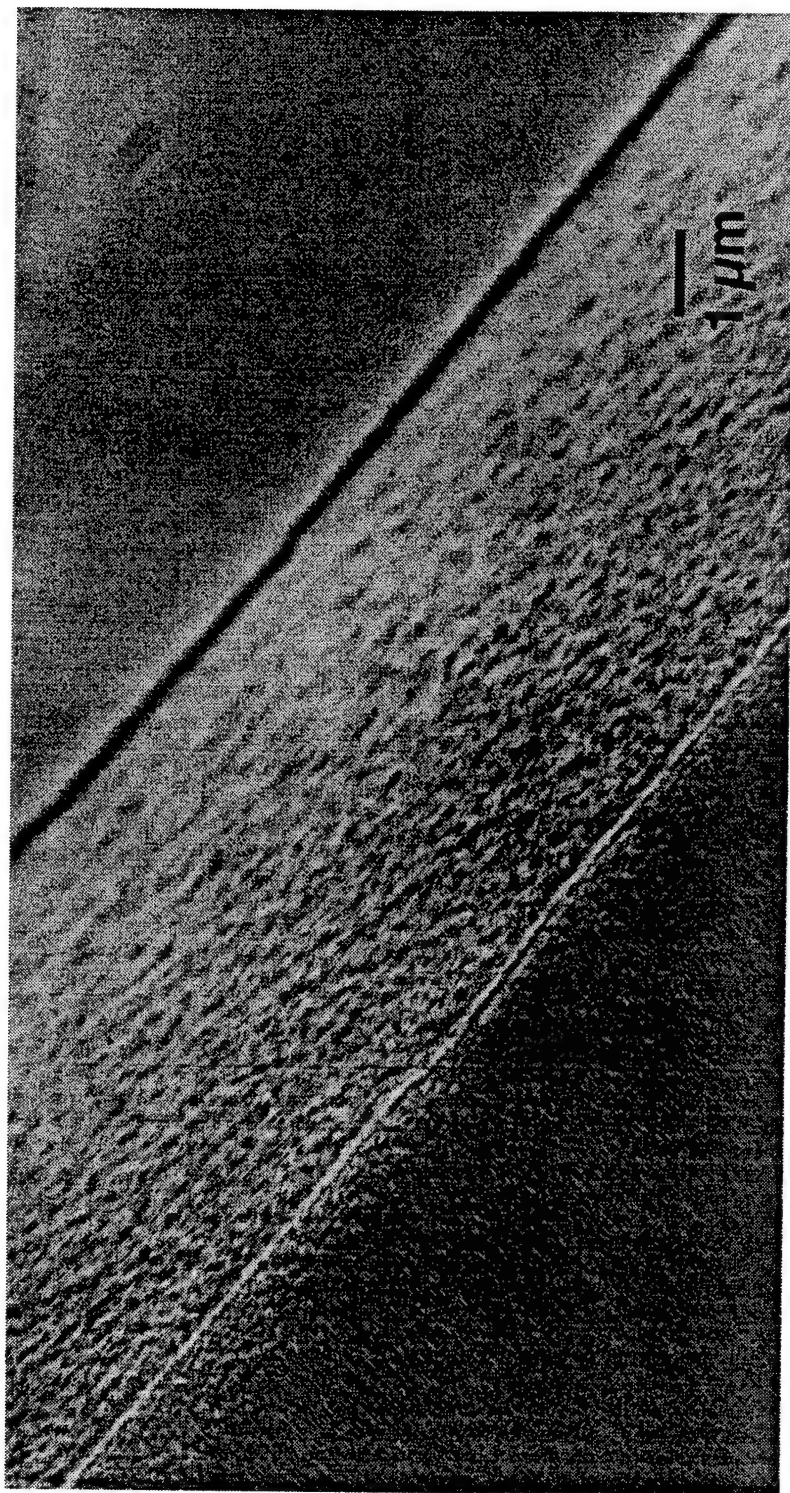
Figure 4.14 Scanning Electron Microscopy image of feature edge on Si etched by RIE using a photoresist film of **9.** Diagonal feature is above the level of the substrate

The amount of solvent used to develop the films was small and the pattern was developed in seconds which makes it attractive for high throughput processes. In addition, because the insolubility is not caused by formation of a flexible network, swelling in this system may be decreased greatly from the common polymer negative resist systems and allow systems of this type to be used to much lower feature sizes. Exposure times were too long for commercial use, but more highly reactive functional groups could solve that problem. The benefits of a liquid crystalline material over a conventional polymeric photoresist may lie in improved processing properties. The viscosity of this material is strongly dependent on temperature. From room temperature to 200°C the material is a smectic liquid crystal which tends to be viscous. But above 200°C, the material is either a nematic liquid crystal or an isotropic liquid with much lower viscosity. This change in flow properties results in a film that may flow to fill pinholes and vias more easily—leading to better coverage of a rough surface. Upon cooling, the material again becomes solid-like and thus does not flow. Furthermore, a completely uniform distribution of the reactive chromophores is inherent in the compound nature of the system. Finally, resistance to plasma etch may be helped by the more densely packed mesogens as compared to amorphous polymer matrices.

Chapter 5 Nanostructure Synthesis in Binary Systems

5.1 Introduction

As described in Chapter 2, rodcoil molecules made up of an oligo(styrene) coil and a two biphenyl rod segment (**3**) formed nanoaggregates in the solid state as observed by TEM (Figure 2.10). The electron diffraction pattern of the material showed evidence for both highly ordered crystal E domains of the biphenyl rod segments along with an amorphous halo due to disordered regions. The fact that the biphenyl rods are able to achieve this level of order while covalently attached to an atactic length of oligo(styrene) demonstrates the aggregation ability of the biphenyl ester rod-like segments. In an effort to further study this aggregation behavior in rodcoil molecules, the idea of binary mixtures of rod molecules with rodcoil molecules was developed. The rod molecule chosen was molecule **8** (Chapter 3) which has a nearly identical chemical structure to the rod portion of **3**. There were many reasons for selecting **8**. First its chemical similarity to **3** in order to induce mixing between the rod segment of the rodcoil and molecules of **8** when dissolved in solvent and cast as a solid film. It is unlikely that any favorable interactions could occur between the oligo(styrene) and **8**. Another reason for using **8** was its highly crystalline nature and strong tendency to undergo topochemical polymerization of the diacetylene bonds [78, 79]. Previous attempts to react the diacetylene groups in rodcoil **3** had not been successful. Therefore, incorporation of the more reactive **8** into an aggregate of **3** might lead to topochemical polymerization within ordered nanodomains of both the rodcoil and the discrete molecule. The potential for mixing of rod molecules with the rod segments of the rodcoil molecules in a crystalline aggregate could potentially lead to different topography in the nanostructure that could also prove useful and will be discussed more later.

The chemical difference in the two types of molecules in the binary mixture lies away from the diacetylene group. A pentyl ether group terminates molecule **8** while oligo (styrene) segments terminate rodcoil **3** with distribution in length and meso vs. racemic dyads. If these two materials were to co-crystallize in some fashion, one possible structure for this mixed, ordered aggregate would be an array of 'rods' of both molecules packing in a layered configuration [Figure 5.1(a)]. Others have described this type of structure in the case of rodcoil molecules cast as films.[1, 61, 69, 175] If the two components of the mixture were to mix within an ordered aggregate, the location of the rod molecule within the aggregate could be important. One scenario has the rods, **8**, segregated into the center of the aggregate and rodcoils, **3**, placed around the edge of the aggregate [Fig 5.1(a)]. This configuration would allow the rod segments of the rodcoils to remain crystallized and give the coil segments of the rodcoils more freedom to explore conformational space. If the rodcoils were concentrated in the center of the puck, the oligo(styrene) coils would be forced to stretch to match the dense packing of rod segments. This scenario of nanophase separation may not describe how a continuous film will incorporate two different moieties.

As mentioned before, another consequence of segregating the rod molecules from the rod segments of the rodcoil molecules is the potential of forming topography within a film or within each supramolecular aggregate. Figure 5.1(b) shows a side view of another way a binary mixture may form a layer. In the regions that are rich in rod molecules, cavities may form due to the absence of covalently attached oligo(styrene). This may lead to a general way to create nanoscale topography by molecular self assembly on the surfaces of films.
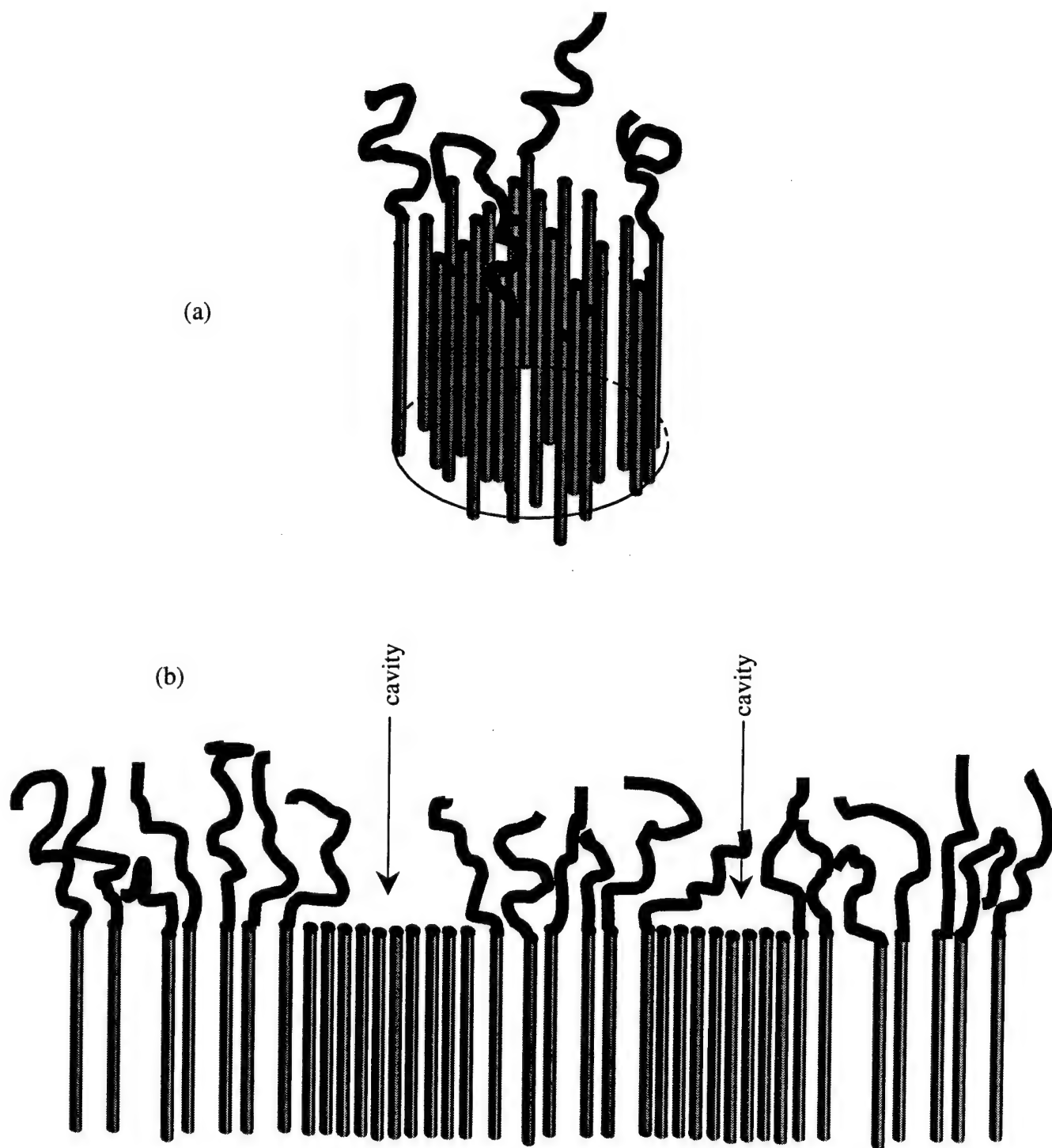
Figure 5.1 (a) schematic drawing of a binary aggregate with rod molecules segregated to the middle and rodcoils on the periphery (b) possible cavities formed by a layer of a binary mixture

5.2 Results

5.2.1 POM

A 1:1 molar ratio mixture of **3:8** was dissolved in dichloromethane with ~50% toluene, cast onto glass and viewed between crossed polarizers on the optical microscope. Compared to the textures of **3** alone, which were almost isotropic, this material was much more birefringent and appeared to be much more like the texture of **8**. On second heating, the material appeared to have cleared to the isotropic state except for highly birefringent spots containing point singularities with four brushes that remained birefringent above 300°C [Fig 5.2]. This is attributed to phase separation where the bulk of the material has become isotropic leaving only small regions that remain birefringent. The fact that the material is still birefringent above 300°C suggests that some of the diacetylene groups in **8** may have polymerized leading to material that will not undergo isotropization. This is suggested because both pure **8** and pure **3** are isotropic at this temperature.

5.2.2 Bulk Polymerization

Solvent cast films of the 1:1 mixture of **3:8** were also investigated for their ability to topochemically polymerize. Films irradiated at 254 nm turned a dark blue/violet color, the result of topochemical reaction of the diacetylene groups, similar to the color of **8** when topochemically polymerized on its own.[79] A sequence of films was cast and then heated to increasing temperatures for 10 minutes and then irradiated at 254 nm (see Figure 5.3). At room temperature and after annealing at temperatures up to ~75°C, the entire film became dark blue/violet in color. At 80°C, there was a change in the intensity of the color although the color was still blue. This is believed to represent a decrease in the amount of reaction.

At 90°C, the topochemical reaction was not producing highly colored polydiacetylene and at 100°C, no change in color could be detected. A similar disruption of the topochemical reaction of **8** can be observed, but not until the film is heated to ~120°C. Thus, the disruption temperature, the temperature needed to perturb order in the film so that topochemical polymerization of **8** can not occur, is 40°C lower in the case of the binary mixture. The physical reason for this is believed to be mixing of **8** with **3** such that the crystalline lattice is distorted and topochemical reaction is hindered. Such mixing can not occur in the case of **8** heated on its own and therefore, topochemical reaction still occurs. TEM studies, detailed below, revealed an interesting morphology and mapped the interdiffusion of the two species with increased temperature annealing.

5.2.3 TEM

Characterization of thin films of the binary mixtures by TEM showed evidence for phase separation in as cast films from solution. Micrographs taken at low magnification showed alternating dark and light stripes that ran parallel to one another [Fig 5.4]. The boundary between the stripes is very diffuse and required defocusing to increase contrast. It is believed that the dark and light stripes are due to alternating crystalline and amorphous (or less-crystalline) domains. The dark and light striped regions are thought to be rich in rods and rodcoil molecules, respectively. Of course, these regions are not exclusively rods or rodcoils but a mixture of both. But because there may be a majority of the rods in the dark bands, this leads to increased crystallinity and hence dark color due to diffraction contrast. Diffraction contrast is caused by Bragg scattering of electrons in the crystalline portions of the film. When the electron beam is refocused after passing through the sample, the loss in electron
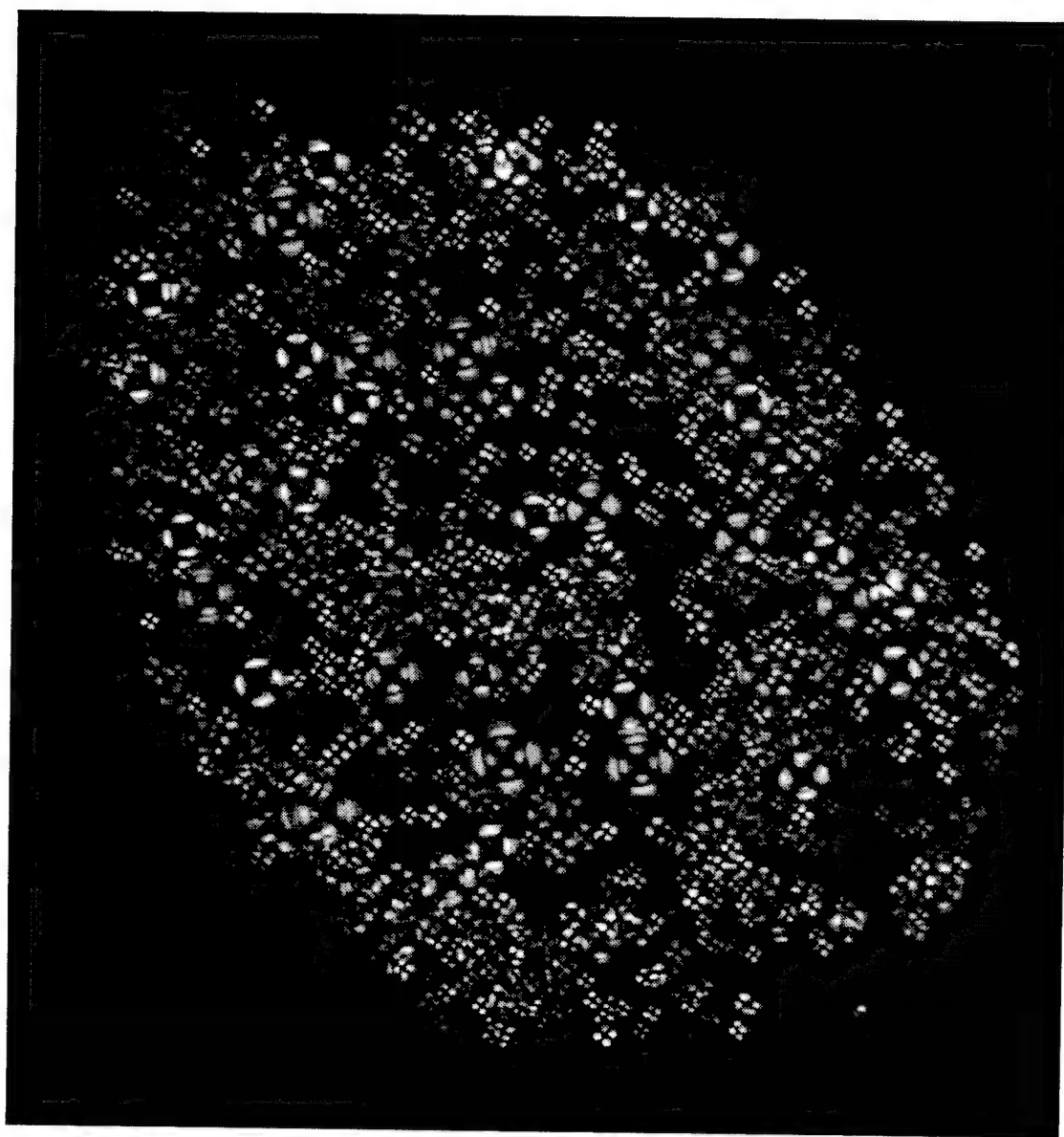
Figure 5.2 Polarized Optical Microscopy image of biphasic texture of binary mixture at 191°C
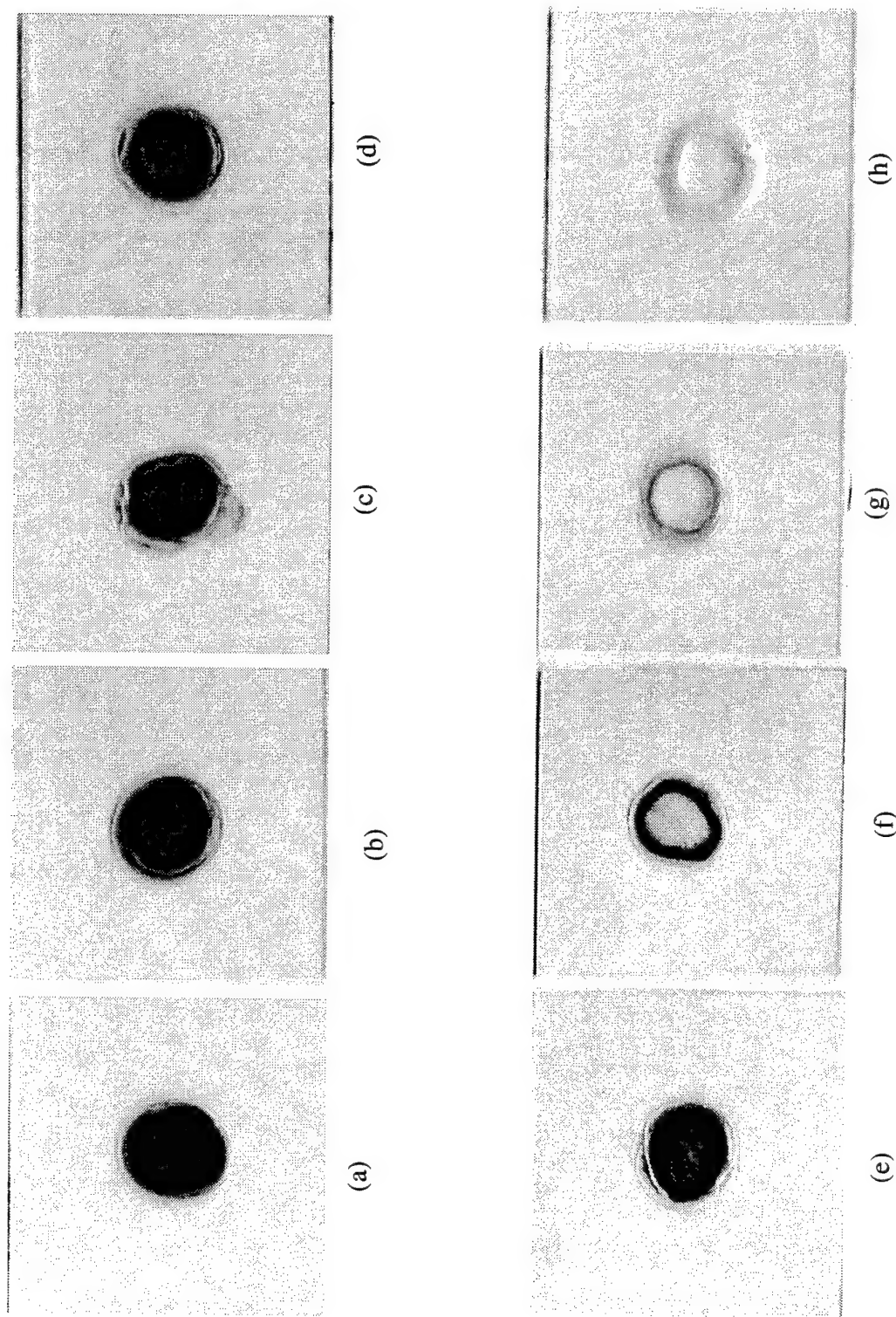
Figure 5.3 Films of binary mixture irradiated after thermal annealing for 10 minutes at increasing temperature (a) room temperature (b) 50°C (c) 60°C (d) 70°C (e) 75°C (f) 80°C (g) 90°C (h) 100°C
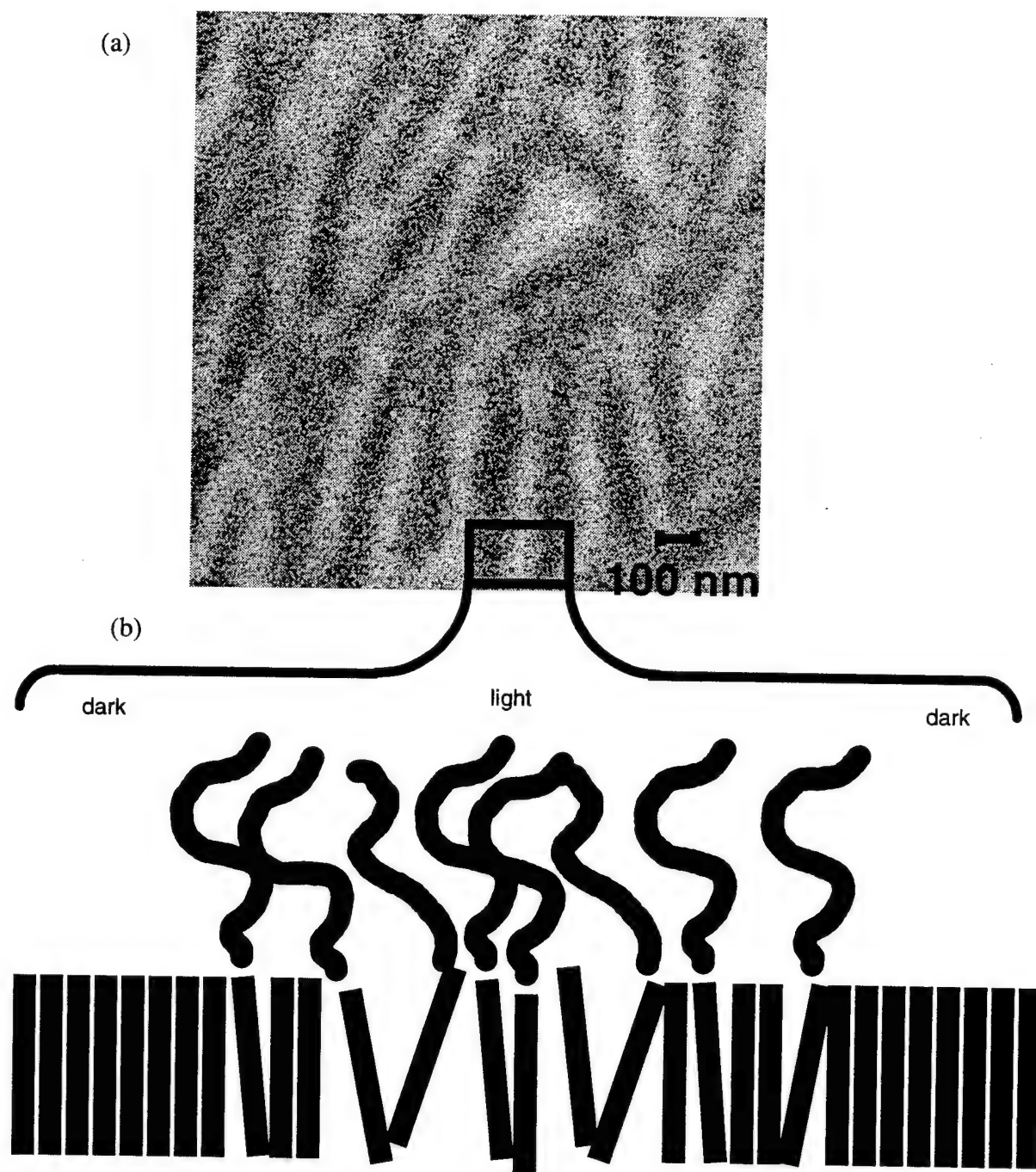
Figure 5.4 (a) Transmission Electron Micrograph of stripes formed in solvent cast films of binary mixtures (b) Schematic representation of the content of the dark and light stripes, as rod and rodcoil rich, respectively

intensity appears as dark regions in the TEM micrograph. Therefore, the light stripes are identified as being less crystalline than the dark regions although it is not known if they are completely amorphous. Interesting changes in the morphology were discovered by TEM analysis of films that were annealed at elevated temperatures for 30 minutes, quenched in air, and then irradiated. Figure 5.5 contains four micrographs showing a decrease in the width of the crystalline stripes with higher temperature annealing and at 120°C, the film is completely homogeneous. The disappearance of the dark stripes is believed to represent mixing of the two domains is thought to be the cause of the disruption of the topochemical polymerization in the binary mixture as discussed above. The crystalline domains are likely to be rich in **8** which undergoes topochemical polymerization as evidenced by the highly colored films in Figure 5.3. But as the two different species are mixed through an interdiffusion process, the crystalline domains are disrupted until at ~100°C, no color is evident in the irradiated film [Figure 5.3]. The width of the crystalline stripes is graphed in Figure 5.6 and does not noticeably drop until above 65°C, which agrees with the bulk polymerization results. Disruption of the topochemical reaction in films of pure **8** annealed in the same manner as the binary mixtures does not occur until the films are heated to 120°C where the material undergoes a phase transition to the crystal E_h phase.[135] Therefore, physical mixing of rodcoil **3,** with rod-like molecule **8,** causes a disruption of the topochemical reaction at 40°C lower than in the case of pure **8**.

Another interesting aspect of the morphology of this material is the large number of 3-10 nm dark spots that reside within the light stripes [Fig 5.7]. These dark spots are believed to be phase separated nanocrystals within the amorphous light stripes. These nanocrystals are fairly regular in size and appear to reside exclusively within the light striped regions. The
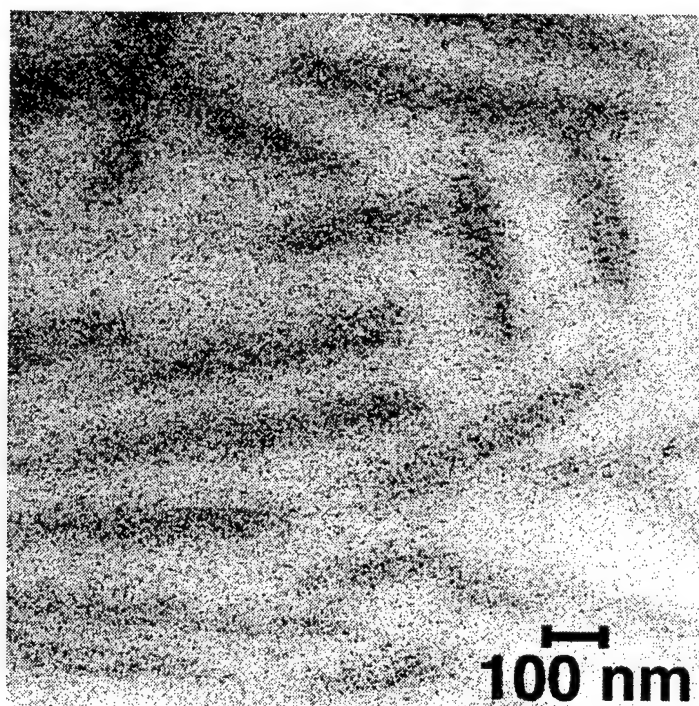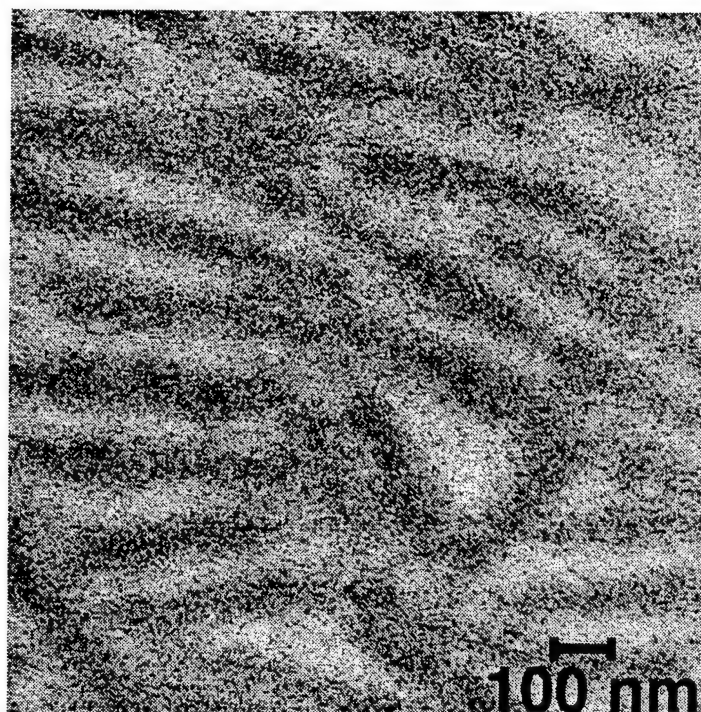
Figure 5.5 Transmission Electron Micrograph of film of binary mixture annealed for 30 minutes, quenched, and then irradiated at 254 nm. (a) as cast, no annealing (b) 65°C
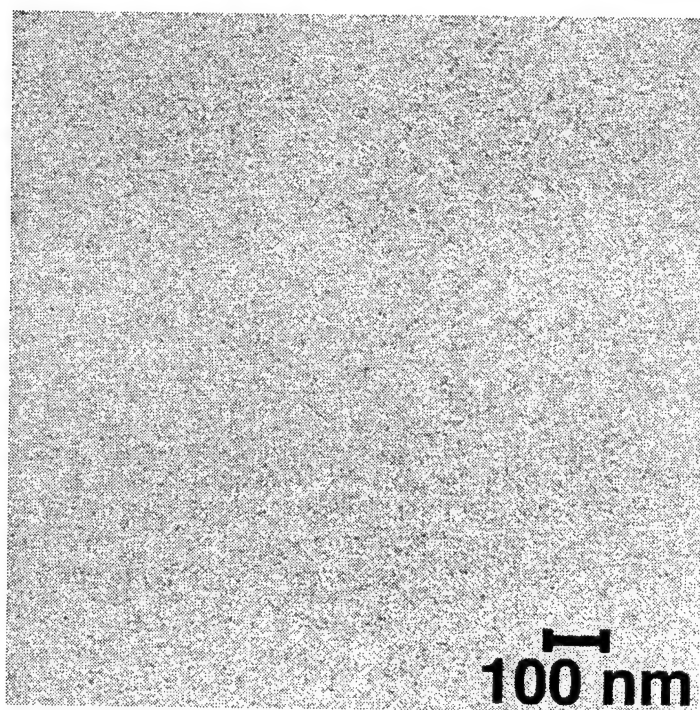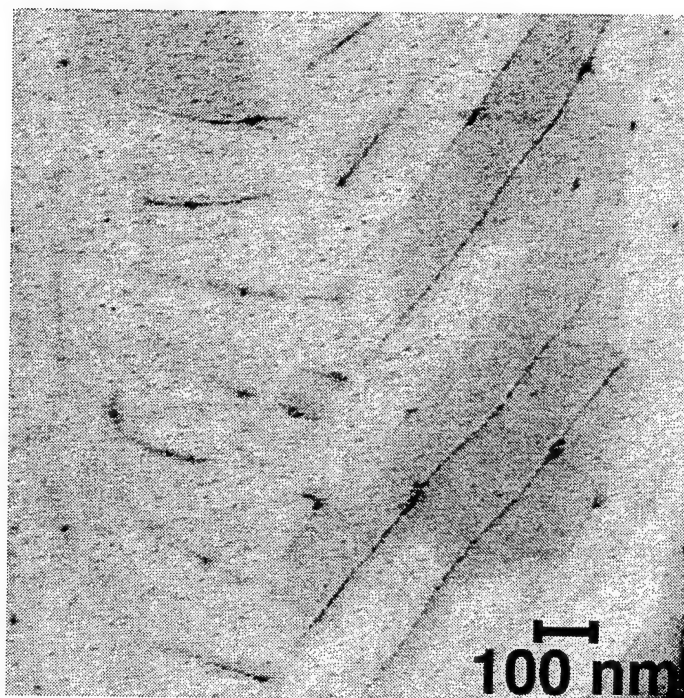
Figure 5.5 (cont.) (c) 100°C (d) 120°C
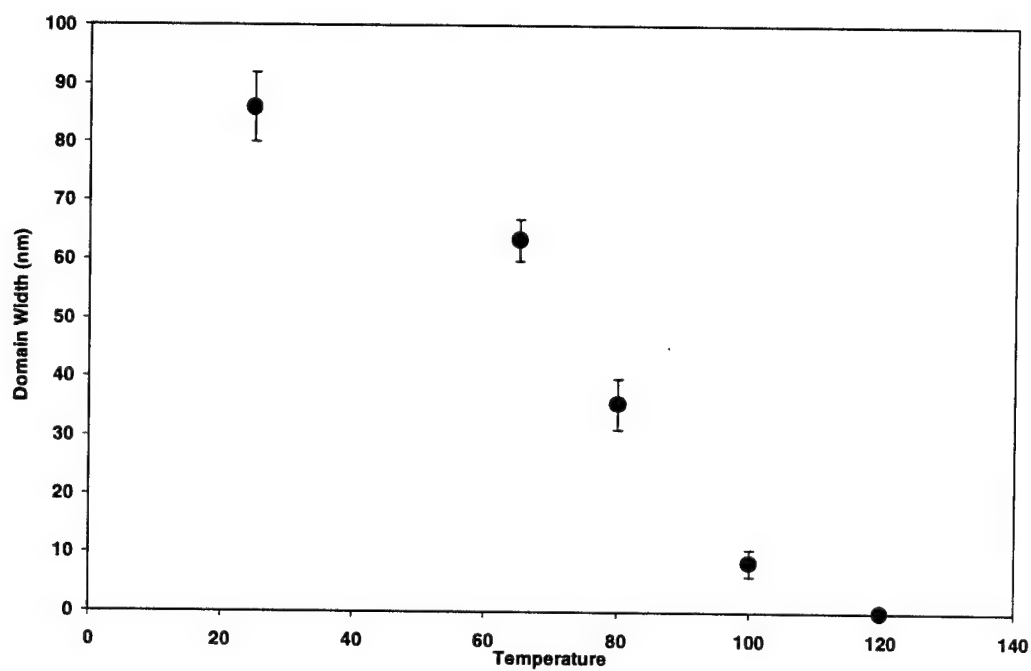
Figure 5.6 Crystalline domain width versus temperatureof annealing in the binary mixture

162
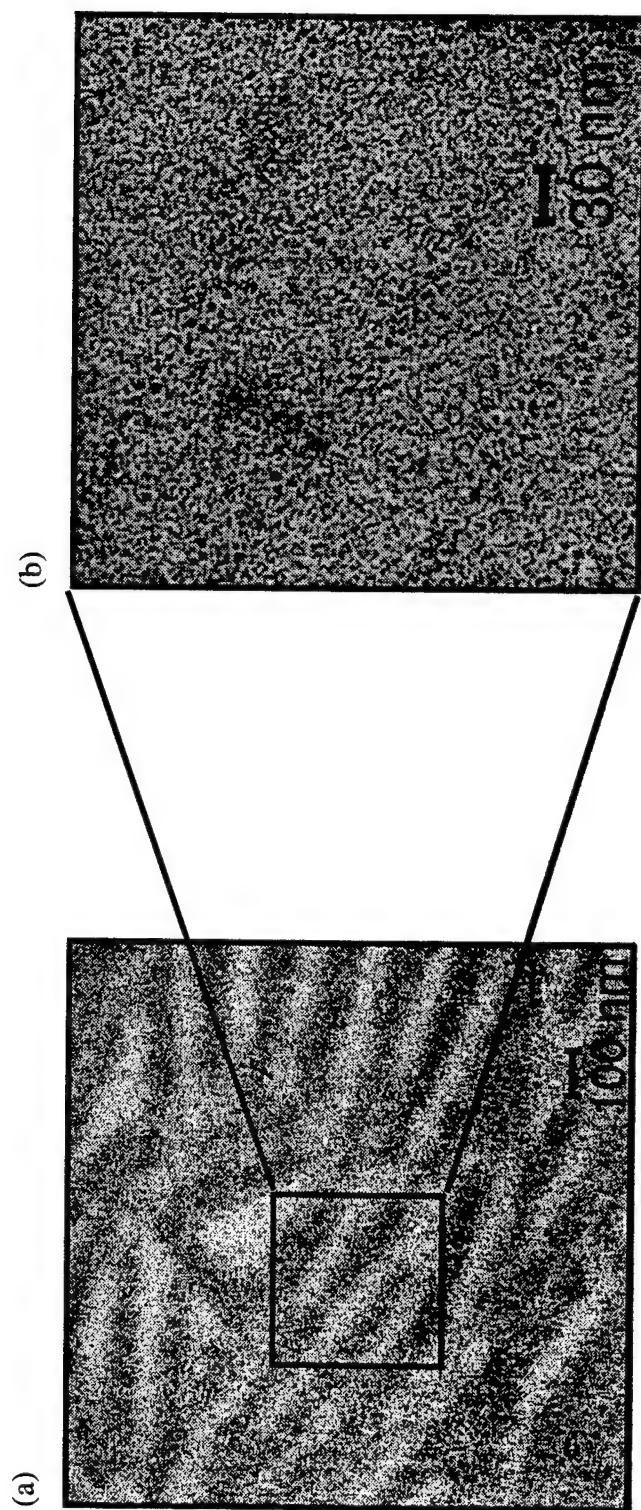
Figure 5.7 (a) Micrograph showing lamellar stripes in a film of the binary mixture (b) Higher magnification micrograph showing nanophase separation into nanocrystals within the light striped domains.

nanocrystals are thought to be predominantly **8**. But because the nanocrystals never changed in size upon annealing, it may be that incorporation of **3** into the aggregate is having a size limiting effect. As mixing is induced by annealing, the morphology transitions from a stripe-like morphology, to a more homogeneous one [Fig 5.5(d)]. The 3-10 nm nanocrystals become more prevalent throughout micron wide areas of the films after annealing at elevated temperatures [Fig 5.8] although they do "melt" above 120°C as the entire film becomes homogeneous [Fig 5.5(d)]. This nanomorphology appears to be thermodynamically more stable than the stripes as films annealed at 80°C for 2 hours showed an almost complete absence of the striped morphology while the nanocrystals appeared to be more prevalent. The nanocrystals also did not Oswald ripen as might be predicted by classical nucleation and growth theory.[176] One possible schematic of the nanocrystals is shown in Figure 5.9. A top view of the nanocrystals is shown in Figure 5.9(a) while an individual nanocrystal is shown from the side in Figure 5.9(b). Note that the single nanocrystal is believed to be limited in its size by interactions with rodcoils. Therefore the rodcoils help define the "nanostructure" which is different than the "nanocrystal" in Fig 5.9(b). The spacing of the rods within the nanocrystal are believed to be regular and smaller than the spacing outside the nanocrystal because of the strong contrast seen in TEM. The aggregates are likely made up of **8** with potentially some molecules of **3** around the edge. The matrix surrounding the nanocrystals is made up of the rodcoils and remaining rods in a less ordered phase. There may be very small (< 3-10 nm) crystalline aggregates of rods and the rod segments of rodcoils in the matrix surrounding the nanocrystals but they were not detected by TEM studies done to date. The fact that the nanocrystals are stable at 80°C after the striped morphology has disappeared may suggest that nanocrystal formation is a way for the phase to lower its energy and that the
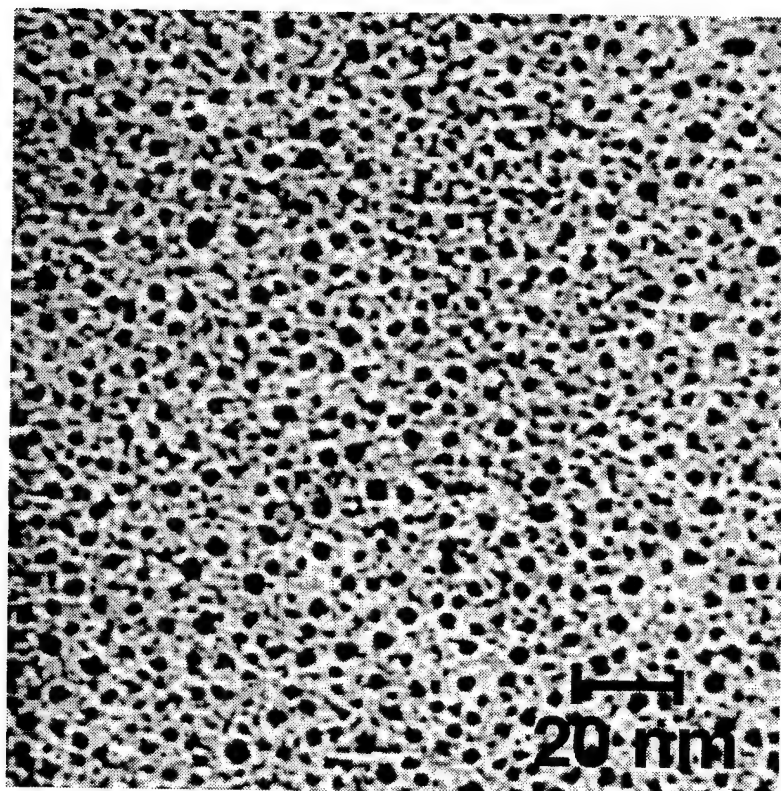
Figure 5.8 Transmission electron micrograph of nanocrystals after a 100° C anneal for 10 min.
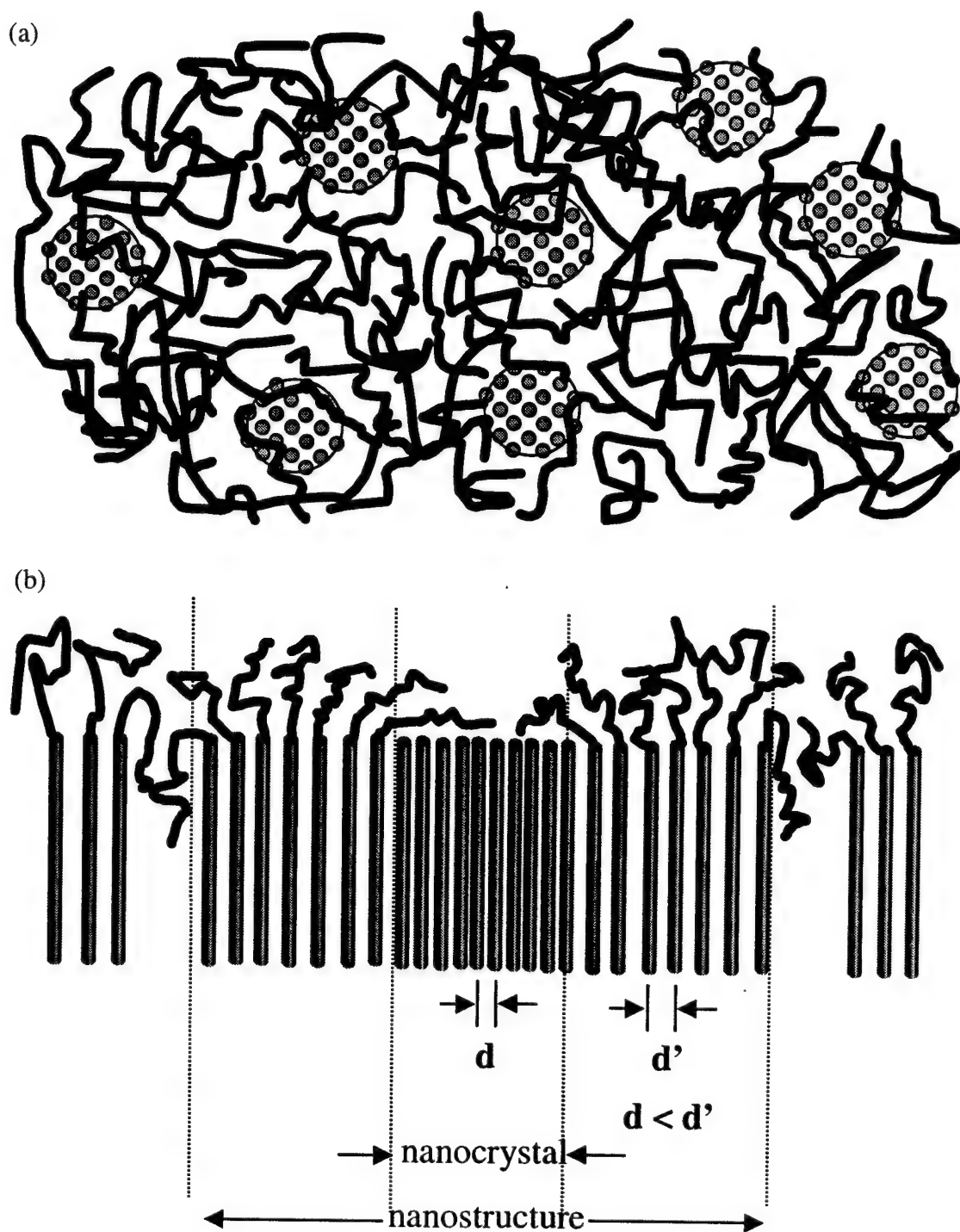
Figure 5.9 Schematic drawings of the nanocrystals in the binary mixture as seen by TEM (a) top view (b) side view of one nanocrystal

completely mixed state is not favorable at this temperature. While it is believed that the nanocrystals are thermodynamically stable between 80-100°C, the experiment has not been done in which the nanocrystals are melted at 120°C and then the film is slowly cooled back to 80°C. If the nanocrystals are thermodynamically stable at this temperature, they should reappear with a slow decrease in temperature from 120°C. This experiment will be done in future collaborative work with Martin Pralle of the author's group. Another binary mixture containing a 3:1 ratio of rods to rodcoils was investigated by TEM. The higher percentage of rods was expected to lead to microphase separation of the rods into crystalline domains that exclude the rodcoil molecules. This is in fact what was observed by TEM. Long platelets with crystalline diffraction patterns identical to those of the rods alone were observed.

If the striped morphology were due to spinodal decomposition of a mixture, longer annealing times at temperatures below the critical temperature should not cause the stripes to disappear, but their boundaries would become more defined.[176-178] But if the stripes are merely a trapped state caused by solvent casting, the longer annealing times should lead to further narrowing of the crystalline regions. An experiment was done at 80°C where the films were annealed for 0 (native solvent-cast state), 30, 90, and 120 minutes before quenching and irradiation. The stripes were found to narrow as is shown in the graph below [Figure 5.10]. Another experiment done to determine whether spinodal decomposition was involved entailed heating a film to 120°C, and then cooling (5°C/min) back to room temperature relatively slowly. At this temperature, the film is homogeneous and no topochemical reaction will occur when the film is quenched in air and irradiated. Relatively slow cooling might allow for spinodal decomposition back into the dark and light stripes, if this were the mechanism
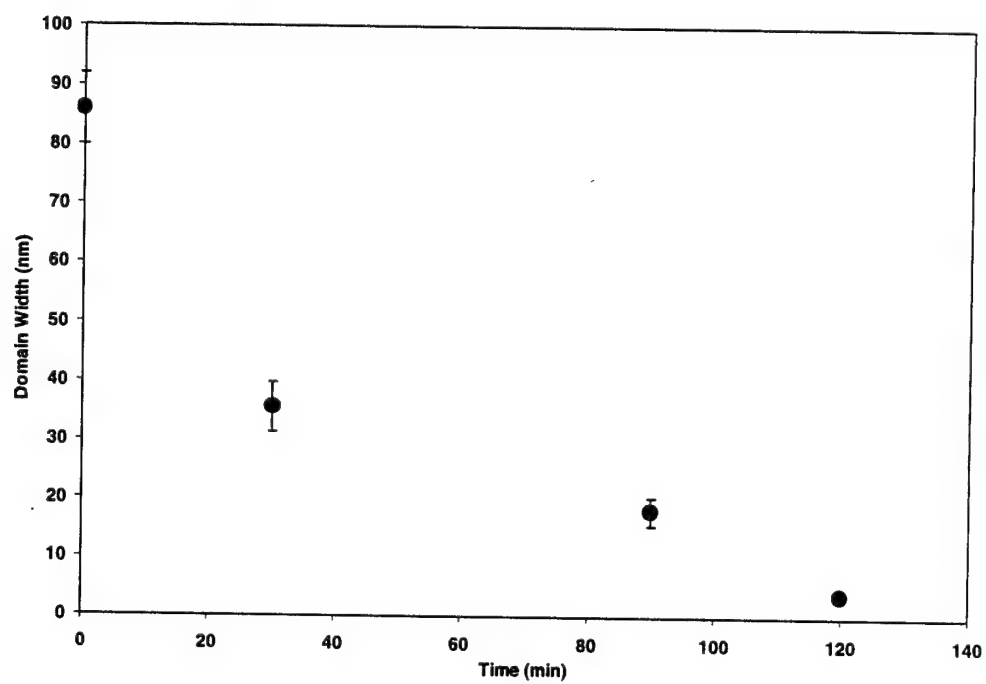
Figure 5.10 Crystalline domain width versus time of annealing at 80°C

involved. Previous attempts to image such a film by TEM were not successful due to destruction of the film during long periods at elevated temperature. However, a correlation has already been shown between films that have dark and light stripes and bulk films that produce a highly colored film upon irradiation. Therefore, the film cooled from 120°C was irradiated as a test for reformation of the striped morphology; the film did not undergo any color change. Finally, films of the binary mixtures was held at 75°C for 12 and 26 hours. When heated to this temperature for 10 minutes and then quenched, the film turned a dark blue color upon irradiation. After 12 hours at 75°C and then quenching in air, irradiation caused only an extremely faint blue color in the film. After 26 hours at 75°C, then quenching in air, the naked eye could still detect an extremely faint change in the film color. Again, if the striped morphology was due to a spinodal decomposition, the stripes should be stable at 75°C and reaction should occur even after the longer annealing times. Therefore, spinodal decomposition is not thought to be the cause of the stripes found in the solvent cast films.

5.2.4 X-ray Characterization

X-ray powder diffraction studies of the binary mixtures supported the findings of TEM. Shown in Figure 5.11 is a series of wide angle diffraction patterns taken of films annealed at various temperatures, quenched, and then irradiated at 254 nm. The peaks of the orthorhombic unit cell are indexed based on electron diffraction data recently published.[135] As the films are heated at increasingly higher temperatures, a disruption of the crystal lattice can be seen in the disappearance of the (200) peak and a broadening of the (110) peak. Interestingly, as the annealing temperature increases past 75°C, the (110) peak begins to sharpen and a new peak with spacing of ~4.02Å becomes apparent at 120°C [Fig 5.11(e)].
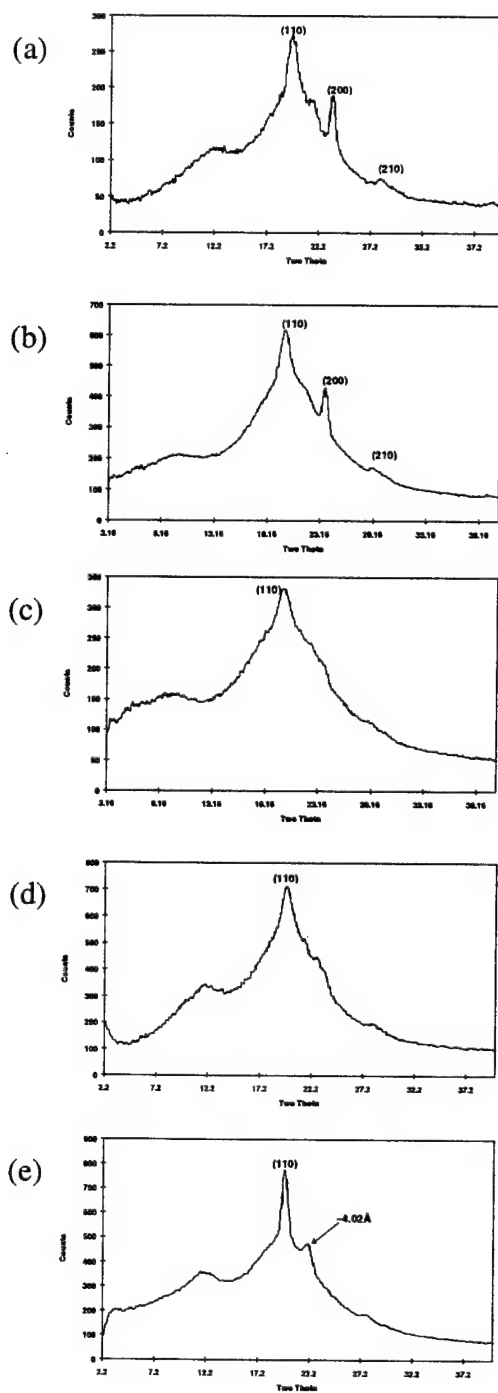
Figure 5.11 Debye-Scherrer patterns of binary mixture with elevated temperatures annealing before 254 nm irradiation (a) room temperature (b) 65°C, 10 min. (c) 75°C, 10 min. (d) 100°C, 10 min. (e) 120°C, 30 min.

The initial broadening of the (110) peak upon annealing at temperatures up to 65°C is thought to be caused by the narrowing of the dark striped regions as the annealing temperature is increased. The fairly sharp diffraction peaks at wide angles can not be coming from the nanocrystals because they are too small to effectively cause Bragg scattering. Therefore, the wide angle peaks must be coming from the dark stripes which are more crystalline than the light stripes and whose disappearance is reflected in the broadening of the (110) peak with annealing. The new peak at 4.02Å and the sharpening of the (110) peak after annealing above 75°C is due to an irreversible phase transformation seen by Li in the poly(diacetylene) form of **8** after heating the film to 200°C.[135] The electron diffraction pattern of a film of the binary mixture heated to 120°C [Fig 5.12], shows the same two characteristic reflections (also seen by X-ray diffraction in Fig 5.11(e)) that Li saw in polydiacetylene film heated to 200°C.[135] The peak at 4.02Å is also faintly visible in the room temperature wide angle diffraction pattern, Fig 5.11(a) and may be visible in the other patterns as well. If this high temperature phase in the binary mixture at 120°C is due to some disordering of **8**, as evidenced by the fact it occurs at high temperature and disrupts the topochemical polymerization, then an effect of the solvent-cast binary mixture may be to cause a small amount of **8** to form this less ordered phase at room temperature. This would likely occur in molecules of **8** that reside in the light striped bands and are not able to crystallize. Therefore, to decrease the enthalpic penalties for being isotropic, the trapped rods take on the disordered phase that would normally occur at higher temperature (200°C) in pure **8**. This small amount of disordered **8** may be what is detected by the wide angle diffraction patterns in Figure 5.11 until 120°C where this disordered phase becomes the dominant phase.
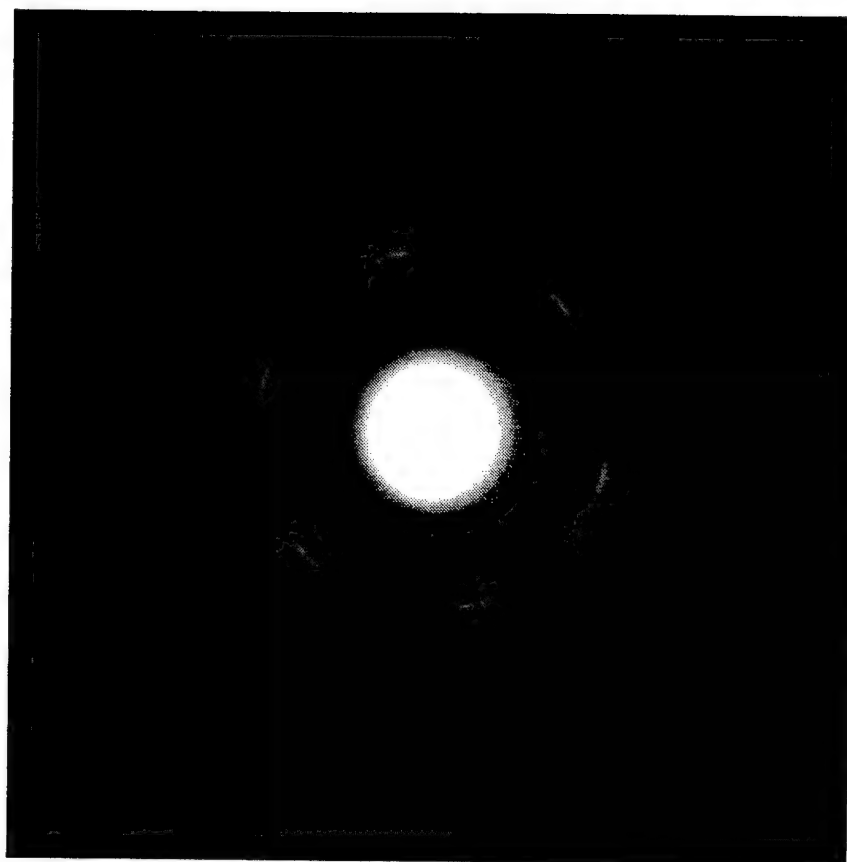
Figure 5.12 Electron Diffraction Pattern of binary mixture after 30 minutes anneal at 120°C, quenched, and then irradiated with 254 nm light.

5.3 Conclusions

Nanostructures, both stripe-like and nanocrystals, were formed from solvent cast films of a binary mixture of a rodcoil, **3**, and a chemically similar rod, **8**. As described in Chapter 2, films of the rodcoil material on its own did form nanoaggregates (1-5 nm) due to the steric effect of oligo(styrene), but they were not as well defined as the nanocrystals in the binary system nor did it form the striped morphology whatsoever. The striped structure, which is believed to be due to alternating crystalline and less-crystalline domains, disappears upon annealing at elevated temperature to produce a homogenous film. Annealing also destroyed the ability of the films to undergo topochemical polymerization due to mixing of the rodcoils with the rods. The make up of the 3-10 nm nanocrystals remains unknown. Due to their dark color in TEM, they are crystalline based on diffraction contrast. They are fairly uniform in size and do not grow after elevated temperature annealing which suggests that mixing of the two dissimilar components is having a size limiting effect on the nanocrystals. One possible schematic of the nanocrystals suggested segregation of the rods into nanoaggregates that contained rodcoils on the periphery [Fig 5.9]. A much less crystalline matrix made up of rodcoils and some rods surrounds these aggregates. The rod molecules themselves are very stable in the pure form and favor crystalline packing. Because of the presence of the rodcoils and the entropic gain of mixing, the rods must mix to some degree and therefore are limited to crystallizing in nanoaggregates. Complete mixing of the phase and disappearance of both the striped and nanocrystal morphology occurs after annealing at 120°C at which point a new disordered phase is detected by both electron diffraction and wide angle X-ray diffraction.

Chapter 6 Experimental

6.1 General Information and Instrumentation

Nuclear Magnetic Resonance (NMR) spectra were collected on either a General Electric QE-300, a Unity 400, a Unity 500, or Unity Inova 500NB instruments. Proton spectra in deuterated chloroform were always internally referenced to 7.26 ppm and carbon spectra were always referenced to 77.0 ppm. If other deuterated solvents were used they are mentioned by the appropriate compound. ^{1}H NMR data are presented in the following condensed format: chemical shift (ppm), multiplicity, integrated intensity. Multiplicities are abbreviated as s (singlet), d (doublet), t (triplet), q (quartet), m (multiplet) and b (broad). Molecular weight distribution data is reported for Gel Permeation Chromatography (GPC) and Field Desorption Mass Spectroscopy (FD) and Matrix-Assisted Laser Desorption/Ionization (MALDI) as appropriate. Calculation of molecular weight distributions from FD and MALDI was done by spreadsheet calculations on raw mass spectroscopy data using relationships described in Chapter 2.[87] Abbreviations used will be Mn (Number average molecular weight), Mw (weight average molecular weight), pdi (polydispersity index). GPC was done on a Waters GPC with Burdick & Johnson HPLC grade THF and calibrated against polystyrene standards at a flow rate of 1mL/minute. The GPC was equipped with Waters 510 HPLC pumps, Waters 486 Tunable UV/Vis detector, and Styragel HMW2 (100-10,000 daltons) and HMW6E (5000-10,000,000 daltons) columns linked in series. Samples were filtered through Alltech 4 mm, 0.45μm PTFE syringe filters before injection onto the GPC. Differential Scanning Calorimetry (DSC) was done on a TA Instruments 2920 MDSC with LNCA cooling device at 5°C/min and 10°C/min in standard aluminum pans. Mass Spectroscopy was performed by the Mass Spectroscopy Laboratory, School of Chemical Sciences, University of Illinois. Low

resolution (FD) spectra were obtained on a Finnigan-Mat 731 spectrometer. Low resolution (MALDI) specta were obtained on a VG TofSpec spectrometer. Elemental analysis was performed by the Microanalytical Laboratory, School of Chemical Sciences, University of Illinois. Fluorescence and UV/Vis spectroscopy was carried out on a Hitachi F-3010 Fluorescence Spectrophotometer and Hitachi U-3300 Spectrophotometer, respectively. Scanning Electron Microscopy was done on a Hitachi S-800 microscope. Transmission Electron Microscopy was done on a Philips CM-12 at 120 kV, and a Philips CM-200 at 120 kV. Thin layer chromatography was done with Silica Gel 60 F_{254} plates from EM Industries. Silica gel for column chromatography was Merck 230-400 mesh, 60Å. Thermal transitions and liquid crystalline textures were analyzed using a Leitz Laborlux 12 POL optical polarized microscope with Bertrand lens and a Linkham THM 600 hotstage

6.2 Lithographic Processing

Spin coating of films onto <100> p-type silicon wafers was done on a Headway Research Photo-Resist Spinner at 3000 rpm for approximately 30 seconds. Solutions of **9** in chloroform (~40 mg/mL) were introduced onto the silicon wafer by a syringe equipped with an Alltech 4 mm, 0.45μm PTFE syringe filter. Thickness of the films was determined using a Gaertner L116C ellipsometer. Irradiation of the films was done through a mask made of quartz with a chrome pattern on one side. The light source was an Oriel 150 Watt Xenon lamp. Development of the irradiated photoresist film was done by pouring 10 mL of 3:1, DCM:Acetone over the wafer which removed the unreacted portions of the film. The wafer was then rinsed with MilliQ water and air dried. Etching of the silicon was done with a Plasma-Therm 790 Series Plasma Processing System. Conditions for etching were a 5% O_2 in

CF$_4$ atmosphere, at 50 mtorr and 150 W for 5 minutes. The photoresist pattern was then removed from the sample by "ashing" in 100% O$_2$ atmosphere, 70 mtorr, 150 W for 2 minutes.

6.3 X-Ray Diffraction

Samples were prepared in two different ways. In the case of the binary mixtures, samples were solvent cast (1:1 DCM:Toluene) onto microscope slides, dried, and then irradiated and/or heated as was called for. The material was then removed from the glass slide with a razor blade and packed into holder with a 3 mm hole and held in place with Scotch tape. Other powder samples were ground in a mortar and pestle and then placed in the 3 mm holder and held in place with Scotch tape. Variable Temperature X-ray diffraction was done on the liquid crystal samples (**9-11**) as described in Chapter 3. Samples were first ground in a mortar and pestle and then placed in 1.5 mm glass capillaries. The capillaries were then placed within a specially built copper block (see Figure 3.8-3.10) heated by 0.134" substrate heater (Omega) and monitored with a K-type thermocouple. Samples were first heated to the clearing point of the liquid crystal and then slowly cooled, taking diffraction data upon cooling.

6.4 TEM Sample Preparation

Samples were prepared by solution casting onto water from a ~0.1% by weight solution of the material in (1:1 DCM:Toluene). Films were then picked up on carbon coated copper TEM grids. Any annealing or irradiation steps were then done directly on the film held on the TEM grid. The binary mixture films were exposed to 1.5 mW/cm^2 ultraviolet light from a mercury penlight (peak =254 nm) for approximately 1 minute.

6.5 Materials

Unless otherwise noted, all starting materials were obtained from commercial suppliers and used as received. Styrene monomer was prepared by washing with 1M NaOH and water to remove inhibitor and then dryed with $MgSO_4$. Further drying was done over CaH_2 followed by vacuum transfer to a Kontes flask which was stored in a dark freezer until needed. Dry benzene was prepared by washing with conc. H_2SO_4, water, 1M NaOH, water, and then dried over $MgSO_4$. This was then stirred over Na and benzophenone until a purple color was formed and then vacuum transferred to a Kontes flask. Dry tetrahydrofuran was prepared by placing commercially bought anhydrous THF over Na and benzophenone and then vacuum transferring into a Kontes Flask. Dry CH_2Cl_2 was obtained by freshly distilling over CaH_2. Diisopropylcarbodiimide (DIPC) was distilled before use.

The following materials were prepared by literature methods: 4-(4-hydroxyphenyl)phenyl(dimethylthexylsilyoxy)-1-methanone (**12**)[59], 4-(4-methoxycarbonyloxyphenol)-benzoic acid (**13**)[78], 12-tert-butyldimethylsilyloxy-5,7-dodecadiyn-1-ol (**14**)[78], 4-(4-pentyloxyphenyl)benzoic acid (**15**)[78], 9-anthroyl chloride (**5a**)[178], cinnamoyl chloride (**4a**)[178], 4-(Dimethylamino)pyridinium 4-Toluenesulfonate (DPTS)[84].

6.6 Synthetic Procedures

<u>1-(4-(4-(12-(4-(4-(4-pentyloxyphenyl)benzoyloxy)phenyl)benzoyloxy)-5,7-dodecadiynyloxycarbonyl)phenyl)phenyloxy)-1-oligo(styrenone) (**2**)</u>

An oven dried, 500 mL round bottom flask equipped with a magnetic stir bar and septum under N_2 was charged with **3c** (0.14g, 0.11 mmol), **8** (0.08g, 0.12 mmol), DPTS

(0.032g, 0.11 mmol), and dry CH_2Cl_2 (30 mL). Under rapid stirring, DIPC (0.1 mL, 0.6 mmol) was added and the reaction stirred for 24 hours. The reaction solution was filtered to remove precipitated urea, and poured into a separatory funnel. The organic layer was washed with brine water (sat. NaCl solution), water, dried ($MgSO_4$) and then concentrated. The resulting tacky white solid was first purified by chromatography (silica gel, CH_2Cl_2) followed by dissolving in a minimum of CH_2Cl_2 and precipitating in 250 mL of rapidly stirring MeOH. The white product was collected on a Buchner funnel.

2

MW: 1971

Yield: 0.07g (53% yield)

GPC: Mn = 2425 Mw = 2635 pdi = 1.09

^{1}H-NMR (300 MHz, $CDCl_3$): δ 0.7-2.5(bm, 86H); 4.01(m, 2H); 4.4(m, 4H); 6.4-7.4(bm, 93H); 7.6(m, 14H); 8.11(d, 2H); 8.28(d, 2H)

Oligo(styrene) carboxylic acid (**3a**)

An oven dried, 250 mL Schlenk flask, equipped with a magnetic stir bar and rubber septum tighted on with copper wire was charged with dry benzene (30 mL), dry THF (10 mL), and styrene (5 mL, 43.6 mmol) under N_2. This was followed by the rapid addition of a solution of n-butyl lithium in hexanes (2.5 mL, 3.96 mmol) under rapid stirring. This resulted in a deep red color in the reaction solution that was stirred for 2 hours. The reaction was quenched with 99.99% CO_2 via copper tubing and cannula for 5 minutes. This produced a clear solution to which was added a solution of acidic methanol (2 mL 6M HCl in 5 mL MeOH) which was stirred for 5 minutes. Solvent was removed to yield a tacky, clear solid

which was loaded onto silica gel and washed with 1.4 L of CH_2Cl_2 to remove uncarboxylated oligostyrene. The carboxylated oligostyrene was then collected off the column by elution with 1.4 L of acetone which yielded 2.45 g (50% yield) of **3a** as a tacky solid.

3a

GPC: Mn = 1304   Mw = 1541   pdi = 1.18

MS FD: Mn = 1137   Mw = 1219   pdi = 1.07

Yield: 2.45g (50%)

Oligo(tert-butyl styrene) carboxylic acid (**6a**)

An oven dried, 250 mL Schlenk flask, equipped with a magnetic stir bar and rubber septum tighted on with copper wire was charged with dry benzene (30 mL), dry THF (10 mL), and t-butyl styrene (5 mL, 27.3 mmol) under N_2. This was followed by the rapid addition of a solution of n-butyl lithium in hexanes (1.15 mL, 2.1 mmol) under rapid stirring. This resulted in a deep red color in the reaction solution that was stirred for 2 hours. The reaction was quenched with 99.99% CO_2 via copper tubing and cannula for 5 minutes. This produced a clear solution to which was added a solution of acidic methanol (2 mL 6M HCl in 5 mL MeOH) which was stirred for 5 minutes. Solvent was removed to yield a tacky, clear solid which was loaded onto silica gel and washed with 1.4 L of CH_2Cl_2 to remove uncarboxylated oligo(t-butyl styrene). The carboxylated product was then collected off the column by elution with 1.4 L of acetone which yielded 0.83 g (18% yield) of **6a** as a tacky solid.

6a

GPC: Mn = 1913   Mw = 2106   pdi = 1.1

MS FD: Mn = 2047 Mw = 2225 pdi = 1.08

Yield: 0.83g (18% yield)

Oligo(styrene-b-butadiene) carboxylic acid (7a)

An oven dried, 250 mL Schlenk flask, equipped with a magnetic stir bar and rubber septum tighted on with copper wire was charged with dry benzene (30 mL), dry THF (10 mL), and styrene (5 mL, 43.6 mmol) under N_2. This was followed by the rapid addition of a solution of n-butyl lithium in hexanes (2.5 mL, 3.96 mmol) under rapid stirring. The reaction solution became a deep red color and was stirred for 2 hours followed by addition of butadiene (2.2 mL, 26.4 mmol) which turned the reaction solution an orangish/yellow color. The reaction was stirred for another 2 hours and then quenched with 99.99% CO_2 via copper tubing and cannula for 5 minutes. This produced a clear solution to which was added a solution of acidic methanol (2 mL 6M HCl in 5 mL MeOH) which was stirred for 5 minutes. Solvent was removed to yield a tacky, clear solid which was loaded onto silica gel and washed with 1.4 L of CH_2Cl_2 to remove uncarboxylated product. The carboxylated product was then collected off the column by elution with 1.4 L of acetone which yielded 0.55 g (9% yield) of **7a** as a tacky solid.

7a

GPC: Mn = 1741 Mw = 1937 pdi = 1.11

NMR: Mn = 1412 (see text, Chapter 2)

Yield: 0.55g (9% yield)

1-(4-(4-dimethylthexylsilyloxycarbonylphenyl)phenyloxy)-1-oligo(styrenone) (3b)

1-(4-(4-dimethylthexylsilyloxycarbonylphenyl)phenyloxy)-1-oligo(tert-butyl styrenone) (**6b**)

1-(4-(4-dimethylthexylsilyloxycarbonylphenyl)phenyloxy)-1-oligo(styrene-b-butadienone) (**7b**)

An oven dried, 500 mL round bottom flask equipped with a magnetic stir bar and septum under N_2 was charged with oligo(styrene) carboxylic acid (2.45g, 1.81mmol), **12** (0.71g, 1.99mmol), DPTS (0.53g, 1.81 mmol), and dry CH_2Cl_2 (60 mL). Under rapid stirring, DIPC (1.4 mL, 9.05 mmol) was added and the reaction stirred for 16 hours. The reaction solution was filtered to remove precipitated urea, washed with brine water (sat. NaCl solution), water and then dried ($MgSO_4$) and concentrated. The resulting tacky white solid was purified by chromatography (silica gel, CH_2Cl_2) to give **3b** as a white solid.

3b

MW: 1475

Yield: 2.89g (94% yield)

^{1}H-NMR (300 MHz, $CDCl_3$): δ 0.45(d, 6H); 0.78(m, 3H); 0.8-2.8(b, 88H); 3.4(b, 1H); 6.2-7.4(b, 100H); 7.5(m, 2H); 7.6(m, 2H); 8.1(t, 2H)

6b

MW: 2385

Yield: 0.87g (90% yield)

7b

MW: 1750 (NMR)

Yield: 0.45g (67% yield)

^{1}H-NMR (400 MHz, $CDCl_3$): δ 0.48(s, 6H); 0.78(m, 3H); 0.8-2.6(bm, 115H); 3.35(b, 1H); 4.5-5.2(b,15H); 5.4-6.0(b, 5H); 6.4-7.4(bm, 76H); 7.6(m, 4H); 8.1(d, 2H)

4-(4-(oligostyroyl)oxyphenol)benzoic acid (**3c**)

4-(4-(oligo(tert-butyl-styroyl)oxyphenol)benzoic acid (**6c**)

4-(4-(oligo(styrene-b-butadienoyl)oxyphenol)benzoic acid (**7c**)

To a 500 mL round bottom flask equipped with magnetic stir bar and septum under N_2 was added **3b** (2.89g, 1.96mmol). A solution of 9:1 THF:6M HCl (70mL) was added and the mixture stirred for 2 hours or until done by TLC. The contents were then poured into a separatory funnel along with CH_2Cl_2 (150 mL). The organic layer was washed four times with water, dried ($MgSO_4$), and concentrated. The tacky white product was purified by chromatography (silica gel, CH_2Cl_2) to yield the pure product.

3c

MW: 1333

Yield: 2.65 (100% yield)

^{1}H-NMR (400 MHz, CDCl$_3$): δ 0.78(m, 3H); 0.8-2.6(bm, 86H); 3.4(b, 1H); 6.2-7.4(bm, 91H); 7.5(m, 2H); 7.65(m, 2H); 8.15(m, 2H)

6c

MW: 2243

Yield: 0.78g (96% yield)

MS FD: Mn = 2245   Mw = 2408   pdi = 1.07

^{1}H-NMR (400 MHz, CDCl$_3$): δ 0.78(m, 3H); 0.8-2.6(bm, 151H); 3.4(b, 1H); 6.1-7.4(bm, 39H); 7.6(m, 4H); 8.2(m, 2H)

7c

MW: 1608

Yield: 0.41g (99% yield)

1-(4-(4-(4-(4-dimethylthexylsilyloxycarbonylphenyl)phenyloxycarbonyl) phenyl)phenyloxy)-1-oligostyrenone (**3d**)

1-(4-(4-(4-(4-dimethylthexylsilyloxycarbonylphenyl)phenyloxycarbonyl) phenyl)phenyloxy)-1-oligo(tert-butyl-styrenone) (**6d**)

1-(4-(4-(4-(4-dimethylthexylsilyloxycarbonylphenyl)phenyloxycarbonyl) phenyl)phenyloxy)-1-oligo(styrene-b-butadienone) (**7d**)

An oven dried, 500 mL round bottom flask equipped with a magnetic stir bar and septum under N_2 was charged with **3c** (2.65g, 1.96 mmol), **12** (0.68g, 1.96 mmol), DPTS (0.511g, 1.71 mmol), and dry CH_2Cl_2 (60 mL). Under rapid stirring, DIPC (1.3 mL, 8.54 mmol) was added and the reaction stirred for 24 hours. The reaction solution was filtered to remove precipitated urea, washed with brine water (sat. NaCl solution), water and then dried ($MgSO_4$) and concentrated. The resulting tacky white solid was purified by chromatography (silica gel, CH_2Cl_2) to give **3d** as a white solid.

3d

MW: 1671

Yield: 2.96g (88% yield)

^{1}H-NMR (300 MHz, CDCl$_3$): δ 0.46(s, 6H); 0.78(m, 3H); 0.8-2.6(bm, 76H); 3.45(b, 1H); 6.3-7.3(bm, 83H); 7.35(m, 2H); 7.55(m, 2H); 7.7(m, 6H); 8.1(d, 2H); 8.28(t, 2H)

6d

MW: 2581

Yield: 0.71g (79% yield)

^{1}H-NMR (500 MHz, CDCl$_3$): δ 0.43(s, 6H); 0.78(m, 3H); 0.8-2.6(bm, 163H); 3.45(b, 1H); 6.0-7.3(bm, 46H); 7.38(m, 2H); 7.57(m, 2H); 7.7(m, 6H); 8.2(d, 2H); 8.3(m, 2H)

7d

MW: 1946

Yield: 0.40g (80% yield)

4-(4-(4-(4-oligo(styroyloxyphenyl))benzoyloxy)phenyl)benzoic acid (**3e**)

4-(4-(4-(4-oligo(tert-butyl-styroyloxyphenyl))benzoyloxy)phenyl)benzoic acid (**6e**)

4-(4-(4-(4-oligo(styrene-b-butadienoyloxyphenyl))benzoyloxy)phenyl)benzoic acid (**7e**)

To a 500 mL round bottom flask equipped with magnetic stir bar and septum under N$_2$ was added **3d** (2.96, 1.77 mmol). A solution of 9:1 THF:6M HCl (100 mL) was added and the mixture stirred for 2 hours or until done by TLC. The contents were then poured into a separatory funnel along with CH$_2$Cl$_2$ (150 mL). The organic layer was washed four times with water, dried (MgSO$_4$), and concentrated. The tacky white product was purified by chromatography (silica gel, CH$_2$Cl$_2$) to yield the pure product.

3e

MW: 1529

Yield: 2.75g (100% yield)

^{1}H-NMR (400 MHz, CDCl$_3$): δ 0.78(m, 3H); 0.8-2.6(bm, 70H); 3.4(b, 1H); 6.3-7.3(bm, 67H); 7.38(m, 2H); 7.58(m, 2H); 7.7(m, 6H); 8.2(d, 2H); 8.3(m, 2H)

6e

MW: 2439

Yield: 0.60g (90% yield)

^{1}H-NMR (400 MHz, CDCl$_3$): δ 0.78(m, 3H); 0.8-2.6(bm, 163H); 3.45(b, 1H); 6.0-7.3(bm, 46H); 7.38(m, 2H); 7.57(m, 2H); 7.7(m, 6H); 8.2(d, 2H); 8.3(m, 2H)

7e

MW: 1804

Yield: 0.39g (100% yield)

^{1}H-NMR (500 MHz, CDCl$_3$): δ 0.78(m, 3H); 0.8-2.6(bm, 118H); 3.35(b, 1H); 4.5-5.2(b, 16H); 5.4-6.0(b, 7H); 6.4-7.2(bm, 76H); 7.38(d, 2H); 7.67(m, 2H); 7.71(m, 6H); 8.2(d, 2H); 8.3(m, 2H)

1-(4-(4-(4-(4-(12-tert-butyldimethylsilyloxy-5,7-dodecadiynyloxycarbonyl)phenyl)phenyloxycarbonyl)phenyl)phenyloxy)-1-oligo(styrenone) (**3f**)

1-(4-(4-(4-(4-(12-tert-butyldimethylsilyloxy-5,7-dodecadiynyloxycarbonyl)phenyl)phenyloxycarbonyl)phenyl)phenyloxy)-1-oligo(tert-butyl-styrenone) (**6f**)

1-(4-(4-(4-(4-(12-tert-butyldimethylsilyloxy-5,7-dodecadiynyloxycarbonyl)phenyl)phenyloxycarbonyl)phenyl)phenyloxy)-1-oligo(styrene-b-butadienone) (**7f**)

An oven dried, 500 mL round bottom flask equipped with a magnetic stir bar and septum under N$_2$ was charged with **3e** (2.75g, 1.58 mmol), **14** (0.49g, 1.58 mmol), DPTS (0.47g, 1.58 mmol), and dry CH$_2$Cl$_2$ (60 mL). Under rapid stirring, DIPC (1.2 mL, 7.90 mmol) was added and the reaction stirred for 24 hours. The reaction solution was filtered to remove precipitated urea, washed with brine water (sat. NaCl solution), water and then dried (MgSO$_4$) and concentrated. The resulting tacky white solid was first purified by chromatography (silica gel, 2% MeOH in CH$_2$Cl$_2$) and then by dissolving in a minimum of

CH₂Cl₂ and precipitating in 250 mL of rapidly stirring MeOH. The white product was collected on a Buchner funnel.

3f

MW: 1820

Yield: 2.6g (80% yield)

^{1}H-NMR (500 MHz, CDCl₃): δ 0.05(s, 6H); 0.78(m, 3H); 0.85(s, 9H); 1-2.2(bm, 53H); 2.3(t, 2H); 2.35(t, 2H); 3.4(b, 1H); 3.6(t, 2H); 4.38(t, 2H); 6.3-7.2(bm, 59H); 7.38(t, 2H); 7.55(m, 2H); 7.68(m, 6H); 8.11(d, 2H); 8.28(m, 2H)

6f

MW: 2730

Yield: 0.57g (85% yield)

^{1}H-NMR (400 MHz, CDCl₃): δ 0.05(s, 6H); 0.78(m, 3H); 0.85(s, 9H); 1-2.2(bm, 168H); 2.3(t, 2H); 2.35(t, 2H); 3.4(b, 1H); 3.6(t, 2H); 4.38(t, 2H); 6.0-7.2(bm, 55H); 7.38(t, 2H); 7.55(m, 2H); 7.7(m, 6H); 8.11(d, 2H); 8.3(m, 2H)

7f

MW: 2095

Yield: 0.21g (49% yield)

^{1}H-NMR (500 MHz, CDCl₃): δ 0.05(s, 6H); 0.78(m, 3H); 0.9(s, 9H); 1.0-2.2(bm, 77H); 2.29(t, 2H); 2.38(t, 2H); 3.35(b, 1H); 3.61(t, 2H); 4.38(t, 2H); 4.5-5.2(b, 10H); 5.4-6.0(b, 4H); 6.25-7.2(bm, 56H); 7.35(d, 2H); 7.69(m, 8H); 8.11(d, 2H); 8.3(m, 2H)

1-(4-(4-(4-(12-hydroxy-5,7-dodecadiynyloxycarbonyl)phenyl)phenyloxycarbonyl)phenyl)phenyloxy)-1-oligo(styrenone) (**3**)

<u>1-(4-(4-(4-(12-hydroxy-5,7-dodecadiynyloxycarbonyl)phenyl)</u>

<u>phenyloxycarbonyl)phenyl)phenyloxy)-1-oligo(tert-butyl-styrenone) (**6**)</u>

<u>1-(4-(4-(4-(12-tert-butyldimethylsilyloxy-5,7-dodecadiynyloxycarbonyl)phenyl)</u>

<u>phenyloxycarbonyl)phenyl)phenyloxy)-1-oligo(styrene-b-butadienone) (**7**)</u>

To a solution of **3f** (2.6g, 1.25 mmol), THF (30 mL), water (2 mL), was added p-toluene sulfonic acid monohydrate (2.4g, 1.25 mmol). After stirring for 48 hours, the contents were added to a separatory funnel with CH_2Cl_2 (75 mL), washed with water, dried ($MgSO_4$) and concentrated. The solid was purified by chromatography (silica gel, 2% MeOH in CH_2Cl_2) to yield the pure white solid.

3

MW: 1706

Yield: 2.1g (88% yield)

GPC: Mn = 2435   Mw = 2614   pdi = 1.07

MS (MALDI):   Mn = 2057   Mw = 2222   pdi = 1.08

^{1}H-NMR (400 MHz, $CDCl_3$): δ 0.78(m, 3H); 0.85-2.2(bm, 50H); 2.3(t, 2H); 2.35(t, 2H); 3.45(b, 1H); 3.63(t, 2H); 4.38(t, 2H); 6.3-7.2(bm, 56H); 7.38(t, 2H); 7.55(m, 2H); 7.7(m, 6H); 8.11(d, 2H); 8.28(m, 2H)

6

MW: 2616

Yield: 0.32g (57% yield)

GPC: Mn = 3274   Mw = 3565   pdi = 1.09

MS (FD):   Mn = 2902   Mw = 2972   pdi = 1.02

^{1}H-NMR (400 MHz, CDCl$_3$): δ 0.78(m, 3H); 0.85-2.2(bm, 184H); 2.3(t, 2H); 2.35(t, 2H); 3.45(b, 1H); 3.63(t, 2H); 4.38(t, 2H); 6.1-7.2(bm, 58H); 7.38(t, 2H); 7.55(m, 2H); 7.7(m, 6H); 8.11(d, 2H); 8.28(m, 2H)

7

MW: 1981

Yield: 0.2g (90% yield)

GPC:	Mn = 3087	Mw = 3314	pdi = 1.07
MS (MALDI):	Mn = 2262	Mw = 2377	pdi = 1.05

^{1}H-NMR (400 MHz, CDCl$_3$): δ 0.78(m, 3H); 0.85-2.2(bm, 76H); 2.3(t, 2H); 2.35(t, 2H); 3.45(b, 1H); 3.63(t, 2H); 4.38(t, 2H);); 4.5-5.2(b, 10H); 5.4-6.0(b, 5H); 6.25-7.2(bm, 54H); 7.38(m, 2H); 7.7(m, 8H); 8.11(d, 2H); 8.3(m, 2H)

<u>1-(4-(4-(4-(4-(12-cinnamyl carbonyloxy-5,7-dodecadiynyloxycarbonyl)phenyl) phenyloxycarbonyl)phenyl)phenyloxy)-1-oligo(styrenone) (**4**)</u>

<u>1-(4-(4-(4-(4-(12-(9-anthracenyl carbonyloxy)-5,7-dodecadiynyloxycarbonyl)phenyl) phenyloxycarbonyl)phenyl)phenyloxy)-1-oligo(tert-butyl-styrenone) (**5**)</u>

An oven dried 100 mL round bottom flask with magnetic stir bar was charged with **3** (0.17 g, 0.1 mmol), **4a** (0.028 g, 0.17 mmol), pyridine (1 mL), 4-(dimethylamino)pyridine (0.019g, 0.16 mmol), and dry CH$_2$Cl$_2$ (40 mL). This solution was then refluxed gently under N$_2$ for 12 hours and then transferred to a separatory funnel where it was washed with water, dried (MgSO$_4$) and concentrated. The residue was purified by column chromatography (silica gel, 5% acetone in CH$_2$Cl$_2$) and then stored under N$_2$.

4

MW: 1836

Yield: 0.11g (60% yield)

GPC: Mn = 2403   Mw = 2622   pdi = 1.09

^{1}H-NMR (300 MHz, CDCl$_3$): δ 0.8(m, 3H); 0.85-2.2(bm, 50H); 2.38(m, 4H); 3.45(b, 1H); 4.2(t, 2H); 4.38(t, 2H); 6.3-7.4(bm, 108H); 7.52(m, 4H); 7.68(m, 8H); 8.11(d, 2H); 8.28(m, 2H)

5

MW: 1910

Yield: 0.044 g (50% yield)

GPC: Mn = 1866   Mw = 2038   pdi = 1.09

^{1}H-NMR (300 MHz, CDCl$_3$): δ 0.8(m, 3H); 0.85-2.2(bm, 68H); 2.38(m, 4H); 3.45(b, 1H); 4.38(t, 2H); 4.65(t, 2H); 6.3-7.4(bm, 78H); 7.52(m, 6H); 7.68(m, 6H); 8.05(d, 4H); 8.11(d, 2H); 8.3(t, 2H); 8.55(s, 1H)

4-(4-(12-(9-anthracenyl carbonyloxy)-5,7-dodecadiynyloxycarbonyl)phenyl)phenyloxy (4-(4-pentyloxyphenyl)phenyl)-1-methanone (**9**)

An oven dried 100 mL round bottom flask with magnetic stir bar was charged with **8** (0.78 g, 1.19 mmol), **5a** (0.37 g, 1.43 mmol), pyridine (1 mL), 4-(dimethylamino)pyridine (0.017g, 0.1 mmol), and dry CH$_2$Cl$_2$ (60 mL). This solution was then refluxed gently under N$_2$ for 12 hours. The reaction solution was then poured into a separatory funnel along with CH$_2$Cl$_2$ (50mL). The organic layer was washed with sat. NaHCO$_3$, water, dried (MgSO$_4$), then concentrated. The residue was purified by column chromatography (silica gel, 1% acetone in CH$_2$Cl$_2$).

9

MW: 861.04

^{1}H-NMR (400 MHz, CDCl$_3$): δ 0.95(t, 3H); 1.44(m, 4H); 1.73(m, 4H); 1.82(p, 2H); 1.91(p, 2H); 2.01(p, 2H); 2.37(t, 4H); 4.02(t, 2H); 4.33(t, 2H); 4.61(t, 2H); 7.01(d, 2H); 7.34(d, 2H); 7.52(m, 4H); 7.61(d, 2H); 7.69(m, 6H); 8.02(t, 4H); 8.1(d, 2H); 8.26(d, 2H); 8.52(s, 1H)

$C_{58}H_{52}O_7$ calcd C 80.91 H 6.09

found C 80.79 H 6.17

12-tert-butyldimehtylsilyloxy-1-dodecanol (**10a**)

An oven dried 150 mL Schlenk flask equipped with magnetic stir bar and septum under N$_2$ was charged with 1,12-dodecanediol (3 g, 15.1 mmol), imidazole (2.27g, 33.3 mmol), and dry N, N-Dimethylformamide DMF (25mL). This mixture was stirred until homogeneous at which time tert-butyldimethylsilylchloride (TBDMS) (2.26g, 14.9 mmol) was added and the reaction stirred for 16 hours. The reaction solution was added to a separatory funnel along with CH$_2$Cl$_2$ (50 mL) and the organic layer was washed with sat. NaHCO$_3$ solution, water, dried (MgSO$_4$), and concentrated. Purification by column chromatography (silica gel, 10% EtOH in CH$_2$Cl$_2$, compound is not UV active so 4-bromobiphenyl was added in trace amount to act as marker for solvent front on column) yielded the pure material.

10a

MW: 316.61

Yield: 1.48g (31% yield)

^{1}H-NMR (400 MHz, CDCl$_3$): δ 0.04(s, 6H); 0.89(s, 9H); 1.26(b, 16H); 1.49(p, 2H); 1.55(p, 2H); 3.59(t, 2H); 3.62(t, 2H)

12-tert-butyldimethylsilyloxydodecyloxy(4-(4-methoxycarbonyloxyphenyl)phenyl)-1-methanone (**10b**)

An oven dried, 500 mL round bottom flask equipped with a magnetic stir bar and septum under N_2 was charged with **10a** (1.48g, 4.67 mmol), **13** (1.27g, 4.67 mmol), DPTS (1.38g, 4.67 mmol), and dry CH_2Cl_2 (60 mL). Under rapid stirring, DIPC (2.5 mL, 14.0 mmol) was added and the reaction stirred for 24 hours. The reaction solution was filtered to remove precipitated urea, and transferred to a separatory funnel. The organic layer was washed with water, dried ($MgSO_4$) and concentrated. The residue was purified by column chromatography (silica gel, 1% MeOH in CH_2Cl_2) to yield a viscous white product.

10b

MW: 570.61

Yield: 1.92g (72% yield)

^{1}H-NMR (500 MHz, $CDCl_3$): δ 0.04(s, 6H); 0.89(s, 9H); 1.22(s, 3H); 1.26(b, 12H); 1.36(m, 2H); 1.44(m, 2H); 1.5(m, 2H); 1.77(p, 2H); 3.59(t, 2H); 4.33(t, 2H); 7.2(d, 2H); 7.6(d, 4H); 8.1(d, 2H)

12-tert-butyldimethylsilyloxydodecyloxy(4-(4-hydroxyphenyl)phenyl)-1-methanone (**10c**)

A 500 ml round bottom flask equipped with magnetic stir bar was charged with **10b** (1.92g, 3.36 mmol), CH_2Cl_2 (45 mL), conc. NH_4OH (14 mL), ethanol (33 mL) to form a clear yellow solution. This solution was stirred for 7 hours and then added to a 500 mL separatory funnel along with 75 mL CH_2Cl_2. The organic layer was washed with sat. $NaHCO_3$, and water until the aqueous wash was pH~7. Then the organic layer was dried ($MgSO_4$) and

concentrated. Purification was done by column chromatography (silica gel, 5% MeOH in CH$_2$Cl$_2$).

10c

MW: 512.61

Yield: 1.45g (84% yield)

^{1}H-NMR (400 MHz, CDCl$_3$): δ 0.04(s, 6H); 0.89(s, 9H); 1.26(b, 12H); 1.36(m, 2H); 1.43(m, 2H); 1.5(m, 2H); 1.77(p, 2H); 3.59(t, 2H); 4.33(t, 2H); 6.95(d, 2H); 7.51(d, 2H); 7.6(d, 2H); 8.08(d, 2H)

12-tert-butyldimethylsilyloxydodecyloxy(4-(4-(4-(4-pentyloxyphenyl)benzoyloxy) phenyl)phenyl)-1-methanone (**10d**)

An oven dried, 250 mL round bottom flask equipped with a magnetic stir bar and septum under N$_2$ was charged with **10c** (1.45 g, 2.83 mmol), **15** (0.80 g, 2.83 mmol), DPTS (0.83 g, 2.83 mmol), and dry CH$_2$Cl$_2$ (50 mL). Under rapid stirring, DIPC (1.32 mL, 8.49 mmol) was added and the reaction stirred for 24 hours. The reaction solution was filtered to remove precipitated urea, and transferred to a separatory funnel. The organic layer was washed with brine water, water, dried (MgSO$_4$) and concentrated. The residue was purified by column chromatography (silica gel, CH$_2$Cl$_2$) to yield a white solid.

10d

MW: 778.97

Yield: 1.75g (79% yield)

^{1}H-NMR (500 MHz, CDCl$_3$): δ 0.04(s, 6H); 0.89(s, 9H); 0.95(t, 3H); 1.26(b, 12H); 1.46(m,

10H); 1.81(m, 4H); 3.59(t, 2H); 4.02(t, 2H); 4.33(t, 2H); 7.01(d, 2H); 7.34(d, 2H); 7.6(d, 2H); 7.69(m, 6H); 8.12(d, 2H); 8.26(d, 2H)

12-hydroxydodecyloxy(4-(4-(4-(4-pentyloxyphenyl)benzoyloxy)phenyl)phenyl)-1-methanone (10)

A 100 mL round bottom flask with magnetic stir bar was charged with **10d** (1.75 g, 2.24 mmol), p-toluene sulfonic acid monohydrate (0.13 g, 0.67 mmol), water (1 mL), and THF (35 mL). This solution was stirred for 16 hours at which point the product precipitates as a white solid from the solution. The white ppt was collected on a Buchner funnel, rinsed with 200 mL of THF and then dried under vacuum to yield a white solid. This solid was then dissolved in chloroform (0.8mg/mL) and filtered through a teflon, 0.45 μm syringe filter to yield a pure white product.

10

MW: 664.88

Yield: 0.360 g (24% yield)

^{1}H-NMR (400 MHz, CDCl$_3$): δ 0.95(t, 3H); 1.26(b, 12H); 1.46(m, 10H); 1.81(m, 4H); 3.59(t, 2H); 4.02(t, 2H); 4.33(t, 2H); 7.01(d, 2H); 7.34(d, 2H); 7.6(d, 2H); 7.69(m, 6H); 8.12(d, 2H); 8.26(d, 2H)

$C_{43}H_{52}O_6$ calcd C 77.68 H 7.88

found C 77.47 H 7.81

4-(4-(12-anthracenylcarbonyloxy)dodecyloxycarbonyl)phenyl)phenyloxy(4-(4-pentyloxyphenyl)phenyl)-1-methanone (11)

An oven dried 100 mL round bottom flask with magnetic stir bar was charged with **10** (0.77 g, 1.15 mmol), **5a** (0.30 g, 1.25 mmol), pyridine (1 mL), 4-(dimethylamino)pyridine (0.014g, 0.1 mmol), and dry CH_2Cl_2 (100 mL). This solution was then refluxed gently under N_2 for 12 hours. The reaction mixture was then vacuum filtered on a Buchner funnel and the filtrate washed with sat. $NaHCO_3$, water and then dried ($MgSO_4$) and concentrated. The residue was purified by column chromatography (silica gel, CH_2Cl_2).

MW: 869.20

Yield: 0.58g (58% yield)

^{1}H-NMR (500 MHz, $CDCl_3$): δ 0.95(t, 3H); 1.26-1.5(bm, 20H); 1.82(m, 6H); 4.02(t, 2H); 4.33(t, 2H); 4.61(t, 2H); 7.01(d, 2H); 7.34(d, 2H); 7.5(m, 4H); 7.61(d, 2H); 7.69(m, 6H); 8.02(t, 4H); 8.12(d, 2H); 8.26(d, 2H); 8.52(s, 1H)

$C_{58}H_{60}O_7$ calcd C 80.16 H 6.96

                 found C 79.91 H 6.92

Final Conclusions

The study of a series of styrene derivative diblock rodcoils as opposed to the tri-block rodcoils typified by 1 has led to some interesting observations about the nanophase behavior of these types of systems. The oligo(t-butyl styrene) coil was found too completely disrupt the ability of the rod segments to aggregate as they had when attached to relatively less bulky oligo(styrene) group. This may be due to the increased steric bulk of the t-butyl substituted styrene coil or it may be a kinetic effect of the increased glass transition of the oligo(t-butyl styrene). The higher glass transition temperature may hinder rearrangement of the rodcoil molecules during the solvent casting process and trap the rodcoil molecules as a glass. While some of these diblock rodcoil systems were found to aggregates into nanodomains, the ability of the diacetylene groups to "stitch' aggregates of rod segments together seemed to be completely hindered by the styrene coil although short range order was detected by electron diffraction in selected areas. Some success was achieved in forming dimers of the rodcoil molecules by attaching reactive end groups to the terminal –OH group of 3. The mesophase behavior of three reactive liquid crystalline molecules was fully investigated and allowed for better understanding of the ordered layers formed by these materials. The goal with these compounds was to react them in the ordered state for the formation of two-dimensional objects. The interdigitated packing scheme in 9 was found to lead predominantly to head-to-tail isomers that did not undergo topochemical reaction of the diacetylene groups at low temperatures. Insoluble material was formed by irradiation at higher temperature but the nature of this material is unknown at this time. What is known is that molecule 9 was successfully used as a negative photoresist which led to the transfer of 3-5 μm features onto a silicon wafer. To test the role of the diacetylene in the formation of various one-dimensional and two-dimensional polymers, the non-diacetylene analog of 9, 11, was synthesized.

When employed as a photoresist in identical conditions to 9, 11 failed to achieve the necessary differences in solubility between irradiated and unirradiated material and therefore acted poorly as a negative photoresist. Thus, the diacetylene is believed to play a role in the formation of higher molecular weight material upon UV irradiation of films of 9. It is likely that further improvements on the use of reactive liquid crystals as photoresists could be made as a result of this preliminary investigation. Finally, a potentially rich area of study was introduced in the use of binary mixtures of rodcoil molecules with rod molecules. The interesting nanomorphologies formed and their stability at different temperatures led to some proposed ideas about the aggregation and nanophase separation of these types of molecular systems. A combination of TEM, X-ray, and observation of the topochemical polymerization of bulk films was used to characterization of these structures. Probing the topography of the nanocrystals remains a significant challenge, but one that merits further investigation for the ability to control both the chemical make up and the topographic make up of nanostructures could further lead to new three dimensional materials.

References

1.   Stupp, S.I., *et al. Science* **276**, 384-389 (1997).

2.   Weller, H. *Angew. Chem. Int. Ed. Engl.* **32**, 41-53 (1993).

3.   Colvin, V.L., Schlamp, M.C. & Alivisatos, A.P. *Nature* **370**, 354-357 (1994).

4.   Fendler, J.H. & Meldrum, F.C. *Adv. Mater.* **7**, 607-632 (1995).

5.   Murray, C.B., Kagan, C.R. & Bawendi, M.G. *Science* **270**, 1335-1338 (1995).

6.   Pileni, M.P. *J. Phys. Chem.* **97**, 6961-6973 (1993).

7.   Fendler, J.H. *Current Opinion in Solid State & Materials Science* **2**, 365-369 (1997).

8.   Gabor, A.H., Pruette, L.C. & Ober, C.K. *Chem. Mater.* **8**, 2282-2290 (1996).

9.   Allen, R.D., *et al.* in *Microelectronics Technology* (ed. Reichmanis, E.) 255-270 (American Chemical Socity, Washington, DC, 1995).

10.   Armstrong, R.W., *et al. J. Am. Chem. Soc.* **111**, 7525 (1989).

11.   Xu, Z. & Moore, J.S. *angew. Chem. Int. Ed. Engl.* **32**, 1354-1357 (1993).

12.   Klug, A. *Angew. Chem. Int. Ed. Engl* **95**, 579 (1983).

13.   Klug, A. *Angew. Chem. Int. Ed. Engl.* **22**, 565 (1983).

14.   Seto, C.T. & Whitesides, G.M. *J. Am. Chem. Soc.* **115**, 1330 (1993).

15.   Simanek, E.E., *et al. Tetra.* **51**, 607 (1995).

16.   Whitesides, G.M., Mathias, J.P. & Seto, C.T. *Science* **254**, 1312 (1992).

17.   Whitesides, G.M., *et al. Acc. Chem. Res.* **28**, 37 (1995).

18.   Doig, A.J. & Williams, D.H. *J. Am. Chem. Soc.* **114**, 338 (1992).

19.   Lehn, J.M. *Angew. Chem. Int. Ed. Engl.* **27**, 89 (1988).

20.   Cram, D.J. *Angew. Chem. Int. Ed. Engl.* **27**, 1009 (1988).

21.   Pedersen, C.J. *Angew. Chem. Int. Ed. Engl.* **27**, 1021 (1988).

22.   Lehn, J.M. *Supramolecular Chemistry: concepts and perspectives; a personal account* (VCH, Weinheim, 1995).

23.   Konig, B. *J. prakt. Chem.* **337**, 339 (1995).

24.   Percec, V., *et al. J.M.S.-Pure Appl. Chem.* **A31(11)**, 1719 (1994).

25.   Philp, D. & Stoddart, J.F. *Angew. Chem. Int. Ed. Engl.* **35**, 1155 (1996).

26.   Subramainian, S. & Zaworotko, M.J. *Coord. Chem. Rev.* **137**, 357 (1994).

27.   Fan, E., *et al. Macromol. Symp.* **77**, 209-217 (1994).

28.   Fredericks, J., Yang, J., Geib, S.J. & Hamilton, A.D. *Proc. Indian Acad. Sci. (Chem. Sci.)* **106**, 923-935 (1994).

29.   Zimmerman, S.C., Zeng, F., Reichert, D.E.C. & Kolotuchin, S.V. *Science* **271**, 1095-1098 (1996).

30.   Lehn, J.M. *Angew. Chem. Int. Ed. Engl.* **29**, 1304 (1990).

31.   Lehn, J.M. *Pure & Appl. Chem.* **66**, 1961 (1994).

32.   Rebek, J.J. *Angew. Chem. Int. Ed. Engl.* **29**, 245-255 (1990).

33.   Branda, N., Grotzfeld, R.M., Valdes, C. & Rebek, J.J. *J. Am. Chem. Soc.* **117**, 85-88 (1994).

34.   Mathias, J.P., Seto, C.T., Simanek, E.E. & Whitesides, G.M. *J. Am. Chem. Soc.* **116**, 1725-1736 (1994).

35.   Mathias, J.P., Simanek, E.E., Zerkowski, J.A., Seto, C.T. & Whitesides, G.M. *J. Am. Chem. Soc.* **116**, 4316-4325 (1994).

36.   Mathias, J.P., Simanek, E.E. & Whitesides, G.M. *J. Am. Chem. Soc.* **116**, 4326-4340 (1994).

37.   Bissel, R.A., Cordova, E., Kaifer, A.E. & Stoddart, J.F. *Nature* **369**, 133-137 (1994).

38.   Anelli, P.L., *et al. Chem. Eur. J.* **3**, 1113-1135 (1997).

39.   Ringsdorf, H., Schlarb, B. & Venzmer, J. *Angew. Chem. Int. Ed. Engl.* **27**, 113-158 (1988).

40.   Fendler, J.H. *Membrane Mimetic Chemistry. Characterization and Applications of Micelles, Microemulsions, Monolayers, Bilayers, Vesicles, Host-Guest Systems, and Polyions* (Wiley, New York, 1982).

41.   Lee, Y.-S. & O'Brien, D.F. *Chem. Phys. Lipids.* **61**, 209-218 (1992).

42.   O'Brien, D.F., Whitesides, T.H. & Klingbiel, R.T. *J. Polym. Sci. Polym. Lett. Ed.* **19**, 95-101 (1981).

43.   Hub, H.-H., Hupfer, B., Koch, H. & Ringsdorf, H. *Angew. Chem. Int. Ed. Engl.* **19**, 938-940 (1980).

44.   Singh, A., Markowitz, M. & Chow, G.M. *Nano. Struc. Mater.* **5**, 141-153 (1994).

45.   Wegner, G. *Z. Naturforsch.* **24B**, 824 (1969).

46.   Wegner, G. *Makromol. Chem.* **145**, 85 (1971).

47.   Wegner, G. *Die makromol. Chem.* **154**, 35 (1972).

48.   Wilson, T.E., Spevak, W., Charych, D.H. & Bednarski, M.D. *Langmuir* **10**, 1512-1516 (1994).

49.   Saremi, F., Maassen, E., Tieke, B., Jordon, G. & Rammensee, W. *Langmuir* **11**, 1068-1071 (1995).

50.   Chan, K.C., Kim, T., Schoer, J.K. & Crooks, R.M. *J. Am. Chem. Soc.* **117**, 5875-5876 (1995).

51.   Qian, X. & Litt, M. in *Contemporary Topics in Polymer Science* (eds. Salamone, J.C. & Riffle, J.) 361-369 (Plenum Press, New York, 1992).

52. Douglas, E.P., Langlois, D.A. & Benicewicz, B.C. *Chem. Mater.* **6**, 1925-1933 (1994).

53. Broer, D.J., Mol, G.N. & Challa, G. *Makromol. Chem.* **192**, 59-74 (1991).

54. Hikmet, R.A.M., Lub, J. & Tol, A.J.W. *Macromoleules* **28**, 3313-3327 (1995).

55. Hikmet, R.A.M. *Liquid Crystals* **9**, 405-416 (1991).

56. Hikmet, R.A.M. & Michielsen, M. *Adv. Mater.* **7**, 300-304 (1995).

57. Okuno, T., Fukada, M., Izuoka, A., Sato, N. & Sugawara, T. *Mol. Cryst. Liq. Cryst.* **217**, 59-64 (1992).

58. Campell, C., Milburn, G.H., Shand, A.J., Werninck, A.R. & Wright, J. *Intern. J. Polymeric. Mater.* **22**, 85-90 (1993).

59. Walker, K.A. (University of Illinois at Urbana-Champaign, 1995).

60. Radzilowski, L.H., Wu, J.L. & Stupp, S.I. *Macromolecules* **26**, 879-882 (1993).

61. Radzilowski, L.H. & Stupp, S.I. *Macromolecules* **27**, 7747-7753 (1994).

62. Wu, J.L., Radzilowski, L.H. & Stupp, S.I. *APS Bull., March* **37**, 512 (1992).

63. Chen, J.T., Thomas, E.L., Ober, C.K. & Mao, G.-p. *Science* **273**, 343-346 (1996).

64. Ober, C.K., *et al. Macromol. Symp.* **117**, 141-152 (1997).

65. Chen, J.T., Thomas, E.L., Ober, C.K. & Hwang, S.S. *Macromolecules* **28**, 1688-1697 (1995).

66. Saunders, R.S., Cohen, R.E. & R.R., S. *Macromolecules* **24**, 5599 (1991).

67. Perly, B., Douy, A. & Gallot, B. *Makromol. Chem.* **177**, 2569 (1976).

68. Tew, G., Li, L. & Stupp, S.I. *in preparation* .

69. Williams, D.R.M. & Frederickson, G.H. *Macromolecules* **25**, 3561-3568 (1992).

70. Stupp, S.I., Son, S., Lin, H.C. & Li, L.S. *Science* **259**, 59 (1993).

71. Rehage, H. & Schnabel, E. *Makromol. Chem.* **189**, 2395 (1988).

72.   Nuzzo, R.G. & Allara, D.L. *J. Am. Chem. Soc.* **105**, 4481 (1983).

73.   Marikhin, V.A., Guk, E.G. & Myasnikova, L.P. *Phys. Solid State* **39**, 686-689 (1997).

74.   Guk, E.G., Levinshtein, M.E., Marikhin, V.A., Myasnikova, L.P. & Rumyantsev, S.L. *Phys. Solid State* **39**, 690-694 (1997).

75.   Se, K., Ohnuma, H. & Kotaka, T. *Macromolecules* **18**, 2341 (1984).

76.   Seiferheld, U. & Baessler, H. *Solid State Commun.* **47**, 391 (1983).

77.   Park, Y.W., *et al. J. Polym Sci., Polym. Lett. Ed.* **17**, 203 (1979).

78.   Son, S. in *Materials Science and Engineering* 239 (University of Illinois, Urbana-Champaign, 1994).

79.   Huggins, K.E., Son, S. & Stupp, S.I. *Macromolecules* **30**, 5305-5312 (1997).

80.   Stevens, M.P. *Polymer Chemistry: An Introduction* 1-40-43 (Oxford University Press, Inc., New York, 1990).

81.   Lattimer, R.P. & Schulten, H.-R. *Int. J. Mass. Spectrom. Ion Phys.* **52**, 105-116 (1983).

82.   Lattimer, R.P., Harmon, D.J. & Hansen, G.E. *Anal. Chem.* **52**, 1808-1811 (1980).

83.   Hiemenz, P.C. *Polymer Chemistry: The Basic Concepts* (Marcel Dekker, Inc., New York, 1984).

84.   Moore, J.S. & Stupp, S.I. *Macromolecules* **23**, 65 (1990).

85.   Greene, T.W. & Wuts, P.G.M. *Protective Groups in Organic Synthesis* 1-77-83 (John Wiley & Sons, Inc., New York, 1991).

86.   Wetter, H. & Oertle, K. *Tet. Lett.* **26**, 5515-5518 (1985).

87.   Spickerman, J., *et al. Macromol. Rapid Commun.* **17**, 885-896 (1996).

88.   Kahr, M.S. & Wilkins, C.L. *J. Am. Soc. Mass. Spectrom.* **4**, 453-460 (1993).

89. Vialini, D., Mineo, P. & Scamporrino, E. *Macromolecules* **30**, 5285-5289 (1997).

90. Martin, K., Spickermann, J., Rader, H.J. & Mullen, K. *Rapid Commun. Mass Spectrom.* **10**, 1471-1474 (1996).

91. Ueberreiter, K. & Kanig, G. *J. Colloid Sci.* **7**, 569 (1952).

92. Cowan, D.O. & Drisko, R.L. in *Elements of Organic Photochemistry* 19-72 (Plenum Press, New York, 1976).

93. Fritzsche, I. *J. Prakt. Chem* **101**, 333 (1867).

94. Bouas-Laurent, H., Castellan, A. & Desvergne, J.-P. *Pure & Appl. Chem.* **52**, 2633-2648 (1980).

95. Sapich, B., Haferkorn, J., Lasker, L. & Stumpe, J. *J. Inf. Recording* **23**, 103-106 (1996).

96. Stumpe, J., Ziegler, A., Berghahn, M. & Kricheldorf, H.R. *Macromolecules* **28**, 5306-5311 (1995).

97. Gilbert, A. & Baggott, J. *Essentials of Molecular Photochemistry* 1-275-277 (CRC Press, Boca Raton, 1991).

98. Weil-Malherbe, H. & Weiss, J. *J. Chem. Soc.* , 541-544 (1944).

99. Coulson, C.A., Orgel, L.E., Taylor, W. & Weiss, J. *J. Chem. Soc.* , 2961-2962 (1955).

100. De Schryver, F.C., Anand, L., Smets, G. & Switten, J. *Polymer Letters* **9**, 777-780 (1971).

101. Fages, F., Desvergne, J.-P., Frisch, I. & Bouas-Laurent, H. *J. Chem. Soc., Chem. Commun.* , 1413 (1988).

102. Gilbert, A. & Baggott, J. *Essentials of Molecular Photochemistry* 1-401-405 (CRC Press, Boca Raton, 1991).

103. Hondrogiannis, G., Lee, C.W., Pagni, R.M. & Mamantov, G. *J. Am. Chem. Soc.* **115**, 9828-9829 (1993).

104. Castellan, A., Lapouyade, R., Bouas-Laurent, H. & Lallemand, J.Y. *Tetrahedron Letters* , 2467-2470 (1975).

105. Brandrup, J. & Immergut, E.H. (John Wiley & Sons, New York, 1975).

106. Morton, M. *Anionic Polymerization: Principles and Practice* (Academic Press, New York, 1983).

107. Quirk, R.P., Yin, J., Fetters, L.J. & Kastrup, R.V. *Macromolecules* **25**, 2262-2267 (1992).

108. Quirk, R.P., Yin, J. & Fetteres, L.J. *Macromolecules* **22**, 85-90 (1989).

109. Kelker, H. *Mol. Cryst. Liq. Cryst.* **21**, 1-48 (1973).

110. Poe, E.A. in *The Complete Stories and Poems of Edgar Allen Poe* 706 (Doubleday & Co., Garden City, NY, 1966).

111. Virchow, R. *Virchows Archiv* **6**, 571 (1854).

112. Reinitzer, F. *Monatsh.* **9**, 421 (1888).

113. Lehmann, O. *Flüssige Kristalle, sowie Plastizität von Kristallen im Allgemeinen, molekulare Umlagerungen und Aggregatzustandsänderungen* 1-264 (Engelmann, Leipzig, 1904).

114. Lehmann, O. *Verhandl. d. Deutsche Phys. Ges* **16.3**, 1 (1900).

115. Toyne, K.J. in *Thermotropic Liquid Crystals* (ed. Gray, G.W.) 28-58 (John Wiley & Sons, Chichester, 1987).

116. Gray, G.W. in *The Molecular Physics of Liquid Crystals* (eds. Luckhurst, G.R. & Gray, G.W.) 1-28 (Academic Press, London, 1979).

117. Onsager, L. *Ann. N.Y. Acad. Sci.* **51**, 627 (1949).

118. Chandrasekhar, S. *Liquid Crystals* (Cambridge University Press, Cambridge, 1977).

119. Chandrasekhar, S., Sadashiva, B.S. & Suresh, K.A. *Pramana* **9**, 471 (1977).

120. Friedel, G. *Ann. Phys. (Paris)* **18**, 273 (1922).

121. Leadbetter, A.J. in *Thermotropic Liquid Crystals* (ed. Gray, G.W.) 1-27 (John Wiley & Sons, Chichester, 1987).

122. Gray, G.W. & Goodby, J.W.G. *Smectic Liquid Crystals: Textures and Structures* (Leonard Hill, Glasgow, 1984).

123. de Gennes, P.-G. *The Physics of Liquid Crystals* (Oxford University Press, 1974).

124. Saeva, F.D. in *Liquid Crystals: The Fourth State of Matter* (ed. Saieva, F.D.) 73-98 (Marcel Dekker, Inc., New York, 1979).

125. Hardouin, F., Achard, M.F., Destrade, C. & Tinh, N.H. *J. Physique* **45**, 765-769 (1984).

126. Tinh, N.H., Hardouin, F., Destrade, C. & Gasparoux, H. *J. Physique Lett.* **43**, L-739-L744 (1982).

127. Hardouin, F. & Tinh, N.H. *J. Physique Lett.* **43**, L779-L784 (1982).

128. Shashidhar, R., Ratna, B.R., Prasad, S.K., Somasekhara, S. & Heppke, G. *Phys. Rev. Lett.* **59**, 1209-1211 (1987).

129. Levelut, A.M., Tarento, R.J., Hardouin, F., Achard, M.F. & Sigaud, G. *Phys. Rev. A* **24**, 2180-2186 (1981).

130. Richardson, R.M., Leadbetter, A.J. & Frost, J.C. *Mol. Phys.* **45**, 1163 (1982).

131. Goodby, J.W. & Patel, J.S. in *Proceedings of SPIE Liquid Crystals and Spatial Light Modulator Materials* (ed. Penn, W.A.) 52-59 (SPIE, San Diego, CA, 1986).

132.   Doucet, J., Keller, P., Levelut, A.-M. & Porquet, P. *J. Phys. (Paris)* **39**, 548 (1978).

133.   Gane, P.A.C., Leadbetter, A.J. & Wrighton, P.G. *Mol. Cryst. Liq. Cryst.* **66**, 247 (1981).

134.   Brand, H.R. & Cladis, P.E. *J. Phys. (Paris) Lett.* **45**, 217 (1984).

135.   Li, L.S. & Stupp, S.I. *Macromolecules* **30**, 5313-5320 (1997).

136.   Stupp, S.I., Son, S., Li, L.S., Lin, H.C. & Keser, M. *J. Am. Chem. Soc.* **117**, 5212-5227 (1995).

137.   Ratna, B.R., Shashidhar, R. & Raja, V.N. *Phys. Rev. Lett.* **55**, 1476-1478 (1985).

138.   Brock, J.D., *et al. Phys. Rev. Lett.* **57**, 98-101 (1986).

139.   Doucet, J. in *The Molecular Physics of Liquid Crystals* (eds. Luckhurst, G.R. & Gray, G.W.) 317-341 (Academic Press, London, 1979).

140.   Leadbetter, A.J., Durrant, J.L.A. & Rugman, M. *Mol. Cryst. Liq. Cryst. Lett.* **34**, 231 (1977).

141.   Paul, S., Stein, S., Knoll, W. & Mullen, K. *Acta Polymer* **47**, 67-73 (1996).

142.   Lambert, J.B., Shurvell, H.F., Lightner, D. & Cooks, R.G. *Introduction to Organic Spectroscopy* 1-288 (Macmillan Publishing Company, New York, 1987).

143.   Chapman, O.L. & Lee, K. *J. Org. Chem.* **34**, 4166-4168 (1969).

144.   Anet, R. *Tet. Lett.* , 3713-3717 (1965).

145.   Becker, E.D. *High Resolution NMR: Theory and Chemical Spplications* 1-174-175 (Academic Press, Inc., Orlando, 1980).

146.   Sanders, J.K.M. & Hunter, B.K. *Modern NMR Spectroscopy: A Guide for Chemists* 1-110 (Oxford University Press, Oxford, 1993).

147.   Braun, S., Kalinowski, H.-O. & Berger, S. *100 and More Basic NMR Experiments* 1-

308-317 (VCH Publishers, New York, 1996).

148. Babbitt, G.E. & Patel, G.N. *Macromolecules* **14**, 554-557 (1981).

149. Wenz, G., Muller, M.A., Schmidt, M. & Wegner, G. *Macromolecules* **17**, 837-850 (1984).

150. Plachetta, C. & Schulz, R.C. *Makromol. Chem., Rapid Commun.* **3**, 815-819 (1982).

151. Willson, C.G. in *Introduction to Microlithography: Theory, Materials, and Processing* (eds. Thompson, L.F., Willson, C.G. & Bowden, M.J.) 88-148 (American Chemical Society, Washington, D.C., 1983).

152. DeForest, W.S. *Photoresist: Materials and Processes* (McGraw-Hill Book Company, New York, 1975).

153. Runyan, W.R. & Bean, K.E. *Semiconductor Integrated Circuit Processing Technology* (Addison-Wesley Publishing Company, Reading, Massachusetts, 1990).

154. Gwozdz, P.S. in *Proceedings of SPIE: Semiconductor Microlithography VI* (ed. Dey, J.) 156-163 (SPIE, San Jose, CA, 1981).

155. Wolf, S. & Tauber, R.N. in *Silicon Processing for the VLSI Era: Volume 1--Processing Technology* 407-458 (Lattice Press, Sunset Beach, CA, 1986).

156. Hofer, D.C., Kaufman, F.B., Dramer, S.R. & Aviram, A. *Appl. Phys. Lett.* **37**, 314 (1980).

157. Frechet, J.M.J., Ito, H. & Willson, C.G. *Proc. Microcircuit Eng.* , 260 (1982).

158. Frechet, J.M.J. (U.S., 1985).

159. MacDonald, S.A., Willson, C.G. & Frechet, J.M.J. *Acc. Chem. Res.* **27**, 151-158 (1994).

160. Crivello, J.V. & Lam, J.H.W. *J. Polym. Sci.: Polym. Chem. Ed.* **17**, 977-999 (1979).

161.   Reiser, A. *Photoreactive Polymers: The Science and Technology of Resists* (John Wiley & Sons, New York, 1989).

162.   Umbach, C.P., Broers, A.N., Willson, C.G., Koch, R. & Laibowitz, R.B. *J. Vac. Sci. Technol. B.* **6**, 319-322 (1988).

163.   Ushirogouchi, T., *et al.* in *Microelectronics Technology* (ed. Reichmanis, E.) 240-254 (American Chemical Society, Washington, D.C., 1995).

164.   Tazuke, S. & Banba, F. *J. Polym. Sci. Polym. Chem. Chem. Ed* **14**, 2463-2478 (1976).

165.   Tazuke, S. & Hayashi, N. *J. Polym. Sci. Polym. Chem. Chem. Ed.* **16**, 2729-2739 (1978).

166.   Bartz, T., Klapper, M. & Mullen, K. *Macromol. Chem. Phys.* **195**, 1097-1109 (1994).

167.   Paul, S., Stein, S., Knoll, W. & Mullen, K. *Acta. Polymer* **45**, 235-243 (1994).

168.   Creed, D., Hoyle, C.E., Griffin, A.C., Liu, Y. & Pankasem, S. in *Microelectronics Technology* (ed. Reichmanis, E.) 504-517 (American Chemical Society, Washington, D.C., 1995).

169.   Satoh, S., Suzuki, H., Kimata, Y. & Kuriyama, A. *Synthetic Metals* **79**, 97-102 (1996).

170.   Paul, S., *et al. Thin Solid Films* **288**, 150-154 (1996).

171.   Stein, S. & Mullen, K. *Acta Polymer* **47**, 85-91 (1996).

172.   Jones II, G., Bergmark, W.R. & Halpern, A.M. *Chem. Phys. Lett.* **76**, 403 (1980).

173.   Wolf, S. & Tauber, R.N. in *Silicon Processing for the VLSI Era: Volume 1--Processing Technology* 539-585 (Lattice Press, Sunset, CA, 1987).

174.   Thompson, L.F. & Bowden, M.J. in *Introduction to Microlithography: Theory, Materials, and Processing* (eds. Thompson, L.F., Willson, C.G. & Bowden, M.J.) 161-214 (American Chemical Society, Washington, D.C., 1983).

175.   Halperin, A. *Macromolecules* **23**, 2724-2731 (1990).

176.   Porter, D.A. & Easterling, K.E. *Phase Transformations in Metals and Alloys* (Chapman & Hall, London, 1993).

177.   Young, R.J. & Lovell, P.A. *Introduction to Polymers* 1-203-211 (Chapman & Hall, London, 1991).

178.   de Gennes, P.-G. *Scaling Concepts in Polymer Physics* 1-98-127 (Cornell University Press, Ithaca, 1991).

179.   Wiesler, W.T. & Nakanishi, K. *J. Am. Chem. Soc.* **112**, 5574-5583 (1990).

Vita

Kyle Daniel Gresham was born in Minot, N.D. on June 25, 1968 to David and Linda Gresham. His childhood dream of attending the United States Air Force Academy became a reality in 1987. He graduated four years later, 14th in his class, with a B.S. in chemistry. After shaking President George Bush's hand at graduation he was off to the University of Illinois where he received a M.S. degree in inorganic chemistry. In 1992, he began work in the Laser Hardened Materials Branch of the Materials Directorate at Wright Laboratory in Dayton, Ohio. There he was awarded the Director's Military Award for 1994. Later that year, he began the pursuit of a Ph.D. in Materials Science and Engineering under the guidance of Professor Samuel I. Stupp at the University of Illinois at Urbana-Champaign. His work has focused on the synthesis and characterization of organic molecules which self assemble into nanostructures.